THE
PHYSICAL REVIEW
A Journal of Experimental and Theoretical Physics Established by E. L. Nichols in 1893
VOL. 59, NO. 2 JANUARY 15, 1941 SECOND SERIES

Cloud Tracks of Cosmic Rays in the Substratosphere

G. HERZOG*
University of Chicago, Chicago, Illinois
(Received October 24, 1940)

A cloud chamber in a magnetic field of 708 oersteds was carried in an airplane to a height of 29,300 feet. The maximum measurable $H\rho$ was 5.6×10^5 which, for an electron, corresponds to an energy of 1.7×10^8 ev. Out of 155 pictures taken at altitudes greater than 15,000 feet, 51 slow mesotrons and 39 proton tracks were identified. The number of slow mesotron tracks at these altitudes is 9 percent of the number of electron and fast mesotron tracks. One photograph seems to show a slow mesotron shower. Some of the tracks with very high specific ionization may be due to the fragments of heavy nuclei.

IT is of great importance to get direct evidence for the mass of the mesotron and to make a mass determination. This can be accomplished in a cloud chamber by measuring the number of ions formed in the gas, and by simultaneous determination of the curvature in a magnetic field which gives the momentum of the particle. Figure 1 shows the energy loss in air per g/cm² for single charged particles of mass one (electron), 100 and 300 (range of the mesotron mass) and 1840 (proton). For high momenta the ionization is practically independent of the rest mass of the particle. We can hope to get information concerning the rest mass only if the particle has a momentum low enough to put its energy loss caused by ionization on the increasing part of the curves in Fig. 1. The present experiment was performed to see whether such low momentum mesotrons can be observed in the substratosphere.

Mesotrons with a momentum below 100 mc ($H\rho=2\times10^5$) have losses greater than three times that of fast electrons, whereas for protons this value lies at 1000 mc ($H\rho=2\times10^6$). The great number of cosmic-ray pictures taken at sea level and on mountains, reveal only about 10 tracks with momenta small enough to show such increased ionization. We conclude that the percentage of slow mesotrons at low altitudes is extremely small.

Let us assume that mesotrons are produced as secondaries by γ-rays of the soft component in the atmosphere. According to the cascade theory the average energy of the γ-rays decreases rapidly with the amount of air traversed. On this theory

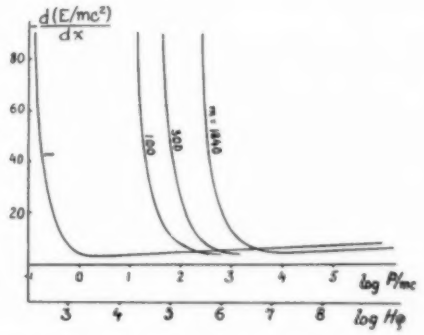

FIG. 1. Energy loss in air per g/cm² for single charged particles of various masses.

* Now at Texas Company, Houston, Texas.

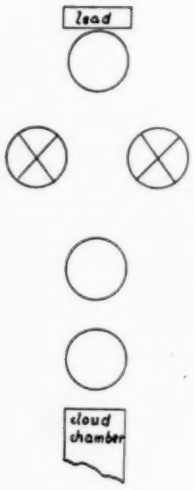

FIG. 2. Arrangement of the threefold counter telescope.

the number F of electrons with energies greater than E electron volts varies with the depth from the top of the atmosphere as

$$F(E, l) = 40(10^8/E)^{1.8} e^{-0.32(l-10)} \text{ min.}^{-1} \text{ cm}^{-2}.$$[1]

l is measured in the units given in the cascade theory. Sea level corresponds to $l=29$, 30,000 feet to $l=10$. The number of γ-rays at a given height is about double that of the electrons. The minimum energy for a γ-ray to produce a mesotron of $\mu=200$ is 10^8 ev. From the above formula one finds

$$2F(10^8, 29) = 0.18 \text{ min.}^{-1} \text{ cm}^{-2},$$
$$2F(10^8, 10) = 80 \text{ min.}^{-1} \text{ cm}^{-2},$$

i.e., the number of photons having enough energy to create the rest mass 200 of a mesotron increases by a factor of 440 from sea level to an altitude of 30,000 feet. Since other than cascade electrons appear at sea level, the actual ratio should be appreciably less than this factor of 440, but should, nevertheless, be large. This large increase suggests that finding slow mesotrons at high altitudes is probable.

Also the experiments of Schein and Wilson[2] and of Jesse, Schein and Wollan[3] have proved the creation of mesotrons in altitudes attainable in an airplane. Although the arrangement of the lead filters in their experiments prevented the detection of mesotrons below 2×10^8 ev (kinetic energy), there is good reason to believe that together with these particles slow mesotrons are also created.

It is worth mentioning that the slow mesotrons have kinetic energies that are near the lower limit for cosmic-ray particles. For a momentum of 100 mc the velocity is $0.45c$ and the kinetic energy 12 Mev. The range is 0.75 cm of lead, or 4.8 g/cm² of air, which corresponds to 37 m at sea level and 110 m at 30,000 feet. This short range is the reason that mesotrons which have been created with low momenta higher in the atmosphere cannot reach sea level. This is quite aside from the possible decay of the mesotron.

THE APPARATUS

The 6-inch diameter cloud chamber has a 1-inch depth of illumination, a rubber piston, and is filled with argon at $\frac{1}{3}$ atmos. overpressure. The expansion is accomplished by tripping a magnet which releases a valve in the back chamber. Special precautions were taken to adjust to the varying outside pressure in the course of a flight. The illumination is accomplished by four photofloodlight lamps which are flashed when the expansion starts. They draw 16 amp. at 150 volts out of 96 No. 6 $1\frac{1}{2}$-volt dry cells. A "Sept" movie camera is used with an f : 1.9 lens and is equipped with an attachment so that all photographs are taken stereoscopically. The timing control of the expansion, illumination

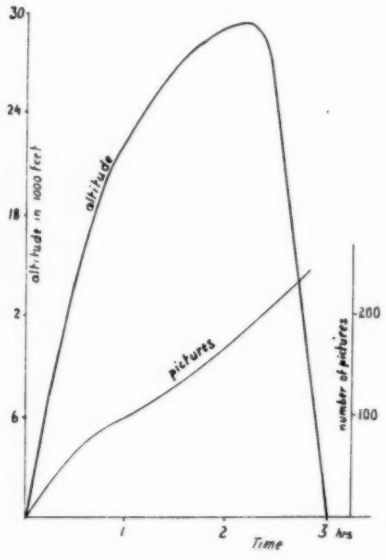

FIG. 3. Record of altitudes reached and number of pictures taken.

[1] W. Heisenberg and H. Euler, Ergeb. d. exact. Naturwiss. **17** (1938).
[2] M. Schein and V. C. Wilson, Rev. Mod. Phys. **11**, 292 (1939).
[3] Schein, Jesse and Wollan, Phys. Rev. **57**, 847 (1940).

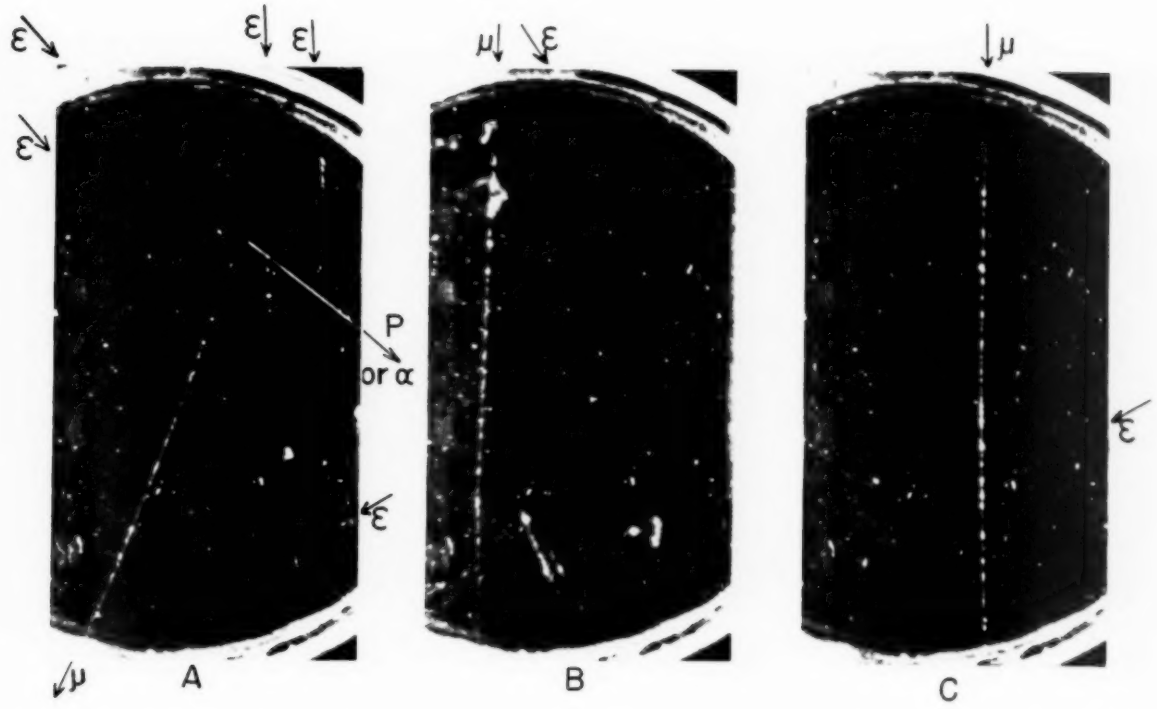

FIG. 4. Cloud-chamber photographs. *A*, negative mesotron ($H\rho = 1.4 \times 10^5$) with an electron shower and α-particle or proton. *B*, mesotron with some scattering after first three-quarters of its path. The sign is positive and initial $H\rho$ is about 5.5×10^5. The electron has an energy of 1.7×10^6 ev. *C*, positive mesotron of $H\rho = 1.4 \times 10^5$.

and exposure is performed by an R C-controlled vacuum-tube circuit. This circuit can work for random expansions with a cycle of 20 seconds between successive expansions, or the cycle can be initiated by the discharge of a G-M counter arrangement.

The magnetic field is provided by a U-shaped permanent magnet weighing 400 pounds. The pole pieces have a square cross section of 4.5 inches on the side. The gap of the magnet is 8 inches. The back part of the cloud chamber (soft iron) forms one pole piece. This reduces the actual gap to 6 inches. The field inside the cloud chamber is 708 oersteds, and it has a homogeneity of 98 percent over the surface of the chamber. The largest radius of curvature which can be measured is about 800 cm (length of tracks 14 cm, deviation from a straight line in center 0.3 mm). This corresponds to a value $H\rho = 5.6 \times 10^5$. For an electron this would be an energy of 1.7×10^8 ev.

The apparatus was installed in a Douglas DC3 transport plane, whose closed cabin was maintained at nearly constant temperature.

The G-M counter arrangement

Figure 2 shows the arrangement of a threefold counter telescope. Placing all counters above the cloud chamber provides for the possibility of catching tracks which end inside the cloud chamber. A lead sheet 2 cm thick in which new mesotrons may be created lies on top of the counters. This lead also would act as an optimum source for shower production. The number of showers tripping the chamber is reduced by the arrangement of two anticounters. They respond to shower electrons at an average of 20 degrees with the vertical. The threefold telescope and the anticounters are connected to an anticoincidence amplifier[4] which controls the expansion. Hence, expansions are made only when a particle crossing the telescope is not accompanied by shower electrons penetrating the anticounters.

The counting rate of this arrangement is 0.125 per minute in the laboratory at sea level, and increased to 2 per minute at an altitude of 26,500 feet. This increase by a factor of 16 may be com-

[4] G. Herzog, Rev. Sci. Inst. **11**, 84 (1940).

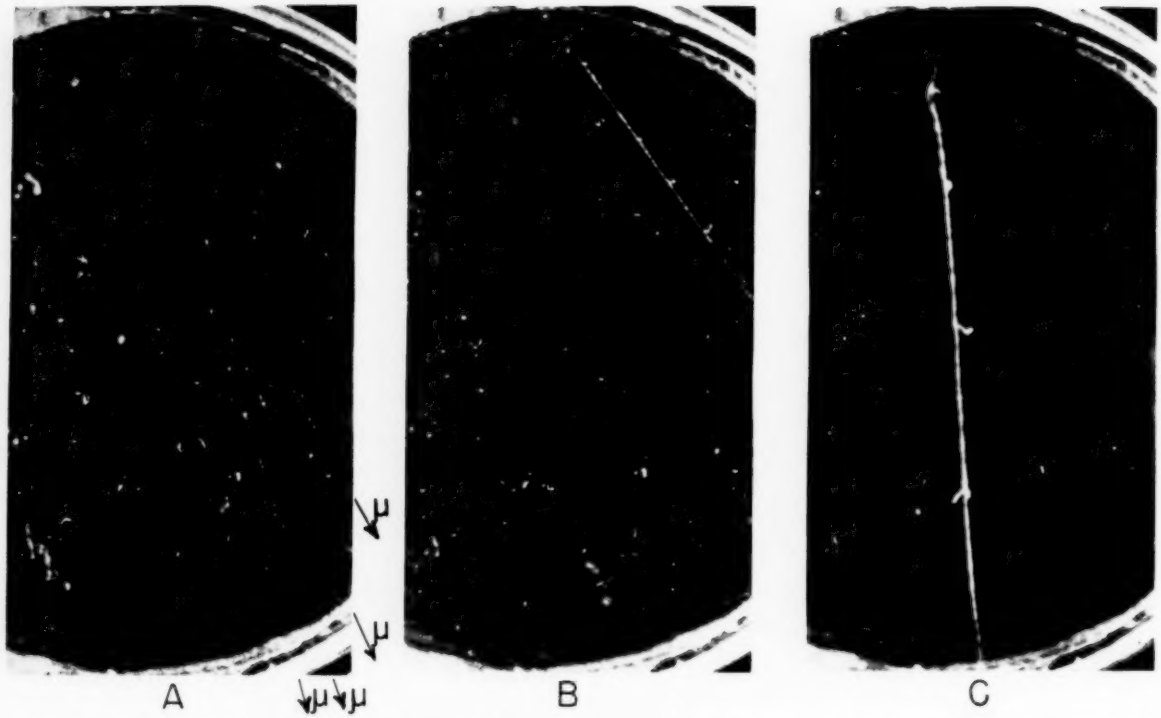

FIG. 5. Cloud-chamber photographs. *A*, shower of slow mesotrons. *B* and *C* show particles heavier than mesotrons with several delta-rays.

pared with the value of 15 for the total vertical counting rate as measured without lead by Pfotzer.[5]

As the airplane left the ground, the random expansion arrangement was used. When the counting rate reached a value of about two per minute the arrangement was switched over to counter-controlled expansions.

THE RESULTS

Figure 3 shows a record of the altitudes reached and the number of pictures taken. Altogether, 230 pictures were taken in a total flying time of three hours.

The pictures show three distinct groups of tracks. Those in the first group have specific ionization similar to that of electrons in the test experiments in the laboratory. These tracks correspond to electrons or heavier particles with speeds approaching that of light. The second group has a definitely higher specific ionization. It can be estimated to be about 3 to 5 times that of the electron tracks, and probably corresponds to slow mesotrons. Both of these groups show clusters of drops and gaps along the tracks, whereas in the third group the ionization is so dense that the tracks are uninterrupted lines. These latter tracks are created by protons and heavier particles.

For the present purpose the most interesting tracks are those of the second group. For a qualitative test the number of clusters per cm path, caused presumably by secondary electrons, was counted for the electrons and mesotrons. The tracks selected by appearance as being of the second group, were found to have two to four times as many clusters as the average electron track. These figures have, however, no

TABLE I. *Number of different tracks.*

ALT. IN 1000 FEET	ELECTRONS		MESOTRONS		PROTONS AND α's		NO. OF PICTURES
	TOTAL	$l>5$	TOTAL	$l>5$	TOTAL	$l>5$	
0 to 5	8	2	—	—	1	—	14
5 to 10	30	9	—	—	9	1	32
10 to 15	33	13	—	—	3	—	29
15 to 20	51	17	2	1	2	—	28
20 to 25	111	38	6	4	5	2	38
above 25	425	137	43	16	32	6	89

[5] G. Pfotzer, Zeits. f. Physik **102**, 34 (1936).

exact numerical significance. In an electron track with its low average ionization, small clusters can be detected which would be obscured in the denser mesotron tracks. The $H\rho$ values for the 14 mesotron tracks which were long enough for measurement lie between 3×10^4 and 5×10^5. Figure 1 shows that this is the region where a large ionization is to be expected for mesotrons It seems quite impossible to explain these tracks as being produced either by electrons or by protons, even if one allows for large errors in the estimate of the ionization and in the curvature determination (see Fig. 1).

Out of these 14 tracks, 8 correspond to positive and 6 to negative particles.

In addition, 37 tracks were photographed whose appearance shows very clearly that they belong in this group of the mesotron tracks, although their curvature could not be measured. Either the length of the track is not sufficient, i.e., the track does not lie in the plane of the cloud chamber, or the radius of curvature is too great for an exact measurement. None of these tracks could have been produced by electrons, because electrons of this ionization would show a very small radius of curvature, which could have been easily measured. The general appearance also makes it very unlikely that they are protons. These tracks, therefore, have been counted as mesotrons.

In Table I the frequency distribution of the different groups with altitude is listed. In each group the total number of tracks is given and then out of those the number of tracks showing a length over 5 cm. The first group headed as electrons also contains all fast particles whose ionization is practically the same as for electrons. The second group contains only the slow mesotrons, the third the protons and heavier particles.

TABLE II. *Number of tracks per expansion.*

ALT. IN 1000 FEET	ELECTRONS		MESOTRONS		PROTONS AND α's	
	TOTAL	$l>5$	TOTAL	$l>5$	TOTAL	$l>5$
0 to 5	0.57	0.14	—	—	0.07	—
5 to 10	0.94	0.28	—	—	0.28	0.03
10 to 15	1.14	0.45	—	—	0.10	—
15 to 20	1.92	0.61	0.07	0.04	0.07	—
20 to 25	2.82	1.00	0.16	0.10	0.13	0.05
above 25	4.77	1.54	0.48	0.18	0.36	0.07

The next column gives the number of pictures taken at the respective altitudes.

In a similar way, the frequency occurrence per expansion is listed in Table II. Table III gives the number of slow mesotrons divided by the number of tracks with electronic appearance.

These figures show that very few slow mesotrons are found below 20,000 feet, and that at 25,000 feet their number becomes 10 percent that of the particles which ionize like electrons. This figure seems very high, and further experiments will be needed to check it. The occurrence of slow mesotrons at these altitudes agrees, however, with the results by Schein and Wilson. They found that in 2 cm lead at 25,000 feet, about as many mesotrons are created as are coming through the atmosphere. If the observed slow mesotrons are the ends of energetic mesotrons produced high in the atmosphere, it can hardly be understood why these ends should be so much more abundant at 25,000 feet than at sea level. It seems much more probable that the slow mesotrons are created in the neighborhood of the cloud chamber, in the lead, the iron of the magnet and in the air.

TABLE III. *Number of mesotrons per electron track.*

ALT. IN 1000 FEET	TOTAL	$l>5$	ALT. IN 1000 FEET	TOTAL	$l>5$
0 to 5	—	—	15 to 20	0.04	0.02
5 to 10	—	—	20 to 25	0.05	0.04
10 to 15	—	—	above 25	0.10	0.04

In Fig. 4*A* a negative mesotron of $H\rho=1.4\times10^5$ occurs simultaneously with an electron shower and α-particle or proton. In Fig. 4*B* the mesotron has some scattering after the first three-quarters of its path. From the upper, undistorted part one finds $H\rho$ about 5.5×10^5 and the sign to be positive. The electron on the same picture has an energy of 1.7×10^6 ev. Figure 4*C* shows a positive mesotron of $H\rho=1.4\times10^5$, and on the same expansion an electron whose ionization is much smaller.

Several expansions have more than one mesotron. There are 6 pictures with two mesotrons, 2 pictures with 3 and 2 pictures with four mesotron tracks. Figure 5*A* seems to be a shower of slow mesotrons. Figures 5*B* and *C* show

particles, heavier than mesotrons, with several delta-rays similar to those observed with alpha-particles.

SUMMARY

This flight shows that slow mesotrons occur in appreciable numbers above 20,000 feet altitude. There seem to be also some heavy nuclei present. These could be the result of nuclear reactions created by neutrons. It is planned to make further flights to get better numerical information.

ACKNOWLEDGMENT

I wish to thank Mr. W. H. Bostick who assisted in the flight and who was very helpful in computing the results. Mr. Leonard Miller was kind enough to help in the construction of the timing set. I have, further, to thank the United Air Lines and their engineer, Mr. W. Davies, for valuable help and cooperation. My special gratitude belongs to Dr. A. H. Compton, who was always ready to give helpful advice and encouragement.

JANUARY 15, 1941 PHYSICAL REVIEW VOLUME 59

Cloud-Chamber Pictures of Cosmic Rays at 29,000 Feet Altitude

G. HERZOG* AND W. H. BOSTICK
Ryerson Physical Laboratory, University of Chicago, Chicago, Illinois

(Received November 9, 1940)

Cloud-chamber pictures (115 in number) of cosmic rays were taken during an airplane flight. The range of slow mesotrons was investigated by inserting a copper plate across the middle of the chamber. The slow mesotron rate above 15,000 feet is 9.6 percent of the occurrence rate of electrons and fast mesotrons. The formation of a pair of positive and negative slow mesotrons was photographed. Statistical evidence is given that mesotrons do not always disintegrate when stopped. One proton was photographed.

RECENTLY one of us[1] reported photographs of cosmic rays made with a cloud chamber at altitudes up to 29,300 feet. The apparatus was installed in a Douglas DC3 airplane, and consisted of a cloud chamber 6 inches in diameter mounted in the gap of a permanent magnet which gives a homogeneous field of 708 oersteds. The results of this first flight indicated that there is a good chance to photograph slow mesotrons at higher altitudes. This conclusion was drawn from an evaluation of the ion density of the tracks combined with a measurement of the momentum of the particle (curvature in the magnetic field).

On April 30th we used the same equipment for a second flight.[2] With a total flying time of four hours and 10 minutes we stayed for three hours above 20,000 feet and reached a top altitude of 29,000 feet. Figure 1 shows the altitude-time record of this flight.

About half of the expansions were made at random, the other half were controlled by the same anticoincidence arrangement of G–M counters as previously described. Because of difficulty with the temperature control in the airplane cabin, convection currents in the cloud chamber caused occasional distortions in the tracks.

In order to obtain additional information two changes were made in the cloud chamber. The first was to mount a horizontal copper plate across the center of the chamber. Careful investigations in the laboratory proved that the plate does not appreciably distort the tracks. The purpose of the plate was to slow down or stop some of the slow mesotrons. For the range of a track which is stopped in the plate, one can give an upper limit. This range determination, together with the curvature measurement, gives

---

* Now with the Texas Company in Houston, Texas.

[1] G. Herzog, Phys. Rev. **59**, 117 (1940) preceding paper, referred to as I.

[2] We wish to thank the United Air Lines for their support in carrying out this flight and Mr. W. Davies, research engineer of this company, for his valuable help.

TABLE I. *Data for electrons, mesotrons ($\mu=200$), and protons for the two ranges of 0.06 cm and 0.32 cm copper.*

PARTICLE	MAX. TOTAL ENERGY MEV	MAX. KINET. ENERGY MEV	MAX. MOMENTUM pc MEV	MAX. VELOCITY v/c	MAX. RADIUS OF CURVATURE CM	MIN. IONIZATION $\frac{\partial E/\partial x}{(\partial E/\partial x)_{\text{ELECTRON}}}$
The stopping power for 0.06 cm copper						
Electron	1.6	1.1	1.5	0.96	7.3	1
Mesotron $\mu=200$	106	6	34.6	0.33	165	3.5
Proton	942	22	200	0.22	950	6
The stopping power for 0.32 cm copper						
Electron	4.55	4.05	4.5	0.99	21.4	1
Mesotron $\mu=200$	119	19	64	0.54	305	2
Proton	967	47	294	0.32	1400	4

the second possibility of evaluating the mass of the particle. The ionization *vs.* curvature method can of course also be used, and sometimes an estimate of the ionization together with the range determination is helpful in discussing the nature of the particle involved. The combination of all these methods is extremely valuable.

In order to cover a larger set of data with one flight, the thickness of the copper plate was 0.06 cm across one half of the chamber and 0.32 cm across the other half. These values were chosen according to information from the first flight, which showed many mesotrons having only a few million electron volts kinetic energy. Such particles should be stopped by a thin plate. The insertion of the plate cuts the length of the tracks in the upper and the lower halves of the cloud chamber to half of its previous value. This reduces considerably the accuracy of the curvature measurements.

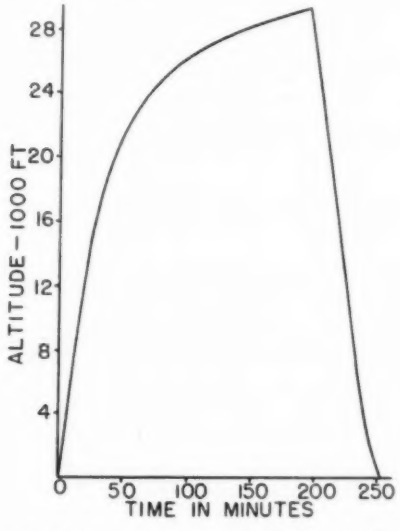

FIG. 1. Altitude-time record of airplane flight.

The second change consisted in replacing the argon in the chamber with helium. Thus we reduced the curvature resulting from multiple scattering in the gas. The scattering increases with the square of the atomic number and is much less in helium than in argon.

STOPPING POWER OF COPPER PLATES FOR VARIOUS PARTICLES

Any particle entering the plate vertically and being stopped in it has a range in copper which is less than the plate thickness. Corresponding to this maximum range one can calculate an upper limit to the energy and to the momentum of the particle before it enters the plate, if the particle is stopped by ionization and radiation processes only. The energy thus calculated depends of course on the mass of the particle. For each assumed mass there is a corresponding maximum radius of curvature which the particle can have in the magnetic field of the cloud chamber (708 oersteds). One also can compute the specific ionization in the gas of the chamber. This ionization decreases with increasing energy for the small energies under consideration.

These data are listed in Table I for electrons, mesotrons ($\mu=200$), and protons for the two ranges of 0.06 cm and 0.32 cm copper. The specific ionization is expressed in terms of the specific ionization of an electron having the same momentum.

The table shows that it is easy to distinguish whether a stopped particle is heavier than an electron. The maximum curvatures for electrons are so small that they can easily be measured with our field. The distinction between a mesotron and a proton is more difficult because

TABLE II. *Data for particles traversing or ending in the copper plates. Electrons are indicated by* ϵ, *mesotrons by* μ, *and protons by* π.

PICTURE	ρ CM	SIGN	IONIZATION FROM INSPECTION	PROBABLE NATURE
Particles passing through 0.06 cm copper				
699	>200		=fast ϵ's	ϵ or fast μ
724	>400		= "	"
738	>400		= "	"
738–1	>100		> "	"
738–2	>100		> "	"
746	14	−	= "	ϵ
759	>150		= "	ϵ or fast μ
770	>300		= "	"
792–1	>200		= "	"
792–2	>200		= "	"
797	>400		= "	"
813	>400		= "	"
Particles ending in 0.06 cm copper				
680–1	2	+	=ϵ's	ϵ
705–3	>150	−	>fast ϵ's	slow μ or π
755	150	+	> "	slow μ
813–1	2	−	=ϵ's	ϵ
813–2	2	−	=ϵ's	ϵ

PICTURE	ρ CM	SIGN	IONIZATION FROM INSPECTION	PROBABLE NATURE
Particles passing through 0.32 cm copper				
712	>300		=fast ϵ's	ϵ or fast μ
721	>400		= "	"
722	>400		= "	"
723	>400		= "	"
739	>400		> "	"
768	>400		= "	"
793	>200		= "	"
803	>300		= "	"
806	>400		= "	"
833	>300		= "	"
879	>300		= "	"
900	>200		= "	"
705	>180		= "	"
Particles ending in 0.32 cm copper				
680–2	3	−	=ϵ's	ϵ
684	>150		>fast ϵ's	slow μ or π
696	>300		> "	"
707	150		= "	slow μ
715	64	−	> "	slow μ
748	>200		= "	slow μ or π
754–1	82	−	$\gg$ "	slow μ
754–2	75	+	$\gg$ "	slow μ
760	>100		= "	slow μ or π
785	>300		= "	"
807–2	28	+	= "	ϵ
807–1	>100	−	= "	slow μ or π
822	>150		$\gg$ "	π
828	>150		= "	slow μ or π
900	>150		= "	"
802	>300		= "	"

the radius of curvature limits are rather large with the magnetic field employed. An estimate of the ionization along the track is very helpful here. This holds especially for slow particles where the ionization losses for mesotrons and protons differ by a factor of two or more. It must be noted, however, that if protons are stopped by processes in which neutrons are ejected, protons of radii of curvature greater than 950 and 1400 may be stopped in the copper plates.

RESULTS

Altogether 115 successful pictures were taken. These show 12 particles traversing the 0.06-cm plate and 12 particles going through 0.32 cm copper. 5 particles are stopped in 0.06 cm copper and 16 in 0.32 cm copper. The stopped tracks are listed in Table II, where column 1 is the number of the picture, column 2 is the radius of curvature, column 3 is the sign of the electric charge assuming that the particle moves downward, column 4 indicates whether the visual inspection shows stronger ionization than for an electron track, and column 5 gives the probable nature of the particle. In several cases only a lower limit for the curvature can be given, and therefore the sign of the charge cannot be determined.

With the exception of picture 746 all the particles which pass through the plate have curvatures above 200 cm. According to Table I both electrons and mesotrons of such curvatures are theoretically able to penetrate the plate and no conclusions can be drawn as to their mass.

Picture 746 is reproduced in Fig. 2. A particle traverses the whole length of the chamber through the thinner half of the plate. Its curvature is $\rho=14.7$ cm above the plate, and $\rho=11.7$ cm below it. The visual inspection identifies the track as an electron. Its energies are then 2.6 Mev above and 2.0 Mev below the plate, which gives an energy loss of 0.6 Mev for 0.06 cm of copper. The theoretical energy loss by ionization

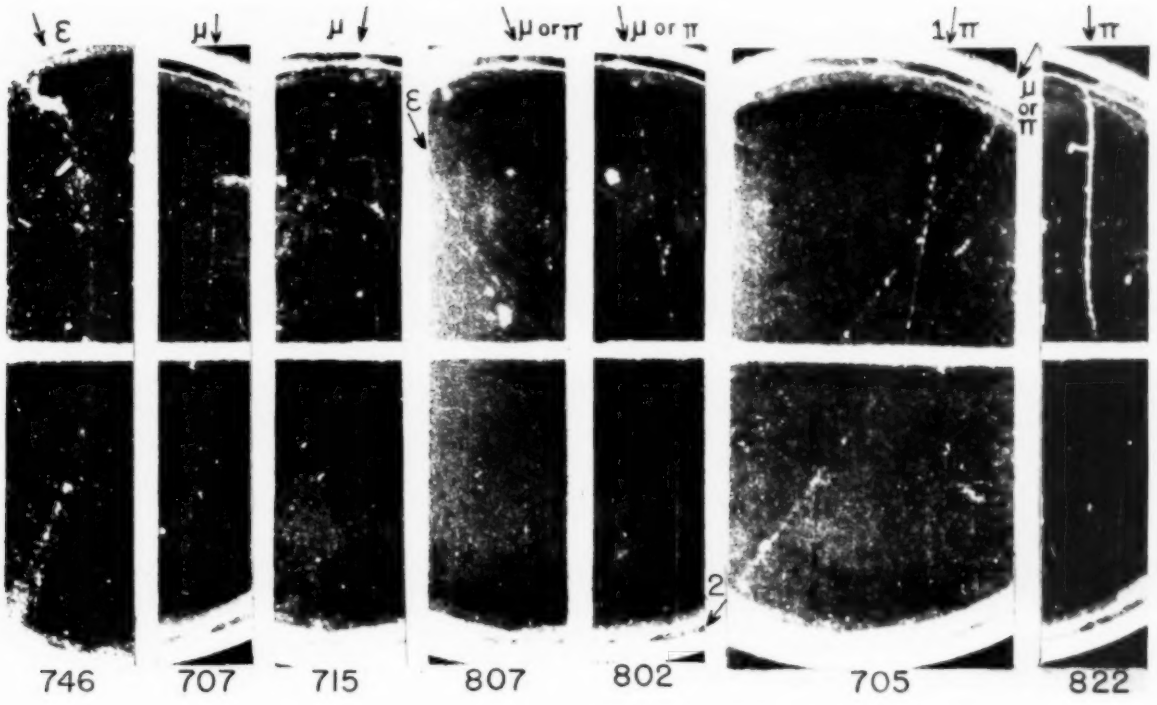

FIG. 2. Cloud-chamber photographs.

and radiation in 0.06 cm copper for an electron of this energy is 0.61 Mev. The agreement between the calculated and the measured values justifies the assumption that the particle is an electron.

The stopped particles, of $\rho<21$ cm and low ionization, are obviously electrons.

As a second group of the stopped particles we may consider those whose radius of curvature, though larger, could exactly be measured, i.e., numbers 755, 707, 715, 754–1 and 2, and of which examples are shown in Fig. 2. Their maximum curvature is 150 cm, a value which is smaller than the critical curvature for mesotrons which is 165 cm and 305 cm, respectively, for the thin and the thick halves of the plate. Thus they can be identified as mesotrons or protons. A differentiation between these possibilities can be made from a consideration of the ionization produced in the gas. Even for the highest curvature of these 5 tracks, which is 150 cm, a mesotron ionizes about 3.5 times as much as a fast electron, whereas a proton ionizes about 30 times as much as a fast electron. Such a strong specific ionization could not be missed in the visual inspection of the photographs. These 5 tracks are thus distinguishable from either electrons or protons, and may be identified as mesotrons.

Of special interest is picture 754 (Fig. 3) with two stopping particles which was recently discussed in a letter to *The Physical Review*.[3] The two particles are stopped in 0.32 cm copper. One has a positive charge with $\rho=75$ cm. The other is negative with $\rho=82$ cm. The curvature measurement, an estimate of the ionization, and the fact that the particles are stopped, give definite evidence for their mesotron nature. They diverge from the same region in the glass ring of the cloud chamber, and may therefore be classified as a mesotron pair. The electron going upwards from the plate is of so low energy that it can hardly be the decay electron from one of the mesotrons.

Examples of photographs of tracks stopped but with radii of curvature for which only a lower limit can be given are shown in Fig. 2,

[3] G. Herzog and W. H. Bostick, Phys. Rev. **58**, 278 (1940). The curvature of the negative mesotron was given wrongly as 45 cm instead of 82 cm. This does not change the conclusions.

FIG. 3. Cloud-chamber photograph showing two particles stopped in 0.32 cm copper.

pictures 807, 802, 822, 705. Because of the large radii of curvature involved it is clear that electrons are excluded. These particles are either mesotrons or protons.

In picture 705 (Fig. 2) track 2 emerges from the plate where 1 enters and has as angle of 30° with the direction of 1. Either track 1 and 2 are produced by the same particle which is scattered at a large angle in the plate, or 1 actually stops in the plate and produces 2 as a secondary. The stereoscopic viewer indicates a higher ionization for 1 than for 2. Unfortunately nothing conclusive can be said from the curvature measurement. Track 1 has $\rho > 180$ cm and track 2 has $\rho > 200$ cm. If in a similar case one could measure the energies precisely and prove that 2 has a momentum larger than 1, this would show that 2 is the decay electron of 1.

Picture 822, Fig. 2: Although gas currents have distorted this track and its energy cannot be given, this picture is very interesting. One may safely estimate that $\rho > 150$ cm. The estimated specific ionization is much larger than that observed for a mesotron of similar momentum. The heavily ionizing secondary particle at the upper end and the big clusters along the track put it in a category with the heavy track reported in the first flight. The new picture, however, gives the additional information that such a particle can be stopped by 0.32 cm copper. We may tentatively identify it with a proton.

It is surprising that out of 5 slow mesotrons and 11 possible mesotrons stopped in the plate only one shows evidence of a disintegration electron, and even in this case the evidence is not conclusive.

Besides the pictures mentioned above, we have good evidence for a total of 28 slow mesotrons on pictures taken above 15,000 feet altitude. The same pictures contain 290 electron-like tracks. We therefore find the number of slow mesotrons to be 9.6 percent of the sum of electrons and fast mesotrons. This agrees well with the value of 9 percent found in the previous flight.

We wish to express our sincere thanks to Dr. A. H. Compton for his continued interest in this work.

Latitude Effect of Cosmic Rays Above 50°N Latitude

PAUL F. GAST AND D. H. LOUGHRIDGE
University of Washington, Seattle, Washington
(Received November 15, 1940)

The latitude effect for cosmic rays above 50° N magnetic latitude has been measured by a continuously operating, ionization type meter mounted on shipboard. From these data the monthly mean temperature coefficient is found to be -0.09 ± 0.03 percent per degree centigrade. When this correction is applied to the data the latitude *vs.* intensity curve is found to be flat within the limits of the probable error over the range of magnetic latitudes from 53° 30′ N (Seattle) to 61° 36′ N (Juneau).

INTRODUCTION

THE latitude effect between about 55° N and 55° S magnetic latitude has been reported by Compton and Turner[1] and by Gill.[2] These observations were carried out by a continuously operating meter mounted on shipboard. North of the region mentioned, observations have been carried out only at isolated stations. Therefore the present investigation was undertaken in order to obtain, at higher latitudes, data of accuracy comparable to those of Compton and Turner and of Gill. It was also hoped that the present investigation would give additional information on the seasonal change in cosmic-ray intensity and on the so-called "atmospheric" latitude effect.

DATA AND RESULTS

The apparatus used has been described in a previous paper.[3] Its location on shipboard enabled the continuous determination of hourly values of the cosmic-ray intensity as the ship traveled over a range of geomagnetic latitude extending from 53° 30′ N geomagnetic latitude (Seattle) to 61° 36′ N (Juneau). A complete round trip was made, on the average, every two weeks. Data were taken over the period from February 1939 to May 1940. A record was kept by the first officer aboard the *Northland*, giving each day the ship's position, reading of ship's aneroid, against which the barometer on the apparatus was checked, maximum and minimum temperature in the meter house since last reading, and shade temperature on deck as well as the time of all observations. Additional checks on the position of the ship were given by the times of arrival and departure at all ports. The hourly values of the cosmic-ray intensity were averaged over six hourly periods and the results reduced to a standard barometer of 30 inches of mercury by using the correction given by Gill[2] for identical apparatus. The mean magnetic latitude of the ship for the six-hour interval was obtained from the data given in the first officer's record.

The data for each 30 minutes of latitude were then averaged by seasons. The results, given in Fig. 1, agree with those of previous investigators[1,2] in showing the greatest intensity in winter and the least intensity during the summer. The results for spring and those for fall (indicated by the crosses) lie intermediate between the two. A yearly mean curve was obtained from the data, and this is shown in the upper, broken line of Fig. 2. One of the outstanding features of all these curves is the decrease in intensity at Juneau amounting to about 2 percent and also the drops at 59° 15′ and 57° 45′. Measurements with a sextant indicate that these drops occur at places where the mountains rise steeply from the water and thus reduce appreciably the solid angle within which the rays can reach the meter.[4] Apart from these sharp drops there is an over-all rise of 0.5 percent from 53° 30′ to 61°, before the

[1] A. H. Compton and R. N. Turner, Phys. Rev. **52**, 799 (1937).
[2] Piara S. Gill, Phys. Rev. **55**, 1151 (1939).
[3] A. H. Compton, E. O. Wollan and R. D. Bennett, Rev. Sci. Inst. **5**, 415 (1934).

[4] An attempt was made to obtain a quantitative check between the actual decreases and those that would be expected, using a $\cos^2 z$ distribution for the cosmic rays, where z is the zenith angle. However, this failed apparently because of the incompleteness of the measurements on the angular elevation of the mountains. There was a definite qualitative check in that increased angles were accompanied by decreased intensities.

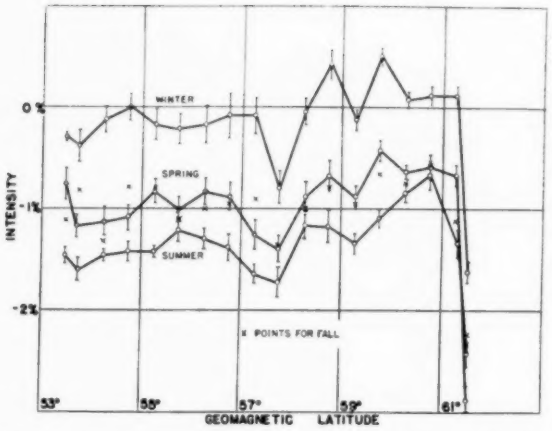

FIG. 1. Seasonal mean cosmic-ray intensities as a function of latitude.

Seattle mean temperature correction has been applied.

I. The temperature effect

Previous investigators[1,2] have ascribed the seasonal variation, as well as the gradual increase of intensity with latitude to the effect of atmospheric temperature on the intensity of the cosmic rays as measured at the earth's surface. In order to determine the effect of temperature on intensity, the daily mean values of intensity were plotted against daily mean temperatures for all the measurements made in Seattle. From this plot a value of -0.11 percent per degree centigrade is obtained for the temperature coefficient. Recently, however, Vallarta and Godart[5] have suggested that a part at least of the seasonal effect may be due to the sun's magnetic field. In order to reduce any contribution which this might make to the true temperature effect the temperature coefficients were computed for each month by computing the mean intensity on the one-way trip having the highest mean temperature for any given month and also the mean intensity on the trip with the lowest mean temperature. The results obtained from these data are listed in Table I. The results for May, 1939, and April, 1940, are undoubtedly affected by the world-wide changes which occurred during these months, as indicated on the apparatus at Huancayo.[6]

It might seem justifiable to eliminate these months from the final result, however; world-wide changes of equal magnitude occurred in April, 1939, and evidently were instrumental in producing the rather large negative value for that month, and also changes of smaller magnitude occurred in other months. Thus it appears that there is no valid reason for excluding some of the above months while preferring others, and the value -0.09 ± 0.03 has been used in making all temperature corrections. This value is identical with that recently given by Hess[7] from data collected during a period of five years on the Hafelekar, but it is somewhat smaller than the value (-0.13) given by Gill for Vancouver and is considerably smaller than the value (-0.22) of Compton and Turner at the same place. It is to be noted that the number of separate readings entering into the computation is considerably greater in the case of the present work than in the results of Compton and Turner and of Gill, but that it is, in turn, considerably less than that of Hess. The fact that the coefficient is slightly higher when computed on the intensity *versus* temperature basis may be an indication of a seasonal effect other than that caused by temperature; however, the difference is not greater than the statistical error and no definite conclusions can be drawn. The mean obtained by omitting the two positive values is also given for comparison.

II. The latitude effect

The upper curve in Fig. 2, which gives the yearly mean intensity as a function of latitude has an over-all upward slope which is about half of that reported by Compton and Turner[1] in the region above the knee but which agrees well with the more recent results of Gill.[2] When a temperature correction based on the coefficient given above is applied the lower curve in Fig. 2 results. The intensity in the region from 55° to 57° seems to fall below that at Seattle, whereas the intensity 59° to 61° is, apart from the fluctuations mentioned before, the same as that at Seattle within the limits of the probable error. No conclusions for the regions from 57° to 59° and above 61° can be drawn because of the

[5] M. S. Vallarta and O. Godart, Rev. Mod. Phys. **11**, 180 (1939).

[6] Private communication from A. H. Compton.

[7] Victor Francis Hess, Phys. Rev. **57**, 781 (1940).

"horizon effect." The probable errors in intensity as computed from the statistical fluctuations vary from 0.05 percent to 0.08 percent for the uncorrected curve, and from 0.05 percent to 0.28 percent for the corrected curve. The greater part of the error in the corrected curve is due to the probable error in the temperature coefficient which also explains the progressive increase in error with latitude which is apparent on the lower curve. It is improbable that the slight decrease between 55° and 57° is a real one and may possibly be caused by a "horizon effect" of smaller magnitude than that producing the decreases at 57° and above 61°. Our conclusions, then, agree with those of Gill that there is no evidence of a geomagnetic latitude effect beyond the knee.

Nature of the Plateau

According to the theory of Lemaître and Vallarta,[8] the cosmic-ray intensity ought to increase monotonically with latitude, the exact character of the increase depending on the energy distribution of the primary rays. The fact that no increase occurs beyond a certain latitude has been attributed by various authors to one or more of the following conditions: (1) The energy spectrum of the primary rays is such that there are very few or no rays with energy less than a certain critical value represented by the threshold energy for the latitude at which the knee occurs. (2) The knee occurs for that minimum energy of the secondary mesotrons which enables them to penetrate the barrier of the earth's atmosphere.[2] (3) Particles below a certain minimum energy are prevented from reaching the earth at all by the action of the sun's magnetic field.[9]

The improbable nature of the energy distribution required to satisfy the first viewpoint is a considerable objection. Against the second viewpoint, Vallarta and Godart[5] have pointed out that the variation in the position of the knee with increasing altitude is not in complete agreement with this hypothesis. In confirmation of this view the fact that the magnetic storm of March 24, 1940, produced a decrease in intensity in the region north of the knee[10] can be taken as an argument in favor of the third view, since the effect of a change in the earth's magnetic field in this region would be merely to shift the latitude of the knee. Thus the "cut-off" appears to be caused, at least in part, by a magnetic effect, external to the earth, which experiences changes at the time of magnetic storms.

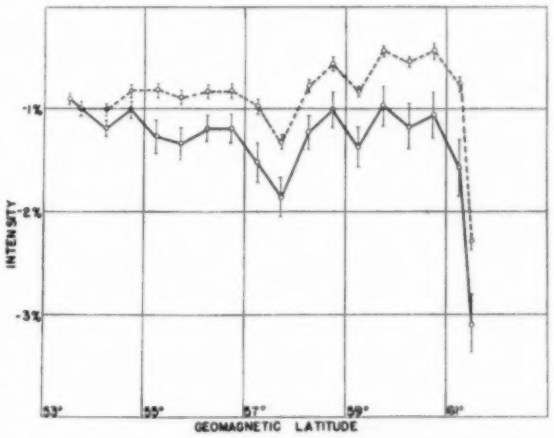

Fig. 2. Upper curve gives yearly mean cosmic-ray intensity as function of latitude, no temperature correction. Lower curve gives same results reduced to Seattle mean temperature as standard.

Table I. *Temperature coefficients for cosmic-ray intensity.*

Month	Coef. in %	Month	Coef. in %
March, 1939	−0.27	November, 1939	−0.34
April	−0.23	December	−0.07
May	+0.25	January, 1940	−0.18
June	−0.11	February	−0.11
July	−0.04	March	−0.14
September	−0.04	April	+0.23
October	−0.15		
Mean			−0.09±0.03
Mean without May, 1939 and April, 1940,			−0.15±0.02

In conclusion, we wish to express our sincere appreciation to Dr. Arthur H. Compton for making available the apparatus and for helpful discussion of the results. Also, we are indebted to the Northland Transportation Company for the use of the space aboard their ship and to Mr. B. W. Joyce, First Officer of the *M.S. Northland* for careful attention to the apparatus.

[8] G. Lemaître and M. S. Vallarta, Phys. Rev. **43**, 87 (1933).

[9] M. S. Vallarta, Nature **139**, 839 (1937).

[10] D. H. Loughridge and Paul F. Gast, Phys. Rev. **57**, 938 (1940).

On the Scattering of Mesons of Spin $\frac{1}{2}\hbar$ by Atomic Nuclei

R. E. MARSHAK AND V. F. WEISSKOPF
University of Rochester, Rochester, New York

(Received November 23, 1940)

The non-electric scattering of charged mesons by protons and neutrons is calculated as a first-order effect in the heavy electron pair theory of nuclear forces. The latter theory regards the mesons as heavy electrons, that is, as particles with spin $\hbar/2$, obeying the Dirac equation and differing from usual electrons only in their rest mass μ. An upper limit for the scattering cross section of mesons by nuclear particles is derived; it is found that the cross section is less than 4×10^{-30} cm^2 for mesons of energy $E=\mu c^2$ and less than 1.6×10^{-29} for $E=3\mu c^2$. These values are about 1000 times smaller than the corresponding cross sections obtained on the basis of meson theories of nuclear forces which ascribe to the meson a spin $\hbar$. In contrast to the latter theories the values obtained in the present paper are in agreement with the upper limits of the scattering cross section found experimentally by Wilson and others. For meson energies large compared to the rest energy of the proton or neutron, the scattering cross section increases linearly with the energy; it first attains the value 10^{-26} cm^2 for meson energies of the order of 10^{11} ev.

§1. Introduction and Discussion of Results

THE scattering of mesons by neutrons or protons has recently been investigated both experimentally and theoretically. The experiments by Blackett and Wilson[1] have shown that the scattering of mesons by nuclei consists mostly of Rutherford scattering due to the Coulomb forces between the electric charges of the nucleus and of the meson. More recently, J. G. Wilson[1a] observed the scattering of mesons by metal plates in a cloud chamber and found that only one track out of 185 showed a scattering angle appreciably outside the range expected from multiple Rutherford scattering; this particular meson had an energy of 1.6×10^9 ev. Wilson also quotes four other tracks of particles with still higher energy, previously measured by Wilson and by Brode and Starr, and which could not be attributed to Rutherford scattering. The cross section for this large angle scattering (due to short range non-electric forces) computed from the three sets of experiments is of the order of 10^{-28} cm^2 per proton. The possibility that the tracks were due to protons scattered by the specifically nuclear forces cannot be excluded. Thus the available experimental material indicates that the cross section of meson scattering by nuclear particles is at most 10^{-28} cm^2 in the energy region: 2×10^8 to 2×10^9 ev.

This result, however, is in striking contrast to the theoretical calculations carried out by Heitler,[2] Bhabha,[3] and Wilson[4] on the basis of the current meson theories of nuclear forces. These theories regard the mesons as particles with spin h obeying Bose statistics, and interacting with nuclear particles (proton, neutron) in a way similar to the interaction between charged particles and light quanta. However, in order to describe the actual nuclear forces by means of a meson field it was necessary (a) to introduce an additional interaction of a kind that does not have its analog in electrodynamics—depending on the spin of the nuclear particles, (b) to introduce neutral mesons besides charged mesons ("symmetric" theory) or even to ascribe the nuclear forces entirely to the virtual emission and reabsorption of neutral mesons alone ("neutral" theory).

These theories (with the exception of Bethe's neutral theory which of course has nothing to say about charged mesons) give rise to a scattering of charged mesons by nuclear particles in virtue of a second-order process, e.g.:

$$N+m_1^{(+)}\rightarrow P\rightarrow N+m_2^{(+)}.$$

Here N stands for neutron, P for proton, $m_{1,2}^{(+)}$ designates a positive meson in two states 1 and 2, respectively. The cross section of this process was first calculated by Heitler[2] with the result

$$\sigma=\frac{4\pi}{3}(g_1^2+2g_2^2)^2\frac{p^4}{E^2\mu^4c^4}. \qquad (1)$$

[1] P. M. S. Blackett and J. G. Wilson, Proc. Roy. Soc. **165**, 209 (1938).
[1a] J. G. Wilson, Proc. Roy. Soc. **174**, 73 (1940).
[2] W. Heitler, Proc. Roy. Soc. **166**, 529 (1938).
[3] H. J. Bhabha, Proc. Roy. Soc. **166**, 501 (1938).
[4] A. H. Wilson, Proc. Camb. Phil. Soc. **36**, 363 (1940).

TABLE I. *Values for the cross section computed from Eqs. (4), (5) and (6) for three characteristic energies.*

Energy (Mev)	89	267	1780
Energy (μc^2)	1	3	20
σ (cm^2) for mesons of spin $\frac{1}{2}$	$<4\times10^{-30}$	$<1.6\times10^{-29}$	$<5.5\times10^{-28}$
σ (cm^2) for mesons of spin 1	1.5×10^{-27}	2×10^{-25}	2×10^{-24}

The quantities g_1 and g_2 are the two factors determining the meson-nuclear particle interaction, both having the dimension of a charge, μ is the meson mass ($\sim$175 electron masses), p its momentum, E its energy; the nuclear particle has been assumed infinitely heavy. The calculations of Wilson[4] taking into account the finite mass of the nuclear particle give in addition to (1) a term proportional to p^2 and a term which does not vanish in the limit of zero p; namely,

$$\sigma_0=\frac{12\pi M^2}{(\mu+M)^2}\frac{(g_1+g_2)^4}{(\mu+2M)^2c^4}. \tag{2}$$

M is the mass of the proton or neutron. The factors g_1, g_2 have been determined by identifying the nuclear forces derived from the meson field with the observed nuclear forces and it is found that $g_{1,2}^2/hc\approx0.16$ and that the order of magnitude does not depend on the particular theory used. The numerical values of the scattering cross section for three characteristic energies can then be calculated and are listed in Table I.

Several authors have tried to remove this large discrepancy with experiment either by introducing new quantum states of the nuclear particle with higher multiples of electric charge or by investigating the possibility that higher approximations would reduce the cross section. The first hypothesis[5] reduces the cross section by introducing new intermediate states which give rise to interference terms of the same sort which occur in the expression for the scattering of neutral mesons by nuclear particles. As regards the second suggestion, Wentzel[6] has shown that the same large cross section $2\pi(\hbar/\mu c)^2$ is obtained in an expansion of the meson-nuclear interaction in powers of $(1/g)$—which represents the limit of strong interaction. It seems therefore improbable that a more exact approximation method would give rise to smaller values for the cross section.

[5] W. Heitler, Nature **175**, 69 (1940).
[6] G. Wentzel, Helv. Phys. Acta **13**, 269 (1940).

In view of these serious difficulties we have tried to calculate the scattering on the basis of a theory of mesons with spin $\frac{1}{2}$ and obeying Fermi statistics. The mesons are supposed to differ from ordinary electrons by the value of the rest mass alone. Thus they are to be described by the Dirac equation, and by a "hole" theory to account for the two signs of charge. We use the term "heavy electrons" for these hypothetical particles, which tentatively may be identified with the observed mesons in cosmic rays.

The interaction between heavy electrons and nuclear particles obviously must be different from the interaction in the theories of the Bose meson. In the present theory the interaction gives rise to a change of state of a heavy electron under the influence of a nuclear particle. This is equivalent to the creation of a heavy electron pair if the change of state consists of a transition from a negative to a positive energy state. It has been shown by one of us[7] that nuclear forces having a suitable spin and spatial dependence can be derived from an interaction of the form:

$$G(\Psi^*\sigma^{(n)}\Psi)(\psi^*\beta^{(e)}\sigma^{(e)}\psi). \tag{3}$$

In (3) Ψ and ψ are the wave functions, $\sigma^{(n)}$ and $\beta^{(e)}\sigma^{(e)}$ the well-known Dirac operators of the nuclear particle and the heavy electron, respectively. The interaction constant G can be computed from the nuclear forces. An upper bound for G is derived in §3 of this paper, namely

$$G<7.8\times10^{-40}\ \text{Mev cm}^3. \tag{4}$$

It is likely that G is considerably smaller.

The scattering of a heavy electron by a nuclear particle is then a first-order process in this theory. The cross section is calculated in §2 and the result for heavy electrons whose energies are small compared to Mc^2 (M is the proton mass) is:

$$\sigma=\frac{3}{2\pi}\frac{G^2}{\hbar^4c^4}(E^2+\mu^2c^4). \tag{5}$$

The cross section for higher energies ($E\gg\mu c^2$) is given by ($E_0=Mc^2$):

$$\sigma=\frac{G^2}{\pi\hbar^4c^4}\left[\frac{EE_0(E+\frac{1}{4}E_0)}{E+\frac{1}{2}E_0}-\tfrac{1}{4}E_0^2\log\frac{2E+E_0}{E_0}\right]. \tag{6}$$

[7] R. E. Marshak, Phys. Rev. **57**, 1101 (1940); this paper will be referred to as I.

The values for the cross section computed on the basis of (4), (5) and (6) for three characteristic energies are given in Table I. They are much smaller than the cross sections calculated using the theories of the meson with spin one. The values quoted are upper bounds, since the actual G is certainly smaller than the value (4) used here. The results are, therefore, smaller than the observed upper limit for the cross section.

The cross section increases for high energies ($E \gg Mc^2$) with the first power of E, just as the corresponding expression for the scattering of mesons with spin 1. In our theory the value 10^{-26} cm^2 is first attained for energies $E \approx 10^{11}$ ev and is therefore not in conflict with any experiment performed thus far. There is, however, reason to doubt the validity of (6) for extremely high energies. It is known that the evaluation of the nuclear forces necessitates a "cut-off" of the potential energy between nuclear particles at small distances. Whatever the reason for this "cut-off" is—it may be caused either by the effect of higher approximations or by the breakdown of the interaction (3) at high energies—it represents a strong argument against the application of our theory to processes involving high energy heavy electrons.

The result that the cross section for the scattering of heavy electrons of spin $\frac{1}{2}$ is so much smaller than of mesons of spin 1 can be traced to the circumstance that the present theory has a much smaller interaction parameter. If we express G by a dimensionless number,

$$G = \Gamma \mu c^2 (h/\mu c)^3, \tag{7}$$

the value of Γ is 0.95×10^{-2}, which is 40 times smaller than the corresponding dimensionless constant $g/(hc)^{\frac{1}{2}}$ of the meson theory. This difference is due to the fact that the nuclear forces are represented by a field of two heavy electrons rather than one meson. Because of the larger statistical factors involved, a field of heavy electron pairs gives rise to relatively stronger nuclear forces than a field of single Bose mesons if the interaction parameters are equated to each other.

The calculations presented here show that a theory which describes the nuclear forces as arising from the emission and reabsorption of pairs of "mesons" of spin $h/2$ is quite compatible with the experiments on the scattering of mesons by nuclei. It must be remembered, however, that the above result is derived by using the first approximation only of the perturbation method. Because of the divergences involved in the higher approximations, it is difficult to decide whether the same conclusion would be borne out by a more rigorous treatment.

§2. The Calculation of the Scattering Cross Section

The differential cross section $d\sigma$ for the scattering of a heavy electron into the solid angle $d\Omega$ by a free neutron or proton at rest is given by the well-known formula:

$$d\sigma = (2\pi/hv) |V_{ab}|^2 \rho d\Omega. \tag{8}$$

In Eq. (8) v is the velocity of the incident heavy electron, V_{ab} is the matrix element of the "tensor" interaction V between the heavy electron and the nuclear particle for the scattering of the meson; ρ is the density of final states of the heavy electron per unit volume, per unit energy and per unit solid angle. The process is of first order. Since we wish to examine the behavior of the scattering cross section for very energetic heavy electrons, we use the relativistic expressions for both nuclear particles and heavy electrons. At the same time the recoil of the nuclear particle and the consequent change of momentum of the heavy electron is taken into account. We may write[8] for V_{ab}:

$$V_{ab} = G \int d\tau^{(e)} \int d\tau^{(n)} \{ (\Psi_Q^* \beta^{(n)} \sigma^{(n)} \Psi_0)(\psi_q^* \beta^{(e)} \sigma^{(e)} \psi_p) + (\Psi_Q^* \beta^{(n)} \alpha^{(n)} \Psi_0)(\psi_q^* \beta^{(e)} \alpha^{(e)} \psi_p) \}. \tag{9}$$

In (9) the quantities Ψ_0, Ψ_Q are, respectively, the initial and final wave functions of the nuclear particle while ψ_p, ψ_q are the corresponding wave functions of the heavy electron; these wave functions are normalized per unit volume. Also $\sigma^{(n)}$, $\sigma^{(e)}$ are the Dirac four-component spin operators of the nuclear particle and heavy

[8] In I the nonrelativistic approximation (3) was used; this sufficed for the calculation of nuclear forces. Eq. (9) is the corresponding relativistic expression; cf. H. A. Bethe and R. F. Bacher, Rev. Mod. Phys. **8**, 82 (1936).

electron, respectively, whereas $\beta^{(n)}$, $\beta^{(e)}$; $\alpha^{(n)}$, $\alpha^{(e)}$ are the well-known Dirac operators. In the initial state a the nuclear particle is at rest so that its energy is[9] $E_0=M/\mu$, while the heavy electron has momentum p and energy $E_i=(p^2+1)^{\frac{1}{2}}$; in the final state b the heavy electron has momentum q and energy $E_f=(q^2+1)^{\frac{1}{2}}$, the nuclear particle acquiring momentum $\mathbf{Q}=\mathbf{p}-\mathbf{q}$ and energy $E=E_0+E_f-E_i=(Q^2+(M/\mu)^2)^{\frac{1}{2}}$. In the notation used the density of states is given by:

$$\rho=qE_f/8\pi^3c^2\hbar^3. \tag{10}$$

In evaluating $|V_{ab}|^2$ we must average over the spins of both heavy electron and nuclear particle in the state a and sum over the spins of both particles in the state b. These operations and integration over the coordinate space of both particles leads to

$$\begin{aligned}|V_{ab}|^2=\frac{G^2}{4}\sum_{k,l=1}^{3}\Bigg[&\frac{Spur}{4}\left\{\beta^{(e)}\sigma_k{}^{(e)}\left(1+\frac{\boldsymbol{\alpha}^{(e)}\cdot\mathbf{p}+\beta^{(e)}}{E_i}\right)\beta^{(e)}\sigma_l{}^{(e)}\left(1+\frac{\boldsymbol{\alpha}^{(e)}\cdot\mathbf{q}+\beta^{(e)}}{E_f}\right)\right\}\\&\cdot\frac{Spur}{4}\left\{\beta^{(n)}\sigma_k{}^{(n)}(1+\beta^{(n)})\beta^{(n)}\sigma_l{}^{(n)}\left(1+\frac{\boldsymbol{\alpha}^{(n)}\cdot\mathbf{Q}+\beta^{(n)}(M/\mu)}{E}\right)\right\}\\&+\frac{Spur}{4}\left\{\beta^{(e)}\alpha_k{}^{(e)}\left(1+\frac{\boldsymbol{\alpha}^{(e)}\cdot\mathbf{p}+\beta^{(e)}}{E_i}\right)\beta^{(e)}\alpha_l{}^{(e)}\left(1+\frac{\boldsymbol{\alpha}^{(e)}\cdot\mathbf{q}+\beta^{(e)}}{E_f}\right)\right\}\\&\cdot\frac{Spur}{4}\left\{\beta^{(n)}\alpha_k{}^{(n)}(1+\beta^{(n)})\beta^{(n)}\alpha_l{}^{(n)}\left(1+\frac{\boldsymbol{\alpha}^{(n)}\cdot\mathbf{Q}+\beta^{(n)}(M/\mu)}{E}\right)\right\}\Bigg].\end{aligned} \tag{11}$$

The cross terms which arise from (9) do not contribute to $|V_{ab}|^2$. Evaluation of (11) by means of the usual rules for taking products of Dirac operators gives:

$$\begin{aligned}|V_{ab}|^2=\tfrac{3}{4}G^2\Bigg\{&\left(1+\frac{1+\frac{1}{3}\mathbf{p}\cdot\mathbf{q}}{(p^2+1)^{\frac{1}{2}}(q^2+1)^{\frac{1}{2}}}\right)\left(1+\frac{M/\mu}{(Q^2+(M/\mu)^2)^{\frac{1}{2}}}\right)\\&+\left(1-\frac{1-\frac{1}{3}\mathbf{p}\cdot\mathbf{q}}{(p^2+1)^{\frac{1}{2}}(q^2+1)^{\frac{1}{2}}}\right)\left(1-\frac{M/\mu}{(Q^2+(M/\mu)^2)^{\frac{1}{2}}}\right)\Bigg\}.\end{aligned} \tag{12}$$

Of course, the second term in brackets which arises from the Dirac current operator, vanishes in the nonrelativistic approximation for the nuclear particle, i.e., in the limit $M\to\infty$. The first term in brackets, arising from the spin operators, does not vanish in the limit $M\to\infty$. We finally obtain the differential cross section $d\sigma$ as a function of the angle of scattering Θ by putting (12) and (10) into (8) and by observing that $v=cp/(p^2+1)^{\frac{1}{2}}$:

$$\begin{aligned}d\sigma=\frac{3\mu^2G^2}{8\pi^2\hbar^4}\Bigg[&(p^2+1)^{\frac{1}{2}}(q^2+1)^{\frac{1}{2}}+\frac{pq}{3}\cos\Theta\\&+\frac{M/\mu}{(p^2+q^2-2pq\cos\Theta+(M/\mu)^2)^{\frac{1}{2}}}\Bigg]\frac{q}{p}d\Omega.\end{aligned} \tag{13}$$

[9] Just as in I, the unit of energy is μc^2, of momentum μc and of length $\hbar/\mu c$.

The momenta p and q are still measured in units of μc. When p is small compared to M/μ then $q\approx p$ for all angles Θ and we get for the total cross section:

$$\sigma=\frac{3\mu^2G^2}{2\pi\hbar^4}(p^2+2)\quad\text{for}\quad p\ll M/\mu. \tag{14}$$

The cross section is therefore finite in the limit of zero velocity. The integration over Θ can also be performed for $p\gg1$; in this case the rest mass of the heavy electron can be neglected and in virtue of the conservation laws of momentum and energy it follows that

$$q=p(M/\mu)/((M/\mu)+p(1-\cos\Theta)).$$

Putting this value for q into (13) leads to an expression which can be integrated exactly with

the result:

$$\sigma=\frac{1}{\pi}\frac{G^2\mu^2}{\hbar^4}\left[\frac{pE_0(p+\frac{1}{4}E_0)}{p+\frac{1}{2}E_0}-\frac{E_0^2}{4}\log\frac{2p+E_0}{E_0}\right]. \quad (15)$$

For energies large compared to M/μ, Eq. (15) reduces to

$$\sigma=\frac{1}{\pi}\frac{G^2\mu^2}{\hbar^4}pE_0. \quad (16)$$

It is seen from (16) that under extreme relativistic conditions the total cross section for the non-electric scattering of heavy electrons by nuclear particles increases linearly with the incident energy of the heavy electron.

§3. The Determination of the Interaction Constant

We follow Bethe's procedure[10] in order to evaluate the interaction constant G from the nuclear forces. Since the experimental material only provides an upper value for the scattering cross section, it will suffice for our purposes to find an upper bound for G; the actual value may be several times smaller.

The strong singularity of the nuclear forces which results from the heavy electron pair theory necessitates a "cut-off" at small distances. The "cut-off" may be made in different ways; in the following we use the "zero cut-off" method which assumes the nuclear potential to vanish within a certain "cut-off" distance r_0. In this way the constant G will be overestimated since we may safely assume that the actual nuclear force does not vanish completely for small distances. There are now two magnitudes to be determined: the constant G and the "cut-off" distance r_0. However, values for G and r_0 may be obtained by making use of the singlet scattering of neutrons by protons and of the fact that the triplet ground state of the deuteron is lower than the singlet state.

The radial part $u(r)$ of the wave function describing the scattering of a neutron of zero energy by a proton is given by the equation:

$$(d^2u(r))/(dr^2)=-V(r)u(r). \quad (17)$$

Here r is measured in units of $\hbar/\mu c$ and $V(r)$ in units of $\mu^2c^4/Mc^2=8.7$ Mev. $V(r)$ is the singlet potential given in I (cf. Eq. (8)):

$$V(r)=aF(r), \quad a=16\pi^3G^2, \quad (18a)$$

with

$$\begin{cases} F(r)=\left(\dfrac{K_0(2r)}{r^3}+\dfrac{4K_1(2r)}{r^2}+\dfrac{K_1(2r)}{r^1}\right) \\ \qquad\qquad\qquad\qquad \text{for } r>r_0, \\ F(r)=0 \qquad\qquad\qquad\qquad \text{for } r<r_0. \end{cases} \quad (18b)$$

In (18) $K_\nu(z)$ is a Bessel function of order ν and related to the well-known Hankel function of the first kind:

$$K_\nu(z)=\frac{\pi}{2}ie^{\pi i\nu/2}H_\nu^{(1)}(iz).$$

Bethe[10] finds from the observed neutron-proton scattering cross section that, for large r, $u(r)$ is given by

$$u=1+0.1r. \quad (19)$$

The constant a in (18a) is to be adjusted so that $u(0)=0$. It is possible to get an upper limit for a by replacing $F(r)$ by another function $F_0(r)$ for which $F(r)\geqslant F_0(r)$ for all values of r. If $u(0)=0$ for the potential $V(r)=b\cdot F_0(r)$, b is an upper limit to the constant a. We have chosen for $F_0(r)$ the function $F_0(r)=Ce^{-\alpha r}$ which coincides in value and first derivative with $F(r)$ at the "cut-off" point; i.e.,

$$F(r_0)=F_0(r_0), \quad F'(r_0)=F_0'(r_0);$$

these two equations determine C and α. The differential equation (17) is now soluble and we obtain with the potential $V=bF_0(r)$ the solution:

$$\begin{cases} u=J_0(se^{-\alpha r/2})-0.1\left(\dfrac{\pi}{\alpha}N_0(se^{-\alpha r/2})-\dfrac{2}{\alpha}\log\dfrac{\gamma s}{2}\right) \\ \qquad\qquad\qquad\qquad \text{for } r>r_0, \\ u=Kr \qquad\qquad\qquad\qquad \text{for } r<r_0. \end{cases} \quad (20)$$

In (20) $s=2(bC)^{\frac{1}{2}}/\alpha$, J_0, N_0 are Bessel functions and γ is the Bernouilli number. The quantity K should be adjusted so that u and du/dr are continuous at $r=r_0$. This is only possible for a suitable value of s, the lowest one of which finally determines b. Several values of b for different "cut-off" radii r_0 are listed in Table II.

[10] H. A. Bethe, Phys. Rev. **57**, 390 (1940).

TABLE II. *Values of b for different "cut-off" radii r_0.*

r_0	0.2	0.4	0.6	0.8
b	0.041	0.27	0.56	0.90

TABLE III. *Values of the distance p for several values of a.*

a	1.5	0.75	0.35	0.12	0.04
p	0.63	0.56	0.50	0.39	0.29

At this point we make use of the fact that the triplet state of the deuteron lies lower than the singlet state. The triplet state is given by two simultaneous differential equations:

$$\begin{cases} (d^2\chi)/(dr^2)-\epsilon\chi = A\chi - D\varphi, \\ (d^2\varphi)/(dr^2)-\epsilon\varphi = -D\chi + C\varphi. \end{cases} \tag{21}$$

ϵ is the energy of the triplet state of the deuteron. In (21) χ is the S wave function and φ the D wave function; also we have:

$$A=\frac{a}{3}F(r); \quad C=\frac{1}{3}aF(r)+\frac{6}{r^2}+\frac{2a}{3}G(r);$$

$$D=\frac{2^{\frac{1}{2}}}{3}aG(r);$$

$$G(r)=\begin{cases} \left(\dfrac{5K_0(2r)}{r^3}+\dfrac{2K_1(2r)}{r^2}+\dfrac{5K_1(2r)}{r^1}\right) & \text{for } r>r_0, \\ 0 & \text{for } r<r_0. \end{cases}$$

According to Bethe[10] these equations are almost equivalent to a single Schrödinger equation with the potential:

$$W(r)=\tfrac{1}{2}(A+C)\pm[\tfrac{1}{4}(A-C)^2+D^2]^{\frac{1}{2}}$$

$$=\frac{a}{3}F(r)+\frac{3}{r^2}+aG(r)\pm\left[\left(aG+\frac{1}{r^2}\right)^2+\frac{8}{r^4}\right]^{\frac{1}{2}}. \tag{22}$$

The lower sign holds for the ground state of the deuteron, and should therefore lead to an eigenvalue lower than the lowest singlet state given by Eq. (17). This state of affairs, however, would be impossible if $[W(r)-V(r)]$ were positive or zero for all values of r. It is easily seen that $W-V\geqslant 0$ for all values of r greater than a certain value p. The distance p is a function of a and several values of $p(a)$ are tabulated in Table III. In order to depress the triplet state below the singlet state, the cut-off radius r_0 must be smaller than p, thereby providing a region in which $W-V$ is negative. We therefore obtain an upper limit for r_0 by the condition $r_0<p$.[11] Let us now compare $p(a)$, which is a monotonically increasing function of a, and $b(r_0)$ which is an upper bound of a and determined in the preceding paragraph; $b(r_0)$ is also a monotonically increasing function of r_0. Supposing there is a value b^* of the second function belonging to a value r_0^*, so that r_0^* in turn is equal to the first function $p(a)$ for $a=b^*$; this is actually the case for $b^*=0.46$. The following inequalities are then valid:

$$b^*>b(r_0)>a.$$

Here r_0 is the actual cutting off radius ($r_0<r_0^*$) and a the actual value of the force constant. Thus b^* is an upper bound of a.

The relation between a and G is given in (18) and we get:

$$G^2=a/(16\pi^3)<b^*/(16\pi^3).$$

Therefore after introducing other units, we have:[12]

$$G^2<0.9\times10^{-4}\mu^2c^4(\hbar/(\mu c))^6. \tag{23}$$

[11] We have checked this procedure by applying it to Bethe's theory; according to Bethe the correct value of a is 1.66 for $r_0=0.3$. For this value of a we find $p=0.8$.

[12] It is interesting to note that one gets a value of G^2 close to (23) by the following approximate method: one takes the experimental proton potential from the paper of Hoisington, Share and Breit (cf. Phys. Rev. **56**, 884 (1939)), i.e., $J(r)=90mc^2e^{-r/\alpha}/(r/\alpha)$, $(\alpha=\hbar/2\mu c)$ and sets it equal to the singlet potential (18) at $r=\alpha$; one finds $G^2=1.6\times10^{-5}\mu^2c^4(\hbar/\mu c)^6$. If one sets the two equal at $r=2\alpha$, one finds $G^2=8.5\times10^{-5}\mu^2c^4(\hbar/\mu c)^6$.

The Density Distribution in the Steady-State Diffusion of Neutrons

E. A. UEHLING
Department of Physics, University of Washington, Seattle, Washington
(Received November 2, 1940)

By carrying the method of Laplace transformations and inversions to its ultimate conclusion, an expression in closed form for the spatial distribution in density of diffusing particles is obtained. This derivation is valid both for the case of incident currents of particles upon the face of a half-infinite medium and for the case of source distributions within that medium. The final expressions are given in terms of a transcendental function and its zeros together with a definite integral, all of which require numerical evaluation. Such numerical calculations have not been performed, since the problem is principally of theoretical interest in the sense that these methods yield for the first time an exact nonseries solution of a well-known, and in this respect, unsolved integral equation. From an experimental point of view it is the ratio of activities at different points within the medium rather than the ratio of particle densities which is of principal interest. These quantities are not the same, and some results for the former based on the exact theory have already been given.

INTRODUCTION

THE problem of neutron diffusion under steady-state conditions has been solved for the emergent distribution from a medium, and the results have been published in previous communications.[1,2] The study of this problem has now been carried one step further in order to find exact expressions for the particle density within the medium in which the diffusion occurs.

The idealizations employed in the statement of the problem are discussed fully in the previous papers.[1,2] We may mention briefly that the diffusion occurs under steady-state conditions within a half-infinite, isotropic, homogeneous medium having a plane boundary face, that the diffusing particles interact isotropically and without the exchange of energy with particles of the medium, and that there are no mutual interactions. Furthermore, the incident current is taken to have azimuthal symmetry about the perpendicular to the boundary face, and to vary only in polar angle, whereas the source distribution is taken isotropic and to vary only in the direction perpendicular to the boundary plane. Under these circumstances the particle velocity enters only parametrically, and the number of independent variables is reduced to two, (x, z), where x is a spatial coordinate measured into the medium and positively to the right from the boundary plane as origin, and $z=\cos\theta$ is the direction cosine of the particle velocity with respect to the positive x axis. The distribution function $f(x, z)$ is taken to represent the density of particles at x per unit solid angle in velocity with the velocity vector lying at z. The emergent distribution of particles from the medium is then represented by $f(0, z)$ with $-1\leq z<0$.

THE EMERGENT DISTRIBUTION

It has been shown[1] that the emergent distribution is given by the value on the real interval $z=(-1, 0)$ of the function

$$f(0,z)=\frac{n\zeta}{\zeta-z}\frac{1}{p_1(z)p_2(\zeta)}\begin{matrix}R(z)<0\\R(\zeta)\geq 0\end{matrix} \tag{1}$$

which is analytic over the entire negative half of the z plane. This result is valid for a particular form of incident current and source distribution, but the validity of superpositions renders the solution for other forms readily available. For a source distribution of the form

$$q(x)=qe^{-x/l\zeta}\quad R(\zeta)\geq 0$$

the constant n is given by

$$n=ql/v, \tag{1a}$$

where l is the total m.f.p. of diffusing particles. For an incident current of the form

$$\begin{matrix}f_0(z)=f\delta(z-\zeta) & 0<\zeta\leq 1,\\ n=f\sigma & \sigma=l/2l_z,\end{matrix} \tag{1b}$$

[1] E. A. Schuchard and E. A. Uehling, Phys. Rev. **58**, 611–623 (1940). Further references to this paper will be to SU.
[2] O. Halpern, R. Lueneburg and O. Clark, Phys. Rev. **53**, 173–83 (1938).

when l_s is the m.f.p. for scattering, which together with the capture m.f.p. l_c contributes to l according to the relation $1/l=1/l_s+1/l_c$. This equivalence of source and incident current distributions insofar as the emergent current is concerned and for values of ζ in the interval $(0, 1)$ has been discussed in SU. The earlier papers[1,2] may be consulted also for a discussion of the functions p_1 and p_2. It will be sufficient for our purpose here to mention only that

$$\left.\begin{aligned} \ln p_1(z) &= -\frac{z}{\pi}\int_0^\infty dt \frac{\ln p(it)}{z^2+t^2} \quad R(z)<0 \\ \ln p_2(z) &= \frac{z}{\pi}\int_0^\infty dt \frac{\ln p(it)}{z^2+t^2} \quad R(z)>0 \end{aligned}\right\}, \tag{2}$$

$$\left.\begin{aligned} p_1(z) &= p_2(-z) \\ p(z) &= p_1(z)p_2(z) = 1+\sigma z\int_{-1}^{1}\frac{d\alpha}{\alpha-z} \end{aligned}\right\}, \tag{3}$$

and that $p_1(z)$ has the branch point and zero of $p(z)$ in the positive half-plane, while $p_2(z)$ has the branch point and zero of $p(z)$ in the negative half-plane. These branch points lie at ± 1, and the zeros lie at $\pm z_0$ where

$$p(z_0) = 1+\sigma z_0\int_{-1}^{1}\frac{d\alpha}{\alpha-z_0} = 0.$$

One finds that $1 \leqq z_0 \leqq \infty$. The value of z_0 is determined only by σ, being unity for $\sigma=0$, and becoming infinite for σ approaching its maximum value $\frac{1}{2}$.

An obvious property of $p(z)$ is

$$\lim_{|z|\to\infty} p(z) = 1-2\sigma.$$

This result shows that in the integrated form

$$p(z) = 1+\sigma z \ln\left[(z-1)/(z+1)\right] \tag{4}$$

with z restricted to points off the real interval $(-1, 1)$, the principal value of the logarithm must be taken. If, furthermore, we write

$$p(z) = 1+\sigma z(\ln \rho + i\alpha), \tag{5}$$

where

$$\rho = \left|\frac{z-1}{z+1}\right| = \left|\left(\frac{(u-1)^2+v^2}{(u+1)^2+v^2}\right)^{\frac{1}{2}}\right|$$

$$\tan\alpha = 2v/(u^2+v^2-1) \quad z=u+iv$$

the same condition requires the vanishing of α at infinity. Thus, one has for α in the neighborhood of the branch points the values consistent with the arrangement given in Fig. 1 instead of the

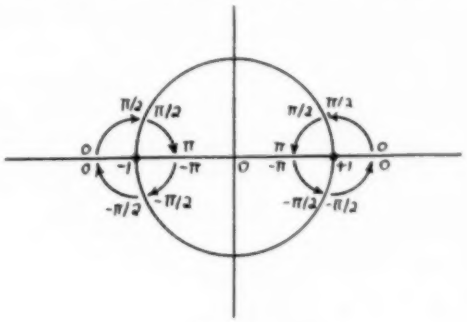

FIG. 1.

alternative arrangement in which 0 and π are substituted for $-\pi$ and 0, respectively, below the real axis.

THE PARTICLE DENSITY

The total density of particles at the plane x is given by

$$F(x) = 2\pi\int_{-1}^{1} f(x, z)dz.$$

It has been shown in SU that the density function must satisfy a well-known inhomogeneous integral equation

$$F(x) = g(x)+\frac{1}{2l_s}\int_0^\infty F(x')K\left(\frac{|x-x'|}{l}\right)dx', \tag{6}$$

where

$$\begin{aligned} g(x) &= 2\pi\int_0^1 f_0(z)e^{-x/lz}dz \\ &\quad +\frac{2\pi}{v}\int_0^\infty q(x')K\left(\frac{|x-x'|}{l}\right)dx', \end{aligned} \tag{7}$$

$$K(s) = \int_0^1 e^{-s/z}\frac{dz}{z} = \int_1^\infty e^{-st}\frac{dt}{t} = -li(e^{-s}), \quad s>0$$

and $f_0(z)$ and $q(x)$ are the incident current and isotropic source distributions, respectively. An integral equation of this type with the symmetric logarithmic integral function as kernel has been encountered in the study of numerous other problems in physics.[3] Particularly, in connection

[3] V. A. Kostitzen, Mem. Sci. Math. **69** (1935). A discussion of the Kundt and Warburg problem of velocity distribution between two parallel plates in relative motion, the Chwolson and Lommel problems of semitransparent sheets and others is given, together with an extensive bibliography. References to some of these papers will be found also in SU.

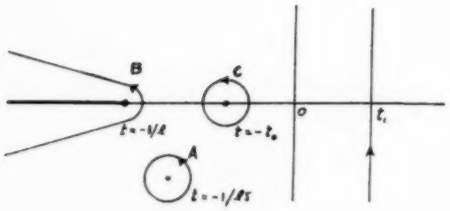

FIG. 2.

with the astrophysical problem of radiant energy transmission through stellar atmospheres, this equation has been the object of considerable study. But no exact solution in closed form has ever been found. Such a solution is required for the case of neutron diffusion, since the development parameter, $2\sigma=l/l_s$, of the iterative solutions is very nearly equal to unity, and such solutions converge very slowly.

It has been shown in SU, Eq. (4a), that $-zf(0, z)$ is the Laplace transform in the variable $-1/lz$ of

$$F(x)/4\pi l_s+q(x)/v$$

for $R(z)<0$. Introducing $z=-1/lt$ this relation is put in the form

$$\frac{f(0, -1/lt)}{lt}=\int_0^x e^{-xt}\left[\frac{F(x)}{4\pi l_s}+\frac{q(x)}{v}\right]dx \quad R(t)>0.$$

Since $F(x)$ and $q(x)$ may be assumed continuous and the integral is absolutely convergent, this transformation has the unique inversion[4]

$$F(x)=-\frac{4\pi l_s q(x)}{v}+\varphi(x), \tag{8}$$

$$\varphi(x)=\frac{2l_s}{il}\int_{t_1-i\infty}^{t_1+i\infty} e^{xt}f(0, -1/lt)\frac{dt}{t}$$

$$t=t_1+it_2 \quad t_1>0, \tag{9}$$

where t_1 is a line parallel to the imaginary axis and lying within a strip of the t plane within which the integrand is analytic. Reference to Eqs. (1) and (2) shows that this region is the entire positive half of the t plane not including the imaginary axis. Considering now the problems of incident currents and source distributions separately, one has in the first case

$$f_0(z)=f\delta(z-\zeta) \quad q(x)=0 \quad 0<\zeta\leq 1,$$
$$g(x)=2\pi fe^{-x/l\zeta}; \quad F(x)=\varphi(x), \tag{10}$$

where $g(x)$ is the inhomogeneous term of Eq. (6), $\varphi(x)$ is given by Eq. (9), and $f(0, -1/lt)$ is given by Eq. (1) with $n=f\sigma$. In the second case one has

$$q(x)=qe^{-x/l\zeta}, \quad f_0(z)=0, \quad R(\zeta)\geq 0,$$
$$g(x)=\frac{2\pi ql\zeta}{v}e^{-x/l\zeta}\ln\frac{\zeta-1}{\zeta+1}-\frac{2\pi ql\zeta}{v}\int_0^1\frac{e^{-x/lz}}{\zeta-z}dz,$$
$$F(x)=-(4\pi ql_s/v)e^{-x/l\zeta}+\varphi(x), \tag{11}$$

where, again, $\varphi(x)$ is given by Eq. (9) and $f(0, -1/lt)$ by Eq. (1) but with $n=ql/v$. The equivalence of incident currents and distributed sources, which holds for the emergent distribution when $0<\zeta\leq 1$ and $ql/v=f\sigma$, is thus modified slightly for the density function. One finds $F(x)$ for sources to be less than $F(x)$ for incident currents by an amount equal to

$$(4\pi ql_s/v)e^{-x/l\zeta}=2\pi fe^{-x/l\zeta}.$$

This quantity is, however, just the contribution to the density at the plane x due to the incident current when account is taken of the kinetic theory probability that a particle incident on the boundary will travel the distance x/ζ without collision. This result may be established, also, directly from the integral equation (6) itself.

Thus, for the determination of $F(x)$ for the case either of incident currents or source distributions, one requires the evaluation of the single function $\varphi(x)$ for all values of ζ such that $R(\zeta)\geq 0$. Introducing Eq. (1) into (9), using the relation $p_1(z)=p_2(-z)$, and introducing $\sigma=l/2l_s$ one has

$$\varphi(x)=\frac{nl\zeta}{i\sigma p_2(\zeta)}\int_{t_1-i\infty}^{t_1+i\infty}\frac{e^{xt}dt}{(1+lt\zeta)p_2(1/lt)}. \tag{12}$$

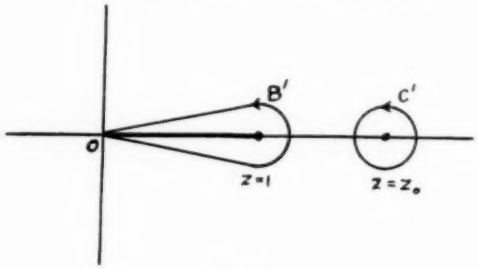

FIG. 3.

[4] G. Doetsch, *Theorie und Anwendung der Laplace Transformation* (Springer, 1937), pp. 40–3.

The integrand, while analytic everywhere to the right of the imaginary axis, has certain singularities in the negative half-plane, which will now be discussed. There exists, first of all, a simple pole at $t=-1/l\zeta$. There is, in the second place, a branch point at $t=-1/l$. The branch cut for $p_2(1/lt)$ may be drawn from the point $t=-1/l$ to the left along the negative real axis to $-\infty$. Finally, there is the zero of $p_2(1/lt)$. This zero is located on the negative real axis at a point $t=-t_0$ where $0\leq t_0\leq 1/l$. Since this zero of p_2 is the zero of p in the negative half of the plane, it may be found, by using Eq. (4) and the subsequent discussion, from the relation

$$p(z_0)=1+\sigma z_0 \ln\left[(z_0-1)/(z_0+1)\right]=0,$$

$$1=\sigma z_0 \ln\frac{z_0+1}{z_0-1}=2\sigma\left[1+\frac{1}{3z_0^2}+\frac{1}{5z_0^4}+\cdots\right], \tag{13}$$

$$t_0=1/lz_0.$$

$\varphi(x)$ for Complex Values of ζ

The function $\varphi(x)$ may be evaluated by deforming the path of integration about the singularities and branch cut in the negative t plane. If ζ is complex, including pure imaginary, or if real it is at least greater than unity and not equal to $1/lt_0$, $\varphi(x)$ may be expressed as the sum of three contour integrals

$$\varphi(x)=(nl\zeta/\sigma)(A+B+C), \tag{14}$$

where A, B and C are the integrals

$$\frac{1}{ip_2(\zeta)}\int\frac{e^{xt}dt}{(1+lt\zeta)p_2(1/lt)}$$

taken about the contours A, B, and C, respectively, of Fig. 2.

Since the contour A contains only a simple pole at $t=-1/l\zeta$, the value of A is obtained immediately. One finds

$$A=\frac{2\pi i}{l\zeta}\frac{e^{-x/l\zeta}}{ip_2(\zeta)p_2(-\zeta)}=\frac{2\pi e^{-x/l\zeta}}{l\zeta p(\zeta)} \tag{15}$$

after introducing the relations given by Eq. (3).

Before evaluating B and C it is convenient to transform back to the z plane by introducing $t=-1/lz$. Introducing Eq. (3) again, one finds that B and C are given by the integrals

$$\frac{1}{il p_2(\zeta)}\int\frac{e^{-x/lz}}{z-\zeta}\frac{p_2(z)}{p(z)}\frac{dz}{z}$$

over the contours B' and C', respectively, of Fig. 3. The branch cut along the interval $(-1/l, -\infty)$ of the t plane is transformed to the interval $(0, 1)$ of the z plane. Since the function $p_2(z)$ is analytic everywhere for $R(z)>0$, and the contours B' and C' do not inclose the point $z=\zeta$, these integrals are taken only about singularities of $p(z)$, its branch cut and zero, respectively.

The evaluation of B may now be carried out. Permitting the contour B' to collapse upon the branch cut, and referring to Eq. (5) and Fig. 1 for the selection of α in $p(z)$ one obtains for this integral

$$B=\frac{1}{il p_2(\zeta)}\int_0^1\frac{e^{-x/lu}}{u-\zeta}\frac{p_2(u)}{1+\sigma u(\ln\rho-i\pi)}\frac{du}{u}$$
$$+\frac{1}{il p_2(\zeta)}\int_1^0\frac{e^{-x/lu}}{u-\zeta}\frac{p_2(u)}{1+\sigma u(\ln\rho+i\pi)}\frac{du}{u}$$
$$=\frac{2\pi\sigma}{lp_2(\zeta)}\int_0^1 e^{-x/lu}\frac{p_2(u)}{(1+\sigma u\ln\rho)^2+(\pi\sigma u)^2}\frac{du}{u-\zeta}, \tag{16}$$

where

$$\ln\rho=(1-u)/(1+u).$$

Finally, we may determine C. Since the only singularity within the contour C' is the zero of $p(z)$, the behavior of this function in the neighborhood of $z=z_0$ must be found. This zero lies on the real axis, and we may set $z_0=u_0\geq 1$ where

$$p(u_0)=1+\sigma u_0\ln\left[(u_0-1)/(u_0+1)\right]=0.$$

Using this condition on u_0 one obtains

$$p(u_0+\Delta z)=\Delta z\frac{1-u_0^2(1-2\sigma)}{u_0(u_0^2-1)}+\cdots.$$

Therefore, $1/p(z)$ has a simple pole at $z=u_0$ and its residue is

$$u_0(u_0^2-1)/\left[1-u_0^2(1-2\sigma)\right].$$

Then

$$C=\frac{2\pi}{lp_2(z)}\frac{(u_0^2-1)}{1-u_0^2(1-2\sigma)}\frac{p_2(u_0)}{u_0-\zeta}e^{-x/lu_0}. \tag{17}$$

Bringing these results together by introducing Eqs. (15), (16) and (17) into Eq. (14) one obtains

$$\varphi(x)=\frac{2\pi n}{\sigma}\Bigg[\frac{e^{-x/l\zeta}}{p(\zeta)}-\frac{\zeta}{\zeta-u_0}\frac{(u_0^2-1)}{1-u_0^2(1-2\sigma)}\frac{p_2(u_0)}{p_2(\zeta)}e^{-x/lu_0}-\frac{\sigma\zeta}{p_2(\zeta)}\int_0^1 e^{-x/lu}\frac{p_2(u)}{(1+\sigma u\ln\rho)^2+(\pi\sigma u)^2}\frac{du}{\zeta-u}\Bigg]. \quad (18)$$

$\varphi(x)$ FOR $\zeta=u_0$

The result for $\varphi(x)$ given by Eq. (18) was obtained subject to $R(\zeta)\geq 0$ but for $\zeta\neq u_0$ and not lying in the interval (0, 1). One may nevertheless obtain the correct result for $\zeta=u_0$ from Eq. (18) by setting $\zeta=u_0+\Delta\zeta$ and canceling the first-order infinities of the first two terms against each other, or one may set $\zeta=u_0$ at the beginning and evaluate $(A+C)$ about the second-order pole then existing at $z=u_0$. Using the first procedure, one has for $\zeta=u_0+\Delta\zeta$

$$e^{-x/l\zeta}=e^{-x/lu_0}[1+x\Delta\zeta/lu_0^2],$$

$$p(\zeta)=1+\sigma(u_0+\Delta\zeta)\ln\frac{u_0-1+\Delta\zeta}{u_0+1+\Delta\zeta}=(\Delta\zeta)\frac{1-u_0^2(1-2\sigma)}{u_0(u_2^2-1)}-(\Delta\zeta)^2\frac{2\sigma}{(u_0^2-1)^2}. \quad (19)$$

Also, one may define a function $a(u_0)$ by the relation valid to the first order in $\Delta\zeta$

$$p_2(u_0)/p_2(u_0+\Delta\zeta)=1-\Delta\zeta a(u_0). \quad (20)$$

Introducing these results into Eq. (18) and passing to the limit of $\Delta\zeta=0$, one obtains

$$\varphi(x)=\frac{2\pi n}{\sigma}\Bigg[\frac{2\sigma u_0^2}{(1-u_0^2(1-2\sigma))^2}e^{-x/lu_0}-\frac{(u_0^2-1)}{1-u_0^2(1-2\sigma)}\left\{1-\frac{x}{lu_0}-u_0a(u_0)\right\}e^{-x/lu_0}-\frac{\sigma u_0}{p_2(u_0)}\int_0^1 e^{-x/lu}\frac{p_2(u)}{(1+\sigma u\ln\rho)^2+(\pi\sigma u)^2}\frac{du}{u_0-u}. \quad (21)$$

Since this result is of interest principally for the sake of completeness, the details for the evaluation of $a(u_0)$ will not be given. In order to find this function one must return to the defining equation for $p_2(z)$, introduce the definition of $p(iz)$, which may be expressed in the form

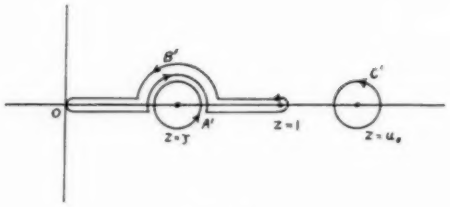

FIG. 4.

$$p(iz)=1-2\sigma z\tan^{-1}(1/z) \quad (22)$$

and then evaluate the logarithm of the desired ratio to the first order. One obtains

$$u_0a(u_0)=\tfrac{1}{2}-\frac{1}{\pi}\int_0^\infty\frac{1+u_0^2t^2(1-2\sigma)}{1-2\sigma u_0t\tan^{-1}(1/u_0t)}\frac{dt}{(1+t^2)(1+u_0^2t^2)}.$$

$\varphi(x)$ FOR ζ IN THE INTERVAL (0, 1)

When ζ takes on real values in the open interval (0, 1) the integrand in the definite integral appearing in the expression for $\varphi(x)$ given by Eq. (18) diverges at one point in the range of integration because of the factor $(\zeta-u)$ in the denominator, and the first term of $\varphi(x)$ is complex and indeterminate because of the appearance of $p(\zeta)$, which, according to Eq. (5) and Fig. 1 has the value

$$p(\zeta)=1+\sigma\zeta(\ln\rho\pm i\pi)\quad\rho=(1-\zeta)/(1+\zeta)$$

on this interval. We will show, however, that Eq. (18) still gives $\varphi(x)$ correctly providing that for ζ lying in the open interval (0, 1) the principal part of the integral is taken, and that $p^{-1}(\zeta)$ is interpreted to mean the average value of $p^{-1}(\zeta)$ on the branch cut. Finally, we will show that the point $\zeta=1$ offers no particular difficulty, because the first term of Eq. (18) vanishes at $\zeta=1$ for all directions of approach, and the integral is finite, though the integrand diverges at the upper limit of the integration range. From these interpretations together with those of the preceding section of the terms in

Eq. (18) this form for $\varphi(x)$ may be regarded as correct for all values of ζ with $R(\zeta)\geq 0$.

In order to establish the desired result we return to the evaluation of $(A+B)$ of Eq. (14) with the point $t=-1/l\zeta$ of the t plane lying on the branch cut. This integral may be performed in either of two ways. We may deform the branch cut and evaluate A and B separately as before. In the z plane the contours then have the form given in Fig. 4. The branch cut is inclosed entirely within B'. Now if B' is divided into two parts, the two small semicircles and the straight line portions, one obtains from the latter the same definite integral as before except that the principal part is meant. For the evaluation of A we recall from Eq. (5) and Fig. 1 that with the branch cut having been deformed upward, the contour for A lies everywhere on that branch of $p(z)$ for which α of Eq. (5) has the value $-\pi$ on the real axis. Then A has the same form as given by Eq. (15), but with $p(\zeta)$ given by

$$p(\zeta)=1+\sigma\zeta\{\ln[(1-\zeta)/(1+\zeta)]-i\pi\}.$$

Therefore

$$A=\frac{2\pi e^{-x/l\zeta}}{l\zeta}\frac{1+\sigma\zeta\ln[(1-\zeta)/(1+\zeta)]}{\{1+\sigma\zeta\ln[(1-\zeta)/(1+\zeta)]\}^2+(\pi\sigma\zeta)^2}+\frac{2\pi^2 i\sigma e^{-x/l\zeta}}{l}\left[\left(1+\sigma\zeta\ln\frac{1-\zeta}{1+\zeta}\right)^2+(\pi\sigma\zeta)^2\right]^{-1}.$$

Now we evaluate the parts of B consisting of the two semicircles. Setting $z=\zeta+\epsilon e^{i\theta}$ where ϵ is the radius of the semicircles, taking the limit for $\epsilon\to 0$, and remembering that the lower and upper semicircles belong to branches of α having the values $-\pi$ and π, respectively, on the real axis, one obtains for this part of B the result

$$-\frac{2\pi^2 i\sigma}{l}e^{-x/l\zeta}\left[\left(1+\sigma\zeta\ln\frac{1-\zeta}{1+\zeta}\right)^2+(\pi\sigma\zeta)^2\right]^{-1}.$$

Thus, this part of B just cancels the imaginary term of A. Now since

$$\frac{1}{2}\left[\frac{1}{p(\zeta+i0)}+\frac{1}{p(\zeta-i0)}\right]=\frac{1+\sigma\zeta\ln[(1-\zeta)/(1+\zeta)]}{\{1+\sigma\zeta\ln[(1-\zeta)/(1+\zeta)]\}^2+(\pi\sigma\zeta)^2}\qquad(23)$$

$$|\zeta|=\zeta,\quad 0<\zeta<1$$

one finds that this result for ζ in the interval $(0, 1)$ is the same as before except for the necessary changes in the interpretations of $p^{-1}(\zeta)$ and the definite integral which were asserted above.

A second method of performing the integration for $(A+B)$ when ζ lies in the interval $(0, 1)$ is to leave the branch cut undeformed, and to integrate over the single closed path inclosing the branch cut. This contour may, however, be regarded as two straight lines broken at $z=\zeta$, giving the principal value integral, plus a small circle about $z=\zeta$. In the integration over the circle it must be remembered that α assumes values belonging to different branches on the upper and lower halves of the circle. It is this method which may be used in particular for the point $\zeta=1$. Considering the circle to be of radius ϵ one obtains the same definite integral as before for the straight line portions of the contour except for the upper limit which is now $(1-\epsilon)$. For the integral over the circle one introduces $z=1+\epsilon e^{i\theta}$, and integrates over θ from $-\pi$ to π. This integral is observed to vanish in the limit of ϵ approaching zero. Returning to the definite integral one finds that for small ϵ, the integrand behaves like $\epsilon^{-1}(\ln\epsilon)^{-2}$. The integrand diverges but the integral is easily shown to be finite. This result for $\zeta=1$ may be obtained, also, directly from Eq. (18) in which ζ is permitted to approach unity from any direction other than along the real segment $(0, 1)$. The definite integral remains finite, and the first term of Eq. (18) vanishes because of the unbounded character of $p(\zeta)$ at $\zeta=1$.

Final Results for $F(x)$

The case of incident currents and source distributions will be expressed separately. For an incident current distribution of the form

$$f_0(z)=f\delta(z-\zeta),\quad 0<\zeta\leq 1$$

one obtains from Eqs. (10) and (18) with $n=f\sigma$, and after inserting (23) since ζ is real and in the

interval (0, 1)

$$F(x)=2\pi f\Bigg[\frac{1+\sigma\zeta\ln[(1-\zeta)/(1+\zeta)]}{(1+\sigma\zeta\ln[(1-\zeta)/(1+\zeta)])^2+(\pi\sigma\zeta)^2}e^{-x/l\zeta}$$
$$+\frac{\zeta}{u_0-\zeta}\frac{(u_0^2-1)}{1-u_0^2(1-2\sigma)}\frac{p_2(u_0)}{p_2(\zeta)}e^{-x/lu_0}+\frac{\sigma\zeta}{p_2(\zeta)}\int_0^1 e^{-x/lu}\frac{p_2(u)}{(1+\sigma u\ln\rho)^2+(\pi\sigma u)^2}\frac{du}{u-\zeta}\Bigg], \quad (24)$$

where, except for $\zeta=1$ the principal part of the integral is to be taken. For a source distribution of the form

$$q(x)=qe^{-x/l\zeta} \quad R(\zeta)\geq 0$$

one obtains from Eqs. (11) and (18) with $n=ql/v$ and setting $2l_s=l/\sigma$

$$F(x)=\frac{2\pi ql}{\sigma v}\Bigg[\left\{\frac{1}{p(\zeta)}-1\right\}e^{-x/l\zeta}+\frac{\zeta}{u_0-\zeta}\frac{(u_0^2-1)}{1-u_0^2(1-2\sigma)}\frac{p_2(u_0)}{p_2(\zeta)}e^{-x/lu_0}$$
$$+\frac{\sigma\zeta}{p_2(\zeta)}\int_0^1 e^{-x/lu}\frac{p_2(u)}{(1+\sigma u\ln\rho)^2+(\pi\sigma u)^2}\frac{du}{u-\zeta}\Bigg], \quad (25)$$

where, if ζ lies in (0, 1) the right member of Eq. (23) is to be substituted for $p^{-1}(\zeta)$ and the principal part of the integral is to be taken, and if $\zeta=u_0$, the limit of the first two terms leading to the result for $\varphi(x)$ given by Eq. (21) is to be taken. In each of these expressions $\rho=(1-u)/(1+u)$, u_0 must be determined as the positive root of

$$1+\sigma u_0\ln[(u_0-1)/(u_0+1)]=0 \quad (26)$$

and the functions $p_2(\zeta)$ and $p(\zeta)$ are obtained from Eqs. (2) and (4), respectively.

The case of a constant source distribution is of particular interest. The result for constant sources q may be obtained from Eq. (25) by letting $\zeta\to\infty$. One shows easily from the defining equations that

$$\lim_{\zeta\to\infty}p(\zeta)=1-2\sigma, \quad \lim_{\zeta\to\infty}p_2(\zeta)=(1-2\sigma)^{\frac{1}{2}},$$

and obtains, therefore, for $q(x)=q$

$$F(x)=\frac{4\pi ql}{v(1-2\sigma)}\Bigg[1-\frac{(1-2\sigma)^{\frac{1}{2}}}{2\sigma}\frac{(u_0^2-1)}{1-u_0^2(1-2\sigma)}p_2(u_0)e^{-x/lu_0}$$
$$-\tfrac{1}{2}(1-2\sigma)^{\frac{1}{2}}\int_0^1 e^{-x/lu}\frac{p_2(u)}{(1+\sigma u\ln\rho)^2+(\pi\sigma u)^2}du\Bigg]. \quad (27)$$

Defining a capture mean time $\tau_c=l_c/v$ where $1/l=1/l_c+1/l_s$ and $\sigma=l/2l_s$, one obtains for $F(\infty)$ and $F(0)$, the density at points located far from the boundary surface and at the boundary surface, respectively

$$F(\infty)=4\pi q\tau_c, \quad (28)$$

$$\frac{F(0)}{F(\infty)}=1-\frac{1}{2}\frac{(1-2\sigma)^{\frac{1}{2}}}{\sigma}\frac{(u_0^2-1)}{1-u_0^2(1-2\sigma)}p_2(u_0)-\tfrac{1}{2}(1-2\sigma)^{\frac{1}{2}}\int_0^1\frac{p_2(u)}{(1+\sigma u\ln\rho)^2+(\pi\sigma u)^2}du. \quad (29)$$

The first result agrees with that obtained from more elementary considerations[5] as it should. The ratio $F(0)/F(\infty)$ depends only on σ, though $F(x)/F(\infty)$ depends on both l and σ.

It is of some interest to compare these results for $F(0)$ with a direct result obtained by integration

[5] H. A. Bethe, Rev. Mod. Phys. **9**, 126 (1937).

over angles of $f(0, z)$ given by Eq. (1). In the limiting case of $\sigma=0$ (pure capture) this comparison is easily made. For the case of source distributions both methods give

$$F(0)=2\pi q\tau_c\zeta \ln (1+\zeta^{-1}).$$

The verification of the expressions for $F(0)$ for the limiting case of $\sigma=\frac{1}{2}$ (no capture) by comparison with the direct calculation is not as easily established. In this limit $F(0)$ for a constant finite source distribution ($\zeta=\infty$) is unbounded for $\sigma\to\frac{1}{2}$. The direct calculation shows that the approach of $F(0)$ to infinity is like $(1-2\sigma)^{-\frac{1}{2}}$. In order to establish this result from Eq. (29) one must first determine the behavior of $p_2(u_0)$ for $\sigma\to\frac{1}{2}$. One finds that whereas[2]

$$\lim_{z\to\infty} p_2(z)=1/\sqrt{3}z \quad \sigma=\tfrac{1}{2},$$

σ having passed to the limit $\frac{1}{2}$ before taking the limit in z, the result of a simultaneous approach to their limits through the maintenance of the relation given by (26) is

$$\lim_{u_0\to\infty} p_2(u_0)=2/\sqrt{3}u_0.$$

Then the second term of (29) may be shown to have a leading term of unity so that the entire expression leads with a term of order $(1-2\sigma)^{\frac{1}{2}}$. Since $\tau_c\sim(1-2\sigma)^{-1}$ the expression for $F(0)$ given by (29) is shown to increase like $(1-2\sigma)^{-\frac{1}{2}}$ for $\sigma\to\frac{1}{2}$, as it should.

JANUARY 15, 1941 PHYSICAL REVIEW VOLUME 59

The Relative Stopping Powers of Carbon and Lead for Slow Mesons

MARTIN A. POMERANTZ AND THOMAS H. JOHNSON
The Bartol Research Foundation of the Franklin Institute, Swarthmore, Pennsylvania

(Received November 18, 1940)

An experimental determination of the relative stopping powers of carbon and lead for slow mesons has been made with an anticoincidence arrangement of G-M counters. For mesons having an average energy of approximately 4×10^7 ev, the experiments revealed that 28.5 g/cm² of carbon is equivalent in stopping power to 24 ± 5 g/cm² of lead. This gives a value for the ratio of the stopping powers of equal masses of carbon and lead, $S_C/S_{Pb}=0.84\pm0.18$, to be compared with the theoretical value of $S_C/S_{Pb}=1.82$ calculated with the ionization theory. However, it is not necessary to invoke a hitherto unknown absorption process to account for this discrepancy, since it may be explained as arising from the scattering and transition effects. The data corrected for these effects show that 28.5 g/cm² of carbon is equivalent in stopping power to 45 ± 7 g/cm² of lead, and $S_C/S_{Pb}=1.6\pm0.3$, in agreement with the theoretical value within the experimental uncertainty. These experiments indicate that in a dense absorber, any additional absorption process is unimportant compared with ionization for mesons having energies of about 4×10^7 ev, or higher.

INTRODUCTION

EXPERIMENTAL evidence consistent with the possibility that some hitherto unknown process is partially responsible for the removal of slow mesons from the cosmic radiation was obtained during the course of several recent investigations relating to the instability of the meson. Of these the following may be mentioned: (1) The value of τ_0, the proper lifetime of the meson, calculated from the observed rate of production of disintegration electrons is larger than that calculated from the rate of disappearance of mesons.[1,2] This arises from a deficiency in the relative abundance of disintegration

[1] M. A. Pomerantz, Phys. Rev. **57**, 3 (1940).
[2] M. Ageno, G. Bernadini, N. Cacciapuoti, B. Ferretti, and G. C. Wick, Phys. Rev. **57**, 945 (1940).

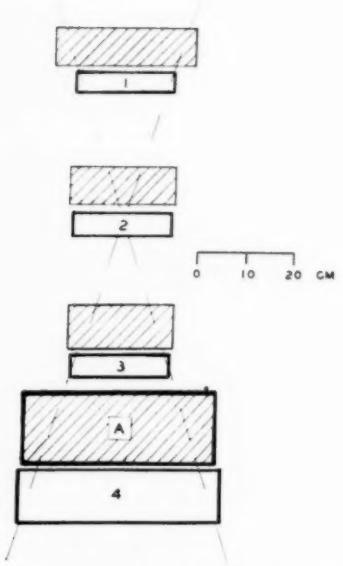

FIG. 1. Scale diagram of the experimental arrangement. Triple coincidences among G-M counter trays 1, 2, and 3, and quadruple coincidences among trays 1, 2, 3 and 4 were recorded simultaneously, with carbon or lead interposed at A.

electrons, and has been interpreted on the hypothesis that slow mesons may disappear in some cases by a process not resulting in the emission of an electron. (2) Behind thin shields at sea level, the electrons from the disintegration of mesons should predominate in burst production. From the observed burst frequency, Montgomery and Montgomery[3] found a value of τ_0 larger than that calculated from the rate of disappearance of mesons, also indicating a slight deficiency in the abundance of disintegration electrons. (3) The delayed coincidence-counter arrangement of Montgomery, Ramsey, Cowie and Montgomery[4] revealed that the delayed emission of disintegration electrons from mesons stopping in 2 cm of lead is less than ten percent of that expected. (4) Although two recent photographs of meson disintegrations have been obtained by Williams, Roberts and Evans,[5] other photographs of mesons stopping in the gas had shown tracks terminating abruptly with no evidence of disintegration electrons.[6] (5) Finally, in an earlier investigation by one of the authors[7] there was an indication that the proper lifetime of high energy mesons was longer than that of mesons with lower energies.

It was therefore considered important to secure direct experimental evidence which would reveal whether or not ionization is the sole process whereby slow mesons are ultimately absorbed in traversing a dense medium. If it is assumed that any other unknown process varies with the atomic number differently than does the ionization, then a determination of the relative stopping powers of carbon and lead would afford a straightforward method of investigating this question. Because of the short geometrical path traversed, disintegration is not a factor in the absorption of slow mesons in a solid. Consequently, if ionization is the only effective process, the experimental value of the ratio of stopping powers of carbon and lead is expected to agree with the theoretical value, a value already established experimentally in the case of fast mesons.[8] A discrepancy between the expected and observed stopping powers would indicate that ionization alone is insufficient to account for the stopping of slow mesons in a dense absorber, and that the other process depends differently upon atomic number than does the ionization.

EXPERIMENTAL PROCEDURE

Method

The experimental value of the ratio of stopping powers S_A/S_B of two absorbers A and B for slow mesons is obtained by determining what thickness of substance A stops the same number of mesons as a given thickness of substance B. Carbon and lead were selected because, if only ionization is considered, their stopping powers are quite different, the former producing a measurably greater absorption per gram per square centimeter than the latter.

Heretofore,[8] a determination of S_A/S_B has consisted essentially of performing the following

[3] C. G. Montgomery and D. D. Montgomery, Rev. Mod. Phys. **11**, 255 (1939).
[4] C. G. Montgomery, W. E. Ramsey, D. B. Cowie and D. D. Montgomery, Phys. Rev. **56**, 635 (1939).
[5] E. J. Williams and G. E. Roberts, Nature **45**, 102 (1940); E. J. Williams and G. R. Evans, *ibid.* **45**, 818 (1940).
[6] S. H. Neddermeyer and C. D. Anderson, Phys. Rev. **54**, 88 (1938).
[7] Reference 1, page 11.
[8] Reference 1, page 4.

two experiments. In the first experiment, the counting rate of a train of coincidence-counters was observed with a given thickness of absorber A interposed within its solid angle. In the second experiment, absorber A was replaced by various thicknesses of absorber B, until the thickness giving the same counting rate as that of experiment I was found. Despite the possibility of minimizing the effect of changes in sensitivity by frequently alternating the two experiments, fluctuations in the cosmic-ray intensity necessitate running the apparatus for very long periods for comparing the absorption in small thicknesses of absorber. The thickness of absorber uniquely determines the upper limit of the energy of mesons which it stops. Therefore, unless the apparatus is run for a very long time, this technique can yield a significant value of S_A/S_B only for fast mesons, i.e., those having an average energy while traversing the absorber of the order of 10^9 ev.

However, the arrangement diagrammed in Fig. 1 has made feasible a determination of S_A/S_B for slow mesons in a short time. Counter trays 1, 2, 3 comprise a triple coincidence train in which is interposed a sufficient thickness of lead to eliminate the soft component. This is designated as the meson selector. Tray 4 is of such dimensions that it fills the solid angle subtended by the meson selector. By means of appropriate circuits, triple coincidences among trays 1, 2, 3 and quadruple coincidences among trays 1, 2, 3, 4 were recorded simultaneously. When an absorbing shield is interposed in position A, the difference between the threefold and fourfold counting rates (corrected for the inefficiency of tray 4) is proportional to the number of slow mesons stopped in the shield. This arrangement has a statistical advantage over one in which the two counts are recorded in separate experiments, and not simultaneously. The standard deviation in the difference between C_3 triple coincidences and C_4 quadruple coincidences recorded separately is $(C_3+C_4)^{\frac{1}{2}}$, whereas it is $(C_3-C_4)^{\frac{1}{2}}$ in the case of simultaneous recording. The statistical advantage is the same as that in the recording of anticoincidences, but the present arrangement has the added feature of providing a continuous check on the sensitivity of the apparatus through the constancy of the counting rate of the three trays included in the meson selector.

Description of apparatus

Trays 1, 2, and 3 each contained twelve G-M counters connected in parallel, and tray 4 contained 48 parallel-connected counters. Each counter tray and the associated vacuum-tube circuits were mounted in a sheet-iron box. The counters were filled with a mixture of hydrogen at a pressure of 5 cm of Hg and argon at a pressure of 33 cm of Hg. The copper cylinders were 8″ long and $\frac{3}{4}$″ in diameter. The individual counters had a constant counting rate over a range of 200 volts, and operated at a potential of approximately 1250 volts. The conventional Neher-Harper[9] arrangement served as the recovery resistors for the counters, and the high voltage was stabilized by the two-stage circuit of Neher and Pickering.[10] The method of recording triple and quadruple coincidences simultaneously is schematically represented in Fig. 2. The apparatus was housed in a wooden structure on the roof of the laboratory.

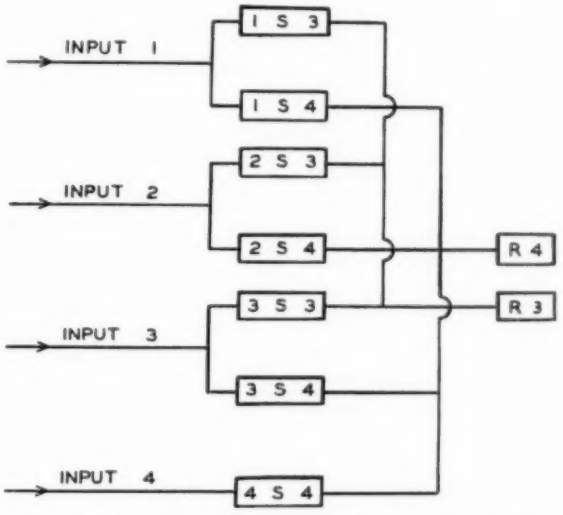

FIG. 2. Schematic diagram of the arrangement for recording triple and quadruple coincidences simultaneously. The amplified pulses from each tray of counters are separated into two channels. The components $S3$ comprise the selection stages for threefold coincidences, and $S4$ those for fourfold coincidences. $R3$ and $R4$ are the recorder units for triple and quadruple coincidences, respectively.

[9] H. V. Neher and W. W. Harper, Phys. Rev. **49**, 940 (1936).
[10] H. V. Neher and W. H. Pickering, Rev. Sci. Inst. **10**, 54 (1940).

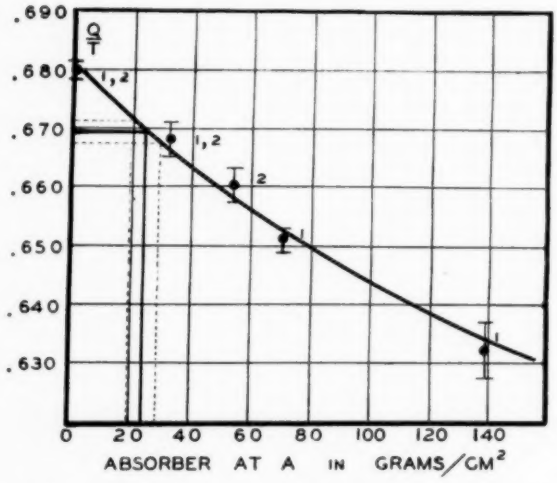

FIG. 3. Uncorrected lead absorption curve for slow mesons. The abscissa of the point on this curve whose ordinate is the ratio Q/T obtained with a given amount of carbon interposed at A is the amount of lead of equivalent stopping power. The numbers at the right of each point refer to the experiment which provided the data for that point.

In order to test the discrimination of the two selection circuits against $(n-1)$-fold coincidences, the high voltage was applied to all but one tray of counters. No counts were recorded during a long period. The bias on the output tube of the quadruple coincidence circuit was intentionally larger than necessary in order to preclude any possibility of spurious counts. This was considered desirable despite the disadvantage that it lowered the efficiency of tray 4 somewhat by inhibiting weak discharges.

Most of the inefficiency of tray 4 is attributable to the fact that the counters did not present an entirely unbroken area, although they did overlap. A test run with the meson selector in operation, but with no high voltage applied to the counters of tray 4 proved that the tripping of the threefold coincidence circuit induced no effect on the fourfold coincidence circuit.

The resolving time of the selection stages, measured with the Ramsey circuit,[11] was shorter than 10^{-5} second. This is in accord with the very small counting rate with tray 3 displaced out of line. The small correction for accidental coincidences and air showers has been subtracted from the original data, to give the final results listed in the table.

[11] Reference 4, page 636.

Results

Table I summarizes the data from which the ratio of stopping powers of carbon and lead is obtained. The uncertainties indicated are standard deviations. Runs with various thicknesses of lead, with 28.5 g/cm² of carbon, and with no absorber interposed in position A were conducted alternately. Shifts of the absorber were made frequently. The counting rate of the meson selector was approximately 6 counts per minute.

Two separate experiments were conducted to serve as a mutual check. At the conclusion of experiment 1, the apparatus was thoroughly retested, and the sensitivity was readjusted for the purpose of obtaining a new set of data.

The final data, after adjusting the results of experiments 1 and 2 with the factor obtained from a comparison of the ratio of quadruples to triples, Q/T, for zero interposed lead thickness, are plotted in Fig. 3. The abscissa of the point on the lead absorption curve having as ordinate the value of Q/T for a specific thickness of carbon, represents the amount of lead equivalent to that thickness of carbon. Figure 3 reveals that 28.5 g/cm² of carbon is equivalent in stopping power to 24±5 g/cm² of lead. Therefore, for slow mesons, the ratio of the stopping powers of equal masses of carbon and lead is $S_C/S_{Pb}=0.84\pm0.18$.

TABLE I. *Cumulative summary of the original data used for determining the ratio of stopping powers of carbon and lead for slow mesons. The values of Q/T obtained in experiment 1 differ from those obtained in experiment 2 because the sensitivity of the apparatus was intentionally changed by raising the selecting biases between experiments.*

Absorber Interposed at A in g/cm²	Total Number of Quadruple Coincidences $=Q$	Total Number of Triple Coincidences $=T$	$\frac{Q}{T}$
	Experiment No. 1		
0	27,124	39,878	0.680±0.002
32.2 Pb	13,318	19,953	0.667±0.004
71.9 Pb	30,823	47,331	0.651±0.002
139.0 Pb	7,387	11,690	0.632±0.005
28.5 C	17,667	26,479	0.667±0.003
	Experiment No. 2		
0	46,742	73,249	0.638±0.002
32.2 Pb	11,660	18,578	0.628±0.004
53.5 Pb	15,096	24,401	0.619±0.003
28.5 C	43,890	69,723	0.629±0.002

Discussion

The theoretical results from which the value of S_C/S_{Pb} is obtained have already been discussed. Several theories of ionization[12–14] are available for calculating the ratio of stopping powers of carbon and lead. However, even though the theories and various experiments do not agree as regards the value for the specific energy loss, the ratio S_C/S_{Pb} is not appreciably altered under the different assumptions made, nor is it sensitive to the energy of the mesons. The theoretical value of S_C/S_{Pb} is 1.82, as compared with the observed value of 0.84 ± 0.18.

The authors' previous comparison of the stopping powers of water and lead had disclosed that the ionization theory affords a suitable method of determining what thickness of one dense absorber is equivalent in stopping power for fast mesons to a given thickness of any other. In that instance, the average energy of the mesons involved was of the order of one billion ev. In the present experiments, however, the mesons concerned were of considerably lower energy. A range of 28.5 g/cm² of carbon corresponds to a meson with an initial energy of about 10^8 ev. This is the *maximum* energy of the mesons included in the observations. The average energy of the mesons as they traversed these thin absorbing shields was approximately 4×10^7 ev. Although lead is not expected to absorb mesons as efficiently per gram per cm² as carbon, the mass absorption law here appears to be approximately valid for slow mesons. At the present time, however, it does not seem necessary to invoke any hitherto unknown process to account for this discrepancy between the theoretical and experimental values of S_C/S_{Pb}. The following two factors appear to be capable of reconciling the observed results with the predictions based upon the theory of ionization:

(a) After taking into account the inefficiency of tray 4, anticoincidences (i.e., a discharge of the meson selector unaccompanied by a discharge of tray 4) are produced by two types of event:

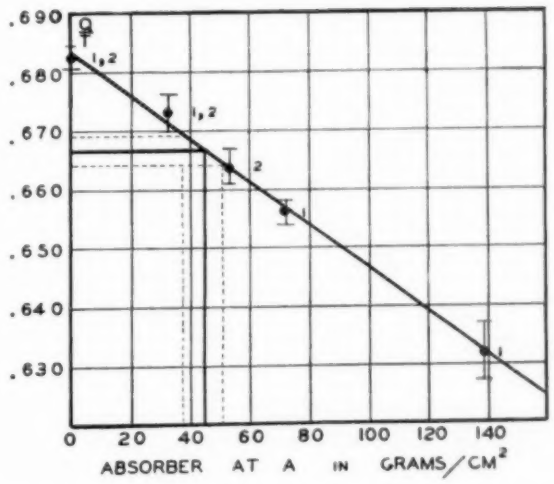

Fig. 4. Plot of the data of Fig. 3 corrected for the scattering and transition effects.

(1) Mesons with energies below the minimum energy required for penetrating absorber A are stopped in A; (2) mesons with energies exceeding this minimum are scattered by absorber A out of the solid angle subtended by the meson selector. The mean scattering angle in lead is larger than that in carbon. Process (2) is therefore more important in lead, and, with a given thickness of lead interposed in position A, the quadruple coincidence rate Q is less than that accounted for by process (1) alone.

(b) The transition effect results in a higher value of Q with a given thickness of carbon interposed in position A than that with an amount of lead equivalent in stopping power. After passing through a sufficient thickness of lead, the knock-on electrons attain equilibrium with their meson primaries. If the radiation passes from lead into carbon, however, the average number of secondaries accompanying a meson increases. The experimental demonstration of this phenomenon was given by the ionization chamber experiments of Schindler,[15] and a particular set of his data is apropos to the present considerations. Upon the addition of 28 g/cm² of aluminum under 25 cm of lead, the total ionization increased, and in fact exceeded by 6 percent that observed when the aluminum was replaced by a quantity of lead of almost equivalent stopping power. The recent experi-

[12] H. A. Bethe, *Handbuch der Physik*, Vol. 24, 1.
[13] F. Bloch, Zeits. f. Physik **81**, 363 (1933).
[14] O. Halpern and H. Hall, Phys. Rev. **57**, 459 (1940). Professor Halpern kindly performed the calculations based upon the Halpern-Hall theory prior to publication of the complete details.

[15] H. Schindler, Zeits. f. Physik **72**, 625 (1931).

ments of Swann and Ramsey[16] also showed the dependence upon atomic number of the average number of single electrons accompanying a meson. Because the efficiency of the fourth tray is not 100 percent, the probability of a fourfold coincidence depends upon the average number of secondaries accompanying a meson through tray 4. Since with carbon interposed in position A this number exceeds that with lead, the efficiency is slightly higher with the carbon. Both this effect and the scattering tend to reduce the experimental value of S_C/S_{Pb}.

In order to determine the effect of these factors upon the experimental value of S_C/S_{Pb}, the estimated corrections have been applied to the data of Table I. The resulting absorption curve for slow mesons is plotted in Fig. 4. In calculating the correction due to scattering, the mean scattering angle was estimated from the cloud-chamber observations of Wilson[17] and Vargus,[18] and the theory of Williams.[19] By taking into consideration the geometry of the arrangement, the percentage of mesons scattered out of the solid angle subtended by the meson selector after having produced a threefold coincidence was estimated to be of the order of 0.7 percent. It was necessary to increase the value of Q for small lead thicknesses by this factor in order to give a value corresponding to the situation in which absorption alone is effective in removing mesons from the beam.

The correction resulting from the transition effect was based upon the experiments of Swann and Ramsey for the determination of the average number of single electrons accompanying a meson under different materials. These experiments, made with a counter apparatus, were considered more directly applicable to the present problem than those of Schindler. Swann and Ramsey observed that 2 percent more of the mesons were accompanied by a single knock-on electron under magnesium than under lead. The inefficiency of tray 4 is halved for those events in which the meson emerges from the carbon accompanied by an electron, and since the efficiency for a single meson was 68 percent, the efficiency for 2 percent of the mesons was 84 percent. Therefore, in order to compare the quadruple rates with the two different absorbers, it was necessary to reduce the quadruple counts with carbon by a number $0.02Q(1-68/84)$. Referring to Fig. 4, we find the corrected rate under 28.5 g/cm^2 of carbon is equal to the corrected rate under 45 ± 7 g/cm^2 of lead, and $S_C/S_{Pb}=1.6\pm0.3$. It must be emphasized that these corrections are only an indication of the order of magnitude of the effects, and it is difficult to assign probable errors to the corrections because of the uncertainty of the dependence of the effects concerned upon the geometry of the apparatus. Hence, it is not possible to state a value of S_C/S_{Pb} of sufficient precision to dismiss definitely the existence of a new absorption process, but the corrected value of S_C/S_{Pb} agrees with the theoretical value of 1.8 within the experimental uncertainty.

Conclusion

These experiments indicate that it is not necessary to assume the existence of a hitherto unknown process in discussing the absorption of mesons having average energies of about 4×10^7 ev, or higher. If such a process exists, it is unimportant compared with ionization at these energies. The possibility of detecting any small effect of this nature with an arrangement of counters is precluded by the present uncertainty in our knowledge of the scattering and transition corrections.

The authors desire to express their appreciation to the National Carbon Company for lending them the large quantity of graphite required for these experiments, and to the Carnegie Institution of Washington for contributing toward the support of this work.

[16] W. F. G. Swann and W. E. Ramsey, Phys. Rev. **57**, 749 (1940).
[17] J. G. Wilson, Proc. Roy. Soc. **174**, 73 (1940).
[18] J. A. Vargus, Phys. Rev. **56**, 480 (1939).
[19] E. J. Williams, Proc. Roy. Soc. **165**, 209 (1938).

A Note on the Density and Compressibility of Nuclear Matter

EUGENE FEENBERG
Washington Square College, New York University, New York, New York
(Received December 2, 1940)

The influence of the Coulomb force between protons on nuclear radii is calculated by using the minimum property of the energy eigenvalue. Several different methods of estimating the compressibility of nuclear matter yield qualitatively concordant results. A small correction to the Coulomb energy is required by the finite value of the compressibility. This correction, which may be called the Coulomb "expansion" energy, is proportional to the square of the Coulomb energy.

I. INTRODUCTION

IT is generally assumed that the density of nuclear matter has approximately the same constant value in all nuclei. Support for this assumption has been found in the approximately linear relation between binding energy and number of particles, in the general trend of nuclear radii in the heavy radioactive elements[1] and in the values of the Coulomb energy required to account for the stability relations among light and intermediate nuclei.[2] The evidence in support of an approximately constant density does not exclude the possibility of small systematic or irregular variations both within a given nucleus[3] and from nucleus to nucleus.[1]

II. THE EFFECT OF COULOMB FORCES ON NUCLEAR DENSITY

One possibility for systematic variations is given by the Coulomb force between protons which might be expected to produce a trend toward decreasing density in heavy nuclei. By utilizing the minimum property of the energy eigenvalue, this effect can be discussed without the introduction of special hypotheses.

Let H_0 represent the nuclear Hamiltonian with the omission of the Coulomb interaction. The equation

$$H_0\psi_0 = E_0\psi_0 \tag{1}$$

determines the normal state eigenfunction $\psi_0(x_1, \cdots)$, eigenvalue E_0 and radius R_0 of a nuclear model in which there is no Coulomb force acting between protons. The eigenvalue E and radius R of the actual nucleus may be obtained by calculating an expectation value of the total Hamiltonian using as wave function $\psi_0(\lambda x_1 \cdots)$ with λ a scale factor to be determined by minimizing E. Thus,

$$E(\lambda) = \frac{\int\cdots\int \psi_0^*(\lambda x_1\cdots) H_0 \psi_0(\lambda x_1\cdots) d\tau}{\int\cdots\int \psi_0^*(\lambda x_1\cdots)\psi_0(\lambda x_1\cdots) d\tau} + \lambda E_{0c}$$
$$= \dot{E}_0(\lambda) + \lambda E_{0c}$$
$$= E_0 + \tfrac{1}{2}(\lambda-1)^2 E_0'' + \lambda E_{0c}. \tag{2}$$

In the last line use has been made of the fact that

$$E_0'(\lambda) = 0 \quad \text{for} \quad \lambda = 1 \tag{3}$$

and terms involving derivatives of $E_0(\lambda)$ beyond the second have been dropped. E_{0c} is the Coulomb energy for the radius R_0. From the condition for a minimum,

$$E'(\lambda) = 0 \tag{4}$$

we obtain
$$\lambda = 1 - E_{0c}/E_0'', \tag{5}$$
$$R = R_0(1 + E_{0c}/E_0''), \tag{6}$$
$$E = E_0 + E_{0c} - E_{0c}^2/2E_0''. \tag{7}$$

The last term in Eq. (7) may be called the Coulomb "expansion" energy.

III. ORDER OF MAGNITUDE ESTIMATE OF E_0''

The facts mentioned in the introduction are consistent with the relations

$$R_0 \sim 0.5A^{\frac{1}{3}}(e^2/mc^2), \tag{8}$$
$$E_0 \sim -16Amc^2. \tag{9}$$

To calculate E_0'' we must know the dependence

[1] G. Gamow, *Atomic Nuclei and Nuclear Transformations* (Oxford Press, 1937), p. 106.
[2] E. Wigner, Phys. Rev. **51**, 947 (1937).
[3] H. Euler, Zeits. f. Physik **105**, 553 (1937).

of E_0 on the nuclear radius R_0. We write

$$E_0 = A[T_0 - W_0(R_0)], \tag{10}$$

in which T_0 is the average kinetic energy per particle and $W_0(R_0)$ the average potential energy per particle. Since the kinetic energy varies inversely with the square of the radius Eq. (10) implies

$$E_0(\lambda) = A[\lambda^2 T_0 - W_0(R_0/\lambda)]. \tag{11}$$

The statistical model and Eq. (8) yield the value[2] $T_0 \sim 28mc^2$. A convenient unit in which to express E_0'' is provided by Eq. (11). We see that the contribution from the kinetic energy to E_0'' is simply $2AT_0 \sim 56mc^2$. The results of the next paragraph show that

$$E_0'' = (2AT_0)k \tag{12}$$

with k in the neighborhood of 2 or 3.

To proceed beyond this point an explicit form must be assumed for $W_0(R)$. Three assumptions are treated here:

$$\begin{aligned} &\text{(a)} \quad W_0(R) = B \exp(-R/a), \\ &\text{(b)} \quad W_0(R) = B \exp(-R^2/a^2), \\ &\text{(c)} \quad W_0(R) = B/(R^2+a^2)^{\frac{1}{2}}. \end{aligned} \tag{13}$$

Some theoretical basis exists for Case (c).[4]

Case (a)

$$\begin{aligned} B \exp(-R_0/a) &= 2T_0 a/R_0, \quad \text{[Eq. (3)]}, \\ E_0 &= AT_0(1-2a/R_0), \\ a/R_0 &= 0.79, \quad \text{(Eq. 9)}, \\ E_0'' &= 1.73(2AT_0) = 97Amc^2. \end{aligned} \tag{14}$$

In the same way we find

$$\text{Case (b)} \qquad E_0'' = 2.73(2AT_0) = 153Amc^2. \tag{15}$$

$$\text{Case (c)} \qquad E_0'' = 1.88(2AT_0) = 105Amc^2. \tag{16}$$

Another type of estimate is provided by using the Hartree approximation to calculate $W_0(R)$ from an assumed Hamiltonian operator. A calculation of this type, based on the exchange force Hamiltonian with error function potentials, has been made by Bethe.[5] He obtains

$$E_0'' = 2.6(2AT_0). \tag{17}$$

IV. Discussion

The numerical results in this section are based on the assumed value $E_0'' = 150Amc^2$. This gives

$$R = R_0(1 + Z^2/125A^{4/3}). \tag{18}$$

[4] E. Feenberg, Phys. Rev. **52**, 758 (1937).
[5] H. Bethe, Rev. Mod. Phys. **9**, 69 (1937), Eq. (319).

The following figures show how R/R_0 varies with charge number. Chemical atomic weights are substituted for A in order to obtain a single valued function of Z

Z	12	32	52	72	92
R/R_0	1.016	1.027	1.034	1.041	1.046

The most interesting aspect of the energy formula Eq. (7) is the way in which the Coulomb energy varies within an isobaric series. If Z is increased by one unit the Coulomb energy increases by the amount

$$\Delta E_c = E_{0c}(Z+1) - E_{0c}(Z) - E_{0c}(Z)2Z/125A^{4/3}. \tag{19}$$

If the Coulomb exchange energy is neglected Eq. (19) becomes

$$\Delta E_c = (6Ze^2/5R_0)(1 - Z^2/125A^{4/3}) = 6Ze^2/5R. \tag{20}$$

The effect of the term in brackets in Eq. (20) is to shift the region of stability toward smaller values of the isotopic number, $N-Z$, as compared with a theory in which nuclear matter is treated as incompressible. Wigner's theory of stability relations in isobaric series is of the latter type. However, the correction to Wigner's energy formula implied by Eq. (19) is not large enough to extend the region in which the theory agrees with experiment, although it is in the right direction. In fact, a considerable extension of the range in which theory and experiment agree could be obtained by arbitrarily taking E_0'' about one-fifth the value used here. Wigner has emphasized that the breakdown of his theory beyond $A = 52$ probably results in large part from the neglect of the effect of the Coulomb interaction in coupling together states with different types of symmetry. Precisely this coupling or mixing effect is neglected in Eq. (2) since the symmetry properties of a wave function are not changed by a change of scale. Consequently it seems best to defer the application of Eq. (20) to the problem of nuclear stability until reliable estimates of the mixing effect and of the Coulomb exchange energy are available. Then it may become possible to determine E_0'' directly from stability relations among isobars.

Resonance Broadening of the Sodium *D* Lines

KENICHI WATANABE*
California Institute of Technology, Pasadena, California
(Received December 2, 1940)

By direct measurement of the contours of the line wings, the resonance broadening of the sodium *D* lines in absorption was determined for vapor pressures of sodium ranging from 10^{-3} to 70 mm Hg with negligible amount of foreign gases. Over nearly the entire range, the half-intensity width varied linearly with the density of the absorbing atoms; i.e., $\Delta\nu_{\frac{1}{2}}/N=0.80\times10^{-7}$ sec.$^{-1}$ cm^{-3}—the constant being 1.6 times that predicted by theory but much less than the corresponding experimental results for potassium. Above 5 mm pressure, $\Delta\nu_{\frac{1}{2}}$ increased slightly faster than N; moreover, the contour for the absorption coefficient was more adequately represented by an inverse cube contour than by the inverse square. Somewhat in contradiction to theory, the relative width, $\Delta\nu_{\frac{1}{2},c}/\Delta\nu_{\frac{1}{2},l}$ was 1.12. No definite evidence of van der Waals force was observed at the higher pressures; likewise no appreciable shifts or asymmetries. The natural width measured was consistent with previous results.

PRIOR to the present investigation of sodium and Chen's simultaneous study of rubidium,[1] the only substantial experimental work on resonance broadening of spectral lines appears to be that by Hughes and Lloyd[2] on potassium resonance lines. They were able to overcome a major experimental difficulty by employing MgO windows[3] which resist alkali vapors to relatively high temperatures. In agreement with theory, their result showed a linear dependence on the half-intensity width, $\Delta\nu_{\frac{1}{2}}$, with the density of the absorbing atoms, N; however, the absolute value of the proportionality constant they obtained was several times larger than theoretical predictions. Particularly, a theoretical paper by Houston[4] raises some doubt as to the accuracy of their results. In addition to the inadequacy of the vapor pressure curve used for potassium, it is thought that their temperature determination involved some uncertainty and their photometry required large corrections. From these considerations, sodium was selected for the present investigation on resonance broadening.

PROCEDURE

The experimental procedure used in this investigation is essentially the same as that described by Hughes and Lloyd.[2] The most important improvement is the provision for a reproducible metallic contact for the Chromel-Alumel thermocouple which measured the temperature of the absorption cell. Repeated *in situ* calibration showed only a small consistent temperature gradient between the thermocouple junction and the absorption cell, whereas in the case of Hughes and Lloyd there was a relatively large gradient with considerable uncertainty and lack of reproducibility. The temperature of the absorption cell was kept constant to within one degree during an exposure and the saturation value of Na vapor was usually assured by the presence of liquid Na.

The following equation by E. Thiele[5] provided the vapor pressure of Na:

$$\log_{10} p(\mathrm{Na}) = -26{,}244/(4.573T) - 1.178\log_{10} T + 11.402, \quad (1)$$

where p is in mm Hg. This equation was considered sufficiently accurate in view of the uncertainties in the photometry. In contrast to the case of potassium, no extrapolation was necessary over the entire range investigated. For relatively high temperatures the vapor pressure of sodium molecules becomes appreciable. Thiele[5] gives

$$\log_{10} p(\mathrm{Na_2}) = -7020/T + 8.149 \quad (2)$$

for the vapor pressure of sodium molecules.

The error in photometry was minimized by repeated *in situ* calibration of the step weakeners used by means of rotating sectors. The Eastman

* Now at the University of Hawaii, Honolulu, T. H.
[1] S. Y. Chen, Phys. Rev. **58**, 884 (1940).
[2] D. S. Hughes and P. E. Lloyd, Phys. Rev. **52**, 1215 (1937).
[3] J. Strong and R. T. Brice, J. Opt. Soc. Am. **25**, 207 (1935).
[4] W. V. Houston, Phys. Rev. **54**, 884 (1938).
[5] E. Thiele, Ann. d. Physik **14**, 970 (1932).

TABLE I. *Results on the resonance broadening of sodium D lines.*

	T	p	N	$\Delta\nu_{\frac{1}{2},1}/N$	$\Delta\nu_{\frac{1}{2},2}/N$	$\Delta\nu_{\frac{1}{2},2}/\Delta\nu_{\frac{1}{2},1}$
1	510	9.34×10^{-4}	1.78×10^{13}	?	?	0.97
2	550	5.50×10^{-3}	9.71	1.14×10^{-7}	1.25×10^{-7}	1.09
3	569	1.18×10^{-2}	2.02×10^{14}	0.79	1.02	1.05
4	570	1.22	2.10	0.73	0.75	1.03
5	601	3.81	6.16	0.73	0.77	1.05
6	601	3.81	6.16	0.57	0.68	1.19
7	$643\frac{1}{2}$	1.50×10^{-1}	2.27×10^{15}	0.80	0.97	1.20
8	645	1.57	2.37	0.80	1.03	1.28
9	669	3.14	4.56	0.90	1.14	1.29
10	701	7.29	1.01×10^{16}	0.93	0.96	1.04
11	719	1.13×10^{0}	1.53	0.63	0.74	1.18
12	783	4.62	5.73	0.59		
13	796	5.96	7.28	0.79		
14	840	1.33×10^{1}	1.54×10^{17}	1.06		
15	878	2.50	2.27	1.17		
16	951	7.23	7.38	1.1		

type I-D and type I-B plates used required for the most part very small corrections for varying sensitivity between the two members of the doublet. The exposure time was usually less than one hour without recourse to hypersensitization. The spectrograms were obtained by using a Rowland grating with 2.64A/mm dispersion in the first order and the traces of the lines and step weakener images were recorded by a Küss microphotometer.

The absorption tube lengths were 0.22 and 7.47 cm. The f values were taken to be $f_1=\frac{1}{3}$ and $f_2=\frac{2}{3}$ for the D_1 and D_2 lines, respectively, although there is some doubt as to the use of f values in the case of lines strongly broadened by resonance forces.

CALCULATION

For the most part the intensity distribution of the line was determined by measuring the transmission of the line wings with the aid of the step weakener traces. Usually the microphotometer traces required only small linear corrections for the varying sensitivity of the plates and the lines were as a rule symmetrical. Consequently when there was no overlapping of the lines, both wings of each line were averaged together.

The experimental intensity distribution was compared with the dispersion equation for the absorption coefficient,

$$\alpha x = -\ln\,(I/I_0) = \frac{Kx\Delta\nu_{\frac{1}{2}}/2\pi}{(\nu_0-\nu)^2+(\Delta\nu_{\frac{1}{2}}/2)^2}, \qquad (3)$$

where $K=(\pi e^2/mc)Nf_i$ sec.$^{-1}$, x is the absorbing path length, e is the electronic charge in e.s.u. and I/I_0 is the transmission (about 0.35 to 0.95). This equation was usually adequate, except for the incompletely resolved lines and the lines corresponding to vapor pressure of Na above about 5 mm.

Equation (3) was transformed to

$$y=C_iz-C' \qquad i=1 \text{ or } 2$$

where $y=(\Delta\lambda)^2$, $z=[-\log_{10}(I/I_0)]^{-1}$ and $C_i=k_iNx\Delta\nu_{\frac{1}{2}}$, k_i being equal to $(\lambda_{0i}^4e^2f_i)/(2mc^3\log_e 10)$. The graph was usually linear and the value C_i gave the half-intensity width.

The incompletely resolved lines were measured by the area method.[6] Near the region of natural broadening the half-intensity widths for resonance broadening and for natural broadening were considered simply additive on the basis of the similarity of their dispersion equations. Hence the theoretical value of natural width was always subtracted from the measured width. Moreover calculation shows that Doppler broadening can be neglected.

For vapor pressure above 0.5 mm, the D lines overlapped partially or completely. For partial overlapping corrections were made according to the degree of overlapping. For completely overlapped lines the wings were treated as caused by a single line—taking into consideration the separation of the two lines. For vapor pressure above 20 mm, measurements become

[6] R. Ladenburg and F. Reiche, Ann. d. Physik **42**, 181 (1913).

difficult because of the conspicuous appearance of the Na_2 bands.

Theoretical Values

Weisskopf,[7] Margenau and Watson,[8] and Furssow and Wlassow[9] have given similar theoretical values for the half-intensity width of resonance broadening,

$$\Delta\nu_{\frac{1}{2}}=k(e^2f/mv_0\pi)N \text{ sec.}^{-1}, \quad (5)$$

where k equals $\frac{1}{4}$, $\frac{1}{2}$, and $\frac{2}{3}$, respectively. Houston[4] has treated the problem in terms of fine structures and has given

$$\Delta\nu_{\frac{1}{2}}=2\pi(6)^{\frac{1}{2}}S(J, J')N/\{h(2J+1)(2J'+1)\} \text{ sec.}^{-1}, \quad (6)$$

where $S(J, J')=(2J'+1)e^2h/8\pi^2mv_0$ for the resonance lines of the alkalis, while J and J' are the inner quantum numbers for the ground and the excited states, respectively. Accordingly

$$\Delta\nu_{\frac{1}{2}}=(6)^{\frac{1}{2}}Ne^2/8\pi mv_0 \text{ sec.}^{-1} \quad (7)$$

for each member of the alkali doublets. This gives

$$\Delta\nu_{\frac{1}{2}}=0.49N\times10^{-7} \text{ for Na.} \quad (8)$$

The natural width for sodium is

$$\Delta\nu_{\frac{1}{2}}=1.01\times10^{7} \text{ sec.}^{-1}. \quad (9)$$

Results

The experimental results are summarized in Table I.

The mean value of $\Delta\nu_{\frac{1}{2}}/N$ is 0.80×10^{-7} sec.$^{-1}$ by taking the values 4–13 as being most reliable. This result is seen to be about 1.6 times the theoretical value given by Eq. (8). Since nearly all the experimental errors tend to broaden the lines, the values 0.80×10^{-7} sec.$^{-1}$ for Na is probably slightly too high and possibly too high by as much as twenty percent, the order of experimental error.

The natural width was measured for the narrowest lines by subtracting the resonance width obtained above from the total measured width. The results were consistent with previous measurement and in agreement with Eq. (10). This provided a rough check for the value of resonance broadening.

A serious discrepancy was the ratio of the half-widths, $\Delta\nu_{\frac{1}{2},s}/\Delta\nu_{\frac{1}{2},l}$, which was found to be 1.12 for Na, while the theory[4] gives unity. Since the more intense line is relatively wider and since the measurement of the ratio is comparatively easy, the experimental value cannot be very much in error.

The microphotometer traces of the D lines showed symmetry in nearly every plate. Slight asymmetries in some were of the order of the variation in the sensitivity of the plates. There were also no appreciable shifts in the lines even at the highest temperature. It was impossible to measure plates for vapor pressure above 70 mm, for there was hardly any measurable background because of the absorption of the Na_2 bands.

The author is indebted to Dr. I. S. Bowen for important suggestions and kind guidance, to Dr. W. V. Houston for clarifying some of the theories, to Mr. Clifford Truesdell for taking some measurements, and to Dr. P. E. Lloyd for valuable suggestions concerning experimental techniques.

[7] V. Weisskopf, Zeits. f. Physik **75**, 287 (1932).
[8] H. Margenau and W. W. Watson, Rev. Mod. Phys. **8**, 22 (1936).
[9] Furssow and Wlassow, Physik. Zeits. Sowjetunion **10**, 379 (1936).

The Absorption of Resonance Neutrons by Boron, Chlorine, Cobalt and Manganese

W. J. HORVATH AND E. O. SALANT
Department of Physics, New York University, Washington Square, New York, New York
(Received November 4, 1940)

Measurements are made of the absorption of neutrons by boron and by several elements which capture the neutrons without activity (or with very weak activity). Rh, In, Ag, Mn, Br and I were used as thermal and resonance detectors, and their known boron absorption coefficients were redetermined more carefully. The resonance levels of only Rh and In appeared to be single. It is shown that, by comparing the boron absorption coefficients with the absorption coefficients of the nonradioactive elements, resonance levels of those elements can be located: Resonances are found for Cl^{36} near 1 volt, for Co^{58} near 1 and 30 volts, for Mn below 0.4 volt. Corrections for nonparallelism of the neutron beam are made semi-empirically and neutron scattering by the absorbers is shown to be quite small compared to neutron capture.

INTRODUCTION

AS is now well recognized, the cross section of boron for slow neutron capture varies inversely as the velocity of the neutrons, and this law has been used by many experimenters[1] to determine the resonance energies of a number of elements showing induced radioactivity. However, many elements capture neutrons with no activity or with only very weak activity, so that for these substances the boron absorption method fails as a means of detecting resonance levels.

We present here measurements which make possible the detection and rough location of resonance levels of such elements. Suppose that there is available a series of radioactive detectors with known resonance levels. Then our method of finding resonance levels in some element consists of using that element as an absorber of the neutrons activating these different detectors.

Since each detector is (under favorable circumstances) activated by neutrons of a single narrow band of energies, we thus obtain the capture cross section of the absorber for the neutrons of energy corresponding to the energies of the known resonance levels. If the absorber has no levels overlapping those of the detectors, then its capture cross section will vary inversely as the velocity of the neutrons detected,[2] as one finds for boron; if, on the other hand, it has a level overlapping a resonance level of one of the detectors, those resonance neutrons will be absorbed more strongly, relative to the resonance neutrons of the detectors, than would be indicated by the inverse velocity law. If, for example, a certain element captures 5-volt neutrons more strongly than 1-volt neutrons, that element has a resonance level in the neighborhood of 5 volts; or, another example, if an element captures 5- and 10-volt neutrons according to the inverse velocity law, but 1-volt neutrons much more strongly than predicted by that law, the element has a resonance level in the 1-volt region.

Of course, all this presupposes an exact knowledge of the resonance levels of the detectors. The levels of the detectors used by us were redetermined rather carefully, by measuring their boron absorption coefficients. This was done both to insure that the geometrical conditions in the measurements of the absorption with boron and with the element to be investigated were the same, and to discover and allow for multiplicity of the levels in any detector, only rhodium and indium being found to have single levels. The presence or absence of a resonance level of an absorbing element in the neighborhood of the levels of the detectors depends, then, on comparing the element's absorption with the boron absorption of the neutrons inducing the activities in the various detectors.

OBLIQUITY CORRECTIONS IN MEASUREMENTS OF NEUTRON ABSORPTION COEFFICIENTS

It is well known that slow neutrons do not emerge from a paraffin surface as a parallel beam.

[1] O. R. Frisch and G. Placzek, Nature **137**, 905 (1937); Weekes, Livingston and Bethe, Phys. Rev. **49**, 471 (1936); E. Amaldi and E. Fermi, Phys. Rev. **50**, 899 (1936); H. H. Goldsmith and F. Rasetti, Phys. Rev. **50**, 328 (1936); Norling and Fleischman, Zeits. f. Physik **108**, 483 (1938).
[2] E. Wigner and G. Breit, Phys. Rev. **50**, 1191 (1936).

Fermi[3] has shown that, theoretically, the number of slow neutrons which leave the paraffin in the element of solid angle $d\omega$ is proportional to

$$f(\theta)d\omega = (\cos\theta + \sqrt{3}\cos^2\theta)d\omega.$$

This law was verified experimentally by Hoffman and Livingston[4] for thermal neutrons and has also been applied to slow neutrons of higher than thermal energy, though without very adequate justification.

Because of the nonparallelism of the beam, the measurement of the transmission of neutrons through a substance in this beam gives us an apparent absorption coefficient which must then be corrected with the aid of the Fermi law to give the true absorption coefficient. This correction is not easily made because the Fermi law holds only for a detector in contact with the paraffin surface. However, under actual experimental conditions, the detector is placed at some convenient height above the paraffin, so that sufficient space is left to insert an absorber. With this arrangement, one must allow for the fact that neutrons emerging at very large angles to the normal to the paraffin will entirely miss the detector, because of its limited size. This, together with the fact that the neutron intensity diminishes in going from the center to the edges of the paraffin, tends to make the obliquity correction smaller than it would be if the detector were placed on top of the paraffin.

Moreover, a different obliquity correction must be applied to each detector, depending on the absorption of neutrons within the detector material. For this purpose we consider only the two ideal cases of "thick" and "thin" detectors. A "thick" detector is one in which all neutrons are captured within a depth from which all electrons emerge; a "thin" detector is one in which only a small fraction of its activating neutrons is captured. It can be shown that the thin detector, because it has a higher probability of capturing neutrons incident obliquely than neutrons incident normally, will, with the same absorber, give a larger absorption coefficient than will a thick detector (for which the probability of neutron capture is independent of the direction). This effect turns out to be quite small in practice.[5]

Undoubtedly, inadequate correction for some of these geometrical effects is one of the chief causes of the many disagreements in boron (and other) absorption coefficients in the literature.

O. R. Frisch[6] has given calculations taking into account these effects. Inasmuch as those neutrons leaving the paraffin surface at a very small angle will miss the detector entirely, he makes the assumption that the Fermi distribution $f(\theta) = \cos\theta + \sqrt{3}\cos^2\theta$ is valid only for angles θ (measured from the normal) less than some critical angle θ_0; and that neutrons making angles greater than θ_0 with the normal will not be detected. In choosing a suitable value of θ_0 one must take into account not only the height of the detector above the paraffin surface but also the shape and size of the detector and of the surface, as well as the distribution of the neutron intensity over the surface. With this assumption, the transmission, T, of an absorber of thickness X is given by

$$T = \frac{\int_0^{\theta_0}\int_0^{2\pi} Je^{-kx}\sin\theta d\theta d\varphi}{\int_0^{\theta_0}\int_0^{2\pi} J\sin\theta d\theta d\varphi},$$

where $J = \cos\theta(1+\sqrt{3}\cos\theta)$ for a thick detector and $J = 1+\sqrt{3}\cos\theta$ for a thin detector.

The integrals were evaluated in Frisch's paper, together with f, the ratio of the measured to the true absorption coefficient, for various critical angles θ_0. For a value of θ_0 as large as 60°, f is nearly independent of absorber thickness, so that the absorption is effectively exponential. For θ_0 smaller than 45°, $f = 2/(1+\cos\theta_0)$ for both thick and thin detectors.

In making the obliquity corrections in our work, we used this formula for angles smaller than 45°; and, as will be seen, the corrections for larger angles were then obtained experimentally from the results for small angles.

[3] E. Fermi, Ricerca Scient. **7**, No. 13 (1936).
[4] J. G. Hoffman and M. S. Livingston, Phys. Rev. **53**, 1020 (1938).
[5] Hornbostel, Goldsmith and Manley, Phys. Rev. **58**, 18 (1940).
[6] O. R. Frisch, Kgl. Danske Vidensk. Selskab. Math. Phys. Medd. **14**, 12 (1937).

Experimental Procedure

Our neutron source consisted of a 200-millicurie Ra-Be mixture, placed 3 cm beneath the top of a paraffin cylinder 15 cm high and 25 cm in diameter. The arrangement for irradiating detectors is shown in Fig. 1. Detectors and absorbers were placed on an aluminum platform which moved on steel rails placed on two sides of the paraffin cylinder. This allows the experimenter to place the detectors and absorbers accurately in position while remaining at a safe distance from the source. The platform was centered over the cylinder by means of steel stops which were placed on the rails. This arrangement proved satisfactorily repeatable, the standard deviation of any set of measurements never being more than that expected from the total number of particles counted.

The detectors were kept at a fixed height of 3.8 cm above the paraffin surface by means of an aluminum stand fastened to the sliding platform. With this arrangement we were able to insert absorbers up to a thickness of 2.5 cm on top of the sliding platform.

The absorbers of the elements investigated were generally made up in powder form. For cobalt and manganese we were able to obtain the pure metal, but for boron we used either anhydrous boric acid (pure B_2O_3), or boron carbide (B_4C). The chlorine absorbers were made up of chemically pure carbon tetrachloride.

The powdered absorbers were placed in thin aluminum cans, of the same cross section as the paraffin cylinder. No absorption of slow neutrons by the empty cans could be detected, and, indeed, calculations with the known total cross section of aluminum showed that, in the thicknesses used by us, the absorption was negligible. The cans were carefully filled to insure a uniform thickness of absorbing material throughout the whole area. The containers for the carbon tetrachloride were of soldered iron, of the same size as the aluminum cans. The effect of the iron was allowed for experimentally by leaving the empty cans in place when the counts without absorber were taken. In order to simplify the geometrical corrections, the absorbers were always inserted directly beneath the detectors rather than on the top surface of the moving platform. The purpose

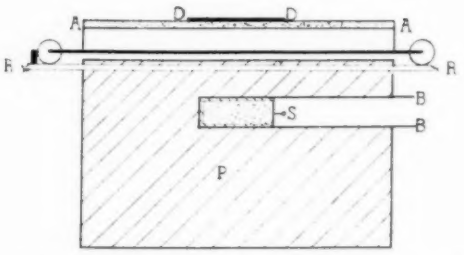

Fig. 1. Neutron source and arrangement for irradiating detectors. *D*—detector, *A*—absorber, *R*—steel rail. *B*—brass tube, *S*—source, *P*—paraffin.

of this arrangement was to minimize the effect of scattering; a discussion of the magnitude of this effect is given in the section on experimental results.

Only six resonance detectors gave sufficient intensity with our source: rhodium, indium, silver, manganese, bromine and iodine. The rhodium, indium and silver were used as rolled foils of the pure metal. The other detectors were in powder form and cast into thin slabs by mixing with a dilute solution of "Duco cement," the amount of slowing produced by the hydrogenous material introduced this way being completely negligible. The iodine, bromine and manganese detectors were used as compounds; for iodine we used lead iodide, PbI_2, and iodoform, CHI_3; for bromine we used lead bromide, $PbBr_2$, and hexabromethane, C_2Br_6; for manganese we used the oxide MnO_2, as well as the pure metal powder. The results obtained with different compounds for the same detector were always consistent with one another and with results obtained using detectors without binder.

All of the resonance detectors except manganese fitted our criterion for "thick" detectors. Manganese and the thermal detectors had such small neutron absorption coefficients that they may be considered "thin."

We found that the most efficient way of using a detector was to cut it into four rectangular pieces, each piece 22 mm by 40 mm. These were placed on the irradiating platform so as to form a detecting surface 44 mm by 80 mm. After irradiation, they were removed and fastened to a rectangular frame, fitting over the Geiger counter, which was thus surrounded on all sides by the activated material. This procedure was carefully standardized, so that the same part of the frame

was always opposite the same part of the Geiger counter.

The recording apparatus consisted of an amplifier with a Neher-Harper circuit, a stabilized high voltage supply and a scale-of-eight counter. All electrical parts were checked to insure stability. Sufficient resolving power was provided so that, even at the highest counting rates used, the number of particles missed was less than 0.1 percent.

Experimental Results

I. Determination of corrections

With the detector at a height of 3.8 cm above the paraffin, evaluation of the critical angle θ_0 from the geometrical arrangements is not very easy. However, by measuring the intensity of neutrons over the surface and by a rather complicated numerical integration, the value $\theta_0 \backsimeq 65°$ was obtained for iodine and rhodium resonance neutrons. Since the calculation of f (the ratio of measured to true absorption coefficient) under these circumstances would not be very accurate, we proceeded to evaluate this factor experimentally.

With rhodium, there was sufficient intensity to place the detector 14.3 cm above the paraffin and to reduce the aperture of the emitting surface of the paraffin to a 10-cm square (by means of a diaphragm of 1.2 g/cm² of boron). The critical angle was carefully evaluated by taking into account the variation of neutron flux from different parts of the surface and was found to be 27°. For this value of θ_0 the correction factor f is accurately determined by the Frisch relation $f=2/(1+\cos\theta_0)$. We obtained a value of 1.06 (± 0.01). Thus, by measuring the boron absorption of Rh resonance neutrons with this good geometry, the true absorption coefficient of B for these neutrons was found to be $K=5.37$ and the same value, to within 1 percent, was found for indium resonance neutrons.

A similar procedure with thermal neutrons gave a true boron absorption coefficient $K_{th}=30.2$ (± 0.3).

Having found the true boron absorption coefficient, we then measured the absorption coefficient with the Rh detector at 3.8 cm above the paraffin, without any diaphragm (that is, under geometrical conditions to be employed in all our other absorption measurements). The ratio of this value to the previously determined true boron absorption coefficient then gave the value of f for the detector at 3.8 cm. Since f, under a fixed geometry, depends, for resonance neutrons, only on the geometry, this value of f, 1.32, could then be used to correct all the absorption measurements with other detectors and other absorbers.

The method employed is, thus, semi-empirical; the true absorption coefficient for boron is obtained under conditions where the Frisch theory is reliable and the correction factor f, under the conditions of our other experiments, is obtained experimentally by comparison with this true coefficient.

The results of the boron absorption measurements with the Rh detector on the 3.8-cm platform appear in Table I. A filter of 0.5 g/cm² of Cd was used to distinguish the thermal neutrons. All transmissions are good to about ± 0.5 percent of the transmission value.

Curves of these values are plotted in Figs. 2 and 3. As predicted by Frisch for a critical angle of about 65°, these curves are closely exponential. However, because of their inhomogeneity, thermal neutrons are not expected to be absorbed exponentially at still lower transmissions; this effect is discussed below.

The two corrected transmission curves appear in Figs. 4 and 5, together with theoretical curves of Frisch for various effective angles θ_0. It will be noticed that the curve for resonance neutrons falls in between Frisch's theoretical thick detector curves for $\theta_0=60°$ and $\theta_0=71°$. In fact, it

Table I. *Transmission through boron.*

δ, g/cm² Boron	% Trans. Rh (44 sec.) Detector	% Trans. Mn Detector
	Thermal Neutrons	
0.0047	80.0	78.7
0.0143	57.3	53.9
0.0230	40.2	37.6
0.0299	32.2	29.2
0.108	—	2.9
	Resonance Neutrons	
0.0143	90.0	
0.0230	84.1	
0.0299	80.4	
0.108	46.5	
0.207	23.2	

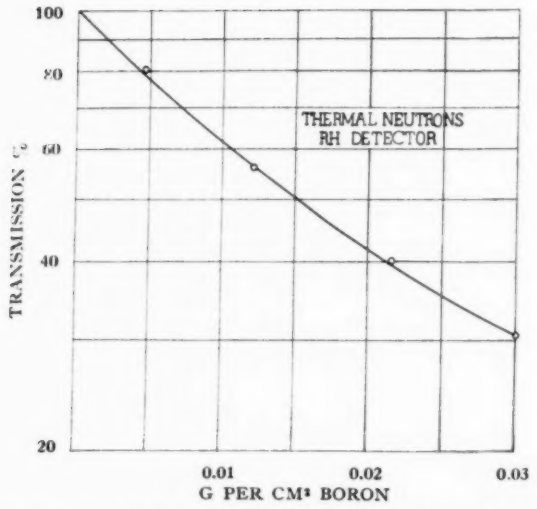

FIG. 2. Transmission of thermal neutrons through boron.

corresponds very closely to the $\theta_0 \backsimeq 65°$ which we had previously estimated for our geometry by an independent method. Our curve for thermal neutrons coincides with Frisch's thin detector curve for $\theta_0 = 60°$. One can understand that thermal neutrons should have a smaller critical angle than resonance neutrons because their longer mean free path in paraffin gives rise to a different intensity distribution over the surface. (The effect is to make the paraffin surface appear larger to a thermal detector than to a resonance detector.)

In order to study the boron absorption of thermal neutrons at low transmission values, we prepared some manganese thermal detectors. These enabled us to follow the curve down to 2.9 percent transmission. Here the observed deviation from the exponential law was equal to the deviation calculated with a Maxwellian distribution of neutron velocities; its amount was such as to make the absorption coefficient at 2.9 percent transmission 1.32 times the absorption coefficient at 53.9 percent transmission. (See Table I.)

It will be noticed that the transmissions measured with the Mn detector are always lower than those measured with the Rh detector. Ag and In, used as thermal detectors, did not show this behavior, their transmissions being in agreement with the Rh values. We were thus led to suspect a resonance level for Mn in the energy region of C neutrons (those not transmitted by cadmium). For this reason, an investigation of manganese as an absorbor was made.

II. Boron absorptions with various resonance detectors

Having determined the geometrical correction with one resonance detector, we measured the boron absorption coefficients with our other detectors under this standard geometry. All absorption coefficients given in this and the following sections are, accordingly, corrected, true absorption coefficients. It is well to note here that our measurements give us only the total absorption coefficient, which includes not only the capture but also a fraction of the scattering coefficient as well; nevertheless, the scattering by boron is sufficiently low[7] to justify equating the total absorption and the capture coefficients of boron, and this equality is assumed throughout this work. A further discussion of scattering is given below.

A more careful investigation of the boron absorption of In resonance neutrons than that mentioned previously appears in Table II.

Thus the absorption coefficient for In, 5.30 ± 0.02 cm²/g, as compared with 5.37 ± 0.02 cm²/g for Rh, indicates that the In resonance level is at a slightly higher energy. As an added check, Hg was used as an absorber with these two detectors:

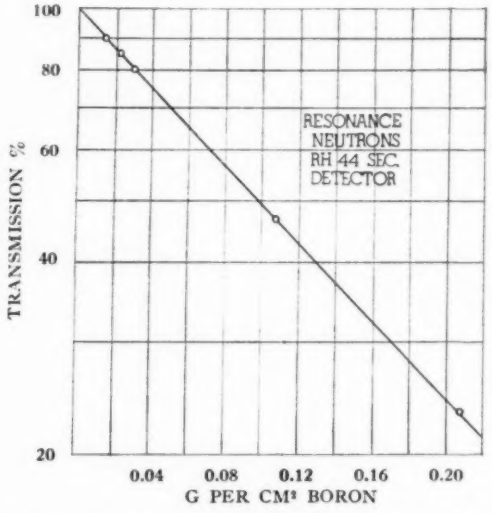

FIG. 3. Transmission of resonance neutrons through boron.

[7] F. Norling and R. Fleischman, Zeits. f. Physik **108**, 483 (1938).

following Goldsmith and Manley,[8] we assume that its absorption varies inversely as the fifth power of the neutron velocity, and hence is more sensitive to energy differences in this region. In this way it was found that the In resonance energy was higher than the Rh by the amount indicated by the boron absorptions, the energy values from these measurements being 0.82 ev for Rh and 0.84 ev for In. These energies differ somewhat from the values of other authors[1] using similar methods, but the values reported by Bacher[9] agree well with ours. The order of the energies is in agreement with those of Goldsmith and Rasetti,[1] though they find a somewhat greater separation. Since the boron absorption curves for both detectors are good exponentials, both In and Rh must have single levels.

The boron absorption coefficients of the silver 22″, manganese 150′, iodine 25′ and bromine 20′ resonance activities are in Table III.

In all four cases the absorption coefficient decreases steadily as the absorber thickness increases, precisely the behavior to be expected if the neutrons are absorbed at two or more separate energy levels. Since we wish to compare the absorption coefficient of some other element with the boron absorption coefficient, we encounter the difficulty, then, of knowing which boron coefficient to choose.

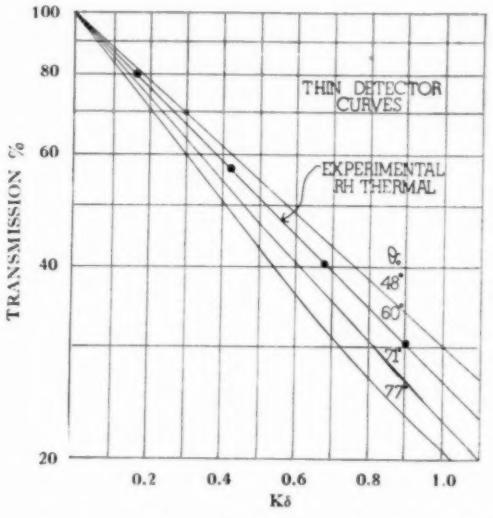

FIG. 4. Corrected transmission values for thermal neutrons with a thin detector and theoretical curves of Frisch for various angles.

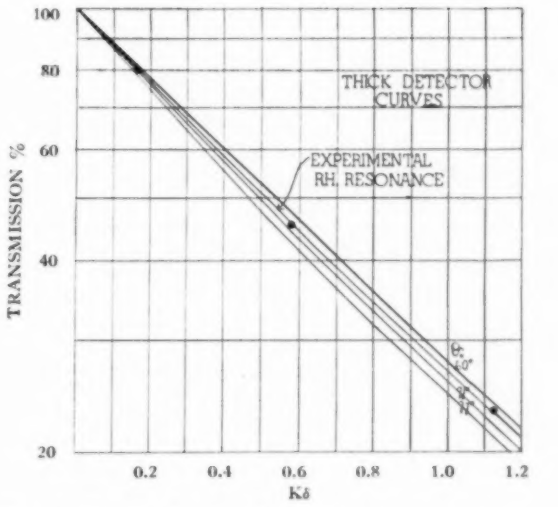

FIG. 5. Corrected transmission for resonance neutrons with a thick detector and theoretical curves of Frisch for various angles.

We are interested in determining whether the absorption of our other element follows the $1/v$ law, that is, the same law as does boron. If both boron and this element follow this law, then their absorption, with a multi-level detector, will vary with absorber thickness in exactly the same way. Thus if we compare their absorption coefficients for any pair of identical values of the transmission, the ratio should be constant. Hence, in comparing the chosen element's absorption coefficient with that of boron, the boron coefficient chosen was the one for the same percentage transmission shown by the element; this was done for several values of the transmission, except with iodine and bromine detectors, where the geometrical arrangements did not permit more than one thickness of absorber.

With boron coefficients selected in this way, the ratio of coefficients for two different detectors, compared to the same ratio with the other element as absorber, will show whether that element follows the $1/v$ law or has resonances, even if the detector has more than one level.

III. Absorption by chlorine, cobalt and manganese

We selected chlorine and cobalt for this work because both elements exhibit a large total cross section for thermal neutrons. Despite their large

[8] H. H. Goldsmith and J. H. Manley, Phys. Rev. **51**, 382A (1937).
[9] C. P. Baker and R. F. Bacher, Phys. Rev. **57**, 1076A (1940).

TABLE II. *Percent transmissions* Rh *and* In *resonance neutrons.*

DETECTOR	δ, 0.030 G/CM² B	δ, 0.108 G/CM² B
Rh	80.4±0.3	46.5±0.2
In	80.8±0.3	46.9±0.2

cross sections we were able to induce only a very weak 40-minute period in chlorine (previously identified as Cl^{38})[10] and a still weaker 11-minute period in Co (Co^{58}).[10] If these activities were to be ascribed to the large neutron capture cross sections, then the activity in Cl should have been 100 times greater than found, and that in Co 600 times greater. Since each element has only two stable isotopes, we concluded that the large capture cross sections are involved in the production of Cl^{36} and Co^{60}. A similar argument has been advanced by Kikuchi[11] on the basis of the cross section for the production of capture γ-rays. Recent work[12] has shown that Co^{60} has a half-life of several years and some unpublished work of Grahame[10] shows a similar behavior for Cl^{36}. Our absorption method is peculiarly suited to the study of their resonance levels, since it is not feasible with a natural source to look for them by the usual method of studying the effect of boron absorbers on the induced radioactivity.

We have already mentioned the reason for investigating the absorption of manganese.

The absorption of neutrons by these elements was measured with the six detectors whose boron absorption coefficients had already been determined. Wherever practicable, several different thicknesses of absorber were used; the absorption coefficients of Cl and Co were good to better than 1 percent, the coefficient of Mn to only 2–3 percent, because of its much weaker absorption.

Rh and Ag served as thermal neutron detectors, and in all cases the same value of absorption coefficient was obtained with both detectors. When Mn was tried as a thermal detector, higher values of the absorption coefficients of Cl, Co, and Mn were found, just as with the boron absorber.

[10] For a summary of induced radioactivities see J. J. Livingood and G. T. Seaborg, Rev. Mod. Phys. **12**, 30 (1940).
[11] Kikuchi, Takeda, and Ito, Proc. Math.-Phys. Soc. Japan **19**, No. 1 (1937).
[12] J. Risser, Phys. Rev. **52**, 768 (1937).

The results of typical runs are given in Table IV, showing the good agreement attainable for different thicknesses when neutrons of homogeneous energy are detected.

Table V shows the absorption coefficients of B, Cl, Co, and Mn, as measured with the various detectors. As already pointed out, the boron absorption coefficients for all neutrons except those of the Rh and In resonances really refer to more than one resonance energy. However, to fix the order of the resonance energies of the different detectors, and to facilitate discussion, the energy corresponding to each boron absorption coefficient is calculated as if due to a single energy and it is in this way that the column of resonance energies in Table V is evaluated.

The following features in Table V are to be noticed, under the assumption, for the moment, that the total absorption coefficient K is not sensibly different from the capture coefficient, K_c, and with our discussion confined to K.

(1) The Cl coefficient is greater at 0.84 ev than at 0.82 ev, just the inverse of the B coefficient; thereafter, the Cl absorption coefficient decreases steadily with increasing energy. We conclude, therefore, that there is a Cl resonance level near 1 ev, somewhat beyond the In resonance level. Additional evidence for this is obtained by com-

TABLE III. *Boron absorption.*

δ, G/CM² BORON	% TRANS.	K, ABS. COEFF. CM²/G
	Silver detector	
0.030	89.0	2.75
0.108	67.4	2.70
0.207	51.5	2.39
0.268	44.9	2.24
0.420	30.7	2.13
	Manganese detector	
0.108	82.5	1.25
0.207	69.2	1.25
0.268	63.2	1.21
0.420	56.8	0.97
0.560	48.0	0.95
0.980	36.5	0.74
	Iodine detector	
0.108	86.9	0.97
0.207	76.8	0.94
0.420	64.9	0.79
0.980	37.9	0.75
	Bromine detector	
0.108	86.2	0.99
0.207	76.0	0.97
0.420	63.5	0.81
0.980	37.1	0.78

paring the ratio K_{th}/K_{Rh} of Cl and of B; this ratio is 4.1 for Cl, and 5.6 for B. In other words, as one goes from thermal energy to 1 volt, the Cl absorption does not diminish as much as does a nonresonance, inverse velocity capture.

(2) In the region of 1 volt, Co behaves like Cl; its absorption coefficient for thermal neutrons is 4.6 times its absorption coefficient at 0.82 volt and the coefficient increases from 0.82 to 0.84 volt. Unlike Cl, the Co coefficient increases again at the Br and I resonance energies, indicating that it has another resonance level beyond the I energy, 27 volts. Downing and Ellis[13] using the method of slowing curves, reported Co resonances at 1 and 40 volts, in good agreement with these results.

(3) For Mn, the ratio of the absorption coefficients at 0.028 and 0.82 volt is 6.5, greater than the ratio 5.6 of the boron absorption coefficients. This indicates a resonance level of Mn below the limit of the Cd cut-off (less than 0.4 volt).

IV. Effect of scattering

We have based our discussion so far on the total coefficients, whereas in actuality the inverse velocity law applies to the capture coefficients only. We shall see, however, that in our experiments the scattering is so small that it does not change the conclusions drawn.

The evaluation of the effects of scattering is based on measurements of absorption by MnO_2. The total absorption coefficient of Mn having already been determined, we can find the effect of oxygen alone by assuming the additivity of cross section. (This is certainly valid at the higher energies.) Oxygen is known[14] to exhibit negligible capture, its effect on the neutron beam being due almost entirely to scattering. Our values of the total coefficient for oxygen are shown in Table VI.

We see that the coefficient is constant for different energies, as to be expected if it represents scattering only. But our value is only one-tenth the value, $K_s=0.15$, found by Goldhaber and others[15] for thermal neutrons. This is not unexpected, since in our arrangement there is considerable scattering into the beam, so that only a fraction of the true scattering coefficient is effective in our experiments. Pb and Fe showed a similar effective fraction of scattering of one-tenth, when their absorption was allowed for, and a rough theoretical evaluation of this effect showed that we might expect a factor of about $\frac{1}{8}$. By taking one-tenth the scattering coefficients of Goldhaber, then, we obtain the scattering coefficients effective in our experiments; these come out to be $K_s=0.005$ cm²/g for Co, $K_s=0.003$ cm²/g for Mn, and since only an upper limit has been given for the scattering of Cl, we can only say that $K_s<0.01$ cm²/g for Cl. These values are to be subtracted from the K values to obtain the coefficients K_c, and are, it is seen, quite unim-

TABLE IV. *Absorption coefficients for* Co *and* Cl.

δ, G/CM²	% TRANS.	K, ABS. COEFF. CM²/G
Thermal neutrons by Co		
0.960	67.0	0.313
1.94	44.8	0.312
3.00	28.8	0.315
Rh *Resonance neutrons by* Cl		
1.00	82.6	0.150
1.94	67.5	0.149
2.94	55.3	0.149

TABLE V. *Absorption coefficients for* B, Cl, Co *and* Mn.

DETECTOR	ENERGY, EV	ABS. COEFF., K, CM²/G			
		B	Cl	Co	Mn
Rh thermal	0.026	30.2	0.610	0.314	0.123
Rh 44 sec.	0.82	5.37	0.149	0.068	0.019
In 54 min.	0.84	5.30	0.161	0.070	0.019
Ag 22 sec.	3.3	2.70	0.110	0.039	0.014
Mn 150 min.	15	1.25	0.065	0.023	(0.79)*
Br 18 min.	25	0.97	0.058	0.032	0.020
I 25 min.	27	0.94	0.054	0.043	0.014

* Abs. coeff. at exact resonance measured with thin detector and thin absorber.

TABLE VI. *Oxygen scattering.*

DETECTOR	K_s, SCATTERING COEFF. CM²/G
Rh thermal	0.015
Rh 44 sec.	0.011
In 54 min.	0.012
Ag 22 sec.	0.012
Br 18 min.	0.012
I 25 min.	0.013

[13] A. E. Downing and C. D. Ellis, Nature **142**, 793 (1938).
[14] M. Goldhaber and G. H. Briggs, Proc. Roy. Soc. **A162**, 127 (1937).
[15] H. Carroll and J. R. Dunning, Phys. Rev. **54**, 541 (1938).

portant, except in the case of Mn, where the ratio of K_e for thermal and 0.82-volt neutrons becomes 7.5 instead of the 6.5 for B, thus making still more prominent the resonance in the thermal region.

It must be realized that, while the method outlined in this paper can show, and has shown, resonances in nuclei which are not activated, it has two drawbacks. One is that, with the few practicable detectors available, the chances are slight that the resonance bands of detectors and absorber will overlap sufficiently for a marked effect, and the other is that, if the absorbing element scatters strongly, the scattering correction is neither unimportant nor accurately calculable.

JANUARY 15, 1941 PHYSICAL REVIEW VOLUME 59

The X-Ray Spectra Arising from the Valence Band—L Transitions of Tungsten, Tungsten Oxide (WO_3) and Platinum*

J. A. BEARDEN AND T. M. SNYDER
Rowland Physical Laboratory, The Johns Hopkins University, Baltimore, Maryland

(Received November 1, 1940)

X-ray emission lines and absorption edges arising from transitions between the L levels and the valence bands of tungsten, tungsten oxide (WO_3) and platinum were studied with a double crystal spectrometer. Manning and Chodorow's calculation of the density of states in the 5*d* and 6*s* bands of tungsten is found to be in good agreement with the observed shapes of the tungsten absorption edges. The tungsten emission lines, on the other hand, do not have the structure expected from their calculation and are 4.5 ev narrower than the region of occupied states calculated for these bands. A comparison of the spectra of tungsten metal with those of its oxide shows: (1) the initial absorption maximum of the L_{II} and L_{III} edges is both broader and higher in the oxide, (2) the L edges of the oxide are shifted 2.5 ev to higher frequencies, (3) the emission lines of the oxide are about 3 ev wider than those of the metal. These differences between the spectra of the oxide and the metal are explained qualitatively in terms of the high electronegativity of oxygen. The platinum absorption edge structures observed are in agreement with what is qualitatively expected from the other properties of this metal. A marked difference in the relative intensity of corresponding structure features of the L_{II} and L_{III} edges is ascribed to a spin-orbit coupling of the valence electrons.

INTRODUCTION

PREVIOUS workers[1–5] have shown that the experimentally observed shapes of x-ray absorption limits and of those emission lines which arise through transitions from the valence bands characteristic of elements in a solid may be interpreted in terms of the density of states in the unfilled and filled portions of these bands. In the present work, the L-absorption edges and L-emission lines which involve transitions from the valence bands of tungsten and tungsten oxide and the L edges of platinum were studied. The shapes of the tungsten spectra are compared with that of the density-of-states of the 5*d* and 6*s* electrons of tungsten calculated by Manning and Chodorow.[6] The WO_3 and W spectra are compared and their differences explained in terms of the high electronegativity of oxygen. The shapes of the L edges of platinum are shown to be compatible with band structure expected for this metal from its other properties.

EXPERIMENTAL

The spectrometer, crystals, high voltage supply and intensity measuring apparatus used in this work have already been described elsewhere.[7] For absorption studies, the target of

* This research was supported by a grant-in-aid from the American Philosophical Society.

[1] H. M. O'Bryan and H. W. B. Skinner, Phys. Rev. **45**, 370 (1934).

[2] H. Jones, N. F. Mott and H. W. B. Skinner, Phys. Rev. **45**, 379 (1934).

[3] H. Jones and N. F. Mott, Proc. Roy. Soc. **162**, 49 (1937).

[4] A. Sandstrom, Zeits. f. Physik **66**, 784 (1930).

[5] W. Beeman and H. Friedman, Phys. Rev. **56**, 392 (1939).

[6] M. Manning and M. Chodorow, Phys. Rev. **56**, 787 (1939).

[7] J. A. Bearden and H. Friedman, Phys. Rev. **58**, 387 (1940).

TABLE I. *Widths of L levels of tungsten.*

	W	Pr	Au
L_{I}	4.9±1.0 ev	8.0±1.0 ev	8.7 ev
L_{II}	3.0±0.5	3.5±0.5	3.7
L_{III}	3.4±0.5	3.6±0.5	4.4

the x-ray tube was gold plated to give high intensity radiation. The absorbers used in the cases of tungsten and platinum consisted of thin rolled foils. In the case of tungsten oxide, the absorber was prepared by smearing a mixture of powdered WO_3 and thinned Duco cement on onion skin paper. Several layers were used to decrease irregularities in thickness. The remaining inhomogeneities caused only a loss of contrast in the absorption spectra. These absorbers were mounted between the tube and the first crystal on a rotating sector which facilitated moving them in and out of the x-ray beam when comparing direct and absorbed intensities and yet insured the absorbers being returned to the same position in the beam. In some cases, aluminum absorbers of known absorbing power had to be used to reduce the intensity of the radiation below the maximum of 8000 counts per minute allowed by the counting system. These foils were mounted either on the rotating sector or between the first and second crystals.

Because the spectrometer can be reset to 0.1 second, the procedure used was to run through the region of an absorption edge repeatedly in steps of ten or twenty seconds of arc, taking counts of both the direct and absorbed radiation at each point for several minutes. The measurements were corrected for scattered radiation which was taken to be the intensity passed by the spectrometer when the second crystal was turned five to ten degrees away from the Bragg angle. The error in an absorption curve caused by second-order radiation was tested for by repeating a number of points at low voltages. Except in the cases of the L_{III} edges of W and WO_3, this correction was found to be less than 6 percent in all cases and was neglected.

In the study of emission lines, the gold was removed from the target. A tungsten button spot-welded onto a nickel backing in hydrogen was soldered on in its place to obtain the tungsten metal lines. To obtain the tungsten lines from the oxide, two different targets were used. The first was made by pounding the WO_3 into a clean copper surface previously picked full of pockets by a fine steel point. The second was made by pounding it into lead. The two sets of measurements obtained from the two targets agreed well with each other. On exposure to the electron beam in the tube, the originally yellow WO_3 was found to acquire a bluish cast indicating the formation of blue W_2O_5. Chemical decomposition was tested for by running, at very low power, critical points of emission lines from a fresh target in order to observe any changes in their position or width with time. As no changes were observed, it was concluded that either (1) the amount of chemical change was negligible, (2) it took place too quickly to be detected, or (3) the emission lines of WO_3 and W_2O_5 are similar. The second possibility is unlikely. If either the first or third is correct, the width and wave-length of the WO_3 lines were obtained.

The wave-lengths of lines and edges were obtained by accurately locating their $(l+l)$ positions and reading off their angles in four microscopes. The $(l-l)$ angles were subsequently obtained and the computed diffraction angles corrected for the height of the slits and reduced[8] to a temperature of 18°C. Calibration corrections for the spectrometer circle, which are always less than 0.3″ of arc, were neglected.

Widths of absorption edges and emission lines

It has been shown by Richtmyer, Barnes and Ramberg[9] that the absorption coefficient of a metal as a function of the frequency in the neighborhood of an x-ray absorption edge is given by

$$\mu(\nu)=c\left\{\frac{1}{2}-\frac{1}{\pi}\tan^{-1}\left(\frac{\nu_{E_0}-\nu}{\Gamma/2}\right)\right\}$$

if there is a uniform density of unoccupied states in the valence bands. Here ν_{E_0} is the frequency corresponding to absorption into the first empty level above the Fermi surface and Γ is the full width at half maximum of the x-ray level involved in the absorption. The position of ν_{E_0} on the absorption edge is characterized by an

[8] J. A. Bearden and C. H. Shaw, Phys. Rev. **48**, 19 (1935).

[9] Richtmyer, Barnes and Ramberg, Phys. Rev. **46**, 843 (1934).

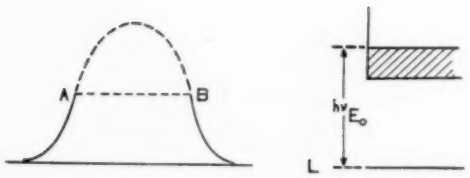

FIG. 1. (left) The shape of an emission band expected from considerations similar to those of Richtmyer, Barnes and Ramberg. A and B denote the inflection points on its sides. Their separation is the width of the region of occupied valence states. The sides below $\overline{AB}$ are arc tangent curves.

FIG. 2. (right) Energy level diagram for x-ray absorption and emission transitions between an L level and a valence band. $h\nu_{E_0}$ denotes energy of transition to Fermi surface. Shading designates region of filled states.

inflection point. These authors have also shown that even if the distribution of states is not uniform, the absorption edge will still have very nearly the same arc tangent form on the low frequency side of ν_{E_0} and the position of ν_{E_0} will still be at the inflection point on the edge. From this equation, the widths of the L levels of tungsten and platinum were obtained by finding for each absorption edge the best match on the low frequency side of the inflection point in a set of arc tangent curves drawn with various values of the parameters C and Γ. The widths so obtained were corrected for the rocking curve width of the crystals according to the equation of Parratt.[10] This correction amounted to between 0.5 and 1.0 electron volt in the present measurements. These widths are listed in Table I. Also listed for comparison are the results obtained by Richtmyer, Barnes and Ramberg[9] for the widths of the L levels of gold. The present results are seen to be in good agreement with these. The value of 3.6 ± 0.5 electron volts obtained for the L_{III} level of platinum agrees within the experimental errors with the value 4.1 ± 0.5 ev obtained by Beeman and Friedman.[5] From these widths, the widths of the other levels of tungsten and platinum could be obtained if the widths of their other emission lines were known, since it has been shown[11] that the width of an emission line is the sum of the widths of the initial and final states involved. In some preliminary tests, the width of the $L\beta_2$ line of tungsten involving the transition $L_{III}\rightarrow N_V$ was found to be 10.6 electron volts. This gives a width of 7.2 electron volts for the N_V level.

In the case of an emission line which arises from transitions from the filled states of a uniform density distribution of states in the valence bands to an unoccupied x-ray level, considerations similar to those of Richtmyer, Barnes and Ramberg[9] in the case of absorption limits show that its sides should have the shape of arc tangent curves below their inflection points. These two inflection points, designated by A and B in Fig. 1, mark the beginning and end of the transitions from the band of filled states. Their separation gives the width of the band. This is illustrated in Fig. 1 where A and B mark the inflection points on the sides of the emission band. (See footnote 6 in reference 7 for discussion of more general case.) This method of consideration is only valid if the width of the x-ray level is considerably less than the width of the band of filled valence states. The widths of the bands of filled valence states obtained in this manner are listed in Table II.

WAVE-LENGTHS OF ABSORPTION LIMITS AND EMISSION LINES

The theory of Richtmyer, Barnes and Ramberg mentioned above indicates that it is logical to call the inflection point in an absorption edge the position of the edge. This point corresponds to the transition from an x-ray level into the lowest unoccupied level in the valence band. This is the transition of energy $h\nu(E_0)$ in the energy level diagram of Fig. 2. For every absorption edge, there should be an emission band corresponding to transitions from the filled portions of the valence band to the x-ray level. Its high frequency side should coincide in wave-length with that of the absorption edge because the region of filled states leaves off where the region of empty states begins. This is seen to be the case for the L edges of tungsten metal and its oxide in Figs. 3 to 8, where the edges and their corresponding emission lines

TABLE II. *Widths of bands of filled valence states.*

TRANSITION	LINE	WO_2	W
	$L\gamma_1$	16.2 ev	16.2 ev
$5d$, $6s$ band$\rightarrow L_I$	$L\gamma_4''$	12.0 ± 6.0	12.0 ± 4.0
$5d$, $6s$ band$\rightarrow L_{II}$	$L\gamma_6$	10.5 ± 1.0	7.0 ± 0.5
$5d$, $6s$ band$\rightarrow L_{III}$	$L\beta_5$	8.9 ± 1.0	6.5 ± 0.5

[10] L. G. Parratt, Rev. Sci. Inst. **6**, 387 (1935).
[11] V. Weisskopf and E. Wigner, Zeits. f. Physik **63**, 54 (1930).

have been plotted together on the same wave-length scale. For convenience, the wave-length has been replaced by a scale of ev with the edge inflection point arbitrarily chosen as zero. It is to be noticed that the relative position of lines and edges in these figures is independent of the choice of the edge inflection point locations, and depends only on the accuracy of angular determinations by the instrument, which is better than ± 0.3 ev.

In Table III the wave-lengths of edges and those of line peaks are listed and compared with the results obtained by previous investigators.[12–15] Because this older work was done with low resolving power instruments, the wave-length of the center of an edge, rather than that of its inflection point, was given. This causes considerable disagreement with the present results in the cases where the edges themselves show structure, as occurs in the L_{I} edges. In all other cases, the agreement is seen to be good.

Discussion

The density of states of the 5*d* and 6*s* bands of tungsten has been calculated by Manning and Chodorow[6] using the cellular method of Wigner and Seitz[16] as modified by Slater.[17] In this method use is made of Bloch's theorem

$$\psi(\mathbf{r}) = u(\mathbf{r}) \exp\left[i(\mathbf{k}\cdot\mathbf{r})\right]$$

which says that any wave function $\psi(\mathbf{r})$ in a crystal is equal to a plane wave $\exp\left[i(\mathbf{k}\cdot\mathbf{r})\right]$ times a function $u(\mathbf{r})$ which is periodic with the

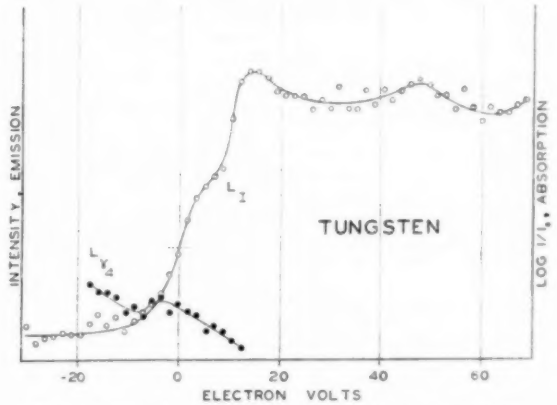

FIG. 3. The $L\gamma_4''$-emission line and L_{I}-absorption edge of tungsten.

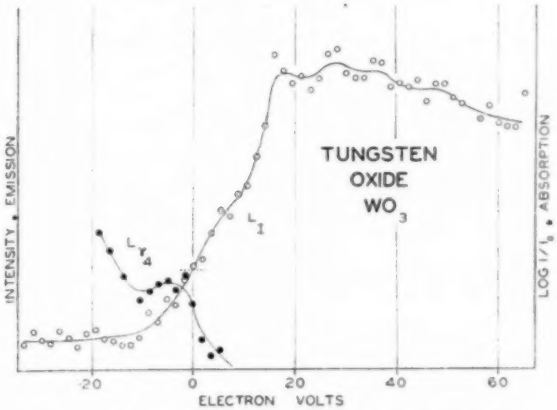

FIG. 4. The $L\gamma_4''$-emission line and L_{I}-absorption edge of tungsten oxide (WO_3).

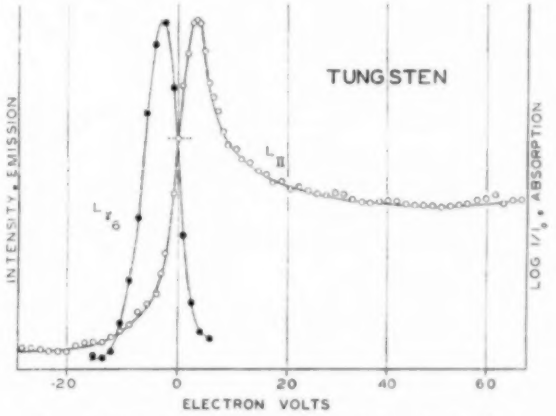

FIG. 5. The $L\gamma_6$-emission line and L_{II}-absorption edge of tungsten.

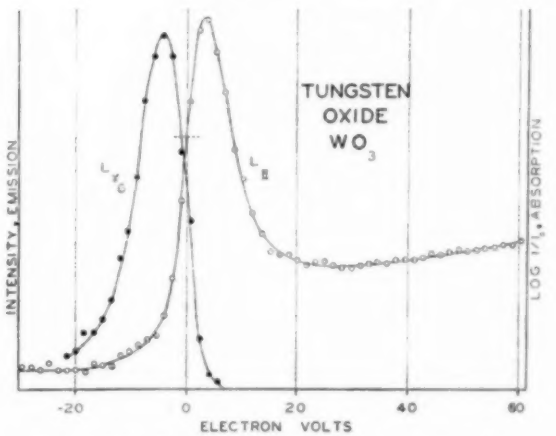

FIG. 6. The $L\gamma_6$-emission line and L_{II}-absorption edge of tungsten oxide (WO_3).

[12] Y. Nishina, Phil. Mag. **49**, 521 (1925).
[13] E. Friman, Zeits. f. Physik **39**, 813 (1926).
[14] S. Idei, Sci. Rep. Tohoku Imp. Univ. **19**, 559 (1930).
[15] A. Sandström, Zeits. f. Physik **65**, 632 (1930).
[16] E. Wigner and F. Seitz, Phys. Rev. **43**, 804 (1933).
[17] J. C. Slater, Phys. Rev. **45**, 794 (1934).

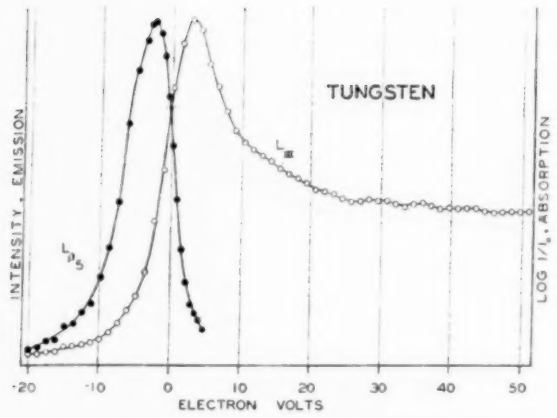

FIG. 7. The $L\beta_5$-emission line and L_{III}-absorption edge of tungsten.

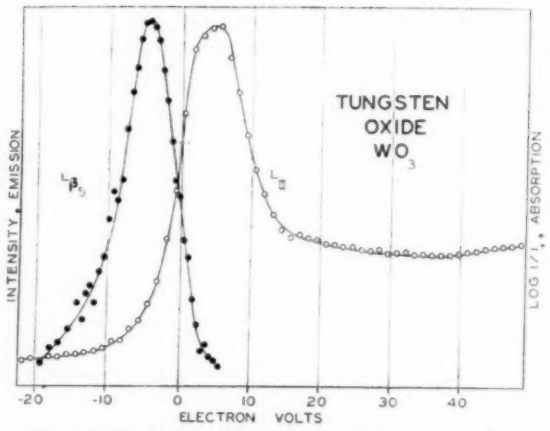

FIG. 8. The $L\beta_5$-emission line and L_{III}-absorption edge of tungsten oxide (WO_3).

period of the lattice. The tungsten lattice is partitioned into fourteen-sided polyhedra by drawing planes perpendicular to radii between nearest and next nearest neighbors at the midpoints. Bloch's theorem shows that the behavior of $\psi(\mathbf{r})$ in one polyhedral cell determines its behavior throughout the lattice. The Schroedinger equation must then be solved in one cell, subject to the condition of lattice periodicity of $u(\mathbf{r})$. A nearly self-consistent tungsten metallic field was used. Wave functions were taken to be linear combinations of fourteen independent wave functions whose angular parts were the fourteen lowest spherical harmonics. The coefficients in the combination were determined by satisfying the Bloch conditions at the midpoints of all cell faces. This was only carried out for certain directions of the wave vector $\mathbf{k}$. In this treatment several approximations were used, since in principle, the wave functions should contain *all* spherical harmonics and the Bloch conditions satisfied over the *whole* cell surface for *all* values of k. Furthermore the cellular method makes no attempt to include interactions between specific pairs of particles. Manning and Chodorow have pointed out that exchange between valence electrons would have the effect of narrowing the $5d$ and $6s$ bands over the results actually obtained. However, from their calculated results, shown in Fig. 9, the electrical conductivity, electronic specific heat, and paramagnetic susceptibility were computed and all but the last were in good agreement with experiment. The fact that their magnetic susceptibility was too small is probably due to the neglected tendency of electrons with parallel spins to keep apart.

The density of states $n(E)$ enters into the intensity $I(E)$ of an x-ray transition through the equation

$$I(E)=n(E)p(E),$$

where $p(E)$, the transition probability, is also a function of the energy. The transition probability $p(E)$ may be taken as proportional to the amount of p function used in the metallic wave function of energy E in the case of transitions involving the L_I level since this is an s level and the l selection rule permits only $s\rightarrow p$ transitions. Similarly $p(E)$ in the case of L_{II} or L_{III} transitions may be taken proportional to the sum of the amounts of d and s function, as L_{II} and L_{III} are p levels. The overlapping of atomic $5d$ wave functions in the tungsten lattice is small enough

TABLE III. *Wave-lengths of edges and those of line peaks.*

	Tungsten	Present Results	Previous Results
L_I	W	1.02253A	1.0205[12]
	WO_3	1.02219	
$L\gamma_4$	W	1.02595	1.0258[13]
	WO_3	1.02596	
L_{II}	W	1.07215	1.0713[12]
	WO_3	1.07189	
$L\gamma_6$	W	1.07232	1.0721[14]
	WO_3	1.07233	
L_{III}	W	1.21252	1.2116[12]
	WO_3	1.21220	
$L\beta_4$	W	1.21294	1.2129[14]
	WO_3	1.21296	
Platinum			
L_I		0.89088	0.8914[15]
L_{II}		0.93213	0.9321[15]

so that the mixing of states in the 5*d* band is not great, and is less for the low energy portions of the band than the high. This means that the 5*d* band consists chiefly of *d* states and one would expect L_{II} and L_{III} x-ray spectra to reflect closely the shape of the density-of-states in the 5*d* band. In the 6*s* band which overlaps the 5*d*, mixing is much greater; in the 6*p* and higher bands it is probably very great indeed, the density of states from there on being dependent chiefly on the crystal structure.

The experimental absorption and emission spectra of tungsten are seen to be in good agreement with this picture of its band structure. The shape of the L_{II} and L_{III} edges is very similar to that of the calculated density-of-states. The high maximum of initial absorption is several volts broader than the corresponding maximum of empty states in the 5*d* band, due to the width of the *L* levels. The lack of structure at higher frequencies may be due to the thorough mixing of the higher states plus the double $p \rightarrow s$, $p \rightarrow d$ possibility for transitions from the L_{II} and L_{III} levels. The L_I edge, on the other hand, shows only a small initial absorption due to the low density of *p* states in the 5*d* and 6*s* bands. This increases in a second jump upon reaching the 6*p* band where there is an extra high density of *p* states which drops off at higher energies. The general increase in structure over that of the L_{II}, L_{III} edges may be ascribed to the fact that absorption into only one type of state, a *p* state, is possible. The emission lines do not show the double peak exhibited by the calculated density of occupied 5*d* states. Furthermore, their widths are considerably less, 6.5 and 7.0 ev compared to the calculated band width of 10 electron volts. It may be that the band is narrowed by exchange to such an extent that the two peaks are no longer resolvable because of the width (>3.0 ev) of the *L* levels. The fact that the particular atom partaking in an x-ray transition is ionized in either the initial or final state may also tend to narrow the energy spread of states in its neighborhood. The low intensity of the $L\gamma_4''$-emission line compared to that of the $L\gamma_6$ and $L\beta_5$ lines is also due to the low *p* character of the 5*d* and 6*s* bands. The asymmetry of these lines is due to the sharp cut-off of filled states at the Fermi level.

A comparison of the corresponding edges and lines of metallic tungsten and tungsten oxide (WO_3) shows that the oxide absorption edges are shifted about 2.5 volts to higher energy although the emission line peaks show no such shift. Both the emission lines and the high initial absorption maxima of the L_{II} and L_{III} edges are broadened by several volts, which is considerably more than any spurious broadening due to inhomogeneities in the absorbers. The shift of the edges may be due to a weaker binding in the oxide; however, exact data are not available. The broadening of the absorption maximum is due to electrons leaving the 5*d* band where they spend relatively little time near the oxygen atoms to go into the 6*s* and 6*p* bands where the time spent near oxygen atoms is considerably greater. This is possible because the high electronegativity of oxygen lowers the energy of the latter states over that of the former. These lower bands are broader than the 5*d* and have a lower density of states. Hence the broadening of the emission lines.

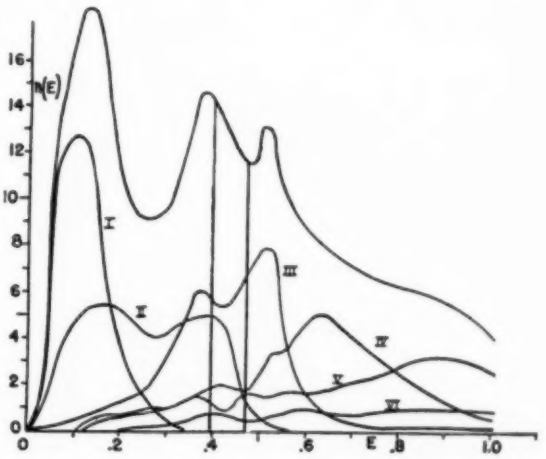

FIG. 9. Density of states in 5*d* and 6*s* bands of tungsten (reference 6). Energy is given in atomic units. Upper curve is total density of states. Curves I to VI give densities in component bands. Right-hand vertical line gives level to which states are filled in tungsten.

There are available, at present, no calculations of the band structure of platinum; however, from its large electronic contribution to the specific heat, anomalous temperature coefficient of resistance at high temperatures, and large paramagnetism, one expects it to have a high but rapidly decreasing density of vacant 5*d* states

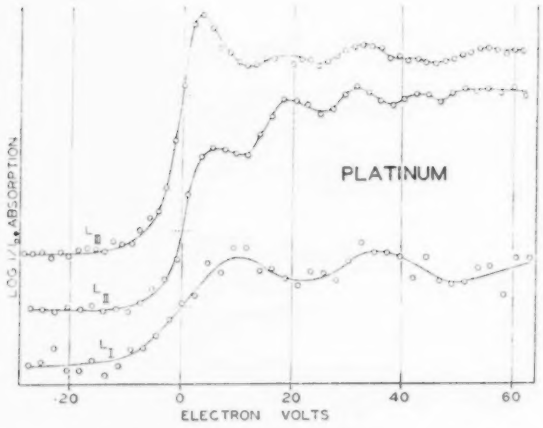

FIG. 10. L-absorption edges of platinum. Circles are experimental points. Positions of flex points are denoted by dashed lines. Edges are plotted to same energy scale and adjusted so that flex points coincide at point arbitrarily taken as the zero of the energy scale.

at the surface of the Fermi level. Because 6*s* electrons overlap more than do 5*d*, one expects the 6*s* band to be broad, highly mixed, overlapping the 5*d*. Due to the increase in nuclear charge in going from W to Pt, which contracts the electronic orbits, one expects all bands in Pt to be narrower and their states to show less mixing than in the corresponding bands of W. Again, the L absorption edges, shown in Fig. 10, are in agreement with the band picture. The L_{II} and L_{III} edges show a high initial absorption, while that of the L_I edge is small. There is much more structure corresponding to less mixing of states, due chiefly to the forbidding of $p \rightarrow p$ transitions in the L_{II} and L_{III} edges. It will be seen that although the positions of L_{II} and L_{III} structure features are in good agreement, their relative intensities are not. For example, the initial L_{III}-absorption peak is only a knee in the L_{II} edge. Differences in the L_{II} and L_{III} edges have also been recorded by other observers.[18] The L_{II} and L_{III} levels differ only in their j value. A large spin orbit coupling of the metallic valence electrons would suffice to account for these differences in a satisfactory manner.

It is a pleasure to acknowledge our indebtedness to Dr. Irving Langmuir of the General Electric Company for preparing the very pure tungsten foils and oxide used in this work. We are also grateful to the American Philosophical Society for a grant-in-aid, and to members of the Baltimore-Washington Solid State Seminar for valuable suggestions and discussions.

[18] J. Veldkamp, Physica **2**, 25 (1935).

JANUARY 15, 1941 PHYSICAL REVIEW VOLUME 59

Fluorescent *K* X-Rays from Ions in Solution and from Gases

T. M. SNYDER
Rowland Physical Laboratory, The Johns Hopkins University, Baltimore, Maryland
(Received November 1, 1940)

The $K\alpha$ lines emitted by cobalt, nickel, copper and bromine contained in chemical compounds were compared with the lines emitted by these elements in pure form. Chemical combination was found to broaden the lines and increase their asymmetry. The magnitude of the effect was greatest for cobalt, progressively smaller for nickel and copper and completely unobservable in the case of bromine. The further effect on the $K\alpha_1$ lines of putting these compounds into water solution at various concentrations was studied. It was found that the lines were unchanged by solution regardless of the dilution. Finally, the $K\alpha$ doublets of liquid and gaseous bromine were studied and found to be identical, showing that the state of physical aggregation has no effect on the $K\alpha$ lines of this element.

INTRODUCTION

THE chemical state of an element is known to affect the shape, width, wave-length and relative intensity of its x-ray emission lines. Because the forces involved in chemical and physical binding are in no way greatly different, the physical state of an element is expected to affect its emission lines just as its chemical state

does. However, as yet no dependence of the emission lines of a substance on its physical state has been found, although pronounced effects on the absorption spectra have been observed. Previous attempts to detect such an effect on the emission lines were of an indirect nature. They made use of the fact that the widths of the $K\alpha$ lines emitted by pure solid elements are smooth functions of the atomic number when it is sufficiently large. Because the widths of the $K\alpha$ lines from liquid gallium[1] and gaseous krypton[2] fell on these curves for solids, it was concluded that the widths were independent of the physical state. In the present work, a direct comparison is made between the x-ray lines emitted from different states of aggregation of the same substance. This provides a more delicate test for such effects. The $K\alpha$ doublet of gaseous bromine (Br_2) is compared with that of liquid bromine. The $K\alpha_1$ lines of crystalline compounds of the elements nickel, cobalt, copper and bromine are compared with the lines obtained from water solutions of these compounds. The lines emitted by solutions were studied over a wide range of concentrations.

Experimental

These studies were made possible by the improved intensity measuring technique of J. A. Bearden and C. H. Shaw,[3] which is especially useful for weak x-ray beams. This technique was applied in conjunction with a tube especially suitable for exciting high intensity secondary radiation. The tube was equipped with a gold-plated target cut at an angle of 45° to the axis of the tube. Primary radiation was taken off through a thin aluminum window. The secondary radiator, situated just outside of this window, was only $\frac{1}{4}''$ from the focal spot. Solid radiators were mounted on a metal support with a suitable adhesive. Gaseous and liquid radiators were contained in glass cells with very thin glass windows. These windows were made by heating the open end of a cell and pressing it while white hot into the side of a thin glass bubble. A single window of this type was used to pass both the exciting and the secondary radiation. The latter was taken off in a direction perpendicular to that of the incident primary beam and analyzed with a double crystal spectrometer which has been described elsewhere[4] as has the high voltage supply[5] for the tube. Intensities were measured with an argon-alcohol high pressure counter[6] in a multivibrator circuit[7] whose output fed through a scale-of-sixteen recorder[8] into a Cenco mechanical counter. Counting intervals were timed by a synchronous motor driven switch. With this apparatus, not only the fluorescent $K\alpha$ lines from bromine gas, but also those from nickel, present in water solution to only one part in 1250 by weight, were studied easily.

Table I. *Widths and indexes of asymmetry. In column 3 $K\alpha_1(1+1)$ width is given in seconds except for the last two entries where the width is $K\alpha_2(1+1)$. In column 4 probable error (P.E.) is given in seconds. In column 5 the index of asymmetry, I, is listed.*

Substance	State	Width	P.E.	I	$\Delta\lambda'$
(1)					
Cu	Metal	42.5	0.3	1.17	0.0
$CuSO_4$	Anhydrous powder	44.3	0.3	1.26	1.8
$CuSO_4 \cdot 5H_2O$	25% sol'n	45.3	0.3	1.22	2.8
$CuNo_3 \cdot 6H_2O$	Crystal	45.0	0.3	1.25	2.5
$CuNo_3 \cdot 6H_2O$	70% sol'n	45.0	0.3	1.24	2.5
(2)					
Cu	Metal	40.3	0.3	—	0.0
$CuSO_4 \cdot 5H_2O$	Crystal	43.0	0.3	1.21	2.7
(3)					
Cu	Metal	41.6	0.3	—	0.0
Ni	Metal	46.0	0.3	1.22	0.0
$NiSO_4 \cdot 7H_2O$	Crystal	56.3	0.3	1.89	10.3
$NiSO_4 \cdot 7H_2O$	16% sol'n	56.0	0.3	1.81	10.0
$NiSO_4 \cdot 7H_2O$	4% sol'n	56.3	0.5	1.7	10.3
$NiSO_4 \cdot 7H_2O$	0.4% sol'n	56	1.0	1.7	10
Co	Metal	57.4	0.5	1.4	0.0
$CoCl_2 \cdot 6H_2O$	Crystal	84.3	0.5	1.65	26.9
$CoCl_2 \cdot 6H_2O$	10% sol'n	84.3	0.9	1.67	26.9
$CoCl_2 \cdot 6H_2O$	4% sol'n	84	1.4	1.7	26.6
Br_2	Liquid	29.5	0.5	1.0	0.0
Br_2	Gas	29.5	0.5	1.0	0.0
KBr	Crystal	30	1.6	1.0	0.5
KBr	1% sol'n	29.6	2.0	1.0	0.1
$CuBr_2$	Crystal	29.9	0.5	1.0	0.4
Br_2	Liquid	30.5	0.5	1.0	0.0
Br_2	Gas	31	1.0	1.0	0.5

Discussion of Results

In Table I are given the widths and indexes of asymmetry of the lines studied. The increase in

[1] J. A. Bearden and C. H. Shaw, Phys. Rev. **48**, 18 (1935).
[2] Wilhelmy, Zeits. f. Physik **97**, 312 (1935).
[3] C. H. Shaw, Phys. Rev. **57**, 877 (1940).
[4] H. H. Roseberry and J. A. Bearden, Phys. Rev. **50**, 204 (1936).
[5] L. Obert, Phys. Rev. **54**, 1000 (1938).
[6] A. Trost, Zeits. f. Physik **105**, 399 (1937).
[7] I. A. Getting, Phys. Rev. **53**, 103 (1938).
[8] J. Giarratana, Rev. Sci. Inst. **8**, 390 (1937).

width, ΔW, over that obtained for a pure element in its normal state, is also listed. These measurements were made in three groups. Between groups, because the spectrometer crystals were removed and replaced, the line widths obtained were altered. In a single group of measurements the crystal characteristics remained fixed. To compare results in different groups the (1+1) widths of Cu $K\alpha_1$ are given for reference at the beginning of each group.

A comparison of the lines emitted from these elements in compounds with those emitted by the same elements in pure form shows that the effect of chemical combination is to broaden the lines and increase their asymmetry. The magnitude of the effect is seen to vary from element to element. In the case of bromine the lines of Br_2, KBr and $CuBr_2$ were found to be identical within the experimental error. In the case of copper, the lines of both the nitrate and the sulphate were several seconds broader and somewhat less symmetrical than that of the metal. The nickel sulphate line was 10″ wider and very much more asymmetrical than that of pure nickel, and the $CoCl_3 \cdot 6H_2O$ line was 27″ wider than that of cobalt although the change in asymmetry was not as marked as in the case of the nickel salt.

It is expected that those features of x-ray emission lines that are sensitive to chemical combination should also be sensitive to changes in physical state. A comparison of widths and asymmetries of lines emitted from different physical states of a substance should reveal the effect of such a change. It will be seen that the $K\alpha_{1,2}$ doublets of gaseous and liquid bromine are the same and furthermore that the $K\alpha_1$ line of KBr is the same whether the substance is in crystalline form or in rather dilute aqueous solution. From the fact that the $K\alpha$ lines of bromine showed no dependence on its chemical state, no dependence of these lines on the physical state is to be expected, due to the similar nature of the two effects.

In the cases of copper, nickel and cobalt where there is a very marked chemical effect, however, no dependence on the physical state is observed either. The lines from crystalline solids and their solutions are the same. However, there is a difference between the lines from the anhydrous and hydrated salt in the case of $CuSO_4$. These facts may be understood when one considers that in order to eliminate chemical changes on putting the compounds into solution only those compounds were used in which the metallic ions were already surrounded by the appropriate number of coordinated water molecules which they would otherwise acquire on solvation. Each ion in the hydrated crystals used, then, is protected from the action of external forces by a layer of surrounding water molecules which one may conveniently consider as an equivalent layer of dielectric constant 81. This layer is introduced into the crystal on transforming the anhydrous to the hydrated form. It reduces the Coulomb forces between ions by a factor greater than 81. The effect of thickening this layer of water, which is effectively what happens on putting the salt into solution, is to reduce this already small force to zero. The main effect occurs then, on introducing the first layer of water molecules; the effect in the case of $CuSO_4$ is seen to be comparable to that of chemical combination. The effect of putting such a hydrated salt into solution should be expected even in the case of cobalt to produce a change in line width of less than 0.25″. As this quantity is considerably smaller than the experimental error, it is understood why no effect on the $K\alpha_1$ line width of these compounds due to putting them into solution was found.

The author wishes to express his appreciation to Professor J. A. Bearden for suggesting this problem, and for his continued interest in its development. He is also indebted to Dr. C. H. Shaw for many helpful suggestions, and to the Naval Research Laboratory for the generous loan of the double crystal spectrometer.

Fine Structure in the Far Infra-Red Spectrum of NH_3

H. M. Foley* and H. M. Randall
Department of Physics, University of Michigan, Ann Arbor, Michigan
(Received November 7, 1940)

The pure rotation absorption spectrum of NH_3 for final state $J=11, 12, 13, 14, 15$ has been examined with high resolution. A multiplet splitting is found which may be expressed by the formula

$$\nu = 19.89J - 0.00294J^3 + 0.00279JK^2,$$

where K is the quantum number of angular momentum about the symmetry axis. This equation is shown to be in good agreement with the theoretical expression of Slawsky and Dennison when the potential anharmonicities are taken into account. A calculation of the permanent dipole moment is made from the absolute intensity of one absorption, giving the value 1.3×10^{-18} c.g.s. e.s.u.

THE far infra-red rotation spectrum of NH_3 has been observed by Wright and Randall[1] and by Barnes.[2] Wright and Randall examined the 70–100μ region and found three doublets, the centers of which may be represented by the formula

$$\nu = 19.89J - 0.00178J^3, \qquad (1)$$

where J has the values 5, 6, and 7. The value of J corresponds to the total angular momentum quantum number for a symmetric rotator in the final state. The doublet splitting is 1.32 cm^{-1}. As is well known, this is due to the tunnel effect, or resonance between the two equilibrium configurations of the molecule.[3] Barnes, in the 45–65μ region observed the absorptions corresponding to transitions to the final states $J=8, 9, 10, 11$, with less resolving power. The doublet separation is not in evidence.

In this paper are reported observations of the absorptions due to transitions to J values 11, 12, 13, 14, and 15. This work was undertaken because of the recent theoretical investigation of Slawsky and Dennison[4] on the effect of centrifugal distortion on the rotational energy levels of NH_3, which indicates that a fine structure should be observable in the higher rotational lines.

Experimental

The spectrometer employed is the wide-aperture, vacuum instrument with automatic recording, described by Randall and Firestone.[5] The radiation source was a strip of platinum coated with thorium oxide, through which about 60 amperes were passed. This was mounted directly before the entrance slit, the strip being of the right width to fill out the large mirror. Source and spectrometer case were evacuated together to remove atmospheric absorption. To purify the spectrum two filters, composed of selenium evaporated onto nitrocellulose films at six mm pressure, were placed in the optical path. These, together with a single reststrahlen reflection from sodium chloride or calcium fluoride plates, and shutters of potassium bromide, provided pure radiation throughout the 30–50μ region. The thermopile had a polystyrene window, and was evacuated separately with a diffusion pump.

The cell containing the gas was mounted inside the evacuated case of the spectrograph behind the emergent slit. Provision was made to pass the gas into the cell from outside the spectrometer case. The cell is of brass, coated inside with paraffin, and is five cm long. The cell windows are of Pliofilm and are reinforced with a wire grid to hold the gas pressure when in the evacuated case. For the absorptions $J=11$, 12, 13, pressures of 10–12 cm NH_3 were used, and for $J=14$, 15, about 40 cm. The data were

* Chas. Coffin Fellow, 1940–41.
[1] N. Wright and H. M. Randall, Phys. Rev. **44**, 391 (1933).
[2] R. B. Barnes, Phys. Rev. **47**, 658 (1935).
[3] D. M. Dennison and G. E. Uhlenbeck, Phys. Rev. **41**, 313 (1932); D. M. Dennison, Rev. Mod. Phys. **3**, 208 (1931).
[4] Z. I. Slawsky and D. M. Dennison, J. Chem. Phys. **7**, 509 (1939).
[5] H. M. Randall and F. A. Firestone, Rev. Sci. Inst. **9**, 404 (1938).

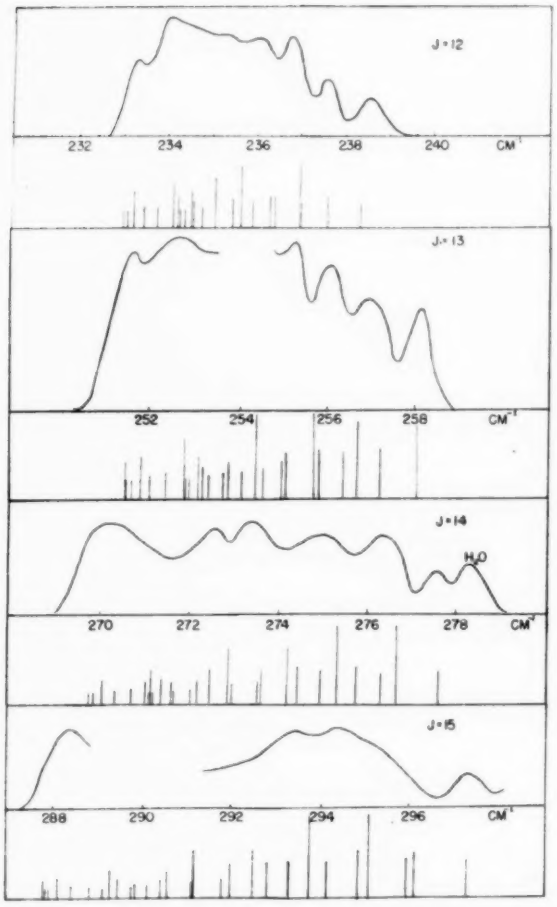

FIG. 1. The absorption lines of ammonia for $J=12$, 13, 14, and 15. Beneath each curve are plotted the positions of the fine structure lines predicted by Eq. (3).

obtained, by the automatic recording device, as photographic records of the galvanometer trace. Three to five records were taken of each absorption. Echelette gratings of 600 and 900 lines per inch, ruled by the Michigan engine, were employed. From the observed zero images it was determined that single lines of 0.5-cm^{-1} separation should be resolved.

The envelopes of the absorptions are shown in Fig. 1 in which the ordinates are proportional to the absorption. Although the ammonia gas was dried and then evaporated from the frozen state, traces of water vapor showed in the spectrum. Possibly this came from the cell walls, which could not be baked out. These lines were easily identified from the known water vapor spectrum,[6] and gaps in the envelopes indicate their positions. The frequencies of the absorption maxima are given in Table I. Most of these positions are considered accurate to a few hundredths cm^{-1}, and all to a tenth cm^{-1}. The $J=14$; 15; absorptions should be the most clearly resolvable, but apparently the larger amount of gas brought on pressure broadening.

[6] H. M. Randall, D. M. Dennison, N. Ginsburg, and L. Weber, Phys. Rev. **52**, 160 (1937).

Comparison with Theory

The effect of centrifugal distortion on a semirigid molecule of the NH_3 configuration has been calculated by Slawsky and Dennison.[4] The influence on the rotational spectrum is predicted to be (1) a displacement of the lines proportional to J^3, and (2) separation of each line into a multiplet with a spread approximately proportional to J^3. Formulas are given, showing the displacement and spread as functions of the normal frequencies and potential constants. These quantities were determined approximately by Slawsky and Dennison, neglecting the effect of anharmonicities in the potentials. They found a formula

$$\nu=19.89J+0.00160J-0.00250J^3+0.00190JK^2. \quad (2)$$

This equation accurately predicts the positions of the lines found by Wright and Randall. However, lines of such a small J value show little spread, and hence no adequate check is possible.

This formula, when applied to the present lines, is in good qualitative, but only fair quantitative agreement. We have fitted a formula of this type to our observed lines. They may all be expressed by the formula

$$\nu=19.89J-0.00294J^3+0.00279JK^2. \quad (3)$$

The deviation of any observed line from this equation is only of the order of magnitude of the experimental error. In Fig. 1 we have plotted the absorption lines $J=12$, 13, 14, and 15, and beneath, the positions of the lines predicted by Eq. (3). The intensities are obtained from the rules given by Slawsky and Dennison.

Dennison[7] has recently made a much better approximation to the normal frequencies and potential constants in the lowest state by taking

[7] D. M. Dennison, Rev. Mod. Phys. **12**, 175 (1940).

into account the anharmonicities. In the same paper he has given new values of the internuclear distances and moments of inertia of NH_3. When substituted into the Slawsky and Dennison formula these new constants yield

$$\nu = 19.89J + 0.00140J - 0.00300J^3 + 0.00271JK^2. \quad (4)$$

It is seen that this is very close to the above empirical formula, and in fact the lines predicted by it would differ only very slightly from the observed lines. The agreement is very satisfactory, and forms an argument for the more recent calculation of the potential constants.

In principle one further effect, not considered by Slawsky and Dennison, might influence the positions of the lines and perhaps account for some of the slight difference between the observed and predicted spectrum. Centrifugal distortion alters the effective double minimum potential, and consequently the resonance splitting. Sheng, Barker, and Dennison,[8] in an analysis of the parallel vibration band of NH_3 have found this perturbation in the excited level. A rough calculation shows that the influence of centrifugal distortion on the splitting in the ground state is about 1/120 of the effect in the excited vibrational level. The ultimate result is a contribution to the doublet separation of

$$-0.00290J^2 + 0.0040K^2.$$

This will shift the lines by not more than 0.2 cm^{-1}. If we adjust our empirical formula to take care of this, we obtain

$$\nu = 19.89J - 0.00303J^3 + 0.00290JK^2. \quad (5)$$

It is evident that this effect will account for the difference between the recalculated Slawsky Dennison formula[4] and the observed positions.

Although these observations were not intended as intensity measurements, certain features make these absorptions a very favorable case to compare the absolute intensities with the theoretically calculated values. The continuous radiation from the spectrometer is very constant across any one absorption, so that the percentage absorption may be calculated easily. More important, large errors in intensity measurement always occur when the absorption coefficient P_ν changes appreciably in a frequency interval equal to the slit width. This effect gives too low an apparent intensity, and consequently too small a value for the dipole moment. In our case, because of the spreading out of a single J line by the multiplet structure, we have in effect a very wide absorption, the spread being more than ten times the slit width. The total intensity of absorption is given by

$$I_J^{J-1} = \frac{8\pi^3 \nu N}{3ch} \mu^2 (1 - e^{-h\nu/kT}) F,$$

where μ is the permanent dipole moment of NH_3, and N the number of molecules per cc.

$$F = \frac{\sum_{K=0}^{J-1} g'_{JK} \exp\left[-E_{JK}/kT\right]}{\sum_{J=0}^{\infty} \sum_{K=0}^{J} g_{JK} \exp\left[-E_{JK}/kT\right]}.$$

We have chosen $J=14$ from which to calculate, as this absorption shows the least structure and is not overlaid with water vapor lines. The pressure here was 21 cm. The sums in this calculation were approximated by the integrals given by Gerhard and Dennison.[9] The measured intensity, integrated across the absorption, is $I = \int P_\nu d\nu = 2.8 \times 10^{10}$. This gives for the dipole moment $\mu = 1.3 \times 10^{-18}$ c.g.s. e.s.u. This value may be compared with the moment obtained from dielectric constant measurements of about 1.45×10^{-18}.[10]

TABLE I. *Observed Absorption Maxima.*

$J=11$	12	13	14	15
214.26 cm^{-1}	233.22	251.63	270.30	288.36
215.16	233.95	252.50	272.56	293.46
216.23	235.41	255.24	273.35	294.40
217.82	235.94	256.08	274.95	297.30
218.59	236.72	256.93	277.60	
	237.53	258.02		
	238.47			

The authors are indebted to Dr. Dennison for making known to them his recent calculations in advance of publication, and for several helpful discussions.

[8] Unpublished, but see reference 7.

[9] S. L. Gerhard and D. M. Dennison, Phys. Rev. **43**, 197 (1933).

[10] J. H. Van Vleck, *Electric and Magnetic Susceptibilities* (Oxford, 1932).

Measurement of Cathode Emission by Use of the Electron Microscope

G. W. Fox and F. M. Bailey*
Physics Laboratory, Iowa State College, Ames, Iowa
(Received July 30, 1940)

The electron microscope has been used in connection with photographic technique to make quantitative measurements of electron emission from the oxides of barium, strontium, and calcium. The instrument proves to be an excellent emission comparator. Time lapse exposures allow the observation of activation processes in detail. The emitting properties of barium compounds other than the oxide are compared.

I. Introduction

ELECTRON microscope studies of thermionic emission from alkaline earth oxides have revealed much information concerning the nature of such emitting surfaces. The work of Heinze and Wagener,[1,2] and Benjamin, Huck and Jenkins,[3] deals with the activation processes and show the dependence of emission properties on the particle size. Fluorescent image pictures have previously provided only qualitative information concerning the pattern of electron emission. The technique of intensity measurement by photographic means as applied to spectroscopy made it appear possible to determine current strength quantitatively from photographs of the fluorescent electron image.

Precise measurement of the temperature of an oxide-coated cathode is difficult, but absolute temperature determinations can be avoided by comparing the emission of two or more substances under the same conditions. In the electron microscope the cathode samples can be heated on the same base metal and the emission from each can be focused to show its pattern on a fluorescent screen. The intensities of such images are independent of the total area of the cathode, and the brightness or intensity per unit area on the screen is a measure of the current emitted from the corresponding area on the cathode surface. The current density at the cathode surface can be obtained by multiplying the density at the screen by the square of the linear magnification.

The objectives of this investigation were: (1) To make quantitative measurements of emission currents photographically, and to test the method by obtaining thermionic emission curves for BaO, SrO, and CaO. (2) To investigate the use of the electron microscope as an emission comparator. (3) To compare the electron emitting properties of barium compounds other than the oxide.

Construction of the Microscope

The apparatus is shown diagrammatically in Fig. 1. It was patterned after the design employed by McMillen and Scott.[4] The main body of the instrument was constructed from 45-mm Pyrex tubing with an inside coating of Aquadag to provide a conducting field-free space. This coating along with the anode ring A was maintained at a potential of three thousand volts.

A reflecting fluorescent screen R was enclosed at the upper end of the tube. Although this type of screen necessitates photographing through a curved glass surface, this objection was overruled by two principal advantages. As outlined by Maloff and Epstein[5] they are: (1) An increase of fifty to one hundred percent in screen efficiency due to direct viewing. (2) An increase in maximum contrast obtainable caused by the absence of halation. Both conditions result in a greater range of useful photographic exposure.

The cathode assembly was introduced into the main tube at the ground glass joint G and

* Now at General Electric Company, General Engineering Laboratory, Schenectady, New York.
[1] W. Heinze and S. Wagener, Zeits. f. tech. Physik **17**, 645 (1936).
[2] W. Heinze and S. Wagener, Zeits. f. tech. Physik **20**, 16 (1939).
[3] M. Benjamin, R. Huck and R. C. Jenkins, Proc. Phys. Soc. **50**, 345 (1938).
[4] J. H. McMillen and G. H. Scott, Rev. Sci. Inst. **8**, 288 (1937).
[5] I. G. Maloff and D. W. Epstein, *Electron Optics in Television* (McGraw-Hill, New York, 1938), p. 231.

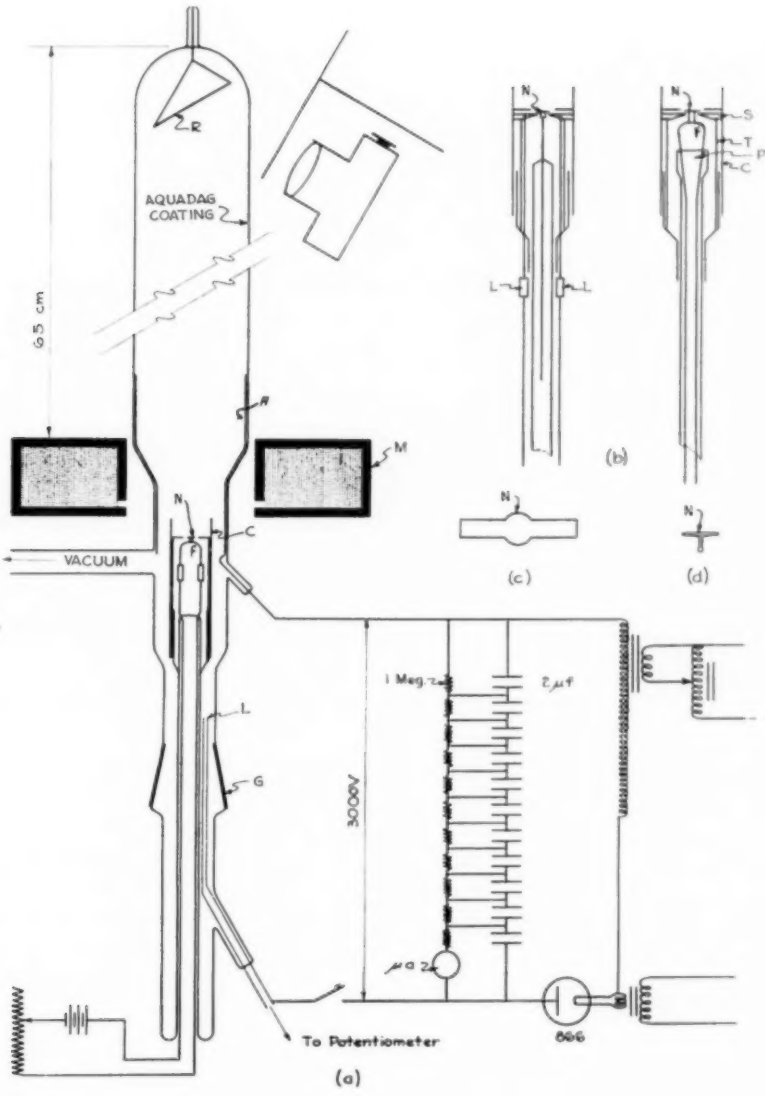

FIG. 1. Circuit of the electron microscope and construction details.

sealed with Picein wax. This assembly was made of a brass guard cylinder C with a sliding sleeve T to hold the soapstone light shield S in place. The heating filament F was made of 10-mil tungsten wire. The cathode plates N were cut from 5-mil nickel sheet in the form of Fig. 1(c), and the protruding strips were folded around the filament wire as shown in Fig. 1(d).

To measure the temperature of the cathode, 5-mil tungsten and nickel wires were spot-welded to the bottom center of the cathode and fastened to the thermocouple leads L. The use of a nickel-tungsten thermocouple enabled the cathode itself to act as one thermocouple metal.

CALIBRATION OF THE MICROSCOPE

In the form of Dushman's equation used for experimental data, $\log_e J_{th}+2\log_e 1/T=\log_e A_0 - b_0(1/T)$,[6] the current strength must be expressed as a natural logarithm. Fortunately, the relation between photographic density and $\log_e J_{th}$ results in a curve similar to the characteristic curve for photographic film.

Pictures of the fluorescent screen were taken with a 35-mm camera supplied with an auxiliary lens to give an object distance of 8.5 cm. To maintain accurate exposure times, a sector disk driven by a synchronous motor was used. The

[6] Saul Dushman, Rev. Mod. Phys. 2, 383 (1930).

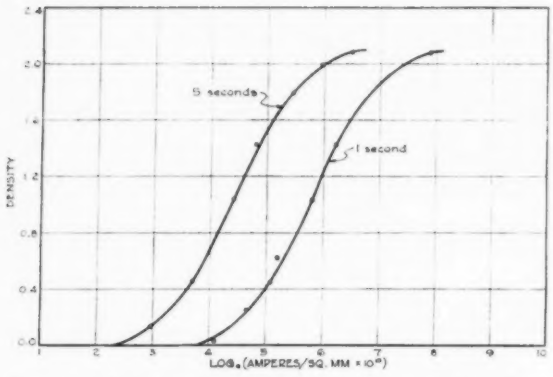

FIG. 2. Calibration curves for the electron microscope—photographic density *vs.* electron current density.

time intervals chosen were one and five seconds, as this choice provided two calibration curves which overlapped and increased the useful range of the method. The exposures were made at f : 4.5 on du Pont Micropan, and the film was developed under standard conditions.

An electron "gun" system was substituted in the cathode position to provide a uniform calibration spot on the screen, while a galvanometer placed in the cathode lead of the microscope measured the current represented by the beam.

In the calibration curves of Fig. 2 the $\log_e J_{th}$ is in amperes/sq. mm at the photographic film. That is, the photographic density is a function of the current arriving at the screen divided by the area of the image on the photographic film surface. To obtain $\log_e J_{th}$ at the cathode, the $\log_e$ of the area magnification between the photographic film and the cathode must be added to the abscissa.

PREPARATION OF THE CATHODE SURFACES

The emitting material was ground with water in a small mortar to form a suspension which

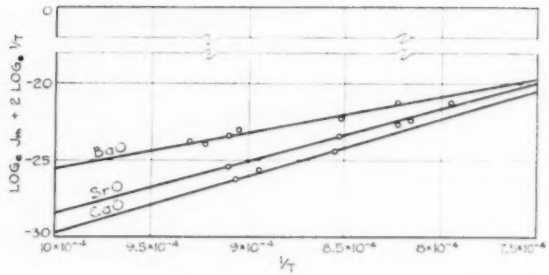

FIG. 3. Logarithmic temperature—emission curves for BaO, SrO, and CaO.

could be applied to the cathode in the form of a liquid drop. The concentration was controlled by the amount of material and water placed in the mortar and was adjusted until the material would form a coating of approximately 5 mg per sq. cm. For comparison measurements, the materials were placed on the cathode in the above manner with a dividing space between adjacent spots of less than 0.5 mm. This arrangement insured the same base temperature at the boundaries.

EXPERIMENTAL PROCEDURE

Oxides were reduced from other compounds by subsequent heating in the microscope. When the pressure reached 10^{-3} mm the cathode temperature was raised to 950°C for an hour to decompose the material and heat the cathode assembly. Then the anode voltage was applied and the current drawn for another hour after which the cathode was cooled to the desired temperature and observations made. The cathode was then removed from the tube and measurements made to determine the magnification.

THE TEMPERATURE CORRECTION

A correction to the thermocouple temperature was made to account for the temperature

TABLE I. *Comparison of emission from barium compounds.*

MATERIAL	T°K	RATIO	J MA/CM^2	MATERIAL	T°K	RATIO	J MA/CM^2
$SrCO_3$	1000	1.0	0.35	$Ba(NO_3)_2$	1100	5.1	36.0
$SrCO_3$	1100	1.0	7.0	BaS	1000	1.8	0.63
$SrCO_3$	1200	1.0	86.0	BaS	1100	1.3	9.1
$BaCO_3$	1000	16.0	5.6	$BaSO_4$	1100	1.2	8.4
$BaCO_3$	1100	7.4	52.0	$BaMnO_4$	1100	0.08	0.56
BaC_2O_4	1100	8.9	63.0	$BaCl_2$	1100	0.13	0.91
$Ba(NO_2)_2$	1100	5.4	38.0				

gradient through the emitting material. This correction was obtained by equating the heat conducted by the material to the heat emitted by radiation as described by Blewett.[7] The average thickness of the emitting material applied by the method described was found to be 0.0033 cm which gives a temperature difference of approximately 7°C. It was therefore assumed that the thermocouple recorded a temperature 7°C greater than the temperature of the emitting surface. Heat loss along the thermocouple wire seemed negligible since the nickel cathode constituted one element of the couple and the tungsten wire was surrounded by the cathode for a considerable distance beyond the junction.

The Microphotometer

A microphotometer with an optical system patterned after that of Lange[8] was used to measure the photographic densities. Instead of the usual slit used in spectrographic work a round spot of light was focused on the film. The diameter of this spot was made small enough to include a uniform density area and the average density computed from a number of readings by the expression

$$D_M = \log_{10} \sum_{i=1}^{n} \frac{I_0/I_i}{n}$$

where I_0/I_i is the ratio of incident to transmitted light in the microphotometer.

Curves for Dushman's Equation

The logarithmic temperature-emission curves for BaO, SrO, and CaO are shown in Fig. 3. In plotting these curves, a comparison run of BaO and SrO was made, and then a comparison run of SrO and CaO. It was found that the SrO curve of the second run was shifted a distance of 2.5 units above the SrO curve of the first run. The correction was then applied to the SrO–CaO run in order to bring it in accordance with the BaO–SrO run. This indicated that there is some difference between cathodes, but that a comparison of two materials on the same cathode gives consistent results.

[7] J. P. Blewett, J. App. Phys. **10**, 670 (1939).
[8] B. Lange, Zeits. f. tech. Physik **13**, 600 (1932).

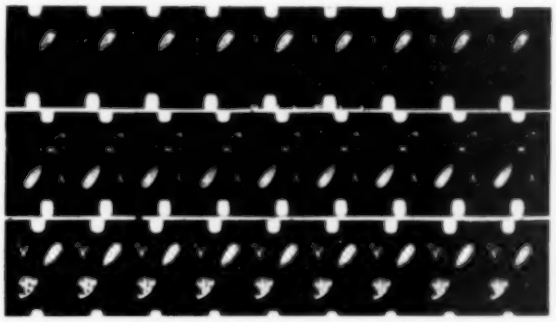

Fig. 4. Motion picture of emission growth.

Comparison of Barium Compounds

Since the emission of other barium compounds is lower than that of BaO, SrO (reduced from the carbonate) was used as a standard material for comparison. The filament current was adjusted until the cathode temperature became steady at 1100°K and then a picture was recorded. Another was taken at 1000°K but in many cases the emission was not sufficient to make an exposure.

The data obtained are recorded in Table I. The first column gives the compounds as applied to the cathode. The third column gives the ratio of the emission of the unknown to that of the $SrCO_3$. The last column gives a value for the current in milliamperes/sq. cm based on an average value obtained for all the data collected on $SrCO_3$.

Motion Picture Records and Sample Photographs

Figure 4 is a series of motion picture frames showing the growth of emission across the surface of a barium oxide cathode. In this case the temperature was held below 1000°K so that the growth proceeded slowly enough to make a

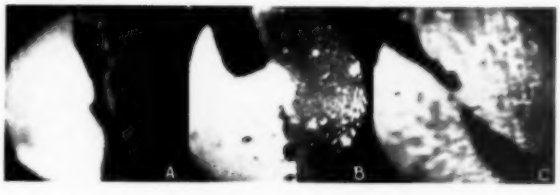

Fig. 5. Fluorescent electron images. (Magnification 36× linear.)

record. It will be noticed that the emission starts from the periphery of the spot and grows inward. Probably the higher temperature of the region adjacent to the nickel plate promoted activation more rapidly than the cooler central portions insulated from the plate by the oxide beneath. The current through the oxide then raised the temperature and caused the emission to spread toward the center. This explanation is the same as that outlined by Myers[9] to account for the hot spots in the emission surfaces.

Prints of the negatives used in comparing emission are shown in Fig. 5. In each picture SrO is the compound on the right, while the compounds on the left are (A) BaO, (B) $Ba(NO_2)_2$, (C) BaS.

[9] L. M. Myers, *Electron Optics, Theoretical and Practical* (Chapman and Hall Ltd., London, 1939), p. 435.

Discussion

The points used to plot the curves of Fig. 3 were obtained from several runs. Since they do not lie above or below the curves a distance of more than 0.25 unit along the ordinate, the error in current density, on a comparative basis, was not greater than the antilog 0.25 or a factor of 1.3.

The absolute values of the current densities appear to be low when compared with the literature.[10,11] This indicates that the absolute measurement of current density by this method is not as reliable as the comparative measurement.

The authors wish to express their appreciation to Dr. P. H. Carr for his suggestions throughout the course of the work.

[10] Saul Dushman, Rev. Mod. Phys. **2**, 381 (1930).
[11] H. J. Spanner, Ann. d. Physik **75**, 609 (1924).

JANUARY 15, 1941 PHYSICAL REVIEW VOLUME 59

Motion of the Earth's Fluid Core: A Geophysical Problem

D. R. Inglis
The Johns Hopkins University, Baltimore, Maryland
(Received October 30, 1940)

The earth's core may be assumed to have a very low viscosity, such as is characteristic of molten metals. The angular acceleration of the earth is sufficiently large, and the radius of the core is sufficiently great, to raise the question whether the rotation of the central part of the core lags appreciably behind the rotation of the solid mantle. The angular acceleration of the mantle, which is known astronomically, consists of a gradual deceleration and a more pronounced change of direction of the angular velocity, the 27,000-year precession. These two aspects are discussed separately. Three types of force might accelerate the core, viscous force in laminar flow, resistance caused by turbulent flow, and the force of induction associated with the earth's magnetic field. The viscous force is so weak that the interior would be practically unaccelerated if the flow were laminar, and the magnetic induction is expected to be weak enough to permit a large lag between the rotation of the mantle and interior of the core. But the core is so large that the flow should be turbulent. Reasonable assumptions on the nature of the flow in this case, based on empirical data on turbulence near a flat boundary, are used to estimate the lag. It is concluded that the axis of rotation of the interior of the core may be expected to lag behind the axis of the mantle in the precession by an angle of the order of magnitude of a few degrees. Apart from the superposed eddies, points rather near the surface of the core would then move relative to the mantle around horizontal closed paths, approximately a hundred kilometers across, with a period of a day. This would cause a diurnal variation of the earth's magnetism much larger than observed if it were not for the shielding of metallic layers above the core.

Introduction

THE fact that transverse seismic waves are apparently not transmitted through the core of the earth[1a] indicates that the matter within the core is almost certainly fluid. The transmission of the longitudinal waves shows[2] that the viscosity is not greater than that of pitch at room temperature, 2×10^{10} g cm sec.$^{-1}$. The viscosity is, however, probably very much

[1] B. Gutenberg, Editor, *Internal Constitution of the Earth* (McGraw-Hill, 1939), (a) Gutenberg, p. 347 and verbal report, Macelwane, p. 277; (b) Jeffries, p. 13.

[2] H. Jeffreys, M. N. R. A. S., Geophys. Supp. **1**, 412 (1926).

less than this upper limit. The core is thought to consist almost entirely of the elements iron and nickel, forming a simple metallic compound which would be expected to have a very definite melting point even at enormous pressure. The plastic state of matter, which reacts as a solid to sudden disturbances but as a fluid to very gradual disturbances, is characteristic of substances consisting of rather complicated molecules, not simple atomic substances like metals. We may, therefore, consider that the most probable order of magnitude of the coefficient of viscosity of the matter in the earth's core is that of molten metals at ordinary pressures, namely, about 10^{-2} g cm sec.$^{-1}$.

It is known that the solid part of the earth outside of the core, which we shall here call the mantle, experiences a rather complicated angular acceleration. This angular acceleration may be separated into two parts, first, a change of the magnitude of the angular velocity, an angular deceleration caused largely by tidal friction, and second, the angular acceleration involved in the 27,000-year precession of the earth's axis about a 24° cone, caused largely by the action of the moon's inhomogeneous gravitational field on the obliquely oriented quadrupole moment of the earth. The question arises whether the rotation of the fluid core keeps up with the rotation of the mantle or whether it lags considerably behind. If it lags behind, there is a rotation of the core relative to the mantle. Since such a relative rotation might have geophysical consequences, including an effect on terrestrial magnetism, we shall here discuss the problem of how much lagging might be expected.

We shall first discuss the effect of the gradual slowing down of the earth's rotation, and leave until later a discussion of the 27,000-year precession. Even though the precession is more important than the deceleration and the two are not actually separable dynamically, it will be helpful first to obtain the orders of magnitude of the various forces in the hypothetical case of deceleration without precession. In order to show that the problem is not entirely trivial, that is, that there might under certain circumstances be a very great lagging effect, we shall first consider the ideal case of laminar flow.

Laminar Flow

The dimensions are so great that this angular deceleration is transmitted to most of the core extremely slowly, if the core is as fluid as molten metal. The deceleration is, of course, transmitted most quickly to the outer layers of the fluid core, and gradually to successively deeper layers. We may obtain an upper limit for the depth of penetration of angular velocity by substituting an initial difference of angular velocity for the gradual deceleration. Since the angular speeds of revolution of the moon and rotation of the earth show that the earth once rotated about six times as fast as it does at present,[1b] we may assume that the initial angular velocity difference is 5Ω, where $\Omega = 7\times10^{-5}$ sec.$^{-1}$ is the present angular speed of the earth.

Anticipating the result that the penetration during the lifetime of the earth is much less than the radius of the core, we may also replace the spherical boundary by a plane solid boundary of a deep fluid. We take this boundary to be the x-y plane, with z directed inward along the radius, and let the velocity have only an x component, u. The equation of motion in the fluid is then

$$\dot{u} = s\partial^2 u/\partial z^2, \tag{1}$$

where $s = \eta/\rho$, the coefficient of viscosity, η, divided by the density, ρ. At $t=0$, we have the initial conditions

$$u = 0 \quad \text{for} \quad z = 0,$$
$$u = u_0 \quad \text{for} \quad z > 0.$$

The problem is identical in form with that of heat conduction into a solid from a hot boundary, and the solution is familiar from the work of Fourier:

$$(u_0 - u)/u_0 = (\pi st)^{-\frac{1}{2}} \int_0^\infty e^{-(\lambda+z)^2/4st} d\lambda$$
$$= 2\pi^{-\frac{1}{2}} \int_q^\infty e^{-\beta^2} d\beta = 1 - \Theta(q), \tag{2}$$

where $q = z/(4st)^{1/2}$ and $\Theta(q)$ is the probability integral, of which tables are available. Θ is equal to 0.84 if q is unity, and rapidly approaches unity for somewhat larger values of q. The condition for

$$(u_0 - u)/u_0 \ll 1$$

is thus that

$$z \gtrsim (4st)^{1/2}. \tag{3}$$

Inserting the plausible values $\eta = 10^{-2}$ g cm^{-1} sec.$^{-1}$ and $\rho = 10$ g cm^{-3}, we have $s = 10^{-3}$ cm^2 sec.$^{-1}$. For t we take the age of the earth, say 6×10^{16} sec., and find

$$z \gtrsim 1.5 \times 10^7 \text{ cm}. \tag{3'}$$

With these values of the constants, the depth of penetration of the transverse velocity into the fluid is thus much less than the radius of the core $R = 3 \times 10^8$ cm.

Turbulent Flow

One would not, however, expect the flow to be laminar in so large a fluid. In predicting the behavior of the flow, one must be guided by considerations of dynamical similarity. The Reynolds number for this case,

$$uR/s = \omega_r R^2/s$$

is of the order of magnitude 10^{15} or more, if the relative angular speed ω_r is comparable with the rotation of the earth. Experimental data on the flow of fluids past flat plates or through pipes are available up to a Reynolds number of almost 10^{10}. The data on flat plates with an adequately streamlined entering edge indicate a sudden transition from laminar to turbulent flow at about the value 10^5. Without streamlining, the flow is turbulent at even smaller values of the Reynolds number. In the interior of the core, with a Reynolds number of about the order of magnitude 10^{15}, the flow would certainly be expected to be turbulent, unless there should be a stratification of different materials according to density, which would hinder the turbulence.

To make an estimate of the degree of penetration in the extreme case of turbulent flow, we may make use of the empirical relations[3]

$$u(z) = u_0(z/\delta)^{1/7} \quad \text{for} \quad 0 < z < \delta, \tag{4.1}$$

$$\tau_0 = 0.02\rho u_0^{7/4}(s/\delta)^{1/4}, \tag{4.2}$$

where δ is the depth of penetration of the deceleration from a stationary surface into a deep moving fluid, and τ_0 is the tangential force per unit area on the surface. In analogy with the possibility of an initial relative rotation of the core and mantle of the earth, we first consider the case in which the stationary boundary is introduced at a time $t = 0$ (even though this does not correspond very closely with the methods of obtaining data on turbulence). The change of momentum of the flow caused by the influence of the boundary, per cm^2, is

$$\rho \int_0^\delta (u - u_0)dz = -\rho u_0 \delta/8.$$

The penetration δ increases with the time, and τ_0 decreases slowly. By equating the rate of change of momentum per cm^2 to τ_0 in (4.2), we obtain

$$\delta^{1/4} d\delta/dt = 0.16 u_0^{3/4} s^{1/4}. \tag{5}$$

After integrating this from zero to T, the age of the earth, we have

$$\delta = 0.3 u_0^{3/5} s^{1/5} T^{4/5} \approx 10^{16} \text{ cm}. \tag{6}$$

This is, of course, very much larger than the dimensions available within the core of the earth. However, even with this enormous depth of penetration, the velocity at a depth less than the radius of the core is still appreciable. According to (4.1) we have

$$u(10^8 \text{ cm}) \approx 10^{-1} u_0. \tag{7}$$

This estimate would not apply to the motion in the earth's core except as a very rough upper limit, because the central part of the core has a comparatively small inertia and can be accelerated to its final equilibrium speed much more easily than can the infinite fluid beyond the region of greatest shear in the case just treated.

Since the failure to treat the inertia properly is probably by far the worst feature of Eq. (7) as applied to the earth, we may make a much better estimate of the motion in the earth's core by improving the treatment of the inertia while retaining the data on turbulence derived from observations of flow past a straight boundary.[3] For this estimate, it will be sufficiently accurate to replace the spherical problem of the earth's core by the problem of an infinite cylinder of radius R

[3] T. v. Kármán, (a) Zeits. f. angew. Math. u. Mechanik **1**, 233 (1921), Eqs. (16) and (17); (b) J. Aero. Sci. **1**, 1 (1934). There Eq. (14), which corresponds to our Eq. (4.2), gives a force about half as great at $R_x = 10^{10}$, and about a third as great at $R_x = 10^{12}$, as his Eqs. (40) and (39) which are more exact for high R_x. We may thus expect the use of the convenient but approximate formula (4.2) to give too large values of the lag of the core, but to lead to results of about the correct order of magnitude, since our final result corresponds to a Reynolds number of about 10^{14}.

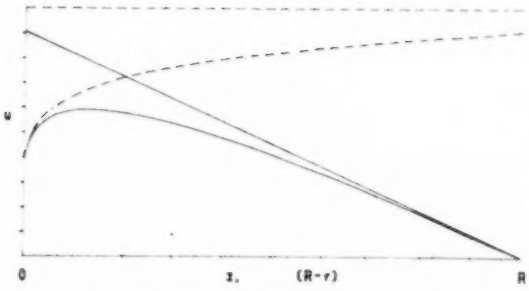

FIG. 1. Average horizontal speed as a function of depth beneath a plane boundary (broken curve) and a cylindrical boundary (solid curve) in the case of turbulent flow. The straight lines indicate initial speeds.

rotating about its axis, since the ratio of the moment of inertia to the area of the surface has the same order of magnitude in both problems. The depth of penetration, δ in Eq. (4) no longer has any meaning. Instead of it, we propose to express the empirical data in terms of the parameter $u(a)$, the velocity at an arbitrarily chosen radius a, considerably less than R. Our initial conditions at $t=0$ become

$$u_0(R)=0,\ u_0(r)=\omega_0 r \quad \text{for} \quad r<R.$$

As an assumption which we shall expect to lead to the correct orders of magnitude only, we shall suppose that the variation of the percentage reduction of velocity with depth in the cylindrical problem is similar to that in the plane problem, as given by (4) with $\delta>R$. This is plausible because by far the most rapid variation takes place in the topmost layer, where the plane and cylindrical problems are similar. We must bear in mind that the fluid is now decelerated from an initial velocity proportional to the radius. We thus substitute for (4) the equations

$$u(r)=u(a)(r/a)\{(R-r)/(R-a)\}^{1/7}$$
$$=\omega_r r\{(R-r)/R\}^{1/7}, \quad (8.1)$$

$$\tau_0=0.02\rho\{u(a)R/a\}^{7/4}\{s/(R-a)\}^{1/4}$$
$$=0.02\rho\{\omega_r R\}^{7/4}(s/R)^{1/4}. \quad (8.2)$$

Here we have defined the angular speed of the core relative to the mantle, ω_r, as $u(a)/a$ for $a\ll R$. The different aspects of (4.1) and (8.1) are illustrated by the broken lines and the solid lines, respectively, of Fig. 1. The straight line in each case shows the initial state of flow before the deceleration of part of the fluid by the turbulence.

By use of (8.1) in the appropriate integration, we obtain for the angular momentum, per centimeter along the axis, the expression

$$1.2\rho R^4\omega_r.$$

The time rate of change of this angular momentum is equal to the torque per centimeter, $2\pi R^2\tau_0$, as given in (8.2). We thus have the equation

$$\dot{\omega}_r=-10^{-1}s^{1/4}R^{-1/2}\omega_r^{7/4}=-10^{-6}\,\text{sec.}^{-1/4}\,\omega_r^{7/4} \quad (9)$$

with $R=3\times10^8$ cm, $s=10^{-3}$ cm^2 sec.$^{-1}$. By integrating this we obtain

$$\omega_r^{-3/4}=\omega_0^{-3/4}+(3/40)s^{1/4}R^{-1/2}t. \quad (10.1)$$

If we put $t=6\times10^{16}$ seconds, the first term on the right side may be neglected, and we have

$$\omega_r=32s^{-1/3}R^{2/3}t^{-4/3}$$
$$=6\times10^{-15}\ \text{sec.}^{-1}\approx10^{-10}\Omega \quad (10.2)$$

independent of the initial speed of relative rotation, within reasonable limits. The result is also quite insensitive to the value assumed for the coefficient of viscosity. Equation (10.2) corresponds to one revolution of the core within the earth in about 10^{10} days $=3\times10^7$ years.

For the sake of discussing the possible decay of a large difference of angular velocity, we have, above, treated the case in which the mantle has a constant angular velocity, and have found that the difference would in that case be reduced to a small value within the lifetime of the earth. For relative rotations as slow as this result, the angular acceleration of the mantle may no longer be neglected. Still considering only the gradual slowing down of the earth's rotation, and leaving until later the precession, we have for the angular acceleration of the mantle $-5\Omega/T=-6\times10^{-21}$ sec.$^{-2}$. Instead of (9) we would now have

$$-\dot{\omega}=10^{-6}\ \text{sec.}^{-1/4}\ \omega_r^{7/4}, \quad (9')$$

where $\dot{\omega}$ is the angular acceleration of the core in an astronomical coordinate system, and ω_r is again the angular speed of the core relative to the mantle, which is responsible for the torque. If the angular speeds of the core and mantle are

to remain very nearly equal, $\dot{\omega}$ must be equal to the angular acceleration of the mantle. The value of ω_r thus determined,

$$\omega_r = 10^{-8}\ \text{sec.}^{-1} = 10^{-4}\Omega \qquad (11)$$

is much greater than (10.2). From these two results we may infer the result of the combined problem. If there were a considerable initial relative rotation in addition to the deceleration of the mantle, the relative rotational speed would approach the value (11) within a time shorter than the life of the earth. The time of approach to this order of magnitude of ω_r may be estimated by putting $\omega_r = 10^{-8}$ sec.$^{-1}$ in (10.1), with the result $t = 3\times10^4$ years.

The Reynolds number corresponding to (11) is still above 10^{10}, so turbulence would be expected to persist at this speed, as was assumed in the derivation of (11).

Magnetic Drag

The transfer of angular momentum into the core may also be due to the inductive effect of a magnetic field arising within the mantle and penetrating into the metallic core. This effect would be closely analogous to the torque exerted on a suspended copper disk by a rotating magnet, or to the functioning of a magnetic speedometer. There would also be such an inductive drag if the magnetic field should arise in the core and penetrate into a metallic mantle, but this would cause large variations in the observed magnetic field at the surface unless the relative rotation were extremely slow or the field penetrating to the surface should be stabilized by an inductive effect in the mantle. For the sake of simplicity, we shall assume in this section that the magnetic field arises in the mantle and penetrates into the core. An analysis of the geographic variations of the earth's magnetism shows that it may be attributed to a strong central dipole making an angle of $11\frac{1}{2}°$ with the axis of rotation of the earth, and to 14 subsidiary dipoles located at the surface of the core, each only about 1/100 as strong as the central dipole.[4] We shall neglect the irregularities in the field which are described by the subsidiary dipoles and consider only the main part of the earth's field which in the analysis is attributed to the central dipole. A uniformly magnetized spherical shell gives rise to a field outside it identical with the field of a dipole at the center. In our treatment we may, therefore attribute this field to a uniform magnetization of the mantle or of a shell within the mantle, or to an equivalent distribution of current. It might, for example, be caused by a suitable distribution of core-encircling current near the surface of the core. Without an inductive effect, the field in any case would be practically uniform within the core. Its strength would depend upon the location of the magnetization: It would be about as strong as the field at the surface (1 dyne$^{1/2}$ cm^2) if the entire mantle were magnetized, but about 8 times that strong if the magnetization or current were confined to the deepest layers of the mantle. Thus we may take the magnitude of the field in the core as about 10 dyne$^{1/2}$ cm^{-1} or somewhat less. In discussing the gradual deceleration, we may consider that the axis of relative rotation of the core and mantle is the geographic axis. Then only the equatorial-plane component of the field within the core produces an inductive effect, and this component we shall call H_0. Its magnitude is about 2 dyne$^{1/2}$ cm^{-1} or less.

The problem of the rotation of a conducting sphere in a uniform magnetic field is simplest if the sphere is rigid. This simple case is not entirely unrelated to the problem of the earth's core if we consider the simultaneous effects of turbulence and magnetic drag. Turbulence allows most of the slip to take place near the boundary, so that the curved velocity distributions shown in Fig. 1 are somewhat similar to the straight lines associated with rigid motion. Before considering the other extreme case in which only magnetic drag decelerates a fluid core, we first treat the simple case of a rigid core rotating, with free slip at its boundary, in a transverse field H_0. With very slow rotation this field induces in the moving matter of the core a current proportional to the rotational speed. The current interacts with the field in such a way as to produce a decelerating torque which is also proportional to the angular speed. At higher speeds, the induced current effectively opposed the penetration of the field into the core. This

[4] A. G. McNish, Trans. Am. Geophys. Union 2, 287 (1940).

"skin effect" is so strong that the decelerating torque actually decreases with increasing speed at high rotational speeds.

This problem of the rotation of a spherical conductor in a uniform magnetic field has been treated quantitatively by R. Gans, who finds for the decelerating torque[5]

$$P=(3/2)H_0^2R^3\{(2\gamma)^{-\frac{1}{2}}-\gamma^{-1}+\cdots\},\ \gamma \text{ large}, \tag{11.1}$$

$$P=(3/22)H_0^2R^3\gamma\{1-10^{-2}\gamma^2+\cdots\},\ \gamma \text{ small}, \tag{11.2}$$

$$\gamma=4\pi\sigma R^2\omega_r,$$

where σ is the specific conductivity of the core in electromagnetic units, which we assume to be about 10^{-6} sec. cm^{-2} (that is, 10^4 ohm cm, a representative value for metals). The division between "γ large" and "γ small" is about $\gamma=10$, or $\omega_r=10^{-11}$ sec.$^{-1}\approx10^{-7}\Omega$, a very small fraction of the angular speed of the earth. From the first term of (11.1) and from the equation of motion

$$\dot{\omega}=-(15/8\pi\rho R^5)P, \tag{12}$$

with $\dot{\omega}=\dot{\omega}_r$ because of the steady rotation of the mantle, we obtain

$$\omega_0^{3/2}-\omega_r^{3/2}=4\times10^{-24}\text{ sec.}^{-5/2}\,t \tag{13.1}$$

with the evaluation of the constants suggested above. In the case of an initial rotation $\omega_0\approx\Omega$ for example, Eq. (13.1) tells us that it would take about 2×10^{17} sec., or about 10^{10} years for $\dot{\omega}$ to become very small. For small values of γ we have instead

$$\ln(\omega_r/\omega_0)=-4\times10^{-7}\text{ sec.}^{-1}\,t. \tag{13.2}$$

Thus the magnetic drag would stop the relative rotation practically completely within about a year if it should ever become rather slow.

We turn again to the problem of the core within a decelerating mantle. With this magnetic drag, which rises to a maximum and then falls off with increasing ω_r, there are two values of ω_r for which the torque is just sufficient to supply the core with a deceleration equal to that of the mantle. These are obtained by setting the average deceleration of the mantle, 6×10^{-21} sec.$^{-2}$, equal to $-\dot{\omega}$ in (12) for both large and small γ, and are

$$\omega_r=2\times10^{-7}\text{ sec.}^{-1},\quad \gamma \text{ large} \tag{14.1}$$

$$\omega_r=1.5\times10^{-11}\text{ sec.}^{-1},\quad \gamma \text{ small}. \tag{14.2}$$

For any ω_r between these values, the magnetic drag is great enough to reduce ω_r in spite of the deceleration of the core, and throughout most of that range the drag is great enough that the deceleration is negligible.

It is probable that the violent separation of the earth from the sun left the core and mantle (as soon as they could be distinguished) with an initial relative rotation of the order of magnitude Ω, or somewhat more. Our hypothetical problem in which we ignore the precession is then as close as possible to reality if we consider both an initial relative rotation and the deceleration. We have seen in Eqs. (10.2) and (11) that the torque caused by turbulence is in this case capable of reducing ω_r down to 10^{-8} sec.$^{-1}$. This lies between the limits (14), so the magnetic drag would be strong enough to reduce ω_r further, down to the value given by (14.2), if the rotation were approximately rigid.

In the case of a fluid core accelerated by magnetic drag alone, the penetration of the magnetic field is greatly facilitated by the possibility that the successively deeper layers may each be first penetrated, then accelerated, by the magnetic field. We consider a fluid core initially rotating with angular speed ω_0 in a transverse field H_0 which does not penetrate it initially. The penetration is most rapid where H_0 is tangent to the sphere. There the penetration is governed by the equation, derivable from Maxwell's equations,

$$\dot{H}_x=(4\pi\sigma)^{-1}\partial^2H_x/\partial z^2$$

if z is the axis normal to the boundary. Comparison of this with Eqs. (1) and (3) shows that the depth of penetration of a tangential field into a stationary conductor in time t is

$$z\approx(t/\pi\sigma)^{\frac{1}{2}}. \tag{15}$$

The field at a part of the surface of the rotating core is reversed after a time $t=\pi/\omega_r$, so the depth of penetration when the outer layers rotate with angular speed ω_r is about

$$\zeta=(\omega_r\sigma)^{-\frac{1}{2}}.$$

The lines representing the field then slope

[5] R. Gans, Archiv f. Elektrotechnik **9**, 413 (1921).

inward from the surface to this depth as they wind $\frac{1}{4}$ of the way around the sphere, so the average radial component of the field is about

$$H_z = H_0\zeta/R.$$

The angular acceleration of the shell of thickness ζ caused by the currents induced by H_z is then approximately

$$\dot{\omega}_r = (\sigma\zeta^2 H_0^2/\rho R^2)\omega_r = H_0^2/\rho R^2 = \Omega/(2\times 10^{13}\ \text{sec.}).$$

We may then say that the time required to decelerate a layer of thickness ζ from $\omega_0 = \Omega$ to rest is about 2×10^{13} sec. With $\omega_r \approx \Omega$, we have $\zeta \approx 10^5$ cm. If we should assume that the deceleration of the next deeper layer would not begin until this outer layer is completely decelerated, we might then estimate roughly that it would require a time

$$(R/\zeta)2\times 10^{13}\ \text{sec.} = 6\times 10^{16}\ \text{sec.} = T$$

for the deceleration to penetrate to the center. This estimate is somewhat too large, both because a smaller value of the radius should be used for the inner layers and because the deceleration of one layer will commence before the layer above it is brought to rest.

With only magnetic drag, the penetration would then be complete within the lifetime of the earth, T. The angular speed of the core relative to the mantle which is necessary to transmit to any layer of the core the average deceleration, $\dot{\omega} \approx 5\Omega/T$, of the mantle, is then

$$\omega_r \approx (\rho/\sigma H_0^2)\dot{\omega} \approx (5\rho/\sigma H_0^2 T)\Omega \approx 2\times 10^{-10}\Omega$$

in agreement with (14.2) for the rigid case. Since we obtain the same result for ω_r in both extremes, it may be expected to apply in order of magnitude to the intermediate case in which we have turbulent drag in addition to magnetic drag. This ω_r, or even that in Eq. (11) given by turbulence alone, is so much less than Ω that we may take the angular speeds of the mantle and core to be equal, and turn to consideration of the precession.

The 27,000-Year Precession

We have as yet been considering only the smaller component of the vectorial angular acceleration of the earth. The magnitude of the angular acceleration associated with the 27,000-year precession about a 24° cone is $10^{-1}\ \text{year}^{-1}\ \Omega = 2\times 10^{-16}\ \text{sec.}^{-2}$. This is about 4×10^4 times as great as the deceleration discussed above. The angular acceleration of the mantle is thus represented by a vector $\dot{\boldsymbol{\omega}}_m$ about normal to its angular velocity $\boldsymbol{\omega}_m$. We shall now investigate whether the turbulent and magnetic interaction between the core and mantle might be strong enough to cope with this larger component of the angular acceleration also.

If $\boldsymbol{\omega}$ and $\boldsymbol{\omega}_m$ should have both different magnitudes and considerably different directions, as in Fig. 2(a), we may assume that $\boldsymbol{\omega}_r$ may be divided, at least roughly, into two parts: a part, either normal to $\boldsymbol{\omega}$ or making equal angles with $\boldsymbol{\omega}$ and $\boldsymbol{\omega}_m$, which causes a turbulent interaction between the core and mantle tending to reduce the angle α between $\boldsymbol{\omega}$ and $\boldsymbol{\omega}_m$; and a part parallel to $\boldsymbol{\omega}$, which causes an interaction tending to reduce the magnitude of $\boldsymbol{\omega}$, as discussed in the preceding section. Although this assumption is intuitively rather plausible as an approximation, it is not obvious, both because of the nonlinear relation between relative velocity and turbulent drag, and because of the necessity of discussing relative velocity in a rotating coordinate system. The nonlinearity would be expected to decrease the decay times of the relative rotation estimated below. Before we make such estimates, we shall discuss the relative velocity in more detail in the following section.

The usual discussion of fluid friction, laminar or turbulent, depends on a persistent motion of the mass of the fluid in one direction, relative to a boundary which is at rest in an inertial coordinate system. In our case, the relative motion which is responsible for the interaction is the difference of the motions of two bodies neither of which is even approximately unaccelerated relative to an inertial system. The following discussion of some details of the motion will form a basis for a plausible extension of the usual treatment.

Relative Motion in the Precession

We have seen that the interactions are of an order of magnitude to cause a change of angular velocity comparable to $\boldsymbol{\Omega}$ only in many years: $\boldsymbol{\omega}$ and $\boldsymbol{\omega}_m$ are practically constant for times as short as a few days. For such short times, the relative velocity $\boldsymbol{\omega}_r$, which is the difference of $\boldsymbol{\omega}$

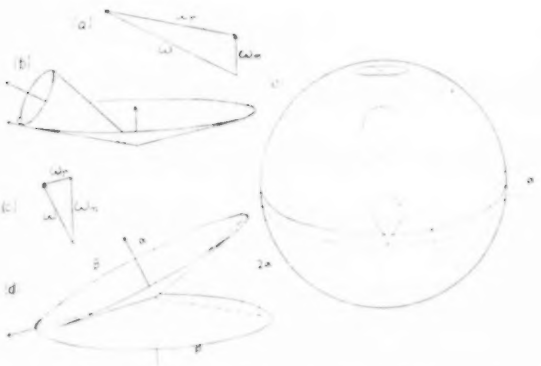

FIG. 2. (a) and (b) describe a possible initial rotation of the core and mantle with quite different angular speeds. (c) and (d) describe the probable present rotation with the angle between the axes exaggerated. On the sphere (e) are shown the paths, fixed relative to the mantle, followed by representative points of the core.

and ω_m and is parallel to neither, is practically constant in space and therefore rotates with a period of one day in the coordinate system of the mantle. As the mantle rotates about the axis of ω_m, the direction of ω_r sweeps out a cone in the mantle-fixed coordinate system. The axis of the cone is the polar axis. Likewise ω_r sweeps out a cone whose axis is the axis of rotation of the core in the core-fixed coordinate system. Since these two cones always have a line of contact, which is the instantaneous axis of rotation, the motion of the core relative to the mantle may be described as the rolling of the core-fixed cone on the mantle-fixed cone.

The shapes of the cones, of course, vary with the angles between the vectors ω, ω_m and ω_r. In the extreme case in which ω is considerably greater in magnitude than ω_m, with a considerable angle between them, the angle between ω and ω_r is comparatively small (Fig. 2(a)), and the core-fixed cone is a rather narrow one, although the mantle-fixed cone may be rather wide, as shown in Fig. 2(b). In the limit in which the core-fixed cone becomes very narrow, the motion of the core relative to the mantle is a fast rotation with a very slow change in the general direction of the axis, relative to the mantle. In this limit the motion is not essentially different from that discussed in the preceding section, and the result of that discussion leads us to expect that ω would decrease until it is not much larger than ω_m in a time much shorter than the age of the earth.

In the case in which ω and ω_m are equal in magnitude, and when they have an angle α between them considerably less than $\pi/2$, the cones are equal and very wide, with apex angle $\pi-\alpha/2$, as in Fig. 2(c) and (d). In describing the motion of the core relative to the mantle, we may think of the lower cone in Fig. 2(d), the mantle-fixed cone, as stationary, with the upper cone rolling on it. A point on the core-fixed cone describes a closed glass-drop shaped figure with a cusp at the point of contact with the mantle-fixed cone, as sketched on the sphere in Fig. 2(e). The points on the polar axis of the core describe circles. A point above the cone but not on the axis describes a figure intermediate between the glass-drop shape and a circle, a pear-shaped figure without a cusp. A point between the core-fixed cone and the equatorial plane of the core describes a figure-of-eight. The diametrically opposite points trace the same figures. The motion of points on the inner surface of the mantle relative to the core is of course similar; they trace closed paths, of over-all north-and-south dimensions $2\alpha R$. The velocity of the surface of the mantle past a given point near the surface of the core rotates periodically into all directions of the compass, in the core-fixed coordinates.

If the core-fixed coordinate system were an inertial system, this would mean that the impulse imparted to the upper layers of the core during one half-cycle would be largely canceled by the impulse imparted during the next half-cycle. There would thus be comparatively little penetration of the turbulent flow, for example, and no net drag on the interior of the core. This cancellation is not very effective in the rotating core because of the Coriolis forces in the rotating coordinate system. In order to see that the Coriolis forces, which are a way of expressing the conservation of momentum and of angular momentum, act in the right way, let us consider a model in which an intermediate layer between the core and mantle originally rotates with the core, and has a frictional interaction with the mantle which may be turned on and off at will. We shall consider as typical the interaction, with the mantle, of the point which traces the pear-shaped figure in Fig. 2(e). During the instant represented by Fig. 2(d) and (e), this point is

moving up the left side of the pear, so the adjacent surface of the mantle moves down past it. Let the interaction be turned on instantaneously at this time. This impulse makes an increment of angular velocity of the intermediate layer, $\mathbf{d\omega}$, in the direction opposite to $\boldsymbol{\omega}_r$. We next turn the interaction on instantaneously a half-cycle later, when the point is moving down the right side of the pear, and the mantle up past it. In a space-fixed coordinate system, both of the cones in Fig. 2(d) are spinning in such a way that their line of contact remains stationary, with no slipping, and the sphere in Fig. 2(e) rotates with the core-fixed cone. At this second instant, the pear is around behind the sphere. In the space-fixed system, the conservation of angular momentum maintains the first increment of angular velocity $\mathbf{d\omega}$ intact, and the second increment is in the same direction, so the two are additive. In the core-fixed coordinates it is the Coriolis force which maintains $\mathbf{d\omega}$. Thus we see that the forces acting during the different parts of the periodic relative motions do not effectively cancel one another.

A third case to be discussed is similar to the last, but with ω slightly greater than ω_m, so that $\beta > \beta'$ in Fig. 2(d). In this case the circumference of the mantle-fixed cone (at a radius R) is greater than the circumference of the core-fixed cone and points in the mantle-fixed cone advance relative to the core by an angle $2\pi(\sin\beta - \sin\beta')$ during each revolution of the core, instead of returning to the same point and making a closed figure. Other points on the inner surface of the mantle similarly fail to make closed figures, and progress circuitously and slowly around the core. Their paths are somewhat similar to trochoids (generalized cycloids). Just as in the case of an electron following a trochoidal path in crossed magnetic and electric fields, we can speak of a net velocity of translation after averaging out the irregularities of the path, so here we can speak of a net angular speed with which the points of the core-fixed cone, for example, effectively rotate in the mantle-fixed system. This net relative angular speed is the scalar quantity

$$\omega(\sin\beta - \sin\beta')/\sin\beta = (\omega - \omega_m). \qquad (16)$$

The first member is derived by considering the gradual progress of the cusp (Fig. 2(e)) about the lower cone in Fig. 2(d), and the second member is obtained from the first by use of the law of sines in Fig. 2(c). Thus points on most of the surface of the mantle circulate around the core with a net relative angular velocity whose magnitude is approximately the difference of the angular speeds and whose direction is that of $-\boldsymbol{\omega}$. This may be expected to be effective in decelerating the core, in keeping with the assumption that the two components of $\boldsymbol{\omega}_r$ may be considered separately.

Turbulent Force in the Precession

We next investigate whether the forces are adequate in order of magnitude to reduce α to a small value. Although the two processes would probably take place at the same time from general initial conditions, we may consider that the core has already been decelerated so that $\omega = \omega_m$ in magnitude. We then have the second case discussed above, with $\beta = \beta'$ in Fig. 2(c) and (d). Having seen that the vacillating direction of the relative motion in the core-fixed coordinate system does not bring about an effective cancellation of the frictional impulses imparted at various times, we assume that we may obtain a sufficient approximation to the torque effective in the astronomical coordinate system from the relative motion by use of Eq. (8.2) above. In making this assumption, we take into account, in the core-fixed system, the Coriolis forces due to the horizontal average motion of the various layers of fluid near the surface. We have no way of showing that the vortex-like fluctuations from this average, which describe the turbulence itself, would not behave quite differently, under the influence of the Coriolis forces and the closed-path motion of Fig. 2(e), than in the simple case. Qualitatively, one might expect large-scale turbulence to be less fully developed here than in a corresponding rotation about a steady axis. Such an effect would tend to make the lag between the axes larger than estimated below, but, even if extreme, would not make it larger than 24°. The inaccuracies discussed in footnote 3 tend in the opposite direction.

Even a comparatively small interaction, one capable of changing ω by as much as Ω in less than the lifetime of the earth, would gradually

bring ω into coincidence with the axis of the 24° cone about which ω_m precesses. But it requires an interaction which may have a considerable effect in less than 27,000 years to bring ω closer to ω_m and thus make α remain less than 24°. Starting with ω along the axis of the 24° cone, the time during which the rate of change of ω remains in the same general direction is about $27{,}000/2\pi$ years $= 1.3\times10^{11}$ sec. This value of t in Eq. (10.1) gives $\omega_r = 2\times10^{-7}$ sec.$^{-1} = 3\times10^{-3}\Omega$. This shows that the interaction is quite strong enough to make ω approximately parallel to an element of the cone, rather than stay near the axis of the cone. How closely it may keep up with ω_m in its precession may be found by substituting $|\dot{\omega}|$ for $-\dot{\omega}$ in Eq. (9′) and putting it equal to the magnitude of $\dot{\omega}_m$ in its precession, 2×10^{-16} sec.$^{-2}$. One finds

$$\omega_r = 3\times10^{-6}\ \text{sec.}^{-1} = \Omega/25.$$

Under the influence of turbulence alone, the axis of the core is thus expected to lag behind the axis of the mantle in the precession by an angle of about 2°. The relative angular velocity is great enough that it would correspond to about one revolution of the core inside the mantle in 25 days, if it were not for its rapid change of direction relative to the mantle. Because of its rapid change of direction, the motion of the core inside the mantle, as here estimated, can be described as the rolling of two cones on one another, as in Fig. 2(d) with $\alpha \approx 2°$. Each point in the core-fixed coordinate system then describes in the mantle-fixed coordinates a small closed figure daily (Fig. 2(e)). Near the surface of the core these figures have linear dimensions of about the order of magnitude $10^{-1}R = 300$ km.

Magnetic Drag in the Precession

The rapid change in the direction of the axis of rotation of the core in the mantle-fixed coordinate system completely alters the treatment of the magnetic drag. The earlier treatment considered the rotation of a conducting sphere about a fixed axis in a homogeneous field. In that case, only the component of the field normal to the axis could cause a drag, and the penetration of this component into the sphere was opposed by the induced currents, because of the steady flow of conducting matter across the lines along which the field seeks to establish itself. In the motion of the core relative to the mantle described in the preceding paragraph, the motion of the conducting matter is not steady, but is a periodic motion about small closed figures. Such a motion is not effective in opposing the penetration of the field. The time of penetration would be about the same as if the core were stationary. It may be estimated by putting $z = R$ in Eq. (15). One obtains, for the time of penetration to the center of the earth, about 3×10^{11} sec. $= 10^4$ years, which is much less than the age of the earth. This agrees in order of magnitude with the fact noted above that the division between "γ large" and "γ small," which is presumably the division between incomplete and complete penetration, lies at $\omega_r = 10^{-11}$ sec.$^{-1}$. We thus expect the magnetic field of the mantle to penetrate through the core from north to south.

We shall make a rough estimate of the effect of this penetrating field on the motion of the core. If this is at all comparable with the effect of the torque caused by turbulence, so that we are left with a motion of points of the core about closed paths with a period of one day, we should expect the lines representing the field to bend periodically near the surface of the core in such a way as to allow the lines deep within the core to follow the motion of the core rather closely. The angle at which the lines cross the surface of the core near the pole may be estimated from the requirement that the field supply an angular acceleration $|\dot{\omega}| = 2\times10^{-16}$ sec.$^{-2}$, as demanded by the precession. The tangential force per unit area applied to a surface by a field H penetrating the surface at an angle θ to the normal is found from the Maxwell magnetic stress tensor to be $(H^2/4\pi)\sin\theta\cos\theta$. Since the integrated normal component is not changed by the bending of the field at the surface, we may on the average say that the normal component of the earth's field at the surface of the core is $H_n = H\cos\theta$, and we have placed an upper limit to its magnitude at the poles, 10 dyne$^{1/2}$ cm^{-1}. The average value of H_n^2 over the surface is one-third of the value at the poles. For the magnetic torque on the core we obtain

$$\tfrac{1}{3}H_n^2R^3\sin\theta/\cos\theta,$$

where H_n is the value at the poles. For this to

be equal to $I|\dot{\omega}|$ in the precession, θ must satisfy

$$\tan\theta \approx (8\pi/5)\rho|\dot{\omega}|R^2/H_n^2 \approx 10 \qquad (17)$$

with the evaluation of constants suggested above.

Before applying this to the fluid core, let us consider a hypothetical case in which a rigid core is free to rotate with easy slipping at the surface. If this is accelerated by the magnetic drag, to keep up with the precession, the depth of penetration of the horizontal component of H is estimated, by putting $t=\frac{1}{2}$ day $=4\times10^4$ sec. in (15), to be about 10^5 cm. The angle α by which the core must lag behind the mantle in order that the magnetic drag shall supply the required acceleration is then roughly equal to this depth multiplied by $R^{-1}\tan\theta$, or $\alpha\approx3\times10^{-3}$. (In this connection, one may note that the error function $\Theta(q)$ in Eq. (2) is almost linear in q nearly up to the value $q=1$ which we have taken to correspond to the depth of penetration.) Such a small value of α is, of course, largely caused by the rigidity which was arbitrarily introduced in this case. But it is instructive to observe that the transverse motion of the magnetic lines through the matter is very small, even in this extreme case in which the induction in the outer skin of the core, less than $10^{-3}R$ thick, is responsible for the angular acceleration of the entire core.

In the case with only magnetic drag accelerating a fluid core, which we consider next, we may, therefore, neglect the transverse motion of the magnetic lines through the matter. In this case the axes of rotation of the successively deeper spherical shells of the core are expected to lag behind the axis of the mantle by successively greater angles, but, when an equilibrium has been reached in which these angles are constant in time, the torque required to maintain a steady angular acceleration of the core is the same as in the rigid case. Thus, even though the core is not a rigid body, (17) applies to this case also. Moreover, the analogous equation

$$\tan\theta(r) \approx (8\pi/5)\rho|\dot{\omega}|r^2/H_n^2 \approx 10r^2/R^2 \qquad (17')$$

serves to determine the inclination $\theta(r)$ of the magnetic lines at any radius r within the core. The angle of lag in the vicinity of the center is

$$\alpha=\int_0^R r^{-1}\tan\theta(r)dr \approx 5. \qquad (18)$$

The lines would spiral inward with almost one complete revolution if ω_m should precess in a plane. The magnetic drag alone would thus leave the interior rotating about the axis of the 24° cone. This value of α, which is necessary to make the magnetic drag sufficiently strong, is so much larger than the value 1/25 estimated in the case of turbulence alone that the mere *superposition* of the magnetic drag cannot be expected to modify that result appreciably.

Here we have not considered the possible *interaction* of the magnetic force and the turbulence—the manner in which the vortex motion within the turbulent flow might be modified by the presence of the magnetic field. In treating the possible penetration of the field through the vortex motion, we may consider that the angular speed of the eddies is at least of the order of magnitude of ω_r, say 10^{-6} sec.$^{-1}$. Then the parameter γ for the eddy, as discussed for the entire cone in connection with (11) above, is large if the size of the eddies is as great as 10^6 cm $=3\times10^{-3}R$. Since the eddies are probably larger than this, it seems unlikely that the field penetrates the eddies enough to make the interaction appreciable.

In the present state of geophysics, it seems impossible to be sure that one's hypotheses concerning the deep interior of the earth correspond to reality. An attempt has been made to discuss the situation which at present seems most plausible, but it may be that the results will merely serve in some way to prove—perhaps to disprove—the hypotheses. Our main result is that, if the core is a fluid at all similar to molten metals, the bulk of it has an angular velocity relative to the mantle, in order of magnitude a few percent as fast as the earth's rotation itself, in spite of the force due to turbulence and the smaller forces of direct viscosity and of magnetic induction.

The very helpful suggestions of Professor E. Teller and Dr. Ross Gunn have been appreciated. This investigation is, in fact, a sequel to a series of conversations with them on possible sources of the earth's magnetism, and to discussions at the Sixth Washington Conference on Theoretical Physics.

Perturbation of Boundary Conditions

H. FESHBACH AND A. M. CLOGSTON
Massachusetts Institute of Technology, Cambridge, Massachusetts

(Received November 18, 1940)

The perturbation method of solving boundary value problems with irregular boundary conditions has been re-examined and generalized. Problems are considered for which the boundary of the region is changed and the boundary conditions are unaltered, and also the inverse case where the boundary is fixed and the boundary conditions are changed. It is pointed out that the integrations involved in obtaining the perturbed eigenvalues will be in general very difficult, but that this difficulty can be avoided in two important cases. The perturbed eigenfunctions, however, can always be simply obtained. An application of the method was made to a problem in room acoustics which requires the calculation of second-order terms in the perturbation, and the results obtained for the pressure distribution and frequency were found to check well with experiment. A simple formula is found for the problem of the absorbing wall. The method is useful in calculating electromagnetic resonators of the "rhumbatron" type, and may also be useful in calculating electronic wave functions for metals. In Appendix III the method is applied to the scattering problem, and the results are related to Huygens' principle.

INTRODUCTION

MANY physical problems reduce to finding the eigenvalues and eigenfunctions of an equation of the type $H\phi+K\phi=0$ where H is some differential operator. It often happens that solutions are desired under circumstances differing slightly from conditions for which the solutions are well known. This perturbation can be introduced into the problem in two ways. First, small additional terms may enter the differential operator, whereupon the usual methods of perturbation theory are employed. Secondly, it may happen that the boundary conditions for the eigenfunctions are slightly different than in the case of the problem whose solutions are known. Problems of the second type arise in the Wigner-Seitz theory of metals, in problems in room acoustics, in electromagnetic radiation problems and in certain problems in quantum mechanics. In many cases problems of the second type can be reduced to the first kind as has been shown by Brillouin[1] and Cabrerra.[2] A method of obtaining first-order corrections to the unperturbed eigenvalues for problems of the second type has been indicated by Froelich,[3] but this method is not essentially different from that of Brillouin and Cabrerra (Appendix I). The method that is to be employed in this paper is nearly the same as that of Brillouin and Cabrerra. It is desired to bring out various aspects of the problem that have not been considered, and to show how solutions are actually to be obtained in certain cases.

METHOD

Let x represent some set of coordinates x_1, x_2, x_3, and let S_0 be a surface enclosing a region R_0. Suppose that the eigenvalue equation

$$H^0(x, \partial/\partial x)\phi_n^0(x)+K_n^0\phi_n^0(x)=0 \qquad (1)$$

has been solved with the ϕ_n^0 satisfying boundary conditions I on S_0. Suppose that the boundary conditions are such that the solutions are orthonormal. Two cases will be considered in this paper: case 1, $\phi_n^0=0$ on S_0; case 2, $\partial\phi_n^0/\partial n=0$ on S_0. Let S be a surface enclosing a region R. It is required to find the solutions of the equation

$$H^0(x, \partial/\partial x)\psi_n(x)+K_n\psi_n(x)=0 \qquad (2)$$

with ψ_n satisfying boundary conditions II on S. It will be supposed that ψ_n does not differ very much from ϕ_n^0. Let T be some operator, and define a function ϕ_n by $\phi_n=T\psi_n$. T must be such an operator that ϕ_n satisfies boundary conditions I on S_0.[4] Suppose that T may be written as $1+\sigma+\rho+\cdots$ where σ is a quantity small in first order and ρ is a quantity small in second order. The equation satisfied by ϕ_n is

$$(H^0+H^1+H^2+\cdots)\phi_n+K_n\phi_n=0, \qquad (3)$$

[1] L. Brillouin, Comptes rendus **204**, 1863 (1937).
[2] N. Cabrerra, Comptes rendus **207**, 1175 (1938).
[3] H. Froelich, Phys. Rev. **54**, 945 (1938).

[4] Brillouin and Cabrerra introduce an operator P such that $P\phi_n^0$ satisfies boundary conditions II on S. This is a more stringent condition than is necessary.

where

$$H^1=\sigma H^0-H^0\sigma, \tag{4}$$

$$H^2=(\rho-\sigma^2)H^0-H^0(\rho-\sigma^2)+\sigma H^1. \tag{5}$$

The problem has thus been reduced to one in which ordinary perturbation methods may be applied. One obtains the formulas

$$K_n=K_n^0-H_{nn}^1-H_{nn}^2+\sum_k{}'\frac{H_{nk}^1H_{kn}^1}{K_n^0-K_k^0}+\cdots, \tag{6}$$

$$\phi_n=\phi_n^0+\sum_k{}'\frac{H_{kn}^1}{K_k^0-K_n^0}\phi_k^0+\cdots. \tag{7}$$

The quantities H_{kn}^1 and H_{nn}^2 are given by

$$H_{kn}^1=\int_{R_0}\overset{*}{\phi}_k^0H^1\phi_n^0dV, \tag{8}$$

$$H_{nn}^2=\int_{R_0}\overset{*}{\phi}_n^0H^2\phi_n^0dV. \tag{9}$$

The prime on the summation sign indicates omission of the term with k equal to n. For these perturbation formulas to be valid, it is necessary that H^1 and H^2 do not introduce singularities into the problem. For ψ_n one may write to first order,

$$\psi_n=\phi_n^0-\sigma\phi_n^0+\sum_k{}'\frac{H_{kn}^1}{K_k^0-K_n^0}\phi_k^0. \tag{10}$$

It will now be assumed that H^0 is given by $H^0=\nabla^2+V(x)$. One then obtains the following results:

$$H_{kn}^1=(K_k^0-K_n^0)\sigma_{kn}-A_{kn}, \tag{11}$$

$$H_{nn}^2=(\sigma H^1)_{nn}-B_{nn}, \tag{12}$$

where

$$A_{kn}=\int_{S_0}\{\overset{*}{\phi}_k^0(\partial/\partial n)(\sigma\phi_n^0)-\partial\overset{*}{\phi}_k^0/\partial n(\sigma\phi_n^0)\}dS, \tag{13}$$

$$B_{nn}=\int_{S_0}\{\overset{*}{\phi}_n^0(\partial/\partial n)(\rho-\sigma^2)\phi_n^0-\partial\overset{*}{\phi}_n^0/\partial n(\rho-\sigma^2)\phi_n^0\}dS. \tag{14}$$

For ψ_n there can now be written,

$$\psi_n=(1-\sigma_{nn})\left[\phi_n^0+\{\sum_k\sigma_{kn}\phi_k^0-\sigma\phi_n^0\}-\sum_k{}'\frac{A_{kn}}{K_k^0-K_n^0}\phi_k^0\right]. \tag{15}$$

The expression in curly brackets needs some discussion. The sum $\sum_k\sigma_{kn}\phi_k^0$ is the expansion of $\sigma\phi_n^0$ and will be equal to it inside S_0. Aside from a normalization factor, ψ_n there depends only upon the surface integrals A_{kn}, and this means that ψ_n can always be easily obtained. This would not be the case, as will be seen later, if ψ_n really depended upon H_{kn}^1. In general, $\sigma\phi_n^0$ does not obey the same boundary conditions as ϕ_n^0. If it did, A_{kn} would vanish, and there could be no first-order change of the wave pattern. This is seen from the fact that a necessary condition for the orthogonality of the ϕ_n^0 is the vanishing of the integral

$$\int_{S_0}[\overset{*}{\phi}_k^0(\partial\phi_n^0/\partial n)-(\partial\overset{*}{\phi}_k^0/\partial n)\phi_n^0]dS. \tag{16}$$

Therefore, it is not necessarily true that the sum equals $\sigma\phi_n^0$ on S_0. If ϕ_n^0 is zero on S_0, the expression in curly brackets will be discontinuous on S_0, while if $\partial\phi_n^0/\partial n=0$ on S_0, it will show merely a discontinuity in slope. However, ψ_n will not show any discontinuity. This discontinuity on S_0 presents difficulties in obtaining the eigenvalues in certain cases and will be mentioned again in discussing the eigenvalue formulas.

The eigenvalue (6) may be written

$$K_n=K_n^0+A_{nn}+B_{nn}+\sigma_{nn}A_{nn}+[\sum_k\sigma_{nk}H_{kn}^1-(\sigma H^1)_{nn}]+\sum_k{}'\frac{H_{kn}^1A_{nk}}{K_k^0-K_n^0}.$$

One can usually represent σ by a first-order differential operator. In this case, it is possible to show that

$$(\sigma H^1)_{nn}=\sum_k\sigma_{nk}H_{kn}^1.$$

This formula does not follow obviously from the usual rules of matrix multiplication, because the conditions for application of these rules are not always fulfilled in the present case. Equation (11)

is an example of their failure. One can now write,

$$K_n = K_n^0 + A_{nn} + B_{nn} + \sigma_{nn}A_{nn} + \sum_k{}' \frac{H_{kn}^1 A_{nk}}{K_k^0 - K_n^0}. \quad (17)$$

Transformation Operators

Let $X_i(x)$ be defined so that, if x_i represents the coordinates of a point on S_0, $x_i + X_i(x)$ gives the coordinates of a point on S. An operator R is defined by

$$Rf(x) = f(x+X). \quad (18)$$

If one writes $R = 1 + \mu + \nu + \cdots$, then one has

$$\mu = \sum_i X_i \partial/\partial x_i, \quad \nu = \tfrac{1}{2}\sum_{i,j} X_i X_j (\partial^2/\partial x_i \partial x_j). \quad (19)$$

Case 1. Suppose that $\phi_n = 0$ on S_0 and $\psi_n = F(x)$ on S, where F is a small quantity. Then one has,

$$\begin{aligned} \psi_n(x) &= F(x) \quad x \text{ on } S, \\ R\psi_n(x) &= RF(x) \quad x \text{ on } S_0, \\ RT^{-1}\phi_n(x) &= RF(x) \quad x \text{ on } S_0. \end{aligned} \quad (20)$$

Placing $\phi_n = \phi_n^0 + \phi_n^1 + \phi_n^2 + \cdots$ and separating into orders one finds,

$$\text{first order:} \quad \sigma\phi_n^0 = \mu\phi_n^0 - F \quad (21)$$

$$\text{second order:} \quad \sigma\phi_n^1 + (\rho - \sigma^2)\phi_n^0 = \mu\phi_n^1 + \nu\phi_n^0 - \mu(\sigma\phi_n^0 + F). \quad (22)$$

Some special cases are worth mentioning:

Case 1a. If F is zero, it follows at once from (20) that a solution for T is $T = R$.

Case 1b. If S coincides with S_0, $R = 1$ and the equations become,

$$\sigma\phi_n^0 = -F, \quad (21a)$$

$$\sigma\phi_n^1 + (\rho - \sigma^2)\phi_n^0 = 0. \quad (22a)$$

Case 2. Suppose that $\partial\phi_n/\partial n = 0$ on S_0, and $\partial\psi_n/\partial n = F$ on S, where F is again a small quantity. Let the surface S be determined by the equation $S(x) = 0$ for x on S. Then one has that $S(x+X) = 0$ for x on S_0. Hence the function $S_0(x)$ determining S_0 may be defined by $S_0(x) = RS(x)$. Thus one has

$$\begin{aligned} S &= S_0 - \mu S_0 + (\mu^2 - \nu)S_0 + \cdots\cdots, \\ \nabla S &= \nabla S_0 - \nabla\mu S_0 + \nabla(\mu^2 - \nu)S_0 + \cdots\cdots. \end{aligned}$$

If $S(x)$ is given the proper sign, one has

$$\begin{aligned} \nabla S \cdot \nabla\psi_n &= |\nabla S| F \quad x \text{ on } S, \\ R(\nabla S \cdot \nabla T^{-1}\phi_n) &= R(|\nabla S| F) \quad x \text{ on } S_0. \end{aligned} \quad (23)$$

This last condition can be worked out in general as before, but the equations are very complicated. Some special cases are of more interest:

Case 2a. If F is zero, the conditions can usually be satisfied as before with $T = R$. Under these circumstances, the conditions become,

$$\text{first order:} \quad \nabla S_0 \cdot [\mu\nabla]\phi_n^0 + \nabla\phi_n^0 \cdot [\mu\nabla]S_0 = 0; \quad (24)$$

$$\begin{aligned} \text{second order:} \quad & \nabla S_0 \cdot [\mu\nabla]\phi_n^1 + \nabla\phi_n^1 \cdot [\mu\nabla]S_0 \\ & + \nabla S_0 \cdot [\nu\nabla]\phi_n^0 + \nabla\phi_n^0 \cdot [\nu\nabla]S_0 \\ & - \nabla S_0 \cdot [\mu\nabla]\mu\phi_n^0 - \nabla\phi_n^0 \cdot [\mu\nabla]\mu S_0 \\ & + [\mu\nabla]S_0 \cdot [\mu\nabla]\phi_n^0 = 0, \end{aligned} \quad (25)$$

where $[\mu\nabla]$ is a symbol for $(\mu\nabla - \nabla\mu)$. In a particular two-dimensional case that has been worked out, these somewhat complicated conditions simply demanded that the X_i satisfy Cauchy conditions on S_0. This could be anticipated.

Case 2b. If S coincides with S_0, the conditions become,

$$(\partial/\partial n)(\sigma\phi_n^0) = -F, \quad (26)$$

$$(\partial/\partial n)(\sigma\phi_n^1) + (\partial/\partial n)(\rho - \sigma^2)\phi_n^0 = 0. \quad (27)$$

Case 3. Suppose that $\partial\phi_n/\partial n = 0$ on S_0, and $\partial\psi_n/\partial n = F\psi_n$ on S_0. Here F is again a small quantity. In this case the conditions are

$$(\partial/\partial n)(\sigma\phi_n^0) = -F\phi_n^0, \quad (28)$$

$$(\partial/\partial n)(\sigma\phi_n^1) + (\partial/\partial n)(\rho - \sigma^2)\phi_n^0 = -F\phi_n^1 + F\sigma\phi_n^0. \quad (29)$$

The operators σ and ρ that are determined by these conditions should really carry another index that has been suppressed for simplicity. This index would indicate to which solution ϕ_n the σ was appropriate. Thus, the perturbation introduced into the equation for ϕ_n may be different from that introduced into the equation for ϕ_k.

Further Discussion of the Eigenvalues

In the previous section there have been worked out the conditions that must be fulfilled by σ and ρ in various cases. The notable fact about these conditions is that they must hold only upon the surface S_0. Nevertheless, in the eigenvalue formulas there enter matrix components that involve integrals of σ over the region R_0. If σ is

not specified in any way inside R_0, it would seem that any answer at all could be obtained by a suitable choice of σ. This certainly cannot be the case, for in any particular problem there will be introduced some parameter λ measuring the magnitude of the perturbation, and the eigenvalue will be a power expansion in this parameter. This expansion must be unique. Thus one comes to the conclusion that the results for each order must be independent of the volume behavior of σ, as long as it does not introduce singularities that will cause the expansions in the orthogonal set ϕ_n^0 to diverge. To find a σ satisfying all the boundary conditions and of sufficient continuity may be, in all but extremely simple cases, very difficult. Even if σ has been found, the matrix components σ_{kn} may be impossible to obtain except by numerical integration. One is led to suspect that, as in the case of the eigenfunctions, the eigenvalues can always be obtained in terms of surface integrals and thus made independent of the volume behavior of σ. It has not been found possible to do this in general. The difficulty is illustrated by the cases 1b and 2b for which conditions were deduced in the last section. The eigenvalues may be written,

$$\text{case 1b:}\quad K_n = K_n^0 + \int_{S_0} (\partial \overset{*}{\phi}_n^0/\partial n) F dS + \sigma_{nn} \int_{S_0} (\partial \overset{*}{\phi}_n^0/\partial n) F dS;$$

$$\text{case 2b:}\quad K_n = K_n^0 - \int_{S_0} \overset{*}{\phi}_n^0 F dS - \sigma_{nn} \int_{S_0} \overset{*}{\phi}_n^0 F dS,$$

where there is a direct dependence in second order upon σ_{nn}. The value of σ_{nn} must therefore be unique, but it has not been found possible to verify this in any way.

In certain cases, however, the eigenvalue can be written in a form depending only upon surface integrals. For case 3 where $\partial\phi_n/\partial n = 0$ on S_0 and $\partial\psi_n/\partial n = F\psi_n$ also on S_0, the eigenvalue formula becomes

$$K_n = K_n^0 + A_{nn} - \sum_k{}' \frac{A_{kn}A_{nk}}{K_k^0 - K_n^0} \tag{30}$$

with

$$A_{kn} = -\int_{S_0} F \overset{*}{\phi}_k^0 \phi_n^0 dS.$$

This equation is indeed independent of anything but known quantities and is in a very simple form. This case is of interest because of its application to acoustic problems. The boundary condition $\partial\psi_n/\partial n = F\psi_n$ describes conditions at an absorbing wall, F being a complex function related to the acoustic impedance.

In one other case the eigenvalue formula may be reduced to a form involving only surface integrals. This is for the case 2a. From Eq. (9) in Appendix II, it can be deduced that

$$K_n = K_n^0 + A_{nn} + \int_{S_0} (\sigma\phi_n^0)(\partial/\partial n)(\overset{**}{\sigma\phi}_n^0) dS - \int_{S_0} (\mathbf{n}\cdot\mathbf{D}) \overset{*}{\phi}_n^0 H^1 \phi_n^0 dS + B_{nn} - A_{nn} \int_{S_0} (\mathbf{n}\cdot\mathbf{D}) \overset{*}{\phi}_n^0 \phi_n^0 dS - \sum_k{}' \frac{A_{kn}\overset{*}{A}_{kn}}{K_k^0 - K_n^0}. \tag{31}$$

This formula has been applied as described below to calculating a certain problem in room acoustics.

The other very simple case 1a does not yield to this treatment. The eigenvalue expression may be written,

$$K_n = K_n^0 + A_{nn} + B_{nn} - \int_{S_0} (\partial \overset{*}{\phi}_n^0/\partial n)(\sum_k \sigma_{kn}\sigma\phi_k^0) dS - \sum_k{}' \frac{A_{kn}A_{nk}}{K_k^0 - K_n^0}.$$

But since $\sigma\phi_n^0 \neq 0$ on S_0, the series $\sum_k \sigma_{kn}\sigma\phi_k^0$ will diverge on S_0, and the series

$$\sum_k{}' \frac{A_{kn}A_{nk}}{K_k^0 - K_n^0}$$

must therefore also diverge. Since from Eq. (9) in Appendix II, $A_{nk} = \overset{*}{A}_{kn}$, an expression like (31) cannot be obtained. No other way of writing the eigenvalue has been found.

If it is assumed that the formulas are independent of the volume behavior of σ, a procedure can be given by means of which a closed form for the eigenvalue may be obtained in all cases. It amounts essentially to choosing a particular σ. Suppose that σ is such that one has

$$H^1 = \sigma H^0 - H^0\sigma = cH^0 \tag{32}$$

where c is some constant. It is seen at once that c must be A_{nn}/K_n^0. Thus one has $H_{kn}^1 = -A_{nn}\delta_{kn}$.

The eigenvalue expression then becomes

$$K_n = K_n^0 + A_{nn} + B_{nn} + \sigma_{nn} A_{nn} \tag{33}$$

and the problem is to find σ_{nn}. One has from (32)

$$H^0(\sigma\phi_n^0) + K_n^0(\sigma\phi_n^0) = A_{nn}\phi_n^0. \tag{34}$$

Let $G(x, x')$ be the Green's function for the region R_0 and the equation $H^0\phi + K_n^0\phi = 0$. Then,

$$\sigma\phi_n^0 = \int_{R_0} G(x, x') A_{nn}\phi_n^0 dV' + \int_{S_0} \{\partial G(x, x')/\partial n' [\sigma\phi_n^0]_{x'} - G(x, x')[(\partial/\partial n)(\sigma\phi_n^0)]_{x'}\} dS' \tag{35}$$

and

$$\sigma_{nn} = A_{nn} \int_{R_0} \int_{R_0} G(x, x') \overset{*}{\phi}_n^0(x) \phi_n^0(x') dV dV' + \int_{R_0} \overset{*}{\phi}_n^0 dV \int_{S_0} \left\{ \frac{\partial G(x, x')}{\partial n'} [\sigma\phi_n^0]_{x'} - G(x, x')[\partial/\partial n(\sigma\phi_n^0)]_{x'} \right\} dS'. \tag{36}$$

The Green's function used must be appropriate to having $\sigma\phi_n^0$ or $(\partial/\partial n)(\sigma\phi_n^0)$ specified on S_0. The expression obtained for ψ_n is of interest.

$$\psi_n = \phi_n^0 - A_{nn} \int_{R_0} G(x, x')\phi_n^0(x') dv' + \int_{S_0} \{\partial G(x, x')/\partial n' [\sigma\phi_n^0]_{x'} - G(x, x')[\partial/\partial n(\sigma\phi_n^0)]_{x'}\} dS'. \tag{37}$$

An application of formula (31) has been made to a problem in room acoustics. A rectangular box with perfectly reflecting walls was distorted into a trapezoidal cross section, and the distortion of the standing wave pattern and change of frequency computed for a particular mode of vibration. Experiments of this type have been made,[5] and it was possible to compare the results with experimental data. It was found that the pressure distribution was predicted closely, mostly within experimental error. The change of frequency from the unperturbed case was experimentally +4.9 percent while the calculated change was +4.2 percent.[6]

[5] R. H. Bolt, J. Acous. Soc. Am. **11**, 184 (1939).

[6] These calculations will be published in *The Journal of the Acoustical Society of America*.

Conclusion

It has been found that the perturbed eigenfunctions ψ_n can always be found by a surface integration over known quantities. The perturbed eigenvalues, however, as given by Eq. (17), may involve volume integrals of the transformation operator σ, and no general way has been found of eliminating these integrals. In two cases, 2a and 3, however, where the unperturbed eigenfunctions have normal boundary conditions, the eigenvalue can be so expressed as to depend only upon surface integrals and can therefore be easily calculated. Of these two cases, the first has direct application to the Wigner-Seitz theory of metals, to electromagnetic resonators and to acoustic problems, where it has been found to give accurate results. The second case can lead to complex eigenvalues and applies directly to the problem of the slightly absorbing wall. If it is assumed, as seems to be necessarily true, that the eigenvalues are independent of the volume behavior of σ, then for all cases formulae involving a Green's function of the unperturbed region can be obtained for the perturbed eigenfunctions and eigenvalues.

We wish to thank Professor P. M. Morse for reading this paper and for the interest he has taken in it during its preparation.

Appendix I

In this appendix it will be shown that the method employed by Froelich if extended to include second-order terms leads to results identical with the perturbation method. One has obviously,

$$K_n = K_n^0 + \frac{\int_{S_0} \{\psi_n \partial\overset{*}{\phi}_n^0/\partial n - \overset{*}{\phi}_n^0 \partial\psi_n/\partial n\} dS}{\int_{R_0} \psi_n \overset{*}{\phi}_n^0 dV}. \tag{1}$$

Take for ϕ_n the expression

$$\phi_n = \phi_n^0 + \sum_k{}' B_{kn}\phi_k^0$$

where

$$B_{kn} = \frac{\overset{1}{H}_{kn}}{K_k^0 - K_n^0} + \text{second-order terms.}$$

Then for ψ_n to second order one obtains

$$\psi_n = \phi_n^0 + \sum_k{}' B_{kn}\phi_k^0 - \sigma\phi_n^0 - \sum_k{}' \frac{\overset{1}{H}_{kn}}{K_k^0 - K_n^0}\sigma\phi_k^0 + (\sigma^2 - \rho)\phi_n^0.$$

If this is employed in (1), there is obtained directly Eq. (17).

Appendix II

A formula used in Eq. (31) will be established in this appendix. First, the integral $\int_R f(x)dV$ taken over the region R will be expressed as an integral taken over the region R_0. Consider

$$\int_R f(x)dV=\int_R f(x)J(x)dx_1dx_2dx_3, \tag{1}$$

where J is a quantity dependent upon the coordinate system chosen. A new set of variables x_i' is now introduced by the equations

$$x_i=x_i'+X_i(x'). \tag{2}$$

One now has,

$$\int_R f(x)dV=\int_{R_0} R'(fJ)\frac{\partial(x_1, x_2, x_3)}{\partial(x_1', x_2', x_3')}dx_1'dx_2'dx_3'. \tag{3}$$

If the following quantities are defined,

$$\alpha=\sum_i\frac{\partial X_i}{\partial x_i}, \quad \beta=\tfrac{1}{2}\sum_{i,j}\left(\frac{\partial X_i}{\partial x_i}\frac{\partial X_j}{\partial x_j}-\frac{\partial X_i}{\partial x_j}\frac{\partial X_j}{\partial x_i}\right), \tag{4}$$

the integral may be written, dropping the primes,

$$\int_R f(x)dV=\int_{R_0} R(fJ)(1+\alpha+\beta+\cdots)dx_1dx_2dx_3. \tag{5}$$

If for $f(x)$ one takes $\overset{*}{\psi}_n(x)\psi_k(x)$, the integral (5) becomes on evaluation to first-order terms,

$$\begin{aligned}\int_R \overset{*}{\psi}_n\psi_k dV=&\int_{R_0}\overset{*}{\phi}_n\phi_k dV\\&+\int_{R_0}\sum_i(\partial/\partial x_i)(\overset{*}{\phi}_n{}^0\phi_k{}^0JX_i)dx_1dx_2dx_3\\&-\int_{R_0}[\overset{*}{\phi}_n{}^0\sigma\phi_k{}^0+\phi_k{}^0\overset{**}{\sigma}\overset{*}{\phi}_n{}^0]dV.\end{aligned} \tag{6}$$

From (6) there are obtained two results, one for $k\neq n$ and one for $k=n$. To write these, a vector $\mathbf{D}$ is defined by the equation

$$\mathbf{D}=\sum_i(\partial\mathbf{r}/\partial x_i)X_i, \tag{7}$$

where $\mathbf{r}$ is the radius vector. In terms of $\mathbf{D}$ one has,

$$\sigma=\mathbf{D}\cdot\nabla, \quad (1/J)\sum_i(\partial/\partial x_i)(JX_i)=\nabla\cdot\mathbf{D}. \tag{8}$$

Except for second-order terms, $\mathbf{D}$ is the vector displacement corresponding to the increments X_i. For $k\neq n$, one obtains, using Eq. (11),

$$\int_R\overset{*}{\psi}_n\psi_k dV=\left(\frac{A_{nk}-\overset{*}{A}_{kn}}{K_k{}^0-K_n{}^0}\right)+\int\mathbf{n}\cdot\mathbf{D}\overset{*}{\phi}_n{}^0\phi_k{}^0dS. \tag{9}$$

For $k=n$, there is found

$$\int_R\overset{*}{\psi}_n\psi_n dv=1+\int_{S_0}\mathbf{n}\cdot\mathbf{D}\overset{*}{\phi}_n{}^0\phi_n{}^0dS-(\sigma_{nn}+\overset{*}{\sigma}_{nn}). \tag{10}$$

Equation (8) gives information about the relation of A_{nk} and $\overset{*}{A}_{kn}$. If ψ_n obeys boundary conditions that make the solutions orthogonal, and if $\phi_k{}^0$ is zero on S_0, then $A_{nk}=\overset{*}{A}_{kn}$. The surface integral also vanishes in cases where S coincides with S_0. The formula (9) relates the normalization of ψ_n and ϕ_n.

Appendix III

Here the method developed in this paper will be applied to the continuous eigenvalue case, the problem of scattering. The equation satisfied by ϕ_n is to first order,

$$H^0\phi_n+K_n\phi_n=-H^1\phi_n{}^0. \tag{1}$$

If Φ_n is the solution of the homogeneous equation, the solution of the inhomogeneous equation may be written,

$$\phi_n=\Phi_n+\int_{R_0}G(x, x')H^1\phi_n{}^0dV, \tag{2}$$

where it has been specified that ϕ_n behave as Φ_n plus a first-order term, and where $G(x, x')$ is the Green's function for the region R_0. From the properties of the Green's function, Eq. (2) becomes

$$\begin{aligned}\phi_n=\Phi_n+\sigma\phi_n{}^0+\int_{S_0}\{&G(x, x')[(\partial/\partial n)(\sigma\phi_n{}^0)]_{x'}\\&-[\sigma\phi_n{}^0]_{x'}(\partial/\partial n)G(x, x')\}dS'.\end{aligned} \tag{3}$$

For ψ_n, one has to first order,

$$\begin{aligned}\psi_n=\Phi_n+\int\{&G(x, x')[(\partial/\partial n)(\sigma\phi_n{}^0)]_{x'}\\&-[\sigma\phi_n{}^0]_{x'}(\partial/\partial n)G(x, x')\}dS'.\end{aligned} \tag{4}$$

This result is related to Huygens' principle. It is the result that would be obtained by solving the equation $H^0\psi_n+K_n\psi_n=0$ by means of a Green's function and using in the surface integral, as a first approximation, the Green's function for the region R_0 and the unperturbed functions $\phi_n{}^0$. This is the method employed by Sommerfeld.[7]

[7] P. Frank and R. von Mises, *Reimann-Weber Differential Gleichungen der Physik*, Vol. 2 (Fred. Vieweg & Sohn, 1927), p. 478.

On an Asymmetrical Metric in the Four-Space of General Relativity

GUNNAR RANDERS
Yerkes Observatory of the University of Chicago, Chicago Illinois
(Received October 1, 1940)

Physical space-time allows of a metric of asymmetrical properties because of the unidirection of time. The simplest possible asymmetrical generalization of Riemannian metric is considered. The study of this metric is here mainly confined to the mathematical aspects. However, the physical consequences by application to space-time are obvious, and may be of interest by leading directly to a description of the electromagnetic field. A close formal connection with five-dimensional Riemannian geometry is shown, which might carry interest for the physical interpretation of five-dimensional relativity.

1. INTRODUCTION

IN the geometry of affinely connected spaces the metrical and the affine properties are completely independent. The characteristics of the space described by the curvature tensor are derivable from the definition of parallel displacement, or covariant derivation. Only when we want to compare vectors of different directions, the need for a metric arises. We are, however, quite free in the choice of metric. That is, we can choose at will measuring units in every direction at each point of the space. The locus of the end points of all the unit lengths radiating from a certain point x_0, is called the indicatrix. In Euclidian geometry this locus is a (hyper-) sphere around x_0. In Riemannian geometry the indicatrix is a quadratic surface around x_0, with coefficients equal to the fundamental tensor $g_{\mu\nu}$, which already exists in each point by the definition of the Riemannian parallel displacement.

There would be nothing to prevent the choice of another tensor, $h_{\mu\nu}$, to define the metric. As far as the application to physical space-time goes, however, there is no indication of the need for a new tensor, because there is no need for twenty independent potentials. However, the Riemannian metric has one property which does not seem quite appropriate for the application to physical space-time, and that is the perfect symmetry between opposite directions for any coordinate interval. Perhaps the most characteristic property of the physical world is the unidirection of time-like intervals. Since there is no obvious reason why this asymmetry should disappear in the mathematical description it is of interest to consider the possibility of a metric with asymmetrical properties.

2. THE ECCENTRIC METRIC

It is known that many reasons speak for the necessity of a quadratic indicatrix.[1] The only way of introducing an asymmetry while retaining the quadratic indicatrix, is to displace the center of the indicatrix. In other words, we adopt as indicatrix an eccentric quadratic (hyper-) surface. This involves the definition of a vector at each point of the space, determining the displacement of the center of the indicatrix. The formula for the length ds of a line-element dx^μ must necessarily be homogeneous of first degree in dx^μ. The simplest "eccentric" line-element possessing this property, and of course being invariant, is

$$ds = k_\mu dx^\mu + (g_{\mu\nu} dx^\mu dx^\nu)^{\frac{1}{2}}, \qquad (1)$$

where $g_{\mu\nu}$ is the fundamental tensor of the Riemannian affine connection, and k_μ is a covariant vector determining the displacement of the center of the indicatrix. If a space of Riemannian affine connection is given, we are, as mentioned earlier, completely free in our choice of metric, and consequently free in our choice of the vector k_μ. This vector, therefore, does not describe any properties of the Riemannian space considered, but only the properties of the units chosen for measuring intervals. To change from one vector field k_μ to another, only means to change from one system of asymmetrical units to another. By each of the measuring systems

[1] H. Weyl, "Die Einzigartigkeit der Pythagoreischen Massbestimmung," Math. Zeits. **12**, 114–146.

we can determine certain paths in the space, defined by the condition

$$\delta \int ds = 0. \tag{2}$$

We may now divide the variety of arbitrary vector fields k_μ into classes giving the same paths (2). If we only allow changes of units within each class, the vector k_μ has attained a certain significance besides describing the units chosen, namely by defining a set of paths. The only change of k_μ which will not affect the path defined by (2) is the addition of an arbitrary gradient vector,

$$k_\mu' = k_\mu + \partial\phi/\partial x^\mu. \tag{3}$$

The change (3) will according to (1) result in the addition of a total differential $d\phi$ to ds. Hence

$$ds' = ds + (\partial\phi/\partial x^\mu)dx^\mu \tag{4}$$

and this addition does not affect Eq. (2). The change of units corresponding to the transformation (3) will be called a k transformation. The fundamental difference from the gauge-transformation of Weyl should be noticed. Weyl's transformation is a change of units at different points, while the k transformation is a change of units in different directions at the same point.

3. The Asymmetry of Time-Like Intervals

The quadratic form with coefficients $g_{\mu\nu}$ is indefinite. When the invariant

$$g_{\mu\nu}dx^\mu dx^\nu \tag{5}$$

is positive, the interval is "time-like," when negative, it is "space-like." For space-like intervals the square root in (1) becomes imaginary, and ds consequently complex. But the results of measurements are real numbers. We, therefore, assume that the result of measurement is given by the absolute value $|ds|$. Time-like intervals are purely real, so that we have simply

$$(\pm)\,|ds| = k_\mu dx^\mu + (g_{\mu\nu}dx^\mu dx^\nu)^{\frac{1}{2}}. \tag{6}$$

Space-like intervals are complex, the square root being the imaginary part. The absolute value becomes

$$|ds| = [(k_\mu k_\nu - g_{\mu\nu})dx^\mu dx^\nu]^{\frac{1}{2}}. \tag{7}$$

It follows that a reversal of sign of a space-like interval dx^μ does not affect the measured length, because the form (7) is purely quadratic. For time-like intervals this is different. The linear term $k_\mu dx^\mu$ will change its sign with dx^μ, and we have different values of $|ds|$ for opposite directions.

It might seem as though our introduction of an asymmetrical line-element has also introduced an absolute preferred direction, at each point, defined by the vector k_μ. However, this preference arises only as a result of the special system of units chosen. We can change k_μ by changing to new units by a k transformation, without affecting the properties of space, or even of the paths of extreme length as measured by our system. The direction of k_μ is, therefore, not determined before we have specified the units we want to use. And as these units are a matter of convention, there is obviously no absolute direction given.

If k_μ is a given time-like vector, we can, of course, transform our coordinates so as to make the time-coordinate go in the k_μ direction. In this coordinate system k_μ has no components perpendicular to the time-axis, and measurements perpendicular to the time-axis will by (7) give the usual Riemannian length

$$|ds| = (g_{\mu\nu}dx^\mu dx^\nu)^{\frac{1}{2}}. \tag{8}$$

However, since quite generally the asymmetry does only affect time-measurements, there is no reason for considering this system of coordinates as unique.

4. The Paths of Extreme Length

We shall study the type of extreme paths resulting from our choice of measuring units, as defined by the eccentric line-element (1). The equation for the path is

$$\delta \int [k_\mu dx^\mu + (g_{\mu\nu}dx^\mu dx^\nu)^{\frac{1}{2}}] = 0. \tag{9}$$

We consider a path of time-like direction, i.e., ds is real. Now choose a parameter τ, and denote differentiation with respect to τ by a dot:

$$\delta \int [k_\mu \dot{x}^\mu + (g_{\mu\nu}\dot{x}^\mu \dot{x}^\nu)^{\frac{1}{2}}] d\tau = 0.$$

The equivalent Eulerian equations are

$$\frac{d}{d\tau}\frac{\partial}{\partial \dot{x}^\nu}[k_\mu \dot{x}^\mu + (g_{\mu\nu}\dot{x}^\mu \dot{x}^\nu)^{\frac{1}{2}}] - \frac{\partial}{\partial x^\nu}[k_\mu \dot{x}^\mu + (g_{\mu\nu}\dot{x}^\mu \dot{x}^\nu)^{\frac{1}{2}}] = 0,$$

or

$$\frac{d}{d\tau}\left(k_\nu + \frac{1}{2}\frac{(g_{\mu\nu}+g_{\nu\mu})\dot{x}^\mu}{(g_{\alpha\beta}\dot{x}^\alpha \dot{x}^\beta)^{\frac{1}{2}}}\right) - \frac{\partial k_\mu}{\partial x^\nu}\dot{x}^\mu - \frac{1}{2}\frac{\dot{x}^\mu \dot{x}^\alpha \partial g_{\mu\alpha}/\partial x^\nu}{(g_{\alpha\beta}\dot{x}^\alpha \dot{x}^\beta)^{\frac{1}{2}}} = 0. \quad (10)$$

We now specify the arbitrary parameter by putting

$$d\tau = (g_{\alpha\beta}dx^\alpha dx^\beta)^{\frac{1}{2}}, \quad (11)$$

which makes the square root $(g_{\alpha\beta}\dot{x}^\alpha \dot{x}^\beta)^{\frac{1}{2}}$ equal to unity. We can do so without inconsistency because the square root mentioned is an integral of the resulting Eq. (14).[2] Performing the differentiation in (10), and changing some summation indices, we get

$$g_{\mu\nu}\ddot{x}^\mu + \frac{1}{2}\left(\frac{\partial g_{\mu\nu}}{\partial x^\alpha}\dot{x}^\mu \dot{x}^\alpha + \frac{\partial g_{\alpha\nu}}{\partial x^\mu}\dot{x}^\mu \dot{x}^\alpha - \frac{\partial g_{\mu\alpha}}{\partial x^\nu}\dot{x}^\mu \dot{x}^\alpha\right) + \left(\frac{\partial k_\nu}{\partial x^\alpha} - \frac{\partial k_\alpha}{\partial x^\nu}\right)\dot{x}^\alpha = 0.$$

Using the familiar notations

$$\{\mu\alpha, \sigma\} = g^{\sigma\nu}[\mu\alpha, \nu] = g^{\sigma\nu}\cdot\frac{1}{2}\left(\frac{\partial g_{\mu\nu}}{\partial x^\alpha} + \frac{\partial g_{\alpha\nu}}{\partial x^\mu} - \frac{\partial g_{\mu\alpha}}{\partial x^\nu}\right) \quad (12)$$

$$F^\sigma{}_\alpha = g^{\sigma\nu}F_{\nu\alpha} = g^{\sigma\nu}\left(\frac{\partial k_\nu}{\partial x^\alpha} - \frac{\partial k_\alpha}{\partial x^\nu}\right) \quad (13)$$

we obtain after multiplication by $g^{\nu\sigma}$

$$\ddot{x}^\sigma + \{\mu\alpha, \sigma\}\dot{x}^\mu \dot{x}^\alpha + F^\sigma{}_\alpha \dot{x}^\alpha = 0. \quad (14)$$

As we expected, Eq. (14) is invariant for k transformations. If k_μ is a gradient vector, the path reduces to the Riemannian geodesic.

It will be noted that starting a path (14) with initial conditions given in the form of "velocities" $(dx^1/dx^4, dx^2/dx^4, dx^3/dx^4, 1)$, there are two paths possible. This is because a reversal of the signs of all dx^μ does not affect the "velocities," while the effect on Eq. (14) is to reverse the sign of the term $F^\sigma{}_\alpha \dot{x}^\alpha$.

5. Connection with Five-Dimensional Riemannian Geometry

Suppose we assign to a space not only the affine properties, but also the property of possessing certain paths of extreme length. If there exist laws describing these properties, it is obvious that such laws must be covariant for coordinate transformations as well as for k transformations. In order to treat both kinds of transformations under one, we can proceed in the following way:

By the formula for the eccentric line-element the length of a vector A^μ is

$$A = k_\mu A^\mu + (g_{\mu\nu}A^\mu A^\nu)^{\frac{1}{2}}. \quad (15)$$

Moving $k_\mu A^\mu$ to the left-hand side and squaring the equation gives

$$(g_{\mu\nu} - k_\mu k_\nu)A^\mu A^\nu + 2k_\mu A^\mu A - A^2 = 0. \quad (16)$$

Consider now a 5-dimensional Riemannian space with fundamental tensor γ_{mn}, $(m, n = 1, 2, 3, 4, 5;\ \mu, \nu = 1, 2, 3, 4)$

$$\gamma_{\mu\nu} = g_{\mu\nu} - k_\mu k_\nu;\ \gamma_{\mu 5} = \gamma_{5\mu} = k_\mu;\ \gamma_{55} = -1. \quad (17)$$

It follows immediately from (16) that a 5-vector in the space (17) with components A^1, A^2, A^3, A^4, and A, is a zero-length 5-vector. In other words, the fifth component A^5 of a null-vector in the 5-space (17) represents the measured length of the 4-vector A^μ composed of the first four components of the 5-vector. This property makes the 5-space (17) useful for expressing the metrical properties of our 4 space. It is obvious that any 5-space conformal with (17) would do, since it is only the ratio of the coefficients that count. However, the affine properties of our Riemannian 4-space are determined by $g_{\mu\nu}$, and not by this quantity multiplied by an arbitrary function. It is therefore necessary to specify the tensor γ_{mn} to the values (17) if we want to describe the properties of the 4-space by the properties of the corresponding 5-space. It should be remarked, however that a constant factor of proportionality may always be introduced in (17), because such

[2] Multiplying (14) by $g_{\sigma\beta}\dot{x}^\beta$ gives

$$g_{\sigma\beta}\dot{x}^\beta \frac{d}{d\tau}\dot{x}^\sigma + \frac{1}{2}\left(\frac{d}{d\tau}g_{\sigma\beta}\right)\dot{x}^\sigma \dot{x}^\beta = 0$$

or $g_{\sigma\beta}\dot{x}^\sigma \dot{x}^\beta = \text{const.}$

a factor does not affect the affine properties of space.

A 5-dimensional space of the type (17) has been used frequently for representing gravitational and electromagnetic laws by Riemannian geometry,[3] and also for introducing the quantum concept into the geometrical picture. The lack of physical interpretation of the fifth coordinate seems to be the main obstacle to the theory.

If the length A is denoted by A^5, the formula for the length of A^μ can be written

$$\gamma_{mn}A^m A^n = 0. \tag{18}$$

Similarly for the interval length

$$\gamma_{mn}dx^m dx^n = 0, \tag{19}$$

where $dx^5 = ds$. It must, however, be remembered that the interpretation $dx^5 = ds$ is only valid for null-directions and cannot be integrated to give $x^5 = s$. This is obvious because ds is not a perfect differential.

It is easily realized that a coordinate transformation in 5-space of the form

$$x^{\mu'} = x^{\mu'}(x^1, x^2, x^3, x^4); \quad x^{5'} = x^5 \tag{20}$$

has the same effect on the fundamental quantities $g_{\mu\nu}$, k_μ, and on 4-vectors A^μ as the corresponding coordinate transformation in 4-space. The length A^5 is left unchanged. Similarly it is realized that a 5-coordinate transformation

$$x^{\mu'} = x^\mu; \quad x^{5'} = x^5 + \phi(x^1, x^2, x^3, x^4) \tag{21}$$

has the same effect as a k transformation. By combining (20) and (21) we can therefore treat k transformations and coordinate-transformations simultaneously as a single coordinate-transformation in 5-space. This transformation leaves the "cylindricity" of the space (17) unaffected.

Because of the one-to-one correspondence between the 4-space of $g_{\mu\nu}$ and k_μ, and the Riemannian 5-space of γ_{mn}, the properties of one are determined by the properties of the other, and we can study the combined metrical and affine properties of the four space by studying the affine properties of the Riemannian 5-space. Instead of looking for equations in $g_{\mu\nu}$ and k_μ, being covariant for k and coordinate-transformations, we can use 5-dimensional tensor equations involving γ_{mn}.

It is easy to show that the x^μ-projection of a Riemannian null-geodesic in the 5-space (17) is identical with the extreme path (14) in our 4-space of eccentrical metric.

The role played by the Riemannian 5-space can now be described shortly as follows: By means of the fundamental quantities $g_{\mu\nu}$ and k_μ of a space of Riemannian affine connection and eccentric metric we can construct a 5-dimensional Riemannian space (17). There is a direct correspondence between simultaneous coordinate- and k transformations in 4-space and simple coordinate-transformations in 5-space. Only null-directions in 5-space have a correspondence with 4-space, and the fifth component of a null-vector or line-element represents the measured length of the vector. The advantage of using the 5-dimensional method of representation arises from the fact that tensor equations in the 5-space represent, in 4-space, equations that are covariant for k transformations as well as coordinate-transformations.

The 5-space is introduced merely as a mathematical auxiliary. The fifth coordinate does only enter by its differential, and its interpretation is then clear: it is the measured interval length of dx^μ. The transformation of the fifth coordinate represents the change to new measuring units in 4-space, giving the same extreme paths.

6. "Physical" Space

The *Einstein-Ricci* tensor of the 5-space (17), expressed in the quantities $g_{\mu\nu}$ and k_μ have components of the form[4]

$$G^{\mu\nu} = (R^{\mu\nu} - \tfrac{1}{2}g^{\mu\nu}R) + \tfrac{1}{2}E^{\mu\nu}; \tag{22}$$

$$G_5{}^\nu = \tfrac{1}{2}F^{\nu\alpha}{}_{;\alpha} \tag{23}$$

$$G_{55} = \tfrac{1}{2}(R - \tfrac{3}{4}F^{\alpha\beta}F_{\alpha\beta}). \tag{24}$$

Here $E^{\mu\nu} = -F^{\mu\alpha}F_\alpha{}^\nu + \frac{1}{4}g^{\mu\nu}F_{\alpha\beta}F^{\alpha\beta}$, and $R^{\mu\nu}$ is the 4-dimensional *curvature* tensor. The quantities G^{mn} can be calculated if one knows the fundamental quantities $g_{\mu\nu}$ and k_μ.

[3] Originally by T. Kaluza, Preuss. Akad. Wiss. **54**, 966 (1921); Also O. Klein, Zeits. f. Physik **46**, 188 (1927); L. Rosenfeld, Bull. Akad. Roy. Belg. **13**, 304 (1927). For further references see O. Veblen, *Projective Relativitätstheorie* (Springer, 1933).

[4] See L. Rosenfeld, reference 3, p. 310.

We recall the fact that only null-vectors in 5-space have an immediate significance in terms of measurements in 4-space. Multiplying G_l^m by an arbitrary null-vector A^l gives a new 5-vector

$$B^m = G_l^m A^l. \tag{25}$$

We will now demand that B^m has also an interpretation in 4-space, as a vector and its length, which means that B^m must be a null-vector. This gives the condition

$$\gamma_{mn}(G_l^m A^l)(G_q^n A^q) = 0$$

or

$$(\gamma_{mn} G_l^m G_q^n) A^l A^q = 0.$$

But A^l is an arbitrary null-vector,

$$\gamma_{lq} A^l A^q = 0.$$

Consequently

$$G_{nl} G_q^n = \theta \gamma_{lq} \tag{26}$$

where θ is a function of the coordinates. Equation (26) gives the condition to be satisfied by the fundamental quantities $g_{\mu\nu}$ and k_μ in our space. There are fifteen equations (symmetrical 5-tensor of second rank), and fifteen functions, $g_{\mu\nu}$, k_μ and θ. We shall consider some examples of such spaces.

(1) One possible way to satisfy (26) would obviously be to put

$$G^{mn} = \lambda \gamma^{mn}. \tag{27}$$

Here $\lambda = \theta^{\frac{1}{2}}$ must be a numerical constant because the divergence of G^{mn} is known to vanish identically. Expressed in 4-dimensional quantities (27) becomes

$$(R^{\mu\nu} - \tfrac{1}{2} g^{\mu\nu} R) + \tfrac{1}{2} E^{\mu\nu} = \lambda g^{\mu\nu}; \quad F^{\nu\alpha}{}_{;\alpha} = 0. \tag{28), (29}$$

Contracting (28) gives $-R = 4\lambda$, which together with the (5,5)-component of (27) becomes

$$\lambda = -\tfrac{3}{8} F^{\alpha\beta} F_{\alpha\beta}. \tag{30}$$

If $\lambda = 0$ the above equations are those of Einstein and of Maxwell for space containing plane electromagnetic waves only. If $F^{\alpha\beta}$ is also zero, (28) is Einstein's law for empty space.

(2) Writing (26) in the form

$$G_n{}^l G_q^n = \delta_q^l \cdot \theta$$

it is obvious that this equation can also be satisfied by the following system, in which $\theta^{\frac{1}{2}}$ need not be constant:

$$\begin{aligned} G_1^1 &= \theta^{\frac{1}{2}}, \quad \text{(a)} & G_4^4 &= \theta^{\frac{1}{2}}, \quad \text{(d)} \\ G_2^2 &= -\theta^{\frac{1}{2}}, \quad \text{(b)} & & \\ G_3^3 &= -\theta^{\frac{1}{2}}, \quad \text{(c)} & G_5^5 &= \pm\theta^{\frac{1}{2}}, \quad \text{(e)} \end{aligned} \tag{31}$$

while $G_{mn} = G^{mn} = G_n^m = 0$ when $m \neq n$. Putting $E_1^1 = -E_2^2 = -E_3^3 = E_4^4 = \frac{1}{4} F^{\alpha\beta} F_{\alpha\beta} = \frac{1}{2} F^{14} F_{14}$ as in a static symmetrical field with $k_4 = \epsilon/r$ the equation (e) gives

$$3E_1^1/2 = \pm\theta^{\frac{1}{2}}$$

and (31) becomes

$$R_1^1 = R_4^4 = \begin{cases} -2E_1^1 \\ +\ E_1^1 \end{cases}, \quad R_2^2 = R_3^3 = \begin{cases} +2E_1^1 \\ -\ E_1^1 \end{cases}, \tag{32}$$

which gives solutions of the type known as Nordström's solution[5] for the field of a charged particle. There appear to be two possibilities, one in which the gravitational effect of the charge counteracts the term m/r of the Schwarzschild line-element, another where the two act in the same direction.

(3) The static, symmetrical field

$$ds^2 = -\frac{dr^2}{1+\alpha/r^2} - r^2 d\theta^2 - r^2 \sin^2\theta d\varphi^2 + dt^2 \tag{33}$$

where k_μ vanishes identically is also a possible solution of (26). It is a solution of the form (31) with

$$G_1^1 = -G_2^2 = -G_3^3 = -G_4^4 = -G_5^5 = \theta^{\frac{1}{2}} = \alpha/r^4.$$

If interpreted as a particle-solution, (33) represents a particle without any first-order interaction with other particles (because $g_{44} = \text{const.}$). A "neutrino" field might be the nearest suggestion.

The *fundamental equation* (26) is seen to be a generalization of Einstein's equation for empty space. Besides the well-known particle solutions of general relativity (26) appears to be satisfied by the field of an electromagnetic wave and by the "neutrino" field (33).

I am indebted to Dr. H. P. Robertson for helpful criticism of the present work.

---

[5] See A. S. Eddington, *Mathematical Theory of Relativity* (Cambridge University Press, 1924), second edition, p. 185

Conduction of Electricity by Dielectric Liquids at High Field Strengths

H. J. PLUMLEY*
Commonwealth Edison Company, Chicago, Illinois
(Received November 14, 1940)

The conductivity of highly purified heptane has been measured between optical flats at field strengths up to 600,000 volts per cm and at temperatures ranging from −190°C to 20°C. Electrode separations down to 0.005 cm were used in order to minimize the effect of space charge and ionic recombination. It is concluded that electronic or collision processes are unlikely as the source of high field conductivity in heptane and probably most other liquid dielectrics as well. It is suggested that the highly nonconducting dielectric liquids should be included as extreme cases in the general class of weak electrolytes. The presence of appreciable conductivity under high electric fields is ascribed to the lowering of the energy of the hydrogen bond by the applied field.

INTRODUCTION

IN spite of a considerable revival of interest in recent years in the problem of the high field electrical conductivity of dielectric liquids, no one of the several theories proposed to explain the observed phenomena has ever managed to obtain widespread acceptance. In this paper the results of some new experiments designed to determine which of the various theories is most valid will be presented. There is no essential indeterminacy since the predictions of the different theories differ widely for certain critical effects. In addition, there will be presented one new viewpoint, C(2) in the outline below, as well as the mathematical development of certain of the effects of space charge and ionic recombination which must be taken into account in the interpretation of any experiments on electrical conductivity in dielectric liquids.

The most reasonable of the theories available at present fall logically into the following three groups:

A. Electron emission theories

1. Baker and Boltz[1] have proposed that in the presence of a dielectric liquid the work function of a metal is lowered to such an extent that high field currents in dielectrics may consist entirely of electrons emitted thermionically from the cathode. LePage and DuBridge[2] have recently reexamined the theoretical basis of the thermionic emission theory and have revised the form of the stress-current relationship.

2. Dornte[3] has suggested that the mechanism of cold-cathode emission may explain the observed effects. The fact that greater currents are observed in dielectrics than in vacuum at the same field strengths is correlated with the lowering of the work function in the former case by the presence of the dielectric.

B. Theories involving collision ionization

1. Nikuradse[4] has been chiefly responsible for the development of the view that the great increase in dielectric currents at high field strengths is due to a collision multiplication of the extremely small number of ions normally present in an insulating liquid.

C. Theories involving field-facilitated ionization in the body of the dielectric

1. Reiss[5] has applied the Onsager theory of weak electrolyte dissociation[6] to the explanation of dielectric high field conductivity. His supposition is that even the most chemically pure of dielectrics contain traces of polar impurities whose ionization is sufficiently enhanced at high fields to explain the observed conductivities.

---

* This work was conducted at Ryerson Laboratory, University of Chicago, under the sponsorship of the Utilities Research Commission.

[1] E. B. Baker and H. A. Boltz, Phys. Rev. **51**, 275 (1937).

[2] W. R. LePage and L. A. DuBridge, Phys. Rev. **58**, 61 (1940).

[3] R. Dornte, Ind. Eng. Chem. **32**, 1529 (1940).

[4] A. Nikuradse, *Das flüssige Dielectrikum*, pp. 138–152.

[5] K. Reiss, Ann. d. Physik **28**, 325 (1936).

[6] L. Onsager, J. Chem. Phys. **2**, 599 (1934).

2. It is not unreasonable to assume as a working hypothesis that the high field conductivity of even the most highly insulating of liquids is, after normal purification, due not to the ionization of some easily ionizable remaining impurity, but to the ionization of the molecules of the dielectric itself.

Theory of Field-Facilitated Ionization of Dielectric Molecules

According to this last viewpoint, the difference between the ionization of weak electrolytes and of the pure nonpolar solvents such as heptane, which have always been considered as completely non-ionized substances, is one of degree but not of kind. The rapid progressive decreases in electrical conductivity as one considers, for instance, first acetic acid, then water, and finally a paraffin hydrocarbon are to be ascribed to the progressive increase in the ionization energy in the liquid phase of the hydrogen bond in this series. On this assumption, it is reasonable to suppose that in order to detect any evidence of ionization in a medium such as a paraffin hydrocarbon, it should be necessary to apply an electric field of such a magnitude that the energy of the bond is appreciably lowered. It is for this reason that the usual liquid dielectrics display easily measurable conductivities only at high field strengths.

A rough estimate of the effect of an electric field, X, on the dissociation constant $K(X)$ may be obtained by use of the following argument.

Let v be the concentration of undissociated material in molecules/cm^3. Then by definition of the dissociation constant

$$-dv/dt = vK(X). \tag{1}$$

Let U_X be the energy required for the removal in the liquid phase of an ion from the molecule under consideration, when the applied field is X. From a theorem of statistical mechanics it follows that

$$d \log_e K(X)/dT = U_X/kT^2. \tag{2}$$

On integration this yields

$$K(X) = C \exp [-U_X/kT]. \tag{3}$$

In the presence of an external field, the ionization energy for favorably oriented ionic bonds is lowered by an amount

$$\Delta U_X = -\epsilon^2/Dr_0 - Xr_0\epsilon, \tag{4}$$

where r_0, the separation of the ions at the maximum of the potential barrier, is given by $r_0 = (\epsilon/DX)^{\frac{1}{2}}$, D being the dielectric constant of the medium.

It follows at once, U_0 being the normal ionization energy, that

$$U_X = U_0 + \Delta U_X = U_0 - 2\epsilon^{\frac{3}{2}}(X/D)^{\frac{1}{2}} \tag{5}$$

and

$$K(X) = K(0) \exp\left[\frac{2\epsilon^{\frac{3}{2}}(X/D)^{\frac{1}{2}}}{kT}\right]. \tag{6}$$

Onsager[6] has computed the effect of an external field on the dissociation constant of weak electrolytes from the equations of Brownian motion of ions in a combined Coulomb and external field. This result for $K(X)$ checks our result (6) above asymptotically for large values of the field strength but departs rather widely at low values.

The Stress-Current Relation

The general functional relation between current and applied field in a dielectric is necessarily complex. We shall set up the conditions which must be satisfied for conduction between plane parallel electrodes and then demonstrate how the experimental conditions must be chosen to simplify the correlation between theory and experiment.

The dielectric or, in the case of theory C(1), the more easily ionizable impurity, whose concentration in molecules per cc is given by v is considered to dissociate yielding positive ions of concentration m and negative ions of concentration n having mobilities of w_m and w_n cm^2 per sec. volt, respectively. m and n are functions of x, the space coordinate normal to the electrodes, while v is a constant under any theory, since the currents are always extremely small.

$\bar{X}$ is the mean applied field in volts per cm, equal to the applied voltage divided by d, the

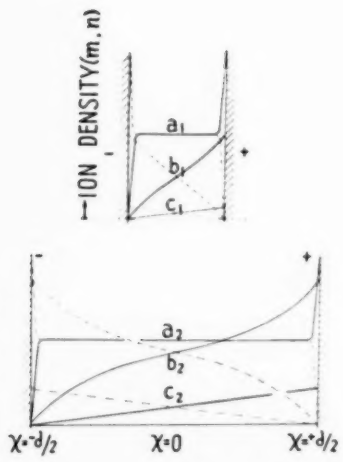

FIG. 1. Ion densities in the inter-electrode space for two electrode-spacings. Positive ion density (m) is shown by dotted lines, negative ion density (n) by solid lines. a_1, a_2 conductance; b_1, b_2 intermediate; c_1, c_2 saturation current.

electrode separation. X is the actual field in the dielectric and must satisfy Poisson's equation.

$$dX/dx = -4\pi(m-n)\epsilon 300/D, \tag{7}$$

$$\int_{-d/2}^{d/2} X dx = \bar{X}d. \tag{8}$$

The current in elementary charges per cm² is given by the following equation, which must hold for every x,

$$I = X(w_m m + w_n n). \tag{9}$$

From the equation of continuity, neglecting the diffusion terms,

$$d(Xw_n n)/dx = -d(Xw_m m)/dx = vK(X) - Amn. \tag{10}$$

Onsager has shown that for a binary electrolyte the coefficient of recombination, A, takes the simple form

$$A = 4\pi\epsilon(w_m + w_n)300/D. \tag{11}$$

In principle, Eqs. (7) through (10) may be solved, subject to the boundary conditions that $m=0$ at $x=d/2$ and $n=0$ at $x=-d/2$, to yield a complex relation between I and $\bar{X}$, which is the connecting link between theory and experiment. However, in the event that the following conditions are satisfied, the stress current relation becomes greatly simplified because the effect of space charge becomes negligible.

1. Dielectric under investigation has a high intrinsic resistivity and a low viscosity (resulting in high ionic mobilities).

2. The separation between the electrodes is made small.

As an illustration of an experiment conforming to these conditions, suppose that a dielectric in which the ionic mobilities are known to be 10^{-3} is tested between electrodes about 0.01 cm apart at a field strength of 300,000 volts per cm and is found to conduct 10^{-6} ampere per cm². The maximum stress distortion due to space charge as estimated from Eqs. (7) and (9) will be of the order of 100 volts per cm. It is evident that the effect of space charge is unimportant in this case. However, unless experimental conditions are carefully chosen as outlined above, it is not possible, in general, to neglect space charge.

The conditions under which ionic recombination becomes relatively unimportant are more stringent but substantially the same as those given above. It is instructive to solve for the stress-current relation under the assumption that space charge is negligible and that mobilities of anions and cations are equal. Under these conditions, the m distribution becomes the mirror image of the n distribution, and there results

$$\bar{X} = X; \quad I = wX(m+n); \tag{12}$$

$$wXdn/dx = vK(X) - An(I/wX - n). \tag{13}$$

On integration, there results

$$n = \frac{B}{2A}\tan\frac{xB}{2wX} + \frac{I}{2wX}, \tag{14}$$

where $B = [4AvK(X) - (AI/wX)^2]^{\frac{1}{2}}$.

The stress-current relation is implicitly contained in

$$\tan(dB/2wX) = AI/wXB. \tag{15}$$

It can be shown that, in the limit of large values for w, small values for $K(X)$, and in particular small values for d, Eq. (15) reduces to the expression for a saturation current

$$I = vK(X)d. \tag{16}$$

Similarly for small values of w, large values of $K(X)$, and large values for d, Eq. (15) reduces to

the expression for a conductance current

$$I = 2wX[vK(X)/A]^{\frac{1}{2}}. \qquad (17)$$

The ionic distributions corresponding to a saturation, a conductance, and an intermediate case are shown in Fig. 1 for two electrode separations. It is evident that in the intermediate case the current partakes of the nature of a saturation current (16) when the spacing is small. As the spacing is increased, recombination of ions plays an increasing role and ultimately the current exhibits the characteristics of conductance, Eq. (17). As a guide in the interpretation of data, one should notice that if $AId/4w^2X^2 \gg 1$, then the current as measured is a conductance current. If $AId/4w^2X^2 \ll 1$, saturation current is being measured.

Experimental Procedure

Normal heptane was selected for the initial investigation since it satisfies the above-mentioned conditions which simplify interpretation of results and is more easily purified than many of the other liquid dielectrics which are commonly studied. A batch of this material of exceptional purity having a freezing range of only 0.009°C was obtained from the National Bureau of Standards. The purification of the liquid was carried even further in the high vacuum train shown in Fig. 2. The cell in which the conductivity measurements are made is an integral part of the high vacuum system. This system is so arranged that the material under study may be passed through the following cycle as many times as desired, a high vacuum being maintained at all times:

1. Distillation over sodium ribbon for drying.
2. Passage through a column of activated silica gel for removal of polar impurities by adsorption.
3. Passage through two sintered glass filters.
4. Electrical purification.
5. Final distillation into measuring cell.

All distillations are carried out with a maximum temperature differential of 10°C. Under these conditions there is a complete absence of ebullition in the liquid at all times. The cycle is re-initiated at the end of any one run by the operation of the magnetic stopcock shown in Fig. 2.

The electrode assembly is especially designed for work with very small spacings. The upper electrode, of pure nickel, is supported by a fine wire which also serves as the high potential lead. Without breaking vacuum, the nickel electrode may be raised about 6 cm, at any stage of the experiment, and both electrodes heated to a bright yellow temperature by high frequency induction for outgassing. The possibility of vertical displacement of one electrode also serves to make possible the determination at any time of the inter-electrode contact potential by the Kelvin procedure. During conductivity measurements, the nickel electrode is lowered into close proximity to the lower electrode, of platinum-iridium, where it is supported by three quartz pins. The nickel electrode, which is equipped with an iron armature, may be rotated magnetically. The flange of the electrode is equipped with 0.005-cm stepped depressions machined to an accuracy of ±0.0001 cm. By this means, the electrode spacing may be set at any one of a number of very accurately known values without breaking vacuum, and the problem of maintaining the very closely spaced electrodes exactly parallel is made relatively simple.

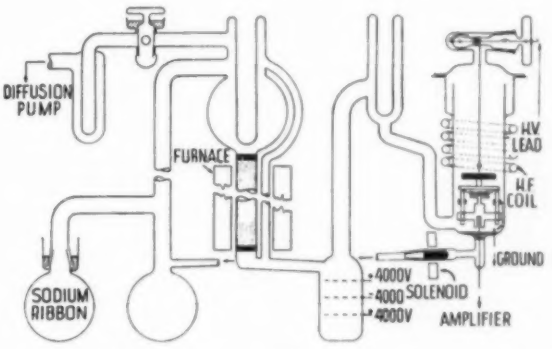

Fig. 2. Vacuum train designed for removal of polar impurities from liquid hydrocarbons. Measuring cell is schematic.

The edges of all electrodes were very carefully shaped to avoid the possibility of stress concentration. All surfaces were ground and polished to optical flats with pitch laps. The materials were so annealed prior to the figuring of the surfaces that the distortion accompanying the degassing in vacuum did not exceed one-fourth of a fringe in the usual optical test.

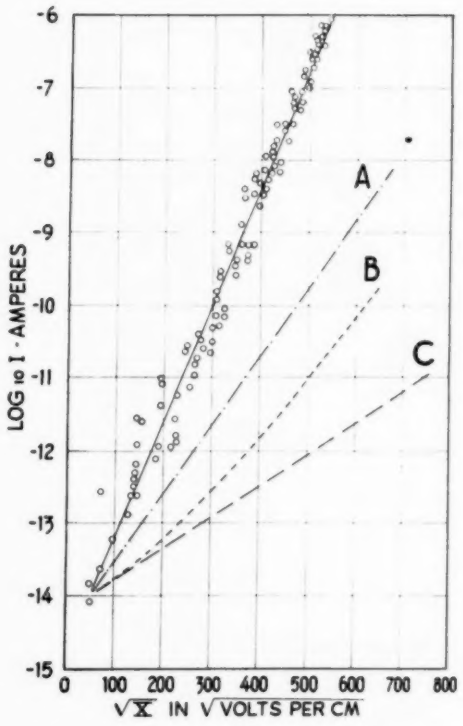

FIG. 3. Stress-current relation for heptane at 20°C. Electrode separation of 0.0055 cm. *A*, *B*, and *C* are theoretical curves based on Eq. (6), Onsager's theory, and thermionic emission theory, respectively.

All currents are measured with an FP-54 amplifier. Extreme freedom from ripple in the applied voltage is required if error is to be avoided in d.c. measurements on dielectrics at small electrode spacings. The 60-cycle impedance of the test cell is usually lower than the grid impedance of the amplifier with the result that the full ripple voltage, if any is present, appears on the grid of the FP-54 and a spurious d.c. reading is obtained since the tube is not linear over large ranges of grid voltage. The voltage source is a 3000-volt television-type rectifier combined with an electronic regulator which is a modification of the type recently described by Neher and Pickering.[7]

In some of the later experiments a measuring cell designed to fit into a Dewar flask was constructed. In this way, data at temperatures down to that of liquid air were obtainable.

[7] H. V. Neher and W. H. Pickering, Rev. Sci. Inst. **10**, 53 (1939).

RESULTS AND DISCUSSION

For the sake of brevity in the following discussion of experimental data, references to the theories listed in the introduction will be by symbol. For instance, A(1) refers to the thermionic emission theory.

1. Effect of electrode work function

Up to 600,000 volts per cm, the highest stress used in our work, no polarity effect was found with the electrode pair nickel to platinum-iridium. This constitutes a check on our previous experiments[8] conducted with electrodes of gold and brass under conditions less ideally controlled. If the dielectric currents are thermionic, the polarity ratio between dissimilar electrodes should have the value

$$I_1/I_2=\exp\left[-\epsilon(\phi_1-\phi_2)/kT\right],$$

$\phi_1-\phi_2$, which is the difference between the work functions of the two electrode metals when immersed in the dielectrics, is also equal to the contact potential as measured in the dielectric by the Kelvin procedure. The measured contact potential between nickel and platinum-iridium in heptane was 0.4 volt from which the deduced current ratio, on the thermionic emission assumption, should have been of the order of 10^6 instead of unity as was actually found. This result tends to invalidate A(1) and, to a lesser degree, A(2).

2. Effect of electrode configuration

On either the thermionic or the cold emission theories, A(1) and A(2), the current should be a function of the cathode gradient and should be entirely independent of the anode gradient. A large polarity effect should be observed at high stresses with unsymmetrical electrode configurations. In a series of experiments on the high stress conductivity of heptane between a nickel needle and a nickel optical flat, no consistent polarity effect was found by us. In agreement with this finding, Dornte[3] reports that with the wire cylinder configuration the polarity effect is very small. In general, the current is seen to be a function, not of the *cathode* gradient, but of the *maximum* gradient. This is exactly what would

[8] H. J. Plumley, Phys. Rev. **52**, 140 (1937).

be expected if either of the theoretical mechanisms, C(1) or C(2), is correct.

3. The effect of progressive purification and long-time application of stress

Figure 3 presents some of the data obtained at an electrode separation of 0.0055 cm with heptane at room temperature. The material was under high vacuum at all times and the electrodes were degassed. Stress-current data were obtained after each successive passage of the material through the purification cycle. The points shown are the superposition of two months of data and include 8 cycles of purification (16 slow distillations). If the mechanism C(1) as outlined in the introduction were correct, a definite trend to smaller currents as the degree of purification of the dielectric is extended should be expected. Although such an effect to the extent of a factor of 1000 was in fact observed in this work for the preliminary stage of purification of heptane, indicating that initially at least impurities are partially responsible for the conductivity, yet no such trend is apparent in the data obtained for any of the successive cycles of purification as shown in Fig. 3. This fact points to the following conclusion concerning the high field conductivity of well purified dielectrics. If the current carriers are created by ionization in the dielectric, the material ionizing

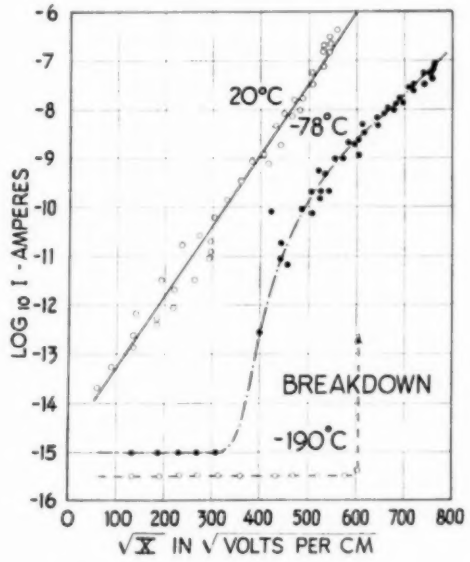

FIG. 4. Effect of low temperatures on stress-current relation for heptane, nitrogen saturated.

is the dielectric itself, as proposed in C(2), and not more easily ionizable impurities, such as contained water. The field-facilitated ionization of a hydrocarbon such as heptane would presumably go according to the following, assuming that all hydrogen ions, when formed, would associate with neutral molecules:

$$2C_7H_{16} \rightleftarrows C_7H_{17}^{+} + C_7H_{15}^{-}.$$

The fact that a hydrocarbon polymer always forms on the anode, never on the cathode, after

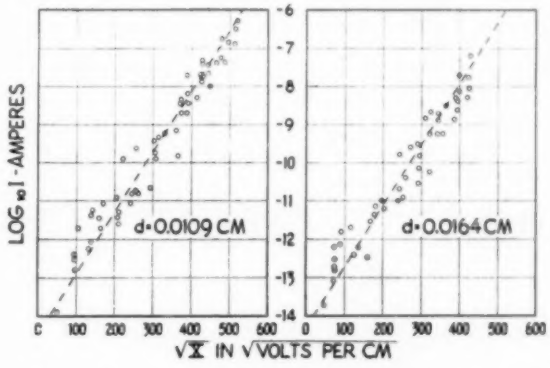

FIG. 5. Stress-current relation for heptane at 20°C. Conditions as for data in Fig. 3 except that electrode spacing is doubled and tripled, respectively.

a long-time application of stress is possibly to be correlated with a reaction involving the negative ion indicated above. The amount of hydrogen to be expected at the cathode would scarcely be detectable since it would immediately dissolve in the liquid.

A second experiment designed to discriminate between C(1) and C(2) consisted of applying a high field to a 0.005-cm inter-electrode film of heptane obtained by filling and then voiding the measuring cell. The current was initially 10^{-6} ampere but fell to about half of this value after a two-hour period. If the heptane contained dissolved water to the extent of $\frac{1}{10}$ of the saturation value, this amount of water would have been completely electrolyzed in 3.7 minutes, and the current, if arising from this source, should have fallen to zero in this short time. The fact that it did not is evidence against the validity of C(1).

4. The stress-current relation

It is probably safe to use 10^{-3} cm^2 per sec. volt as a lower limit to the ionic mobility in heptane.

With this value, it is easily verified that the conditions were so chosen, in the case of the data presented in Fig. 3, that both space charge and ionic recombination were negligible. Equation (16) should accordingly apply, inferring a proportionality between the current and $K(X)$, the dissociation constant of theories C(1) and C(2). The data so far obtained indicate that the function $K(X)$ increases much more rapidly with X than would be predicted from Onsager's function and somewhat more rapidly than predicted from our Eq. (6). The stress-current relation predicted from the thermionic emission theory A(1),

$$I = I_0 \exp\left[\frac{\epsilon^{\frac{1}{2}}(X/D)^{\frac{1}{2}}}{kT}\right],$$

results in the poorest check with experiment.

It is hoped that the discrepancy between theoretical and experimental slopes will yield to further refinement of the theory. The derivation of Eq. (6) is certainly oversimplified.

Applying our criterion for determining whether to expect a conductance or a saturation current in the case of large electrode separations, we expect to find saturation at moderately low field strengths changing to conductance at the highest fields. This implies slopes similar to ours at low fields but decreasing to one-half of this value at high fields. The data of Baker and Boltz with toluene and of Dornte with heptane, obtained with separations of the order of 0.100 cm, exhibit this effect.

Figure 4 contains the results of some low temperature experiments. The slope of the stress-current relation would normally be expected to increase at low temperatures since T occurs in the denominator of the exponent in Eq. (6). If, however, the lowering of the temperature so decreases the ionic mobility that Eq. (17) rather than (16) applies, the net effect will be a decrease in the slope. At the temperature of liquid air, heptane is in the solid phase. The ionic mobilities approach zero and the currents remain on the borderline of detectability up to the breakdown point. This is additional evidence in favor of the ionic over the electronic mechanisms.

5. The effect of electrode separation

In Fig. 5 are presented data taken under similar conditions to that in Fig. 3 except that the electrode separation was increased to 0.0109 cm and 0.0164 cm. Unless some rather artificial assumptions, involving association of ions and neutral molecules, are introduced, the collision ionization mechanism, B(1), must necessarily predict that the current be an exponential function of Xd. This would infer a proportionality, in a log I *versus* X curve, between the slope and the electrode separation, d. On the contrary, the data, which for consistency with Fig. 3 are plotted against $\sqrt{X}$, instead of X as would be required for linearity on theory B(1), show absolutely no change in slope as the electrode separation is changed.

According to A(1) and A(2), the current should be entirely independent of d. On theories C(1) and C(2), the effect of d on the stress-current relation is complex, being embodied in Eq. (15). However, for our conditions Eq. (16) is valid and the effect of the simple proportionality between I and d there indicated would be masked by the inherent dispersion of the data except for greater increases in electrode separation than obtained in our case.

In summary, it would appear that mechanisms A(1), A(2), and B(1) are very unlikely as the source of high field currents in liquid dielectrics. Investigations which should determine whether or not C(1) should be definitely excluded are being continued. The most plausible explanation of the phenomena in the light of this work appears to be the newer viewpoint C(2), which treats the dielectrics of low conductivity merely as special cases in the general class of weak electrolytes. This treatment affords a unified picture of the conductivity of all dielectric liquids, from those with extremely high resistivity to those of rather low resistivity. In any given case, the factor of prime importance is the energy for ionization in the chemical sense and in the liquid phase. This in turn is greatly affected by the dielectric constant of the medium, since the required energy may be greatly lowered by the solvation of the ions.

It is important to note that conductivity in liquid dielectrics is essentially a less complex phenomenon than is the case in solid dielectrics. In the former case, the only requirement for conductivity is the creation of charge carriers—

their transport in the field follows naturally. In the latter case, it is usually more difficult to explain how the carrier can move than it is to explain how the carrier arises.

The writer wishes to thank Mr. Herman Halperin and Mr. K. W. Miller, who encouraged this work, and the Utilities Research Commission, which made funds available for its continuation. A debt of gratitude is due to Professor A. J. Dempster, who extended the facilities of Ryerson Laboratory and provided a number of helpful suggestions, and to the National Bureau of Standards for the loan of a number of pure hydrocarbons.

JANUARY 15, 1941 PHYSICAL REVIEW VOLUME 59

On the Diffuse X-Ray Diffraction Maxima Observed by C. V. Raman and P. Nilakantan

W. H. ZACHARIASEN
Ryerson Physical Laboratory, University of Chicago, Chicago, Illinois
(Received November 22, 1940)

IT has been known for a long time that Laue photographs exhibit radial streaks.[1] When the incident beam contains both characteristic and continuous x-rays diffuse spots (which are not regular Laue spots) may also be observed. These spots were first studied by G. D. Preston[2] who demonstrated beyond doubt that they were produced by the characteristic, the radial streaks by the continuous component of the incident radiation. Preston showed further that both the radial streaks and the diffuse spots increased in intensity when the temperature of the crystal was raised. His observations have later been confirmed by other investigators.[3] A year ago a theory of diffuse scattering of x-rays by crystals was developed[4] (superseding the theory of Debye and of Jauncey and Harvey, but reviving and extending earlier, long-forgotten, results obtained by Faxén[5]) and it was shown that this theory provided an explanation for the phenomenon observed by Preston and others. Lately the diffuse spots have been found also by Raman and Nilakantan[6] who, being unaware of Preston's work, at first believed that they had discovered a new effect. The most recent article by Raman and Nilakantan[7] reports on the diffuse spots observed in Laue photographs of rocksalt. In this article the statement is made that the theory of diffuse scattering does not account for their observations and it is claimed that they are dealing with a new phenomenon and not with a diffuse scattering effect. All qualitative observations reported by Raman and Nilakantan are in perfect accord with the predictions of the theory of diffuse scattering, but the authors nevertheless refuse to accept the applicability of this theory on the ground that it does not give the correct scattering angles for the diffuse spots.

According to the theory of diffuse scattering[4] the diffuse diffraction maxima correspond to

TABLE I. *Data on rocksalt (Raman and Nilakantan, reference 7), $\lambda = 0.7095A$.*

LATTICE PLANE	FIGURE	θ_i	$2\theta_m$ OBS.	$2\theta_m$ CALC.	$2\theta_B$
400	9	11° 51′	29° 5′	28° 50′	
400	11	17° 40′	29° 21′	29° 34′	
400	14	19° 26′	29° 37′	29° 44′	
400	15	25° 9′	30° 13′	30° 9′	29° 12′
420	13	12° 38′	32° 9′	32° 6′	
420	13	13° 1′	32° 19′	32° 10′	
402	9	14° 46′	32° 29′	32° 29′	
420	15	21° 53′	33° 13′	33° 30′	32° 44′
600	14	19° 26′	43° 57′	43° 38′	
600	15	25° 9′	45° 19′	45° 16′	44° 26′

[1] W. Friedrich, Physik. Zeits. **14**, 1082 (1913); A. P. R. Wadlund, Phys. Rev. **53**, 843 (1938).
[2] G. D. Preston, Proc.-Roy. Soc. **172**, 116 (1939).
[3] Stanley Siegel and W. H. Zachariasen, Phys. Rev. **57**, 795 (1940); K. Lonsdale, I. E. Knaggs, H. Smith, Nature **146**, 332 (1940).
[4] W. H. Zachariasen, Bull. Am. Phys. Soc. Nov. 1939; Phys. Rev. **57**, 597 (1940).
[5] H. Faxén, Zeits. f. Physik **17**, 266 (1923).
[6] C. V. Raman and P. Nilakantan, Nature **145**, 667 (1940); Current Science **9**, 165 (1940); Proc. Ind. Acad. Sci. **11**, 379, 389, 398 (1940).
[7] C. V. Raman and P. Nilakantan, Proc. Ind. Acad. Sci. **12**, 141 (1940).

scattering angles $2\theta_m$ given by the equation

$$\tan 2\theta_m = 2 \sin \theta_B \cos \theta_i/(1-2 \sin \theta_B \sin \theta_i), \quad (1)$$

where θ_i is the glancing angle of incidence, θ_B the Bragg angle. When $\theta_i - \theta_B$ is small Eq. (1) becomes

$$2\theta_m = 2\theta_B + 2(\theta_i - \theta_B) \sin^2 \theta_B. \quad (2)$$

Raman and Nilakantan maintain that the scattering angles for the diffuse maxima are just the Bragg scattering angles $2\theta_B$ and hence that they are not given by Eq. (1). The differences $2\theta_m - 2\theta_B$ are small for all diffuse spots which are sufficiently intense to permit measurement and it is consequently necessary to know the distance from crystal to photographic plate with some accuracy. It is not clear from Raman and Nilakantan's article whether this distance was carefully determined for each separate photograph. The regular Laue spots are well defined and they can conveniently be used to calibrate the various Laue diagrams, whether they be the original photographs or reproductions.

In order to verify or disprove the statement made by Raman and Nilakantan the Laue photographs reproduced in their article have been independently measured by four different individuals (the present writer being one of them) in this laboratory. Measurements were made both on diffuse spots and on regular Laue spots, the latter being used to calibrate the reproduced diagrams. On the basis of the average values so obtained the data given in Table I columns 3 and 4 were deduced. If we take into account all possible sources of error an accuracy of 25′ in the scattering angles can be claimed, and in some cases the greatest possible error is definitely less. The observed scattering angles differ considerably from those reported by Raman and Nilakantan, but no explanation for this discrepancy can be offered. Column 5 contains the scattering angles $2\theta_m$ calculated from Eq. (1) while column 6 gives the theoretical Bragg scattering angles (in calculating these the value $a = 5.628$A for the cube edge of rocksalt was used and the value 0.7095A was assumed to be the average wave-length of Mo$K\alpha_1$ and Mo$K\alpha_2$). It is seen from Table I that the observed scattering angles agree with those calculated from Eq. (1) well within the experimental error. On the other hand the differences between the observed values $2\theta_m$ and the calculated values $2\theta_B$ in several cases far exceed the greatest possible error in the measurements.

TABLE II. *Data on rocksalt (Preston, reference 2, Fig. 5a),* $\lambda = 0.560A$.

LATTICE PLANE	θ_i	$2\theta_m$ OBS.	$2\theta_m$ CALC.	$2\theta_B$
$\bar{4}42$	18° 45′	35° 10′	34° 59′	
442	20° 22′	35° 31′	35° 14′	34° 44′
$\bar{6}02$	17° 28′	36° 39′	36° 29′	
602	19° 35′	37° 0′	36° 55′	36° 40′
262	17° 56′	37° 55′	38° 15′	
622	18° 37′	38° 18′	38° 23′	38° 32′

TABLE III. *Data on aluminum (Preston, reference 2)* $\lambda = 0.560A$.

LATTICE PLANE	θ_i	$2\theta_m$ OBS.	$2\theta_m$ CALC.	$2\theta_B$
200	0	15° 23′	15° 27′	15° 45′
311	17° 33′	26° 50′	26° 43′	26° 16′

For comparison Table II contains data deduced from Preston's Laue photograph of rocksalt (Fig. 5a in his article), and again Eq. (1) accounts for the observed scattering angles. Preston also investigated diffuse spots produced by monochromatic Ag$K\alpha$-radiation with aluminum crystals. The scattering angles (accurate to 10′) as reported by Preston are given in Table III. His observed values $2\theta_m$ differ from the Bragg scattering angles $2\theta_B$ by amounts greater than the experimental error, but agree with the values calculated from Eq. (1).

In view of the results given in Table I there seems to be no acceptable basis for the assertion of Raman and Nilakantan that the theory of diffuse scattering is incapable of giving the correct positions of the diffuse maxima. There is thus no experimental justification for the statement that the effect described by Raman and Nilakantan (observed earlier by others) is not a diffuse scattering phenomenon.

The Photo-Disintegration of the Deuteron

WILLIAM RARITA* AND JULIAN SCHWINGER
Department of Physics, University of California, Berkeley, California

AND

H. A. NYE
University of Illinois, Urbana, Illinois

(Received December 9, 1940)

HIGH energy experiments on the photo-disintegration of the deuteron should constitute a source of information concerning the mesotron currents responsible for neutron-proton exchange interactions. Siegert,[1] and Lamb and Schiff[2] have shown that the exchange currents are proportional to the exchange interaction itself, and therefore the essential information obtained from such experiments concerns the nature of the exchange forces, or more precisely, the interaction in states of odd parity, the final states of the process. Fröhlich, Heitler, and Kahn[3] have attempted to show that the exchange currents associated with the strong tensor coupling of the vector mesotron theory should have a predominant effect for high energy γ-rays. Indeed, the photoelectric cross section they compute for the Li γ-rays (17.5 Mev) is seven times that predicted by the formula of Bethe and Peierls, which is based on a zero range approximation for nuclear forces. This conclusion is questionable, however, for the calculation was not performed in a consistent manner; the tensor forces were taken into account in computing the exchange currents, but were completely omitted in determining the wave function which describes the motion of the heavy particles under the influence of the exchange forces. Moreover the large value of the photo cross section arises from the $1/r^3$ singularity of the tensor potential. Although this perturbation calculation gives convergent results, it is obviously a dubious procedure to include singularities which, in other aspects of the theory, imply infinities only lent significance by arbitrary methods.

We have avoided these difficulties by employing simplified potentials which permit exact solution for the pertinent states of the deuteron,[4] and thus allow a consistent solution of the problem. Although the choice of these simplified interactions has been guided by current mesotron theories, we have disregarded the detailed radial dependence of the nuclear forces, obtained from these theories by a highly questionable application of perturbation theory. Two typical forms of the interaction potential are:

$$\text{(I)} \qquad V=\tfrac{1}{3}\boldsymbol{\tau}_1\cdot\boldsymbol{\tau}_2\{A+B\boldsymbol{\sigma}_1\cdot\boldsymbol{\sigma}_2+CS_{12}\}J(r),$$

$$V=-\{A'+B'\boldsymbol{\sigma}_1\cdot\boldsymbol{\sigma}_2+C'S_{12}\}J(r),$$

$$\text{(II)} \qquad S_{12}=3\frac{\boldsymbol{\sigma}_1\cdot\mathbf{r}\boldsymbol{\sigma}_2\cdot\mathbf{r}}{r^2}-\boldsymbol{\sigma}_1\cdot\boldsymbol{\sigma}_2$$

written in terms of the isotopic spin operators $\boldsymbol{\tau}_1$, $\boldsymbol{\tau}_2$; the spin operators $\boldsymbol{\sigma}_1$, $\boldsymbol{\sigma}_2$; and the relative position vector $\mathbf{r}$ of the neutron and proton. (I) and (II) are respectively analogous to the "symmetrical" and "neutral" potentials now in vogue. Both sets of constants (A, B, C) and (A', B', C') are chosen in such a manner that the interaction in states of even parity assumes the form:

$$V_{(\text{even})}=-\{1-\tfrac{1}{2}g+\tfrac{1}{2}g\boldsymbol{\sigma}_1\cdot\boldsymbol{\sigma}_2+\gamma S_{12}\}J(r)$$

with g and γ adjustable constants and $J(r)$ a rectangular well function of adjustable depth V_0 and range r_0. $V_{(\text{even})}$ reduces in triplet and singlet states to

$$^3V_{(\text{even})}=-\{1+\gamma S_{12}\}J(r)$$

$$^1V_{(\text{even})}=-\{1-2g\}J(r).$$

In states of odd parity, however, the two assumptions (I) and (II) are distinguished by their different dependence on the isotopic spin.

* On leave from Brooklyn College, Brooklyn, New York.

[1] A. J. F. Siegert, Phys. Rev. **52**, 787 (1937).

[2] W. E. Lamb Jr. and L. I. Schiff, Phys. Rev. **53**, 651 (1938).

[3] H. Fröhlich, W. Heitler and B. Kahn, Proc. Roy. Soc. **A174**, 85 (1940).

[4] J. Schwinger, Phys. Rev. **55**, 235 (1939).

Thus

(I) ${}^3V_{(\text{odd})} = -\frac{1}{3}\,{}^3V_{(\text{even})}$, ${}^1V_{(\text{odd})} = -3\,{}^1V_{(\text{even})}$,

(II) ${}^3V_{(\text{odd})} = {}^3V_{(\text{even})}$, ${}^1V_{(\text{odd})} = {}^1V_{(\text{even})}$.

The quadrupole moment Q and binding energy $|E_0|$ of the triplet even ground state of the deuteron (${}^3S_1+{}^3D_1$) determine V_0 for a definite choice of r_0. The experimental data:[5] $Q=2.73\times10^{-27}$ cm^2; $|E_0|=2.17$ Mev, are fitted by $\gamma=0.775$, $V_0=6.40|E_0|$ with an assumed range of $r_0=2.80\times10^{-13}$ cm. The value of g is determined as $g=0.0715$ by the cross section:[6] (20×10^{-24} cm^2) for scattering of slow neutrons by free protons.

For the purpose of examining the sensitivity to the radial form of the interaction, the calculation has also been performed with Bethe's neutral interaction,[7] which, in its radial dependence, is more like that employed by F. H. K. but with the $1/r^3$ singularity "cut-off." This potential will be denoted by (III). It should be remembered, of course, that the neutral potentials correspond to no mesotron currents.

Photoelectric γ-ray absorption induces transitions from the ${}^3S_1+{}^3D_1$ ground state of the deuteron to states in the continuum, which are limited by selection rules to: ${}^3P_0$, ${}^3P_1$, ${}^3P_2+{}^3F_2$. By virtue of the noncentral character of the tensor forces, the effective interactions in the states of various total angular momenta differ radically. Thus, with potential (I) ("symmetrical theory"), the interaction in the ${}^3P_0$ state is attractive, while that of both the ${}^3P_1$ and ${}^3P_2$ states is repulsive. While the contrary is true with potential (II) ("neutral theory"). With potential (III) ("cut-off neutral theory") only the ${}^3P_1$ state is attractive. The existence of a strongly attractive force in the final state diminishes the absorption probability when the wave-length of the dissociated particles is comparable with the size of the deuteron. This effect is particularly enhanced in the ${}^3P_1$ state of the "neutral" theories, and produces a reduction of the "neutral" photoelectric cross sections as compared with that of the "symmetrical" theory. The results of the computations for the γ-rays emitted in the Li+H reaction (17.5 Mev) are:

(I) $\sigma=0.768\times10^{-27}$ cm^2,
(II) $\sigma=0.376\times10^{-27}$ cm^2,
(III) $\sigma=0.544\times10^{-27}$ cm^2.

Comparison of these values demonstrates that the results are dependent primarily upon the general nature of the potentials, and not upon their detailed radial dependence. In comparing values (II) and (III) it should be remembered that with potential (II) the ${}^3P_2$ state is attractive, reducing the absorption probability, while with potential (III) that state is repulsive. For comparison we include the cross section calculated by treating the dissociated particles unperturbed: $\sigma=0.774\times10^{-27}$ cm^2, and the Bethe-Peierls cross section: $\sigma=0.423\times10^{-27}$ cm^2. Had the neutron-proton system been described by an ordinary attractive potential well, the photo cross section would be: $\sigma=0.529\times10^{-27}$ cm^2.

A further characteristic of the tensor force is to modify the angular distribution of the emitted particles by the introduction of a spherically symmetric term. That such an effect may be expected is evident from the noncentral nature of the forces. The angular distribution computed from the "symmetrical" theory is but little modified: $\sigma(\vartheta)\sim(\sin^2\vartheta+0.015)$, while the "neutral" theories, with their much larger noncentral forces, give (II): $\sigma(\vartheta)\sim(\sin^2\vartheta+0.36)$ and (III): $\sigma(\vartheta)\sim(\sin^2\vartheta+0.26)$, predicting a large intensity in the direction of the incident 17.5-Mev γ-ray. We quote for comparison the angular distribution for an unperturbed final state: $\sigma(\vartheta)\sim(\sin^2\vartheta+0.010)$.

The large interactions of the "neutral" theories, which produce a diminution of the photoelectric cross section and so significantly alter the angular distribution, profoundly influence the scattering of high energy neutrons by protons. With the neutral potential (II), the total scattering cross section evaluated for a neutron energy of 15.3 Mev is $\sigma=0.98\times10^{-24}$ cm^2, while the angular distribution in the center of gravity system is:

$$\sigma(\vartheta)\sim(1+0.93\cos\vartheta+0.46\cos^2\vartheta)$$

thus indicating a large preferentially forward scat-

[5] J. M. B. Kellogg, I. I. Rabi, N. F. Ramsey, and J. R. Zacharias, Phys. Rev. **57**, 677 (1940); A. Nordsieck, Phys. Rev. **58**, 310 (1940).

[6] V. W. Cohen, H. H. Goldsmith and J. Schwinger, Phys. Rev. **55**, 106 (1939); H. B. Hanstein, Phys. Rev. **57**, 1045 (1940).

[7] H. A. Bethe, Phys. Rev. **57**, 390 (1940).

tering. On the "symmetrical" theory, however, $\sigma=0.62\times10^{-24}$ cm^2 and $\sigma(\vartheta)\sim(1-0.080\cos\vartheta+0.077\cos^2\vartheta)$ which differs but slightly from the results computed with an ordinary attractive potential well in the S state and no P interaction; *viz.*, $\sigma=0.59\times10^{-24}$ cm^2 and, of course, spherically symmetrical scattering. The calculations for potential (III) have been performed by Kittel and Breit[8] for a neutron energy of 16 Mev. The total cross section is $\sigma=0.70\times10^{-24}$ while the angular distribution is:

$$\sigma(\vartheta)\sim(1+0.48\cos\vartheta+0.094\cos^2\vartheta).$$

The preceding discussion shows clearly that no significant evidence regarding the tensor interaction may be expected from rough measurements of the total photoelectric cross section; the large value obtained by Fröhlich, Heitler and Kahn is illusory. The information obtainable from precise measurements of the cross section concerns principally whether the interaction in the P state is effectively attractive or repulsive. On the other hand, the specific effect of the tensor forces is to modify the angular distribution in the direction of isotropic emission. Thus more valuable information will be obtained by studying the angular distribution of the disintegration particles than by attempting the difficult precise measurements of the total cross section. Furthermore, a correlation may be expected between the angular distribution of the photo-particles, and both the total cross section and angular distribution of the fast neutrons scattered by protons. The stated numerical results show that a tensor force of sufficient magnitude to produce appreciable forward intensities of the disintegration products will cause a concomitant increase in the total scattering cross section and the relative intensity of the forward scattering.

We wish to thank Professors Oppenheimer and Serber for their stimulating influence during the progress of this work.

[8] C. Kittel and G. Breit, Phys. Rev. **56**, 744 (1939).

Letters to the Editor

PROMPT publication of brief reports of important discoveries in physics may be secured by addressing them to this department. Closing dates for this department are, for the first issue of the month, the eighteenth of the preceding month, for the second issue, the third of the month. Because of the late closing dates for the section no proof can be shown to authors. The Board of Editors does not hold itself responsible for the opinions expressed by the correspondents.

Communications should not in general exceed 600 words in length.

Thermal Conductivity of Liquids

M. RAMA RAO
Department of Physics, University of Mysore, Bangalore, India
September 11, 1940

AT present it may be said that there is no satisfactory theory of the mechanism of thermal conduction in liquids, although it is recognized[1] that the mechanism of thermal conduction in liquids must be different from that in a gas. The mechanism of thermal conduction outlined here refers to the melting point and leads us to an expression for the thermal conductivity of a liquid near the freezing point in terms of the melting point, molecular weight and molecular volume of the liquid.

A liquid near its freezing point is here considered as an assemblage of a number of linear harmonic oscillators, each vibrating with a frequency ν about a slowly displaced equilibrium position with an amplitude which is comparable with the mean molecular distance σ. This simple picture of a liquid has yielded interesting results[2] about the properties of the liquid state of matter. In dealing with the problem of heat conduction we are concerned with the transport of thermal energy. Let us consider a thermal energy gradient dE/dz along the z axis and layers of molecules parallel to the direction of thermal energy gradient and the molecules vibrating in random directions. Then, on an average, $\frac{1}{3}$ of the molecules will be vibrating along each of three directions normal to one another. The difference of energy between two layers separated by a distance σ is $\sigma(dE/dz)$. Since the amplitude of vibration is large, molecules of one layer come into contact with the molecules of a neighboring layer at each extreme libration, the contact being of a short duration. When there is contact between molecules we shall assume that there is transfer of the excess thermal energy. If we consider a plane normal to the direction of drift, a molecule of a given layer conveying thermal energy crosses this plane twice in every oscillation. A molecule of the adjacent layer also crosses this plane twice in every oscillation. The number of molecules in unit area is $1/\sigma^2$ and, hence, on the basis of the assumptions, it follows that the transfer of thermal energy per unit area per unit time is given by

$$\tfrac{1}{3}4\nu\frac{1}{\sigma^2}\frac{dE}{dz}\sigma.$$

This, by definition of the coefficient of thermal conduction, is equal to $K(d\theta/dz)$ where $d\theta/dz$ is the temperature gradient. Hence we have

$$K\frac{d\theta}{dz}=\frac{4}{3}\frac{\nu}{\sigma}\frac{dE}{dz}.$$

It follows that

$$K=\frac{4}{3}\frac{\nu}{\sigma}\frac{dE}{d\theta}.$$

Since the average energy (both kinetic and potential) of a vibrating molecule is $3k\theta$ where k is Boltzmann constant, we have

$$K=4k\nu/\sigma.$$

For ν we substitute the Lindemann expression

$$2.8\times10^{12}(\theta_s/MV_s^{\frac{1}{3}})^{\frac{1}{2}}$$

where θ_s is the melting point and V_s the molecular volume and M the molecular weight. For σ we substitute, $(3V_s/4\pi N)^{\frac{1}{3}}$ where N is Avogadro number. It then follows that

$$K=2.05\times10^{5}(\theta_s/MV_s^{4/3})^{\frac{1}{2}}.$$

Calculated values of K from the above expression agree fairly well with the observed values. Details will be published very soon.

[1] P. Bridgman, Proc. Am. Acad. Arts Sci. **59**, 141 (1923).
[2] L. Sibaiya and M. Rama Rao, Nature **143**, 723 (1939).

Fission Products of Uranium and Thorium Produced by High Energy Neutrons

E. SEGRÈ
Radiation Laboratory, Department of Physics, University of California, Berkeley, California
AND
G. T. SEABORG
Department of Chemistry, University of California, Berkeley, California
December 12, 1940

IN the uranium and thorium fission by neutrons of energy up to ~10 Mev no fission products with atomic numbers between 43 and 51 have been reported.[1] This fact, together with the experiments on the energy of the fragments,[2] points to unsymmetrical fission for neutrons of such energies, and recent work may show that this has a theoretical explanation.[3]

Recently Nishina, Yasaki, Ezoe, Kimura and Ikawa[4] have reported the production by fission of some radioactive isotopes of palladium, silver, cadmium and indium by bombardment of uranium with ~17-Mev neutrons (3-Mev D^2 on lithium). This is evidence for more symmetrical types of fission produced by higher energy neutrons.

We have investigated the production of radioactive silver and palladium from uranium and thorium fission. With the ~17-Mev neutrons (16-Mev D^2 on beryllium) from the 60-inch cyclotron we have observed both the following chains from uranium and thorium:

$$Pd^{112}\ (17\text{ hr.})\rightarrow Ag^{112}\ (3.4\text{ hr.})\rightarrow Cd^{112}\ (\text{stable})$$
$$Pd^{111}\ (26\text{ min.})\rightarrow Ag^{111}\ (7.5\text{ d.})\rightarrow Cd^{111}\ (\text{stable}).$$

The first chain is in agreement with the results of Nishina and co-workers.[4] The products in the second chain were

also reported by Nishina, but the assignment of the 26-minute palladium as the parent of the 7.5-day silver was not made. We have established this genetic relationship by means of successive extractions of the silver from the palladium.

The isotopic assignments in the first chain are based upon the identification[5] of Ag^{112}. The isotopic assignments in the second chain are based upon the identification[6] of Ag^{111}. By deuteron bombardment of palladium, Kraus and Cork[6] have found a period of 17 minutes which they assign to Pd^{111}. We have found a 26-minute palladium in the palladium fraction of the fission products of uranium and thorium, and repeated extractions of silver from neutron irradiated thorium shows that the 7.5-day period grows from a 26-minute parent. Our neutron irradiation of palladium (no chemical separation) also shows an activity of about 26 minutes half-life. The reason for the discrepancy between these results and those of Kraus and Cork is not yet clear.

The cross sections for the production from thorium of these two chains are comparable and are of the order of one-tenth of the cross section for the formation of the 77-hour tellurium under identical conditions. The comparatively low intensity of these activities makes it imperative to purify the products very carefully in the chemical separations.

We have also looked for radioactive ruthenium among the fission products of uranium and thorium and have found an activity of ~4 hours half-life. An investigation of this region is being continued.

Worth mentioning here is the observation, made during our neutron bombardments of palladium, that a 40 second $Ag^{107*, 109*}$, which may be the same as the 40-second silver formed as the product[7] of the decay of the 6.7-hour $Cd^{107, 109}$ also grows from the 13-hour[6] $Pd^{107, 109}$.

We wish to express our gratitude to the Rockefeller Foundation and the Research Corporation, whose financial support made this work possible.

[1] See, e.g., O. Hahn and F. Strassmann, Naturwiss. **28**, 543 (1940).
[2] See, e.g., L. A. Turner, Rev. Mod. Phys. **12**, 21–23 (1940).
[3] This point is under investigation by R. D. Present and J. K. Knipp. See Phys. Rev. **57**, 751, 1188 (1940).
[4] Y. Nishina, T. Yasaki, H. Ezoe, K. Kimura and M. Ikawa, Nature **146**, 24 (1940); Phys. Rev. **58**, 660 (1940). Also T. Yasaki, Sci. Papers Inst. Phys. Chem. Research (Tokyo) **37**, 457 (1940).
[5] M. L. Pool, Phys. Rev. **53**, 116 (1938).
[6] J. D. Kraus and J. M. Cook, Phys. Rev. **52**, 763 (1937).
[7] L. W. Alvarez, A. C. Helmholz and E. Nelson, Phys. Rev. **57**, 660 (1940).

Anode Spots in Oxygen

J. E. Henderson and Sidney M. Rubens*
University of Washington, Seattle, Washington
December 27, 1940

IT has been shown[1] that anode spots appear in N_2 glow discharges when a certain minimum anode current density is exceeded. Anode spots have never been observed in O_2, and various reasons[2,3] have been proposed for their absence. In these explanations, however, the authors neglect the possibility that in their experiments a sufficiently high anode current density to permit the appearance of the spots might not have been established. Since a method[1] was developed for attaining considerable anode current densities in N_2, it appeared that an application of this same procedure to O_2 might provide the conditions under which anode spots would appear. Should this be the case, it would provide an excellent opportunity to test the conditions proposed as essential for the formation of anode spots.

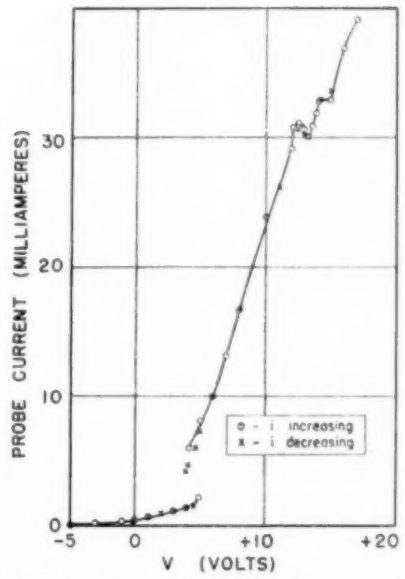

FIG. 1. Current-voltage characteristic for the growth of anode spots in O_2.

The experiment was performed in an oxygen glow discharge maintained in the same apparatus previously described. For O_2 in the same pressure range under which anode spots appeared spontaneously in N_2, neither anode spots nor even a well-defined anode glow could be observed for drift currents up to 500 ma so long as the flat probe auxiliary electrode was maintained at the anode potential. However, when the probe was 5 volts or more positive with respect to the anode, a bright, pale green glow covered the surface of the flat probe, and the probe current rose discontinuously. Holding the drift current constant at 300 ma the current-voltage characteristic curve shown in Fig. 1 was obtained.

It is seen that the current rises discontinuously at 5.0 volts and then increases to a sharp maximum. When the minimum at 13.2 volts was attained, the uniform glow on the auxiliary electrode changed to four brilliant hemispherical spots equally spaced around the probe edge. When the probe potential was further increased, the spots rotated. From these observations, which are similar to those in N_2, we conclude that anode spots might form spontaneously in an oxygen glow discharge at sufficiently great current densities. By dividing the probe current, when the spots appeared, by the probe area, a lower limit for the current density should result. This was found to be of the order of 100 ma/cm^2, a value which would be difficult to obtain in conventional discharge tubes.

The probe potential at which the current maximum occurs, 12.7 volts, is nearly the same as the value found by Guntherschultze and Keller[4] for the anode fall in O_2,

and is also in good agreement with the first ionization potential of O_2, 13.0 volts.

For X/p less than 90 there may be very strong electron attachment in O_2. If the region near the anode is a plasma, X/p would certainly be no greater than 10 for the present conditions, and it might therefore be assumed that strong electron attachment is very probable. Because of this, the anode is bombarded chiefly by O_2^- ions and slow electrons. When the current density is sufficiently great for the development of an anode glow, or anode sheath, then the value of X/p may exceed 90. In this case, when O_2^- ions enter the glow, the electrons readily detach and gain sufficient energy to ionize by collision. Within the sheath, the field strength would be too great for attachment so that a positive space charge would be expected here.

The spots observed on the auxiliary electrode were about 2 mm in diameter at 0.80 mm pressure. If one assumes that the edge of the sheath is spot boundary and that the entire potential drop through the spot is 13.0 volts, an X/p of 160, well above the value for electron detachment, results. These calculations confirm the plausibility of the reasons suggested for the absence of anode spots in oxygen glows.

* Now at University of California at Los Angeles.

[1] S. M. Rubens and J. E. Henderson, Phys. Rev. **58**, 446 (1940).
[2] C. H. Thomas and O. S. Duffendack, Phys. Rev. **35**, 72 (1930).
[3] A. Guntherschultze, W. Bär and H. Betz, Zeits. f. Physik **109**, 303 (1938).
[4] A. Guntherschultze and F. Keller, Zeits. f. Physik **81**, 799 (1933)

Fast Neutrons and Particles with High Specific Ionization in the Cosmic Radiation at High Elevations

S. A. KORFF
Bartol Research Foundation of the Franklin Institute, Swarthmore, Pennsylvania
December 7, 1940

IN a series of flights the number of particles producing large amounts of ionization was measured in the stratosphere with proportional counters. The counters were so adjusted that they did not record pulses produced by ordinary beta- or gamma-rays, but only those produced by particles possessing more than an assignable minimum of specific ionization. In two flights, boron trifluoride counters were used and in two others, different gases were employed.

A proportional counter, filled with boron trifluoride, and adjusted not to detect electrons, will count, in the stratosphere, at a rate equal to the sum of three quantities, A, B and C. A is the number of slow-neutron-induced boron disintegrations, the resulting alpha-particles being counted. B is the number of recoil nuclei produced by fast neutrons traversing the counter, and C is the current of other particles of high specific ionization passing through the counter. In this case it is evident that:

$$A = VN_B\rho\sigma_c v_c$$
$$B = VN\int_{v_2}^{v_1} i(v)\sigma(v)dv \qquad C = S\int_{v_4}^{v_3} I(v)dv, \tag{1}$$

where V is the volume of the counter, N_B the number of B^{10} nuclei per cc, ρ the density of neutrons per cc with energies in the $1/v$ region, σ_c the capture cross section for B^{10} for neutrons of velocity v_c, N the total number of nuclei per cc in the counter, $i(v)dv$ the current of fast neutrons of velocity between v and $v+dv$, σ the recoil cross section of the nuclei of the gas used for neutrons of velocity v, S the cross-sectional area of the counter and I the current per cm², of particles of high specific ionization. The limits of integration, v_1 is the highest and v_2 the lowest neutron velocity producing measurable recoils; v_3 the highest and v_4 the lowest velocity of a particle traversing the counter and producing enough ions to record as a count.

The factor A will be zero for counters using gas other than BF_3. Factor B is proportional to the number of nuclei in the counter (pressure times volume), while C depends on the cross-sectional area of the counter. Hence the use of counters of different sizes and pressures will permit a separation of the effects. Inserting in Eq. (1) the observed counting rates on the four flights, the known S, V and N, taking $(\sigma_c v_c)$ as 10^{-16} and σ as 10^{-24}, we obtain values for ρ, i and I. These are, respectively, at 2 meters of water equivalent below the top of the atmosphere: $\rho = 1\pm1\times10^{-6}$ per cc; $i = 5\pm2$ per cm² and $I = 1.4\pm0.7\times10^{-3}$. These values of ρ and i are in substantial agreement with those previously established by ourselves[1] and others,[2] while no previous measurements exist for I. It is quite impossible to account for the observed results on the basis of fast neutrons alone, by assuming that C is zero, unless the fast neutron flux be supposed increased by a factor of several hundred.

It was necessary to show that gamma-rays had no influence on the counting rate. Before each flight the counter was tested with and without a quantity of radium nearby, which produced in the counter an amount of ionization between 2 and 5 times that encountered in the stratosphere. The backgrounds were thus determined, as was the counting rate in the presence of a known flux of neutrons, with and without the additional gamma-rays.

It seems improbable that large showers could account for the results since (a) it would require over 200 electrons passing simultaneously through the counter to make it discharge, and (b) there was no shower-producing material nearby, the batteries being far below and only the thin glass wall and cardboard container above.

Further tests were made by operating the counter at two voltages during a flight, each voltage being maintained constant for 3 minutes. This, in effect, may be considered as varying the lower limit of the integral in B and C by known amounts. The counting rate could be compared with the previously calibrated rates when the same arrangement was operated in the presence of a known neutron source.

It seems necessary to conclude that fast neutrons alone cannot account for all the observed counts, but that a flux of fast particles of high specific ionization exists. These may be primary protons at the ends of their ranges, or other nuclear particles produced by the radiation. Further details will be published shortly.

Acknowledgment for support is made to the Carnegie Institution of Washington.

[1] H. A. Bethe, S. A. Korff and G. Placzek, Phys. Rev. **57**, 573 (1940).
[2] H. v. Halban, L. Kowarski and M. Magat, Comptes rendus **208**, 572 (1939).

Proceedings of the American Physical Society

MINUTES OF THE PASADENA, CALIFORNIA, MEETING, DECEMBER 20–21, 1940

THE 238th regular meeting of the American Physical Society was held at the California Institute of Technology, Pasadena, California, in the lecture hall, room 201, of the Norman Bridge Laboratory on Friday, December 20, and the morning of Saturday, December 21, 1940.

Sessions for the presentation of ten-minute contributions were held Friday morning and afternoon, starting at 9:30 and 1:30 o'clock. The Saturday morning session consisted in part of contributed papers and in part of an illustrated talk by Dr. John A. Anderson upon problems encountered and progress achieved in the construction of the 200-inch telescope.

About one hundred persons were in attendance.

PAUL KIRKPATRICK,
Local Secretary for the Pacific Coast

ABSTRACTS TO CONTRIBUTED PAPERS

1. Measurement of the Absolute Yield of Gamma-Radiation. J. F. STREIB, W. A. FOWLER AND C. C. LAURITSEN, *California Institute of Technology.*—The number of ion pairs produced per cubic centimeter of sensitive volume by radiation of unit flux (one quantum per cm²) falling on an electroscope completely surrounded by walls of solid material with $Z<20$ has been computed for gamma-radiation extending from 2 to 25 Mev in energy. The calculations of Laurence and others have been extended to take into account the Compton effect, pair production, and the loss of energy by the secondaries through radiation and ionizing collisions. The results in ion pairs per cm³ per quantum per cm² are given below.

WALL	Z	$h\nu$ (MEV)		
		2	10	25
Paraffin	4.5	1.7	4.9	9.4
Air equivalent	7.2	1.8	5.7	12.1
Aluminum	13	1.9	7.2	17.6

Using these results we find the yield of the 6.3-Mev radiation from a thick CaF_2 target bombarded by protons with energy just above the resonance energy at 334 kev to be 1.8×10^{-8} quanta per proton or 11×10^{4} quanta per microcoulomb. This is in good agreement with the yield of $8.9\pm0.5\times10^{4}$ short range alpha-particles per microcoulomb found by Van Allen and Smith and confirms the belief that the quanta are emitted by an excited O^{16} produced in the same reaction as the alphas. The thick target yield at 1.5 Mev is 2.2×10^{-6} quanta/proton.

2. The Photo-Disintegration of the Deuteron. WILLIAM RARITA* AND JULIAN SCHWINGER, *University of California.*—High energy photo-disintegration experiments provide a fruitful source of information concerning the neutron-proton interaction in odd parity states. Fröhlich, Heitler and Kahn[1] have attempted to show that the strong spin-spin coupling of the mesotron theory has a predominant effect at high energies. Unfortunately, their calculation involves the use of inexact, singular wave functions. We have avoided this difficulty by employing a simplified potential which permits exact solutions for the pertinent states of the deuteron. The potential adopted was that following from a symmetrical mesotron theory:

$$V=\tfrac{1}{3}\boldsymbol{\tau}_1\cdot\boldsymbol{\tau}_2\{1+\gamma S_{12}\}J(r),\quad S_{12}=3\frac{\boldsymbol{\sigma}_1\cdot\mathbf{r}\boldsymbol{\sigma}_2\cdot\mathbf{r}}{r^2}-\boldsymbol{\sigma}_1\cdot\boldsymbol{\sigma}_2$$

with $J(r)$ assumed to be a rectangular well of range r_0 and depth V_0. γ was chosen as constant, thus avoiding the singularities which arise in mesotron theory from a highly questionable application of perturbation theory. The constants γ and V_0 were determined by the binding energy and quadripole moment of the deuteron assuming a range of 2.8×10^{-13} cm. The cross sections and angular distributions for electric dipole, magnetic dipole and electric quadripole photo-disintegration were studied, employing the continuum wave functions deduced from this potential. The resultant photoelectric and photomagnetic cross sections for a γ-ray of 17.4 Mev are respectively equal to 0.77×10^{-27} cm², and 0.95×10^{-29} cm². The photoelectric cross section of Fröhlich *et al.* is 4.4×10^{-27} cm². Similar calculations with a simplified neutral potential are in progress.

* On sabbatical leave from Brooklyn College, Brooklyn, New York.
[1] H. Fröhlich, W. Heitler and B. Kahn, Proc. Roy. Soc. **A174**, 85 (1940).

3. Gamma-Rays from C+H². T. W. BONNER, *Rice Institute,* R. A. BECKER, S. RUBIN AND J. F. STREIB, *California Institute of Technology.*—Tuve and Hafstad[1] reported a 2.7-Mev gamma-ray from carbon bombarded by 1.0-Mev deuterons and attributed[2] it to the reaction $C^{12}(d,p)C^{13*}$. Evidence for a weak gamma-ray of higher energy was also obtained. From energy balance considerations Bonner and Brubaker[3] attributed this gamma-ray

to $C^{13}(d,n)N^{14*}$. However, the possibility that it could be caused by the radiative capture reaction $C^{12}(d,\gamma)N^{14*}$ could not be ruled out.[4] We have bombarded a target of ordinary carbon and also one enriched[5] in C^{13} with 1.0-Mev deuterons. Measurements of secondaries ejected from a thin lead lamina by the radiation reveal a strong gamma-ray at 3.0 ± 0.2 Mev and one of approximately 5 percent relative intensity near 5.5 Mev from the ordinary target. Bombardment of the enriched target revealed a large increase in the relative intensity of the higher energy gamma-ray indicating that the original reaction assignments are correct. These results also indicate that the excited state of N^{14} found by Lauritsen and Fowler[6] in the reaction $C^{13}(p,\gamma)N^{14*}$ is at 5.4 rather than 2.8 Mev.

[1] Tuve and Hafstad, Phys. Rev. **48**, 106 (1935).
[2] See also Bethe, Phys. Rev. **47**, 633 (1935).
[3] Bonner and Brubaker, Phys. Rev. **50**, 308 (1936).
[4] Bennett and Bonner, Phys. Rev. **58**, 183 (1940).
[5] Townes and Smythe, Phys. Rev. **56**, 1210 (1939).
[6] Lauritsen and Fowler, Phys. Rev. **58**, 193A (1940).

4. A Magnetic Electron-Pair Spectrograph. E. P. TOMLINSON, *California Institute of Technology.*—A magnetic beta-ray spectrograph has been modified for the purpose of measuring the energy of positive and negative electron pairs. Magnetic fields up to 2000 gauss can be produced across a $2\frac{1}{4}''$ gap between $6''\times18''$ rectangular pole pieces. An evacuated box between the pole pieces has an entrance window for pair members at the center of its top, a slit at each end of the top, and suitable baffles to define semicircular paths of 9.5 cm radius between the entrance window and each slit. Geiger counters, one at each slit, are arranged to record coincidences between members of pairs in which the energy is equally divided between positive and negative electrons. The instrument is to be used for the purpose of comparing the energy of pairs emitted from the O^{16} nucleus produced by bombarding F^{19} by protons with that of pairs ejected from lead by γ-rays from the same reaction.

5. The Lifetimes and Ground States of Be^{10} and C^{10}. E. P. COOPER AND E. C. NELSON, *University of California.* (*Introduced by J. R. Oppenheimer.*)—The lifetimes, $\sim10^6$ years and ~10 seconds, of the unstable isobars Be^{10} and C^{10} show that the transition Be^{10} to B^{10} is forbidden. Since the ground state of B^{10} is a mixture of ^3S and ^3D, the lifetimes might be explained by an assignment of ^1G to Be^{10} and ^1S to C^{10}. However, using the single particle model with a symmetric Hamiltonian,[1] one finds the same order of levels in both Be^{10} and C^{10} with ^1S lowest. Since these two nuclei differ only by the exchange of two neutrons for two protons, this order might be altered by Coulomb forces, though we find from the symmetry of Be^{10} and C^{10} about B^{10}, the center of the p shell, that the first-order contribution of the Coulomb energy[1] does not alter the order of the levels. We have made second-order perturbation calculations to see if it could make the needed level shift. In the Hartree approximation the separation $^1S-{}^1G$ is about 12 mc^2. The first- and second-order Coulomb energy shifts the levels so as to depress ^1G relative to ^1S but by not more than $0.3mc^2$, but the shift is a little more in Be^{10} than in C^{10}. Hence the Coulomb energy could explain the ratio of half-lives, but only if the separation of the levels on the Hartree approximation is too large by a factor of order 10.

[1] E. Feenberg and M. Phillips, Phys. Rev. **51**, 597 (1937).

6. An Interpretation of Fast Neutron Scattering. STANLEY FRANKEL, *University of California.*—The angular distribution of fast neutrons elastically scattered by heavy nuclei, as reported by Kikuchi, Aoki and Wakatuki, shows a smooth rise with decreasing angle of scattering down to about 20° and then a sharp drop-off at the lowest measured angle, 14°. Theoretical distributions have been calculated from five approximate models. The experimental points were fitted by one of these, the Placzek-Bethe shadow-diffraction model, giving satisfactory agreement except for the point at 14° in each case. From consideration of the necessary degree of smoothness and of possible sources of error, it is concluded that this drop-off is probably spurious. This fitting determines rather sensitively an effective "radius" for neutron scattering. The "radii" so determined for seven elements, C, Al, Fe, Cu, Sn, Pb and Bi, are approximately linear in $A^{\frac{1}{3}}$, with one apparent exception, Cu. The linear relation best fitting them has a slope of $(1.25\pm0.10)\times10^{-13}$ cm and gives a "radius" of $(2.3\pm0.2)\times10^{-13}$ cm for $A=0$. These considerations would suggest the use of $R=1.3\times10^{-13}A^{\frac{1}{3}}$ cm for the nuclear radius, and for the elastic scattering distribution

$$\sigma(\theta)\leqq R'^2(J_1(kR'\theta)/\theta)^2,$$

where $R'=(2.3+1.25A^{\frac{1}{3}})\times10^{-13}$ cm.

7. Excitation Energy of Excited Li^7. S. RUBIN, *California Institute of Technology.*—A measurement of the excitation energy of the low lying excited state of Li^7 is being made by comparing the absorption coefficients in lead of the gamma-rays from the excited Li^7 produced by the reaction:[1]

$$Be^7+e_K^-\rightarrow Li^{7*}+\eta$$
$$Li^{7*}\rightarrow Li^7+h\nu$$

and the annihilation radiation from N^{13} positrons. Beryllium carbonate obtained by chemical separation from a Li^6 target bombarded by deuterons[2] and sealed in a small glass capsule was used as a source of the Li^7 radiation. For the N^{13} radiation, scrapings from the surface of a carbon target bombarded by deuterons will be placed in a small lead capsule, of sufficient wall thickness to annihilate all emitted positrons in the walls. These sources can be mounted in a standard position relative to a shielded, lead-lined, Lauritsen electroscope. A series of ten measurements at each of two absorber thicknesses gave an absorption coefficient of 1.635 ± 0.015 cm^{-1} for the Li^7 gamma-ray. Using a coefficient of 1.51 ± 0.05 for the annihilation radiation as determined by Lauritsen and Fowler[3] under very similar geometrical conditions, the energy of Li^7 radiation is calculated to be 465 ± 10 kev.

[1] Roberts, Heydenburg and Locher, Phys. Rev. **53**, 1016 (1938).
[2] Prepared for us by Dr. S. K. Allison, University of Chicago.
[3] Fowler and Lauritsen, Phys. Rev. **56**, 841 (1939).

8. The Theory of Cascade Showers in Heavy Elements. H. C. CORBEN, *University of California.*—The one-dimensional equations of the cascade theory of showers are

solved, account being taken of the Compton effect and of the variation with γ-ray energy of the cross section for pair production, as well, of course, as ionization and bremsstrahlung effects. These modifications are necessary for the discussion of cosmic-ray showers in elements of high atomic number, and the theory is developed in detail for lead. Introducing as usual the units t of length and β of energy, both characteristics of the material traversed ($t, \beta = 240$ m, 90 Mev and 0.4 cm, 6.5 Mev for air and lead, respectively), one finds that the maximum number of particles N_{max} arising from an incident particle of energy $E_0 = \epsilon\beta$ has in lead, for a given value of ϵ, approximately three-quarters the value that it assumes in air. Thus, for lead, $N_{max} \sim \epsilon/a$ where $a \sim 11$ for $\epsilon \sim 100$ and $a \sim 13$ for $\epsilon \sim 10^4$. For a given ϵ, the maximum number of particles occurs at a distance (in units of t) slightly less for lead than for air, and for large distances the effect of the variation with energy of the pair-production cross section is to decrease the number of particles and increase the number of γ-rays to be expected.

9. The Short Range Alpha-Particles from $F^{19}+H^1$. R. A. BECKER, W. A. FOWLER AND C. C. LAURITSEN, *California Institute of Technology.*—A group of α-particles of mean range about 8 mm was previously reported by this laboratory,[1] and by Burcham and Smith,[2] from the reaction $F^{19}(p,\alpha)O^{16*}$. These were found to show a resonance coinciding with that of the gamma-rays from $F^{19}+H^1$ at 334 kv. Energy considerations also indicated that they were associated with the gamma-rays. Subsequent measurements of Burcham and Devons[3] with an ionization chamber at the 334-kv resonance, and with magnetic analysis, at the 660- and 862-kv gamma-ray resonances, showed the excitation function of the α-particles to be identical to that of the gamma-radiation. It was also found that the α-particles showed the same Q at all three resonances. We have confirmed these observations at 862 kv, and have extended them to the 927- and 1363-kv resonances, using a cloud chamber and employing magnetic analysis of the disintegration products. Within experimental error the Q of the short range α-particles at 862, 927 and 1363 kv was in each case found to be about 1.85 ± 0.05 Mev, identical to that at 334 kv bombarding energy. This method of magnetic resolution is now being employed to study the short range α-particles preceding the pair emission[4] from $F^{19}+H^1$.

[1] McLean, Becker, Fowler and Lauritsen, Phys. Rev. **55**, 796 (1939).
[2] Burcham and Smith, Nature **143**, 795 (1939).
[3] Burcham and Devons, Proc. Roy. Soc. **173**, 555 (1939).
[4] Fowler and Lauritsen, Phys. Rev. **56**, 840 (1939).

10. Electron Capture in White Dwarf Stars. P. MORRISON, *University of California. (Introduced by J. R. Oppenheimer.)*—The spherical equilibrium distribution of a cold gas mixture of stripped nuclei and highly degenerate electrons is apparently a good model for white dwarf stars.[1] For great enough mass M the Fermi pressure will not support the weight, and such a body will collapse. The limiting mass is given by Chandrasekhar as $M\mu^2 < 5.75\odot$, where μ, the number of protonic masses per electron, is, for this completely ionized matter, equal to $2/1+X$, where X is the mol fraction of protons in the mixture. There is another limiting value lower than this purely hydrostatic limit. When the free energy per electron exceeds some 800 kilovolts, protons will be unstable against electron capture. The central pressure reaches this critical value for $M\mu^2 = 4\odot$. For masses above this, protons will be unstable in the bulk of the star, and μ must be nearly 2. From the mass-radius relation we can find a radius $R = 0.016R_\odot$ such that for $R\mu > R$ the body can contain hydrogen, for $R < R$ it certainly cannot. This seems consistent with the observed spectra of the white dwarfs of various radii. An unsuccessful attempt has been made to remove the radius discrepancy in Sirius B by constructing a model in which the outer layer contained He^3, which is unstable against electron capture when the free energy per electron reaches 20 kev. This model can account for the observed radius, even with $X = 0$, but is, however, very unstable against mixing.

11. Point-to-Plane Corona in Very Pure N_2 and H_2. GERHARD L. WEISSLER, *University of California. (Introduced by Leonard B. Loeb.)*—These coronas were studied with a hemispherical 0.45 mm diameter Pt point at pressures of 760, 300 and 100 mm Hg. Earlier results reported for + point in N_2 and H_2* were found to have been falsified by minute traces of impurity. Positive points in pure gases gave no pre-corona-onset pulses at all. At corona-onset for the 3 pressures only a large number of minute single avalanche pulses were found with no streamers or burst pulses. Telemicroscopic observation revealed a corona spot of 0.1 mm diameter in distinction to the positive corona in air, which spreads uniformly all over the point. With increasing voltage the discharge extended visibly towards the cathode and before spark breakdown visible streamers appeared giving oscillographic kicks. They cross the gap without causing a spark, obviously being too feeble to create a hot-spot at the cathode. Streamers in H_2 before breakdown were even weaker than in N_2. The negative corona revealed at onset a glow which spread uniformly over the point, in distinction to the localized spot found in air. A few hundred volts above onset the current changed from 10^{-7} amp. to 10^{-4} amp. and the visible corona changed to a characteristic glow-discharge with cathode glow, Faraday darkspace and positive column. At higher potentials the discharge changed smoothly to an arc.

* Phys. Rev. **57**, 340 (1940).

12. An "Ultra-Spectrometer" Technique for Infra-Red Absorption Bands. MARTIN SUMMERFIELD AND JOHN STRONG, *California Institute of Technology.*—The effect of total pressure on the infra-red absorption of ozone in the 9.6μ band was measured, extending the experiments of Strong and Watanabe.[1] Oxygen was the foreign gas used to control the total pressure. Measurements were made with a grating spectrometer of approximately 0.1μ resolution at 9.6μ. The equivalent thickness of ozone in the cell was determined by absorption measurements in the Hartley band near 3100A. Curves are given showing the increase of absorption with pressure until saturation is reached. Further, in the neighborhood of the saturation

pressure it is found that the transmission depends exponentially on thickness, while at very low pressures the absorption increases with square-root of the thickness. This is in accord with calculations of Elsasser.[2] By a quantitative study of this pressure effect based on the theory of collision broadening of spectral lines,[3] an estimate of the spacing of the lines in the band can be made. This opens the possibility of estimating the spacing of the rotational structure in bands of other heavy molecules with data obtained using spectrometers inadequate to resolve that structure. Not only bands but double lines or groups of lines may be similarly investigated to determine otherwise unresolvable details of structure. Calculations for the ozone band are described.

[1] Strong and Watanabe, Phys. Rev. **57**, 1049 (1940).
[2] Elsasser, Phys. Rev. **54**, 126 (1938).
[3] Margenau and Watson, Rev. Mod. Phys. **8**, 22 (1936).

13. The Vacuum Spark Spectra of Cd IV and In V. M. GREEN, *University of California.* (*Introduced by H. E. White.*)—The spectra of Cd IV and In V have been photographed in the region 300A to 1800A with a three-meter normal incidence vacuum spectrograph. The irregular doublet law and the law of constant second difference has been applied in the classification of many of the lines of these two ions. The separation of the $4d^9\,{}^2D$ multiplet of the ground state has been found for both ions. Most of the odd terms arising from $4d^8 5p$ and some of the even terms arising from $4d^8 5s$ have been determined. Some fifty transitions to the $4d^9\,{}^2D$ levels have been classified for Cd IV and forty-two for In V. In cadmium IV some seventy-five lines have been classified as combinations between $4d^8 5s$ and $4d^8 5p$.

14. Excitation of the Auroral Green Line in Nitrogen Afterglows. JOSEPH KAPLAN AND SIDNEY M. RUBENS, *University of California.*—In 1928 Kaplan observed the auroral green line, λ5577, unaccompanied by other auroral radiations in the Lewis-Rayleigh afterglow, and later observed very large relative intensity of this line in weak auroral afterglows. Never before has the green line been recorded with an intensity sufficiently great to indicate that its emission is a primary radiative process in the afterglow as must be the case in the aurora. Not only has this now been accomplished, but 5577 is accompanied by the forbidden lines of oxygen λ2972, and of nitrogen λ3467 and the Vegard-Kaplan bands showing that the emission of forbidden radiations is a primary radiative process in these afterglows. In the present experiments the nitrogen was very pure, and a trace of pure oxygen was added. λ5577 increased in intensity with nitrogen concentration and exhibits the temporal effect of increasing in relative intensity with afterglow decay duration prior to its observation. This appears to be the most faithful reproduction of the auroral process ever achieved in the laboratory.

15. On the Morphology of Nebulae. F. ZWICKY, *California Institute of Technology.*—A study is presented of the structures of extragalactic nebulae. Particular emphasis is laid (a) on the distribution of mass and luminosity in nebulae, (b) on the dynamic characteristics of nebulae and (c) on the problem of the stellar content of nebulae. Those structural features which are subject to substantial changes in periods of time shorter than the lifetime of the average stars are subjected to an analysis utilizing the fundamental results of the hydrodynamics of laminar and turbulent motion supplemented through considerations based on statistical mechanics and on particle dynamics. A satisfactory understanding of the occurrence of globular, elliptical and irregular nebulae as well as of ordinary spirals and barred spirals may thus be arrived at. In addition, a number of the dynamic properties of nebulae are discussed. An attempt is also made to explain the differences in stellar content of various nebulae through a study of possible evolutionary sequences of stars and their relation to structural changes in nebulae.

16. The Forbidden Lines of Pb I. EDWARD GERJUOY, *University of California.*—Calculations have been made on the forbidden lines of the configuration $6p^2$ of Pb I and the results compared with experiment. Line intensities, hyperfine structure and Zeeman effect have all been investigated theoretically and experimentally. Some of the lines of this configuration, in particular ${}^1D_2 - {}^3P_1$ (approximate Russell-Saunders labeling), permit simultaneous magnetic dipole and electric quadrupole radiation. This results in interference between these radiations in the various Zeeman components of experimentally observable magnitude. The interference vanishes after summing over all Zeeman components. The relative intensities of the Zeeman components depend only upon the quadrupole moment of the transition electron and are independent of the coupling. The agreement with experiment among the Zeeman components is good and self-consistent but requires the assumption of a smaller quadrupole moment for the transition electron than is indicated from the comparison of line intensities. An approximate calculation of the quadrupole moment of the transition electron is planned.

17. Measurement of the Total Infra-Red Emission of Atmospheric Water Vapor. WALTER M. ELSASSER, *California Institute of Technology.*—The thermal emission of columns of moist air was measured directly by the method of Hottel[1] which consists in screening off outside radiation by means of an extremely cold background. In our experiments the background was produced by means of a 30-inch searchlight mirror which was aluminized at the front side and at the focus of which a blackbody of liquid-air temperature was located. The receiving apparatus was a small reflecting telescope with a black disk and compensated thermocouple at the focus. Emissivities were measured for distances varying between 13 cm and 315 m corresponding to a range of moisture between 10^{-4} g/cm² and 0.3 g/cm². The known emission of carbon dioxide[1] in each path was subtracted. The water vapor emissivity was found to vary in the interval measured from 2 percent to 50 percent of the blackbody emission (air temperature 20°C). The solution of the problem of radiative heat transfer in the atmosphere has been worked out before;[2]

our new results give corrections of 10–20 percent for numerical values previously used.

[1] H. C. Hottel and H. G. Mangelsdorf, Trans. Am. Inst. Chem. Eng. **31**, 517 (1935).
[2] W. M. Elsasser, Quar. J. Roy. Meteor. Soc. **66**, 41 (suppl. 1940).

18. Design, Assembly and Preliminary Tests of a Curved Crystal γ-Ray Spectrometer. W. K. H. PANOFSKY, J. W. M. DUMOND, R. R. YOST, *California Institute of Technology*, AND H. A. KIRKPATRICK, *Occidental College*.—A curved-crystal γ-ray spectrometer has been constructed, using the (310) reflections of a quartz plate bent to a radius of curvature of 2 meters. The instrument covers the wave-length range from 500 x.u. to about 10 x.u., thus making accurate γ-ray wave-length measurements in the neighborhood of 1 Mev possible. The geometry of the instrument is such that either the source of radiation or the detector remain stationary when a wave-length setting is made; this is accomplished by moving the center of the focal circle simultaneously with rotating the crystal. For work at very short wave-length the beam reflected by the crystal planes diverges by only about ½° from the directly transmitted beam; to make measurements at this wave-length possible, a collimator consisting of a set of wedge-shaped lead plates about 1 m long and spaced by similar spacers was constructed. Tests on the collimator showed that the intensity of radiation deviating 20′ from the desired beam was reduced to 1 percent. Constructional details of the instrument are given and the program of work contemplated is discussed.

19. A Two-Stage Electron Microscope. W. V. HOUSTON AND HUGH BRADNER, *California Institute of Technology*.—An electron microscope has been constructed in which the electrons transmitted by a thin film are brought to a focus in an image of the film. The electrons are emitted from a hot filament and accelerated by a potential difference of 40 kilovolts. The potential is produced by a rectifier and filter circuit and shows a ripple of about one volt. The electrons are focused upon the object by an electrostatic lens, and the transmitted electrons are focused into an enlarged image by two magnetic lenses of the type described by Ruska. Both the image formed by the first lens and the final image can be examined on fluorescent screens for the purpose of adjusting the focus. Magnifications up to 7000 diameters have been used, and it is thought that objects less than 300 angstroms in diameter can be distinguished.

20. The Velocity of Propagation of the Electric Impulse Along the Organs of the Electric Eel. W. A. ROSENBLITH, *University of California at Los Angeles*, AND RICHARD T. COX, *New York University*.—Observations previously reported[1] have shown that in the discharge of the electric organs of the electric eel a pulse of potential gradient runs along the organ from anterior to posterior. The speed of the pulse, roughly estimated, was found much higher than the highest speed recorded for impulses along nerves. Recently more accurate measurements have been attempted. Oscillographic traces of the discharge in two different segments of an electric organ were photographed and then plotted against each other with various assumed time-lags. This plotted figure was compared to the oscillographic trace obtained when the same two segments were connected respectively to the vertical and horizontal deflecting plates so as to give a loop picture corresponding to the true time lag. Though the margin of error may amount to as much as 20 percent it has been possible to confirm very definitely that the velocity of propagation of the discharge along the large organ ranges from several hundred to a thousand meters per sec. Hypotheses as to the possible nature of this velocity of propagation will be suggested.

[1] C. W. Coates, R. T. Cox and L. P. Granath, "The electric discharge of the electric eel, Electrophorus electricus," Zoologica **22** (Part 1), No. 1 (1937).

21. The Deadtime of a Geiger Counter. H. G. STEVER, *California Institute of Technology*. (*Introduced by W. H. Pickering.*)—The deadtime of a fast Geiger counter is the insensitive time measured from the initiation of one count till the counter is again sensitive. In the course of measurements on counter breakdown, an experiment to measure this deadtime directly was devised. The deadtime has been found to be a function of counter constants such as diameter, gas pressure and working voltage, but it does not depend on the external circuit. This deadtime for a counter of 1 inch diameter is of the order of 10^{-4} second.

22. An Extremely Sensitive Biophysical Indicator for Metal Ions. ALEXANDER GOETZ AND S. SCOTT GOETZ, *Cryogenic Laboratory, California Institute of Technology*.—The experimental conditions essential for using living cells as quantitative indicators for the presence of heavy metal ions (Ag, Au, Hg, Pb) have been worked out for Sacch. cerevisiae and Ag^+. As a prerequisite for the applicability of such methods, a staining technique developed whereby the cells affected by metal ions are differentiated from those not affected, renders it possible to obtain sufficient statistical material of cell mortality with microscopic counts. The study of the most efficient mixing technique for ions and cells as well as ways for avoiding wall adsorption of the ions resulted in this: Each cell can adsorb up to 10^9 Ag^+; the value of $n/N \sim Ag^+/\text{cells}$ necessary to produce the stain reaction (ν) is very small and approaches under the optimum temperature etc. conditions $\nu = 1$ when the Poisson probability:

$$\pi_\nu = \frac{x^\nu}{\nu!} \cdot e^{-x} \cdots (x = n/N) \cdots$$

is applied. This extreme sensitivity can be interpreted by assuming the living cell to act as a giant molecule in this reaction. A qualitative indication of the presence of a quantity of 10^{-8} g Ag is shown as lecture demonstration.

23. Preliminary Report on a Redetermination of h/e by the Short Wave-Length Limit of the Continuous X-Ray Spectrum. J. W. M. DUMOND, H. H. BAILEY, W. K. H. PANOFSKY AND A. E. S. GREEN, *California Institute of Technology*.—In order to shed new light on the apparent discrepancy of the natural atomic constants h, e, and m, a redetermination of h/e by the short wave-length limit method is in progress, using the 30-kw Watters x-ray tube at this Institute. The large available intensity makes it

possible to obtain intensity *vs.* voltage curves at constant wave-length for higher resolving power of the two-crystal monochromator than has hitherto been available, thus greatly reducing the "fillet" of the isochromats which appeared in past work. Improved methods of voltage stabilization and measurement were developed. Preliminary values of h/e agree with indirectly determined values.

24. An Absolute Determination of the Continuous X-Ray Energy from Thin Aluminum Targets. J. C. CLARK, *Michigan State College*, AND H. R. KELLY, *Stanford University*.—Ross's method of balanced foils has been used with foils of Cd and Ag to isolate a small region of the continuous x-ray spectrum from thin aluminum targets. The targets were made by the evaporation of aluminum upon a Cellophane supporting film. Preliminary measurements using target thicknesses 360A and 685A, at a distance of 34 cm from the x-ray source and azimuthal angle of 60°, give $J_\nu d\nu = 22.8 \pm 7.5 \times 10^{-36}$ erg per cm² per electron per second per atom per cm² of the target, when the energy of the bombarding electron is 31.7 kev. Sauter's wave mechanics theory[1] predicts $J_\nu d\nu = 1.27 \times 10^{-36}$ erg for the same bombarding electron energy and azimuthal angle. Scherzer's theory[2] predicts 1.22×10^{-36} erg. Measurements of $J_\nu d\nu$ as a function of azimuthal angle compare very favorably with relative intensity measurements by Kulenkampff and Bohm.[3] Measurements are in progress to determine $J_\nu d\nu$ as a function of incident electron energy and atomic number of the target material.

[1] Sauter, Ann. d. Physik [5] **20**, 404 (1934).
[2] Scherzer, Ann. d. Physik [5] **13**, 137 (1932).
[3] Kulenkampff and Bohm, Ann. d. Physik [5] **33**, 315 (1938).

25. A Theory of the Geneses of Primary X-Rays. SAMUEL R. COOK, *Sacramento, California*.—Former theories of x-rays are briefly reviewed and it is shown that the existing theories are lacking in the presentation of a process of the geneses of primary x-rays. It is then suggested that a process of the genesis of a primary x-ray may be formulated by the consideration of the transformation of the electromagnetic field of force, associated with a cathode-ray electron, into the energy of a primary x-ray, during the collision of a cathode-ray electron with a nucleus of the anticathode material. It is then shown that by this suggested transformation an x-ray is generated, which conforms to the necessary requirements of a theory of the geneses and propagation of primary x-rays and fulfills the criteria both for interference and photoelectron emission and the quantum requirements both for emission and absorption. Mathematical formulations for the transformation of the electromagnetic energy associated with the cathode-ray electron into radiant energy of the newly generated x-ray are given. The general differential equations for the propagation of the x-ray quantum are derived and shown to be of the same general form as Maxwell's equations.

26. Crystallization Phenomena, Crystal Structure and Fatigue in Metallic Conglomerates. S. KYROPOULOS, *California Institute of Technology*.—In tensile strength tests on metallic conglomerates at ordinary temperatures, it is invariably in the crystallites themselves where rupture occurs, never in the crystal boundaries. With regard to impact fatigue, an important factor in bearing metal failure, it is generally stated that there is no connection between microstructure and fracture. The appearance of cracked Babbitt and lead bearings suggests, with due consideration of the crystallization process, that the cracks follow essentially the boundaries of the dendrites. Microscopic examination of a large number of cracks confirmed this: With two exceptions, where a brittle single crystal, subject to tensile stress, bridged two dendrites, the cracks were found to follow the dendrite boundaries. The thickness of brittle impurities or constituents, expelled at the boundaries, is the greater, the larger the dendrites, the diameters of which sometimes amount to 15 mm. The large dendrites, very nearly single crystals of high anisotropy with Sn and its solid solutions with Sb, tend to set up high elastic stresses under load or thermal expansion, which would partly account for the higher resistivity to cracking of isotropic metals like the cubic Pb.

27. Burst Production by Mesotrons. R. F. CHRISTY AND S. KUSAKA, *University of California*.—Making certain assumptions we have calculated the frequency of burst production as a function of burst size. For the mesotron of spin 1 and moment $eh/2\mu c$, we have used the previously calculated knock-on formulae, supplemented by our own calculations of the bremsstrahlung: for the latter, the cross section has terms, significant for our work, in E, $\ln^2 E$, and $\ln E$. The *minimum* cross sections we used differ little from those given directly by the Born approximation. Using these cross sections, the cascade theory of showers, and a modified form of the Furry model to take into account the fluctuations, the frequency of burst production was calculated. The sea-level data of Schein and Gill[1] give for the number of bursts of size greater than S, $N_S \sim S^{-\gamma}$, with $\gamma \sim 1{\cdot}8$. Our calculations give for spin 1, $\gamma \sim 1{\cdot}5$ and numerically too many by a factor of 6. Similar calculations for the mesotron of spin 0 give $\gamma \sim 1{\cdot}8$ and the same in number as the observations within an uncertainty of about a factor 1·5. For spin $\frac{1}{2}$ and moment $eh/2\mu c$, the bursts are approximately twice as numerous as for spin 0. This evidence thus favors spin 0, or possibly spin $\frac{1}{2}$, but tends to exclude spin 1.

[1] M. Schein and P. S. Gill, Rev. Mod. Phys. **11**, 267 (1939).

28. A New Circuit for Generating Alternating Electric Pulses of Very Short Duration. G. POTAPENKO, *California Institute of Technology*.—A new generator of alternating electric pulses of short duration has been worked out. The generator uses gaseous triodes with an alternating potential supplied to their plates. The discharge through the tubes starts and stops automatically without requiring any relays or contacts to open or close the circuit. The starting of the discharge is controlled by the phase-shift between the grid and tube potentials. The stopping of the discharge and, therefore, the duration of it is controlled by the charging time of a condenser in the plate circuit of tubes. The frequency of current supplied to the tubes

determines the number of pulses per second. The duration of pulses and their intensity can be controlled independently one from the other. With usual commercial tubes of 885-type the generator delivers pulses up to about 250–300 v peak value and down to about 0.0001 sec in duration.

29. The Value of the Rydberg Constant. RAYMOND T. BIRGE, *University of California.*—From frequency measurements of the fine structure of H, D and He^+ lines, one can calculate the value of R_∞ and of α (the fine structure constant). With an assumed value of the Faraday, one can also calculate e/m. A systematic recalculation has been made of all work in this field during the past 15 years. The present most reliable values of all auxiliary constants (*including* the index of refraction of air) have been used, and several small errors, some theoretical and some arithmetic, have been found and corrected. Because of time limitations, only the values of R are here reported. From the observational data of DRW[1] alone, assuming only the atomic masses of H and D, and with some allowance for systematic errors, $R_H = 109{,}677.5810 \pm 0.0075$ cm^{-1}, $R_D = 109{,}707.4192 \pm 0.0075$, yielding $R_{He} = 109{,}722.264 \pm 0.012$ and $R_\infty = 109{,}737.303 \pm 0.017$, all in the I.A. system. A similar recalculation of Houston's data[2] gives $R_H = 109{,}677.680$ and $R_{He} = 109{,}722.296$, yielding $R_\infty = 109{,}737.312$. Chu's data[3] similarly give $R_{He} = 109{,}722.343$ which, combined with Houston's R_H, gives $R_\infty = 109{,}737.376$. The DRW data are the most reliable and I *adopt* $R_\infty = 109{,}737.30 \pm 0.05$ cm^{-1}, in the c.g.s. system.

[1] Drinkwater, Richardson and Williams, Proc. Roy. Soc. **A174**, 164 (1940).
[2] W. V. Houston, Phys. Rev. **30**, 608 (1927).
[3] D. Y. Chu, Phys. Rev. **55**, 175 (1939).

30. Neutron Stars as Gravitational Lenses. F. ZWICKY, *California Institute of Technology.*—Collapsed neutron stars are so small that light passing near them is deflected through great angles. For a neutron star of mass M, at the distance D this leads to the following conclusions. Any star at a distance $D' \gg D$ in the line of sight of the neutron star will produce a ring-like image of the diameter $\alpha = 4(\Gamma M/Dc^2)^{\frac{1}{2}}$ where Γ and c are the gravitational constant and the velocity of light. *Every* other star will produce one only slightly deflected direct image and one strongly deflected image which lies within the ring α. Within this ring, therefore, appears a *miniature edition* of *all of the unobscured luminous objects* in the universe. If D is small enough, or if the neutron star is favorably located, the miniature image may be observable. The spectrum of the miniature image is a composite weighted spectrum of many stars. If the neutron star theory of supernovae is correct, the number of collapsed stellar remnants of supernovae in our galaxy should exceed one million and several collapsed neutron stars may be expected within a sphere of ten light years. A search for miniature images of the universe produced by neutron stars in our neighborhood is suggested.

AUTHOR INDEX TO ABSTRACTS OF PASADENA MEETING

Bailey, H. H.—see DuMond, J. W. M.
Becker, R. A., W. A. Fowler and C. C. Lauritsen—No. 9
—— see Bonner, T. W.
Birge, Raymond T.—No. 29
Bonner, T. W., R. A. Becker, S. Rubin and J. F. Streib—No. 3
Bradner, Hugh—see Houston, W. V.

Christy, R. F. and S. Kusaka—No. 27
Clark, J. C. and H. R. Kelly—No. 24
Cook, Samuel R.—No. 25
Cooper, E. P. and E. C. Nelson—No. 5
Corben, H. C.—No. 8
Cox, Richard T.—see Rosenblith, W. A.

DuMond, J. W. M., H. H. Bailey, W. K. H. Panofsky and A. E. S. Green—No. 23
—— see Panofsky, W. K. H.

Elsasser, Walter M.—No. 17

Fowler, W. A.—see Becker, R. A.
—— see Streib, J. F.
Frankel, Stanley—No. 6

Gerjuoy, Edward—No. 16
Goetz, Alexander and S. Scott Goetz—No. 22
Green, A. E. S.—see DuMond, J. W. M.
Green, M.—No. 13

Houston, W. V. and Hugh Bradner—No. 19

Kaplan, Joseph and Sidney M. Rubens—No. 14
Kelly, H. R.—see Clark, J. C.
Kirkpatrick, H. A.—see Panofsky, W. K. H.
Kusaka, S.—see Christy, R. F.
Kyropoulos, S.—No. 26

Lauritsen, C. C.—see Becker, R. A.
—— see Streib, J. F.

Morrison, P.—No. 10

Nelson, E. C.—see Cooper, E. P.

Panofsky, W. K. H., J. W. M. DuMond, R. Y. Yost and H. A. Kirkpatrick—No. 18
—— see DuMond, J. W. M.
Potapenko, G.—No. 28

Rarita, William and Julian Schwinger—No. 2
Rosenblith, W. A. and Richard T. Cox—No. 20
Rubens, Sidney M.—see Kaplan, Joseph
Rubin, S.—No. 7
—— see Bonner, T. W.

Schwinger, Julian—see Rarita, William
Stever, H. G.—No. 21
Streib, J. F., W. A. Fowler and C. C. Lauritsen—No. 1
—— see Bonner, T. W.
Strong, John—see Summerfield, Martin
Summerfield, Martin and John Strong—No. 12

Tomlinson, E. P.—No. 4

Weissler, Gerhard L.—No. 11

Yost, R. Y.—see Panofsky, W. K. H.

Zwicky, F.—Nos. 15, 30